



**HAL**  
open science

# In-cell synthesis of cytotoxic phenanthridine through bioorthogonal cyclization : a paradigm in antitumor prodrug development

Hichem Maslah

► **To cite this version:**

Hichem Maslah. In-cell synthesis of cytotoxic phenanthridine through bioorthogonal cyclization : a paradigm in antitumor prodrug development. Organic chemistry. Université Paris-Saclay, 2022. English. NNT : 2022UPASF009 . tel-03641044

**HAL Id: tel-03641044**

**<https://theses.hal.science/tel-03641044>**

Submitted on 14 Apr 2022

**HAL** is a multi-disciplinary open access archive for the deposit and dissemination of scientific research documents, whether they are published or not. The documents may come from teaching and research institutions in France or abroad, or from public or private research centers.

L'archive ouverte pluridisciplinaire **HAL**, est destinée au dépôt et à la diffusion de documents scientifiques de niveau recherche, publiés ou non, émanant des établissements d'enseignement et de recherche français ou étrangers, des laboratoires publics ou privés.

*In-cell synthesis of cytotoxic  
phenanthridine through bioorthogonal  
cyclization: a paradigm in antitumor  
prodrug development*

*Développement de prodrogues antitumorales générant des  
phénanthridines cytotoxiques par cyclisation bioorthogonale in cellulo*

**Thèse de doctorat de l'université Paris-Saclay**

École doctorale n°571, Sciences Chimiques : Molécules, Matériaux, Instrumentation et  
Biosystèmes (2MIB)  
Spécialité de doctorat : Chimie  
Graduate School : Chimie. Référent : Faculté des sciences d'Orsay

Thèse préparée dans l'unité de recherche **Institut de chimie moléculaire et des  
matériaux d'Orsay** (Université Paris-Saclay, CNRS), sous la direction de  
**Raphaël LABRUÈRE**, Maître de conférences (HDR)

**Thèse soutenue à Paris-Saclay, le 11 février 2022, par**

**Hichem MASLAH**

**Composition du Jury**

<b>Paola ARIMONDO</b> Directrice de recherche (HDR), Institut Pasteur, Paris	Présidente & Rapporteuse du jury
<b>Sébastien PAPOT</b> Professeur, Université de Poitiers	Rapporteur & Examineur
<b>Dominique GUIANVARC'H</b> Professeure, Université Paris-Saclay	Examinatrice
<b>Geneviève ESTENNE-BOUHTOU</b> Chagée de recherche, Sanofi	Examinatrice
<b>Jean-Christophe CINTRAT</b> Directeur de recherche, CEA Paris- Saclay	Examineur
<b>Raphaël LABRUÈRE</b> Maître de conférences (HDR), Université Paris-Saclay	Directeur de thèse

**Titre :** Développement de prodrogues antitumorales générant des phénanthridines cytotoxiques par cyclisation bioorthogonale *in cellulo*

**Mots clés :** Réaction spontanée, Chimie organique, cancer, prodrogue, réaction bioorthogonale, ROS.

**Résumé :** L'inactivation pharmacologique des médicaments antitumoraux vis-à-vis des cellules saines est un facteur critique dans le développement de prodrogues. Généralement, les chimistes médicaux greffent des motifs temporaires aux principes actifs antitumoraux existants afin de réduire autant que possible leur activité pharmacologique. Nous avons développé une plateforme où la structure de la prodrogue n'inclut pas le principe actif préexistant. Celle-ci est basée sur un précurseur synthétique inactif capable de générer l'agent cytotoxique par cyclisation bioorthogonale dans un environnement tumoral. En utilisant les phénanthridines comme composés modèles cytotoxiques,

nous avons conçu des précurseurs biaryles à cycle ouvert qui génèrent des phénanthridines par imination bioorthogonale irréversible. Cette réaction a été déclenchée par des espèces réactives de l'oxygène, communément surproduites dans les cellules cancéreuses et ainsi capables de convertir une fonction ester de vinylboronate en une fonction cétone qui réagit avec une fonction aniline en attente. Nous avons préparé un précurseur inactif qui engendre une phénanthridine cytotoxique sur la lignée cancéreuse KB. De plus, la cinétique de cyclisation de cette prodrogue est extrêmement rapide (< 10 ms) dans des sphéroïdes de cellules vivante KB. Cette formation rapide permet de circonscrire l'action du médicament à la tumeur.

**Title:** In-cell synthesis of cytotoxic phenanthridine through bioorthogonal cyclization: a paradigm in antitumor prodrug development

**Keywords:** Spontaneous reaction, organic chemistry, cancer, prodrug, bioorthogonal reaction, ROS.

**Abstract:** Pharmacological inactivation of antitumor drugs toward healthy cells is a critical factor in prodrug development. Typically, pharmaceutical chemists graft temporary moieties to existing antitumor drugs to reduce their pharmacological activity as much as possible. Here, we report a platform where the structure of the prodrug excludes the preexisting antitumor drug motif and is based on an inactive synthetic precursor able to generate the cytotoxic agent by bioorthogonal cyclization within a tumor environment. Using phenanthridines as cytotoxic model compounds, we designed ring-opened biaryl precursors that generated the

phenanthridines through bioorthogonal irreversible imination. This reaction was triggered by reactive oxygen species, commonly overproduced in cancer cells, able to convert a vinyl boronate ester function into a ketone that subsequently reacted with a pendant aniline. An inactive precursor was shown to engender a cytotoxic phenanthridine against KB cancer cells. Moreover, the kinetic of cyclization of this prodrug was extremely rapid (< 10 ms) inside living cells of KB cancer spheroids so as to circumvent drug action.

## Remerciements

*Je souhaite remercier en premier lieu Monsieur Laurent Salmon, Professeur de l'Université Paris Saclay, pour m'avoir accueilli au sein de l'équipe « Chimie Bioorganique et Bioinorganique » de l'Institut de Chimie des Milieux Moléculaire et des Matériaux d'Orsay.*

*J'exprime ma profonde gratitude à mon directeur de thèse, Monsieur Raphaël Labruère, Maître de Conférences de l'Université Paris Saclay qui m'a permis de réaliser et de mener à bien ces travaux. Je lui suis également reconnaissant pour sa disponibilité, ces bons conseils, ces qualités humaines, scientifiques et sa confiance. J'ai beaucoup appris à ces côtés et je lui adresse tous mes remerciements pour ces quatre années.*

*Je tiens à exprimer toute ma reconnaissance à Madame Paola Arimondo, Directrice de recherche à l'institut Pasteur, qui m'a fait l'honneur de présider ce jury de thèse et de juger ce travail.*

*Merci à Madame Paola Arimondo, Directrice de recherche à l'institut Pasteur et Monsieur Sébastien Papot, Professeur de l'Université de Poitiers, pour avoir accepté d'être les rapporteurs de ce travail de thèse et pour leurs jugements très pertinents sur ce manuscrit.*

*Je remercie également Monsieur Ludovic Jullien, Professeur de l'école normale supérieure de Paris, Monsieur Jean-Christophe Cintrat, Directeur de recherche du Commissariat à l'énergie atomique, Madame Dominique Guianvarc'h, Professeure de l'Université Paris Saclay, Madame Geneviève Estenne-Bouhtou, cheffe d'équipe à Sanofi pour avoir participé au jury de cette thèse et pour l'intérêt qu'ils ont porté à mon travail.*

*Je tiens à exprimer toute ma reconnaissance aux membres de l'équipe « Chimie Bioorganique et Bioinorganique » : Stéphanie Pethe, Maître de Conférences de l'Université de Paris Saclay, pour son aide, ses conseils précieux et avec qui j'ai eu un grand plaisir à travailler ; Wadih Ghattas, Chargé de Recherche CNRS, pour sa gentillesse, son écoute et l'aide qu'il a pu m'apporter ; Laurent Salmon, Professeur de l'Université Paris Saclay pour ces bon conseils.*

*Merci également à tous les doctorants, post-doctorants et stagiaires avec lesquels j'ai eu plaisir à travailler : Charles Skarbek, Yoan Chevallier, Kalani Kariyawasam Bowithantri, Guillermo-alexandro Olivera-Udry, Antoine D'Alemand, Antoine Schlichter, Ivanna Amarsy, Benjamin Joyeux.*

*Enfin, je termine par un grand remerciement à mes parents, mes frères, mes sœurs et ma femme pour le soutien qu'ils m'apportent au quotidien, sans eux je n'en serais pas là aujourd'hui, je vous aime.*

Ce projet de développement de prodrogues antitumorales est à l'interface de la chimie, de la biologie et de la biophysique.

La conception, la synthèse et l'étude biologique des différents dérivés ont été réalisées dans le groupe du Dr Raphaël LABRUERE du laboratoire de Chimie Bioorganique et Bioinorganique de l'Institut de Chimie Moléculaire et des Matériaux d'Orsay. En particulier, les essais biologiques ont été réalisés par le Dr Charles SKARBK qui était chercheur associé post-doctoral dans le groupe. D'autre part, l'équipe du Pr Ludovic JULLIEN ainsi que le Dr Thomas LE SAUX du laboratoire PASTEUR de l'Ecole Normale Supérieure de Paris ont été impliqués dans l'analyse cinétique et les études de microscopie de fluorescence.

Un nombre important de thérapies utilisées contre le cancer ont une toxicité sur les cellules saines proche de celle observée sur les cellules cancéreuses. Il y a donc un besoin urgent de développer de nouvelles chimiothérapies. Pour répondre à cette problématique, il serait souhaitable de cibler spécifiquement les cellules cancéreuses afin de réduire la toxicité générale des molécules utilisées en clinique en exploitant les différences entre cellules saines et cellules cancéreuses. Une réponse rapide et adaptée réside dans le développement de prodrogues, des molécules à activité masquée, conçues pour être activées après une réaction enzymatique ou chimique. La stratégie des prodrogues peut non seulement améliorer l'efficacité du médicament mais aussi diminuer sa toxicité sur les organes ou tissus non ciblés. En général, il est nécessaire que la prodrogue soit activée par un stimulus spécifiquement produit par les cellules cancéreuses afin d'obtenir une libération du médicament dans l'environnement tumoral. Dans la majorité des cas, l'activation de ces prodrogues est réalisée par des enzymes fortement exprimées dans la tumeur.

Parmi les différentes voies métaboliques, l'activation des prodrogues antitumorales par les espèces réactives de l'oxygène (ROS) semble être particulièrement prometteuse. En effet, des études biologiques sur les tumeurs ont révélé que les cellules cancéreuses présentent un niveau de stress oxydatif plus élevé que les cellules saines. Ce stress oxydatif se traduit par la surproduction d'espèces réactives de l'oxygène dont le peroxyde d'hydrogène ( $H_2O_2$ ), le radical hydroxyle ( $HO\bullet$ ), l'anion superoxyde ( $O_2 \bullet^-$ ) ou le peroxyde d'azote ( $ONO_2^-$ ).

Les acides boroniques et leurs esters ont été développés comme groupes de masquage temporaire activés par les ROS. En particulier, il a été démontré que le peroxyde d'hydrogène et le peroxyde d'azote surproduits dans l'environnement tumoral réagissent sélectivement avec les acides et les esters boroniques par oxydation de la liaison carbone-bore pour donner un groupe alcool.

Le principal inconvénient de la stratégie typique des prodrogues antitumorales est la faible capacité de la partie temporaire à masquer l'activité pharmacologique du médicament lié de manière covalente. Cette situation nous a conduits à pousser à mener des recherches via cette thèse visant à développer une plateforme où le médicament antitumoral préexistant n'est pas inséré dans la structure de la prodrogue. La conception de la prodrogue repose plutôt sur un précurseur inactif à cycle ouvert capable de générer l'agent cytotoxique par cyclisation bioorthogonale dans le microenvironnement tumoral.

Ce manuscrit de thèse a été organisé en cinq chapitres en fonction des publications des résultats.

Le premier chapitre de ce manuscrit présente des généralités sur le cancer et les traitements actuels. La majeure partie de ce chapitre a été publiée dans *European Journal of Medicinal Chemistry*, 2020, 112670. Dans ce chapitre, nous avons rassemblé les prodrogues anticancéreuses contenant du bore et répondant au stress oxydatif du microenvironnement tumoral qui ont été rapportées dans la littérature.

Le deuxième chapitre de cette thèse annonce le projet de cette thèse et les principaux objectifs sont présentés ici.

Le troisième chapitre de ce manuscrit présente la preuve de concept de la nouvelle stratégie de prodrogue anticancéreuse. Ce chapitre est basé sur la première partie de notre publication dans *Angewandte Chemie International Edition*, 2021, 133, 45, 24245-24249. En utilisant la phénanthridine comme modèle de médicament, nous avons préparé un précurseur biaryle à cycle ouvert qui a généré la 6-méthylphénanthridine correspondante par imination bioorthogonale intramoléculaire. Cette réaction a été déclenchée par des espèces réactives de l'oxygène capables de convertir une fonction ester de vinylboronate en une cétone qui a ensuite réagi avec une aniline. Les cinétiques d'oxydation et de cyclisation ont été déterminées avec précision par une méthode de stopped flow combinée à la spectrofluorométrie.

Dans le quatrième chapitre de ce manuscrit, a été développée une voie originale de synthèse de diverses 6-méthylphénanthridines. L'identification d'un dérivé cytotoxique de la 6-méthylphénanthridine a été réalisée via la détermination de la viabilité des cellules cancéreuses KB 3.1. Le contenu de ce chapitre sera soumis pour publication prochainement.

Le dernier chapitre de ce manuscrit est basé sur la deuxième partie de notre publication dans *Angewandte Chemie International Edition*, 2021, 133, 45, 24245-24249. Dans ce chapitre, le précurseur biaryle ouvert de la 6-méthylphénanthridine cytotoxique sélectionnée a été synthétisé et trouvé inactif contre les sphéroïdes de KB 3.1. La stabilité de la prodrogue a été évaluée dans le plasma de rat et la cinétique d'oxydation et de cyclisation dans les sphéroïdes a été mesurée par épifluorescence. La cinétique de cyclisation de cette prodrogue a été trouvée extrêmement rapide (<10 ms) à l'intérieur de cellules vivantes de sphéroïdes de cancer KB.

Cette thèse se termine par une conclusion générale et une brève mise en perspective de ces résultats.

This project of antitumor prodrug development is at the interface of chemistry, biology and biophysics.

The design, synthesis and biological study of the different derivatives were carried out in the group of Dr Raphaël LABRUERE from the laboratoire de Chimie Bioorganique et Bioinorganique of the Institut de Chimie Moléculaire et des Matériaux d'Orsay. In particular, the biological assays were performed by Dr Charles SKARBEEK who was postdoctoral research associate in the group. On the other hand, the team of Pr Ludovic JULLIEN together with Dr Thomas LE SAUX from the laboratoire PASTEUR at Ecole Normale Supérieure in Paris were involved in the kinetic analysis and the fluorescence microscopy studies.

A significant number of therapies used against cancer have a toxicity against healthy cells close to that observed on cancer cells. There is therefore an urgent need to develop new chemotherapies. To address this issue, it would be desirable to specifically target cancer cells in order to reduce the general toxicity of molecules in clinical use by exploiting the differences between healthy and cancer cells. A rapid and adapted answer lies in the development of prodrugs, molecules with masked activity, designed to be activated after an enzymatic or a chemical reaction. The prodrug strategy can not only improve the efficacy of the drug but also decrease its toxicity on non-target organs or tissues. In general, it is necessary for the prodrug to be activated by a stimulus specifically made by the cancer cells in order to obtain a release of the drug within the tumor environment. In the majority of cases, the activation of these prodrugs is performed by enzymes highly expressed in the tumor.

Among the different metabolic pathways, the activation of antitumor prodrugs by reactive oxygen species (ROS) seems to be particularly promising. Indeed, biological studies of tumors have revealed that cancer cells exhibit a higher level of oxidative stress compared to healthy cells. This oxidative stress results in the overproduction of reactive oxygen species including hydrogen peroxide ( $\text{H}_2\text{O}_2$ ), hydroxyl radical ( $\text{HO}\bullet$ ), superoxide anion ( $\text{O}_2\bullet^-$ ) or peroxynitrite ( $\text{ONO}_2^-$ ).

Boronic acids and their esters were developed as temporary masking groups triggered by ROS. In particular, hydrogen peroxide and peroxynitrite overproduced within tumor environment were shown to react selectively with boronic acids and esters by oxidation of the carbon-boron bond to engender an alcohol group.

The main disadvantage of the typical antitumor prodrug strategy is the often weak ability of the temporary promoiety to extinguish the pharmacological activity of the covalently linked drug. This situation led us to motivate this PhD study aiming to develop a platform where the preexisting antitumor drug is not inserted in the structure of the prodrug. The design of the prodrug rather relies on an inactive ring-opened precursor able to generate the cytotoxic agent by internal bioorthogonal cyclization within a tumor microenvironment.

This PhD manuscript has been organized into five chapters driven by the publications of the results.

The first chapter of this manuscript introduces generalities on cancer and the current treatments. The major part of this chapter was published in *European Journal of Medicinal Chemistry*, 2020, 112670. In this chapter, we gathered the anticancer boron-containing prodrugs responsive to the oxidative stress from the tumor microenvironment which have been reported in the literature.

The second chapter of this dissertation announces the PhD project from the origin and the main goals are presented herein.

The third chapter of this manuscript introduces the proof of concept of the novel anticancer prodrug strategy. This chapter is based on the first part of our publication in *Angewandte Chemie International Edition*, 2021, 133, 45, 24245–24249. Using phenanthridine as drug model, we prepared a ring-opened

biaryl precursor that generated the corresponding 6-methylphenanthridine through intramolecular bioorthogonal imination. This reaction was triggered by reactive oxygen species able to convert a vinyl boronate ester function into a ketone that subsequently reacted with a pendant aniline. The kinetics of oxidation and cyclization were accurately determined by a method of stopped flow combined to spectrofluorometry.

In the fourth chapter of this manuscript, an original one pot synthetic pathway to various 6-methylphenanthridines was developed. Identification of a cytotoxic 6-methylphenanthridine derivate was achieved by determination of the KB 3.1 cancer cells viability. The content of this chapter will be submitted for publication in due course.

The last chapter of this manuscript is based on the second part of our publication in *Angewandte Chemie International Edition*, 2021, 133, 45, 24245–24249. In this chapter, the precursor of the selected cytotoxic 6-methylphenanthridine was then synthesized and found inactive against spheroids of KB 3.1. The stability of the prodrug have been assessed in rat plasma and the kinetic of oxidation and cyclization in spheroids have been measured by epifluorescence. The kinetics of cyclization of this prodrug was found extremely rapid (<10 ms) inside living cells of KB cancer spheroids

This dissertation ends with a general conclusion and a brief outlook of these results.



*« La réussite est la combinaison de la passion,  
l'effort et le sacrifice »*



<b>Abbreviation</b> .....	9
<b>Introduction</b> .....	14
<b>Chapter 1: Cancer treatments and the place of ROS-activated prodrugs</b> .....	16
1.1. Generality.....	17
1.2. Treatments to cure cancer.....	20
1.2.1. Surgery.....	20
1.2.2. Radiotherapy.....	21
1.2.3. Immunotherapy.....	22
1.2.4. Chemotherapy.....	22
1.2.4.1. Antimetabolite drugs.....	22
1.2.4.2. Alkylating agents.....	23
1.2.4.3. Antitumor antibiotics.....	24
1.2.4.4. Mitotic inhibitors.....	24
2. Tumor targeted chemotherapy.....	25
2.1. Active targeting of cancer cells.....	27
2.1.1. Tumor cell targeting.....	27
2.1.2. Antibody Drug Conjugates (ADCs).....	29
2.1.3. Small Molecule Drug Conjugates (SMDCs).....	32
2.2. Metabolic particularities of cancer cells and tumor microenvironment for specific activation of prodrugs.....	33
2.2.1. Drug release by enzymatic activation.....	33
2.2.2. Drug release by chemical activation.....	35
2.2.2.1. pH sensitive.....	35
2.2.2.2. Reducing environment (hypoxia sensitive prodrugs).....	37
2.2.2.3. Oxidizing environment (ROS sensitive prodrugs).....	38
3. Boronic acid /boronate Prodrugs.....	39

3.1. Small-molecule and macromolecular prodrugs.....	41
3.1.1. Precursors of selective estrogen receptor modulators (SERM).....	41
3.1.2. Precursor of epigenetic regulators.....	42
3.1.2.1. Histone deacetylase (HDAC) inhibitors.....	42
3.1.2.2. Lysine-specific histone demethylase inhibitor.....	43
3.1.3. Precursor of tyrosine kinase inhibitors.....	44
3.1.4. Precursors of antimetabolite drugs.....	45
3.1.5. Precursors of cytotoxic drugs.....	46
3.1.5.1. Camptothecin <b>21</b> .....	46
3.1.5.2. Doxorubicin <b>27</b> .....	48
3.1.5.3. Paclitaxel <b>31</b> .....	51
3.1.6. Precursor of nitric oxide.....	51
3.1.7. Precursors of DNA alkylating agents.....	52
3.1.7.1. Nitrogen mustards.....	52
3.1.7.2. Quinone methides as alkylating agents.....	54
3.1.8. Precursors of ROS/RNOS amplifier/accumulator for oxidation therapy .....	54
3.1.8.1. Aminoferrocene.....	54
3.1.8.2. Diethyldithiocarbamate <b>54</b> .....	59
3.1.8.3. Cinnamaldehyde <b>57</b> .....	60
3.1.8.4. Glucose oxidase.....	60
3.2. Pharmacological relevance.....	61
3.3. Conclusion.....	65
<b>Chapter 2:</b> Thesis project.....	66
<b>Chapter 3:</b> Preparation of the model biaryl precursor <b>ProPhen</b> and kinetics of transformation into the 6-methylphenanthridine <b>Phen</b> .....	72
1. Synthesis of biaryl precursor <b>ProPhen</b> .....	73

2. Cyclization analysis of <b>ProPhen</b> into <b>Phen</b> by <sup>1</sup> H NMR.....	77
3. Kinetic analysis of phenanthridine cyclization from open biaryl precursor.....	81
3.1. <b>ProPhen</b> oxidation and subsequent cyclization into <b>Phen</b> .....	83
3.2. Theoretical model.....	83
3.3. Experimental result.....	85
<b>Chapter 4: Preparation of 6-methylphenanthridines and identification of the cytotoxic ToxPhen</b> .....	88
1. Introduction.....	89
2. Synthesis.....	89
3. Cytotoxicity.....	93
<b>Chapter 5: Preparation of the biaryl precursor of <b>ToxPhen</b> and in-cell studies of cyclization</b> .....	96
1. Synthesis of <b>ProToxPhen</b> .....	97
2. Cytotoxicity experiments on KB 3.1 human cancer cells.....	98
2.1. In vitro cell-proliferation assays.....	98
3. Conformational analysis.....	100
4. Live-cell imaging experiments.....	100
5. Kinetic analysis of <b>ProToxPhen</b> conversion into <b>ToxPhen</b> within KB 3.1 spheroids by video microscopy.....	102
6. Plasma stability of <b>ProToxPhen</b> .....	108
<b>Conclusion and perspectives</b> .....	112
<b>Experimental part</b> .....	113
1. Biology.....	114
1.1. Cell culture.....	114
1.2. Cytotoxicity experiments on KB 3.1 human cancer cells.....	114
1.2.1. In vitro cell-proliferation assay (2D).....	114
1.2.2. In vitro 3D tumor spheroid viability assay.....	114

2. Photophysical analyses.....	115
2.1 UV-visible absorption.....	115
2.2 Epifluorescence spectroscopy.....	115
2.3 Epifluorescence Microscope .....	115
3. Chemistry .....	116
<b>Bibliography.....</b>	<b>146</b>
<b>Publications.....</b>	<b>160</b>



## Abbreviation

°C	Degrees Celsius
4T1	Breast cancer cell line
A2780	Ovarian carcinoma cell line
A2780cis	Ovarian carcinoma cisplatin resistant cell line
A549	Lung carcinoma cell line
ADC	Antibody-Drug Conjugate
ADMET	Absorption, distribution, metabolism, and excretion
AR42J	Rat pancreatic cancer
B <sub>2</sub> Pin <sub>2</sub>	Bis(pinacolato)diboron
Boc	<i>Tert</i> -Butoxycarbonyl
CD <sub>3</sub> CN	Acetonitrile- <i>d</i> <sub>3</sub>
BxPC3	Pancreatic cancer cell line
CA	Carbonic Anhydrase
CA4	Combretastatin A4
CAKI-1	Renal cancer cell line
CD <sub>3</sub> CN	Deuterated acetonitrile
CDCl <sub>3</sub>	Deuterated chloroform
ClSnMe <sub>3</sub>	Trimethyltin chloride
CuCl	Copper chloride
D <sub>2</sub> O	Deuterated water
DCM	Dichloromethane
DMP	Dess-Martin periodonane
DMSO	Dimethyl sulfoxide
DMSO- <i>d</i> <sub>6</sub>	Dimethyl sulfoxide- <i>d</i> <sub>6</sub>
DNA	Deoxyribonucleic acid
DU145	Prostate cancer cell line

ESI <sup>+</sup>	Electrospray ionization positive
Et <sub>3</sub> N	Triethylamine
Et <sub>2</sub> O	Diethyl ether
EtOAc	Ethyl acetate
FDA	Food and Drug Administration
H1993	Non-small cell lung cancer cell line
H2228	Non-small cell lung cancer cell line
H <sub>2</sub> O <sub>2</sub>	Hydrogen peroxide
HBr	Hydrobromic acid
HCT-15	Colon cancer cell line
HDAC	Histone Deacetylase
HDFa	Fibroblast cell line
HEK293	Human embryonic kidney cell line
HeLa	Cervical cancer cell line
Hep G2	Hepatocellular carcinoma
HET-CAM	Hen's Egg Test-Chorioallantoic Membrane
HL-60	Human leukemia cancer cell line
HL-60	Leukemia cell line
HOCl	Hypochlorous acid
HPLC	High-performance liquid chromatography
HR-MS	High-resolution mass spectrometry
HT-29	Colon cancer cell line
IARC	International Agency for Research on Cancer
IC <sub>50</sub>	Half maximal inhibitory concentration
ICI	Iodine monochloride
ICyBF <sub>4</sub>	1,3-bis(cyclohexyl)imidazolium tetrafluoroborate
INCa	Institut national du cancer

K	Degrees Kelvin
KB 3.1	Human papillomavirus endocervical adenocarcinoma cell line
L1210	Leukemia cell line
LC-MS	Liquid chromatography–mass spectrometry
MCF-7 MDR	Breast cancer cell line multidrug resistant
MCF-7	Breast adenocarcinoma cell line
MDA-MB-231	Breast adenocarcinoma cell line
MEC1	Immortalized mouse embryonic epicardial cell line
MeCN	Acetonitrile
MeOH	Methanol
MiaPaCa-2	Pancreatic cancer cell line
MM2	Molecular mechanic (Force field)
MRC5	Fibroblast cell line
MTX	Methotrexate
MV4-11	Leukemia cell line
<i>n</i> -BuLi	Butyllithium
NCI-H460	Lung cancer cell line
NIH/3T3	Fibroblast cell line
NOSs	Nitric oxide synthases
NPEC	Normal pancreatic cell line
ON	Over night
PBS	Phosphate-buffered saline
PC3	Human prostate cancer cell line
PCC	Pyridinium chlorochromate
PEG	Polyethylene glycol
PEG-NAM	Polyethylene glycol conjugated to niacin
pH	Potential of hydrogen

PMA	1-Phorbol-12-myristate-13-acetate
ppm	Parts-per-million
PSN1	Pancreatic cancer cell line
PTLC	Preparative thin layer chromatography
PTSA	<i>p</i> -toluenesulfonic acid
RNA	Ribonucleic acid
RNOS	Reactive nitrogen oxide species
ROS	Reactive oxygen species
rpm	Revolutions per minute
RT	Room temperature
RUMH	Non-small cell lung cancer cell line
SIN-1	3-morpholinopyrrolidine
SMDC	Small Molecule Drug Conjugate
SN12C	Renal cancer cell line
SN-38	7-Ethyl-10-hydroxycamptothecin
SOD	Superoxide dismutase
SR	Leukemia cell line
SW620	Colon cancer cell line
T47D	Breast cancer cell line
TBAF	Tetra- <i>N</i> -butylammonium fluoride
TBDMSCl	Tert-Butyldimethylsilyl chloride
<i>t</i> -BuLi	<i>Tert</i> -Butyllithium
<i>t</i> -BuONa	Sodium <i>tert</i> -butoxide
TLC	Thin layer chromatography
Tf <sub>2</sub> O	Trifluoromethanesulfonic anhydride
TMSOTf	Trimethylsilyl trifluoromethanesulfonate
U251	Glioblastoma cell line
U87MG	Glioblastoma cell line

U937

Leukemia cell line

WHO

World Health Organization

## Introduction

This project of antitumor prodrug development is at the interface of chemistry, biology and biophysics.

The design, synthesis and biological study of the different derivatives were carried out in the group of Dr Raphaël LABRUERE from the laboratoire de Chimie Bioorganique et Bioinorganique at the Institut de Chimie Moléculaire et des Matériaux d'Orsay. In particular, the biological assays were performed by Dr Charles SKARBEEK who was postdoctoral research associate in the group. On the other hand, the team of Pr Ludovic JULLIEN together with Dr Thomas LE SAUX from the laboratoire PASTEUR at Ecole Normale Supérieure in Paris were involved in the kinetic analysis and the fluorescence microscopy studies.

A significant number of therapies used against cancer have a toxicity against healthy cells close to that observed on cancer cells. There is therefore an urgent need to develop new chemotherapies. To address this issue, it would be desirable to specifically target cancer cells in order to reduce the general toxicity of molecules in clinical use by exploiting the differences between healthy and cancer cells. A rapid and adapted answer lies in the development of prodrugs, molecules with masked activity, designed to be activated after an enzymatic or a chemical reaction. The prodrug strategy can not only improve the efficacy of the drug but also decrease its toxicity on non-target organs or tissues. In general, it is necessary for the prodrug to be activated by a stimulus specifically made by the cancer cells in order to obtain a release of the drug within the tumor environment. In the majority of cases, the activation of these prodrugs is performed by enzymes highly expressed in the tumor.

Among the different metabolic pathways, the activation of antitumor prodrugs by reactive oxygen species (ROS) seems to be particularly promising. Indeed, biological studies of tumors have revealed that cancer cells exhibit a higher level of oxidative stress compared to healthy cells. This oxidative stress results in the overproduction of reactive oxygen species including hydrogen peroxide ( $\text{H}_2\text{O}_2$ ), hydroxyl radical ( $\text{HO}\cdot$ ), superoxide anion ( $\text{O}_2^{\cdot-}$ ) or peroxynitrite ( $\text{NO}_3^-$ ).

Boronic acids and their esters were developed as temporary masking groups triggered by ROS. In particular, hydrogen peroxide and peroxynitrite overproduced within tumor environment were shown to react selectively with boronic acids and esters by oxidation of the carbon-boron bond to engender an alcohol group.

The main disadvantage of the typical antitumor prodrug strategy is the often weak ability of the temporary promoiety to extinguish the pharmacological activity of the covalently linked drug.

This situation led us to motivate this PhD study aiming to develop a platform where the preexisting antitumor drug is not inserted in the structure of the prodrug. The design of the prodrug rather relies on an inactive ring-opened precursor able to generate the cytotoxic agent by internal bioorthogonal cyclization within a tumor microenvironment.

This PhD manuscript has been organized into five chapters driven by the publications of the results.

The first chapter of this manuscript introduces generalities on cancer and the current treatments. The major part of this chapter was published in *European Journal of Medicinal Chemistry*, 2020, 112670. In this chapter, we gathered the anticancer boron-containing prodrugs responsive to the oxidative stress from the tumor microenvironment which have been reported in the literature.

The second chapter of this dissertation announces the PhD project from the origin and the main goals are presented herein.

The third chapter of this manuscript introduces the proof of concept of the novel anticancer prodrug strategy. This chapter is based on the first part of our publication in *Angewandte Chemie International Edition*, 2021, 133, 45, 24245–24249. Using phenanthridine as drug model, we prepared a ring-opened biaryl precursor that generated the corresponding 6-methylphenanthridine through intramolecular bioorthogonal imination. This reaction was triggered by reactive oxygen species able to convert a vinyl boronate ester function into a ketone that subsequently reacted with a pendant aniline. The kinetics of oxidation and cyclization were accurately determined by a method of stopped flow combined to spectrofluorometry.

In the fourth chapter of this manuscript, an original one pot synthetic pathway to various 6-methylphenanthridines was developed. Identification of a cytotoxic 6-methylphenanthridine derivate was achieved by determination of the KB 3.1 cancer cells viability. The content of this chapter will be submitted for publication in due course.

The last chapter of this manuscript is based on the second part of our publication in *Angewandte Chemie International Edition*, 2021, 133, 45, 24245–24249. In this chapter, the precursor of the selected cytotoxic 6-methylphenanthridine was then synthesized and found inactive against spheroids of KB 3.1. The stability of the prodrug have been assessed in rat plasma and the kinetic of oxidation and cyclization in spheroids have been measured by epifluorescence. The kinetics of cyclization of this prodrug was found extremely rapid (< 10 ms) inside living cells of KB cancer spheroids

This dissertation ends with a general conclusion and a brief outlook of these results.

# **Chapter 1: Cancer treatments and the place of ROS-activated prodrugs**

## 1.1 Generality

Cancer is a generic term for a large group of diseases that can affect any part of the body.<sup>1</sup> Other terms used are malignant tumors and neoplasms. One defining feature of cancer is the rapid creation of abnormal cells that grow beyond their usual boundaries. Indeed, healthy cells develop, divide, and die according to a process written in their genetic material. Cancer cells, on the other hand, are the result of this cycle, thus escaping the mechanisms of regulation and control of cell proliferation by multiplying in an anarchic way, these cancerous cells will give birth to a tumor that will develop by invading and then destroy the organ from which it originated. Throughout the evolution of the pathology, cancer cells may detach from the tumor and may break away from the primary tumor, migrate through the bloodstream or lymphatic bloodstream and attach themselves and new organs to give rise to new tumors called metastases<sup>2</sup>.

Cancer is a major public health problem today due to the number of people affected (19 million per years) and the number of deaths (10 million per years). According to estimations from the World Health Organization (WHO) in 2020, cancer is the second leading cause of death before the age of 70. In 2018, the International Agency for Research on Cancer (IARC) estimated that: 1 in 5 men will develop cancer in their lifetime and 1 in 8 men will die from this disease; 1 in 6 women will develop cancer in their lifetime and 1 in 11 women will die from this disease (figure 1).<sup>3</sup>

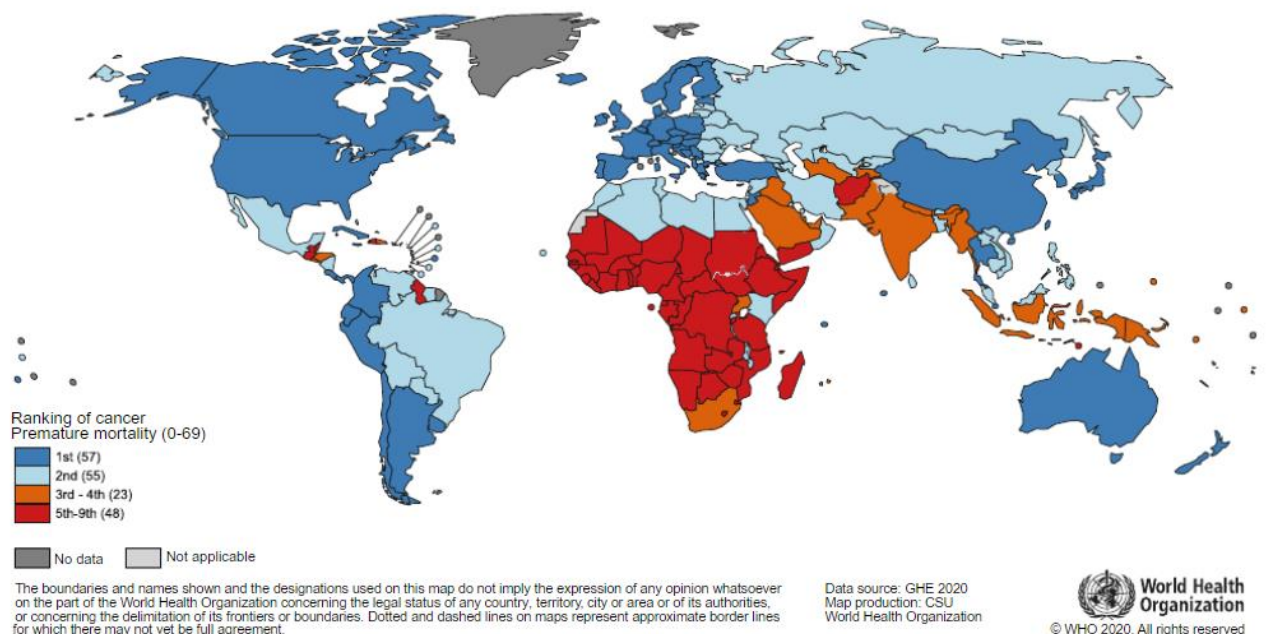
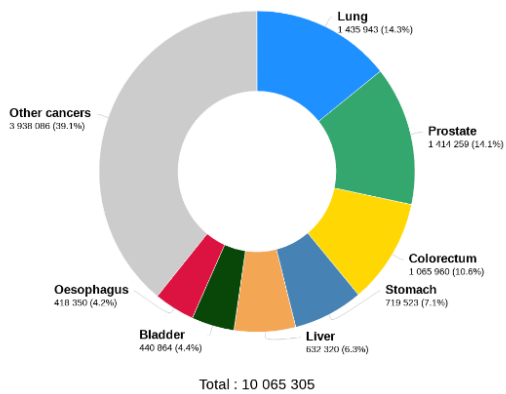


**Figure 1.** National ranking of cancer as a cause of death at ages below 70 in 2019.<sup>3</sup>

In men, the four most frequently encountered cancers are lung, prostate, colorectal and stomach cancers and the deadliest are lung, liver colorectal and stomach cancers. These four types of cancer represent more than 50% of worldwide men deaths (figure 2).<sup>3</sup>

Estimated number of new cases in 2020, worldwide, males, all ages



Estimated number of deaths in 2020, worldwide, males, all ages

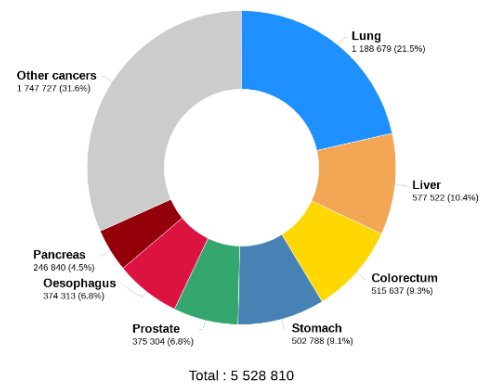
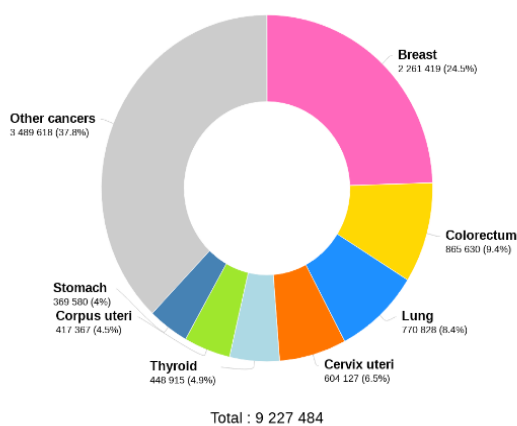


**Figure 2.** Estimated new cases and number of deaths (all age) in males.<sup>3</sup>

In women, the four most frequently encountered cancers are breast, colorectal, lung and cervix uteri cancers. The deadliest are breast, lung, colorectal and cervix uteri cancers. These 4 types of cancer represent around of 50% of worldwide deaths in females (figure 3).<sup>3</sup>

Estimated number of new cases in 2020, worldwide, females, all ages



Estimated number of deaths in 2020, worldwide, females, all ages

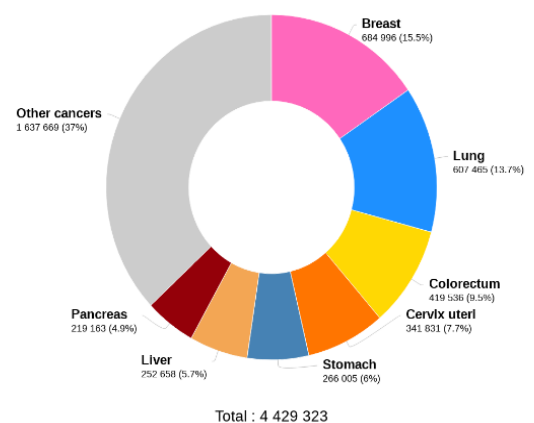


**Figure 3.** Estimated new cases and number of deaths (all age) in females.<sup>3</sup>

There are many different cancers with different causes for each cancer:

- Colorectal cancer is increasing in men and women between the ages of 40 and 50 due to poor diet, sedentary lifestyle, and obesity.
- Lung cancer in women has been increasing at a rate of 5.3% per year for the last 30 years. This is mainly due to women who started smoking in the 70's.
- Liver cancer is increasing in men and women due to obesity, alcohol consumption, tobacco and industrial food.
- Breast cancer increases in women under 40 years old, the main causes are alcohol, hormonal treatments (contraceptives or in case of menopause, delay of the age of the first pregnancy<sup>4</sup>, early puberty or decrease of breastfeeding duration).

According to the INCa, in 30 years there has been an increase in the number of cancers in the French population: +65% in men and + 93% in women.<sup>5</sup>

A part of this increase comes from the increase of the population. We are 8 million more in 2018 compared to 1990. Also, the population is older and therefore more at risk of cancer. If we remove this demographic effect, there remains an increase of 6% in men and 45% in women. This may be because life expectancy has increased and that diagnoses via screening campaigns and imaging techniques are more accurate and done earlier (figure 4).

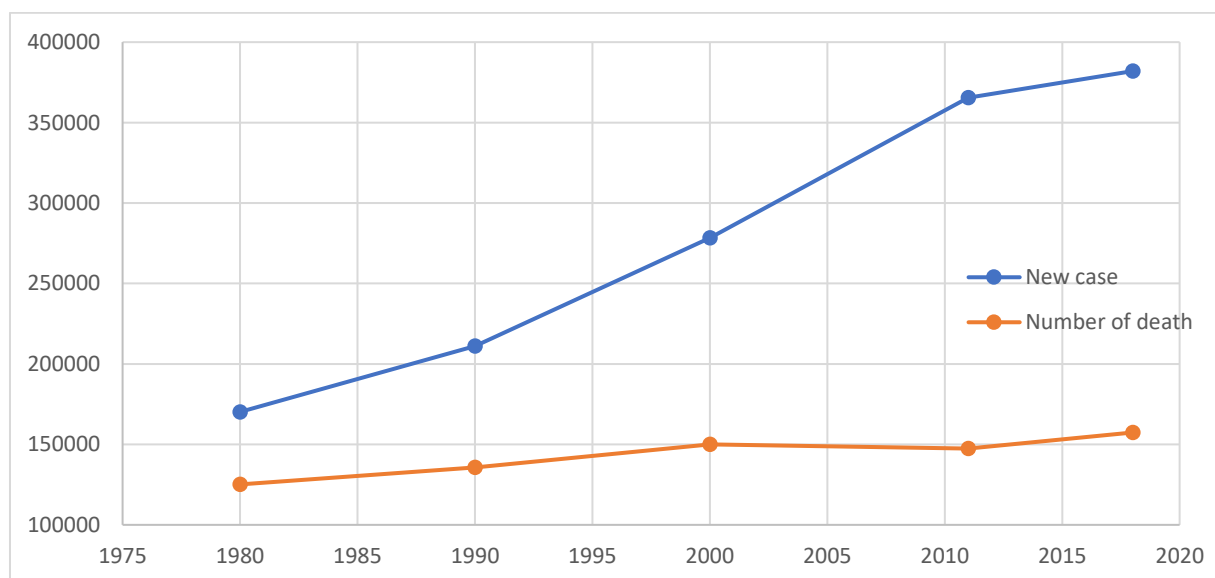


**Figure 4.** Evolution of the number of new cases and deaths due to cancer in France between 1980 and 2018.<sup>6</sup>

Despite the increase in incidence, the mortality of the population is decreasing thanks to earlier detection, earlier diagnosis, and better treatments. Most cancers have a preventable cause (alcohol, tobacco, industrial food...).

In 2011, the French health insurance system (sécurité sociale) spent 14.5 billion € on treating cancer patients. This equates to average expenditure of 10,000 € per patient per year.

## **1.2 Treatments to cure cancer**

Four different approaches coexist to cure cancer, these therapies can be used in combination depending on the type of cancer, its aggressiveness, size, location, and the patient's general condition.

### **1.2.1 Surgery**

The goal of curative surgical treatment of cancer is to remove the malignant tumor and local lymph nodes at a stage where the tumor has not yet metastasized. Surgical resection is said to be complete when all tumor tissue has been resected and the surgical margins are healthy.

In some very specific cancers, surgical treatment is indicated to reduce the tumor mass (debulking) in order to facilitate subsequent eradication of the tumor by chemotherapy and/or radiotherapy. It may also be indicated for the removal of a single metastasis in the liver, lung or brain.

In 2015, 447,391 hospitalizations for cancer surgery (including biopsies and removals of malignant, in situ or invasive tumors) were performed, up by 8.5% from 2010. This represents 8.3% of total hospital activity in oncology (figure 5).

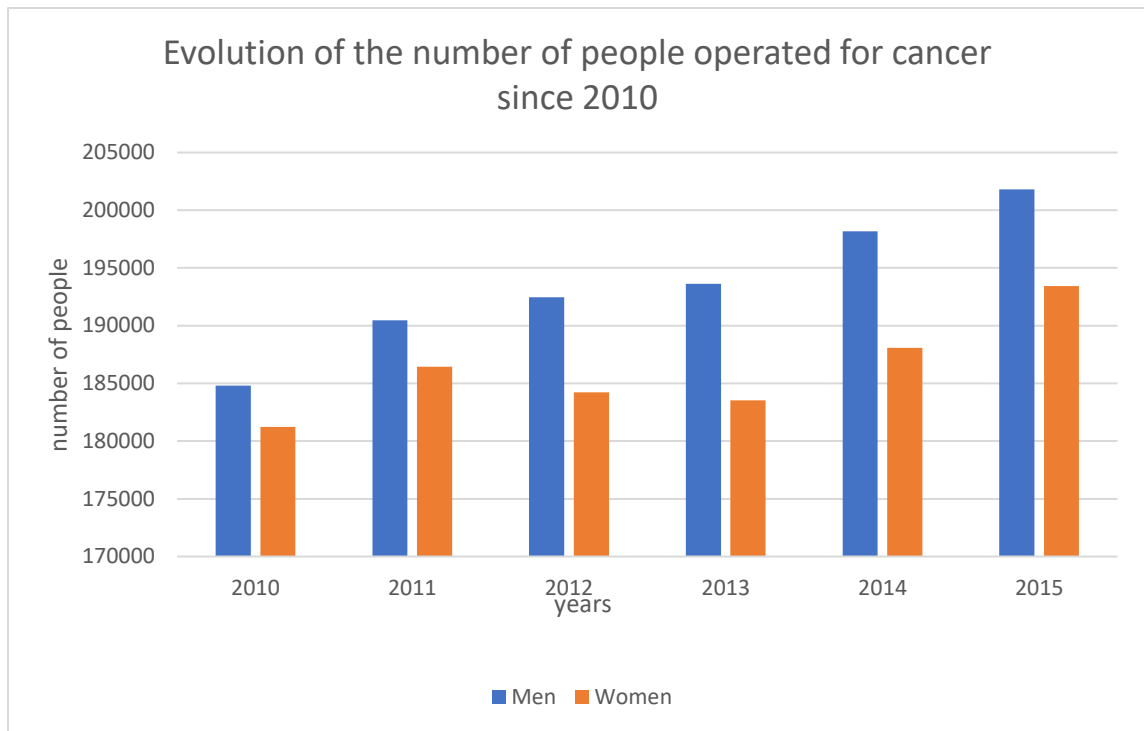


**Figure 5.** Evolution of the number of people operated for cancer since 2010.<sup>5</sup>

In France, in 2016, 408,276 people underwent surgery for cancer and 26.6% of stays were performed on an outpatient basis.

### 1.2.2 Radiotherapy

Radiotherapy is the use of radiation to destroy cancer cells by blocking their ability to multiply.<sup>7</sup> This is a local treatment for cancer. Different types of radiation (x-rays, gamma rays and particles) damage and destroy tumors and, can be combined with surgery or chemotherapy. The radiation can be external (teletherapy) or internal (brachytherapy). The goal of radiation is to destroy cancer cells while preserving healthy tissue and nearby organs as much as possible. More than half of all cancer patients are treated with radiation therapy at some point in their treatment. Radiotherapy may sometimes be combined with chemotherapy (called radiochemotherapy), which makes cancer cells more sensitive to radiation.<sup>8</sup> The goal is to reduce the risk of tumor recurrence and the size of the tumor before surgery. The length of the treatment, as well as the number of sessions, varies according to the area to be treated and the technique used.

### 1.2.3 Immunotherapy

Immunotherapy involves the body's own immune defenses to attack and destroy cancer cells.<sup>9</sup> Different approaches have been used for decades, but recently there has been a shift to a new and very promising strategy: targeting immune cells with drugs to break their tolerance to cancer cells and stimulate their destruction by the body. Immunotherapy is an effective treatment in 20 to 40% of patients. However, they are often accompanied by severe side effects related to the overactivation of the immune system, including the development of autoimmune diseases. These effects are explained by the fact that these therapies make our white blood cells very aggressive: they start to kill the patient's normal cells in addition to the tumor.

### 1.2.4 Chemotherapy

Chemotherapy is a treatment based on the administration of chemical substances and used in different types of cancer to destroy cancer cells.<sup>10</sup> There are many chemotherapy drugs with different mechanisms of action; in the treatment of cancer, these chemotherapy drugs can be used alone or in combination for better efficiency. Each drug differs in the way it works in the cell cycle. Most agents destroy cancer cells by affecting the synthesis or function of DNA during the cell's reproductive cycle or by interacting with RNA and proteins. Herein, only the cytotoxic agents, a major family of chemical drugs used in clinic will be discussed. There are 4 classes of cytotoxic agents.

#### 1.2.4.1 Antimetabolite drugs

The antimetabolites are divided into several subfamilies (table 1 and figure 6):<sup>11</sup>

Pyrimidine analogues	Purine analogues	Folic acid analogues	Other molecule
5-Fluorouracyl (5-FU)	Mercaptopurine	Methotrexate (MTX)	Sepacitabine
Gemcitabine	Cytrabine	Pralatrexate	

**Table 1.** Subfamilies of antimetabolites drugs.

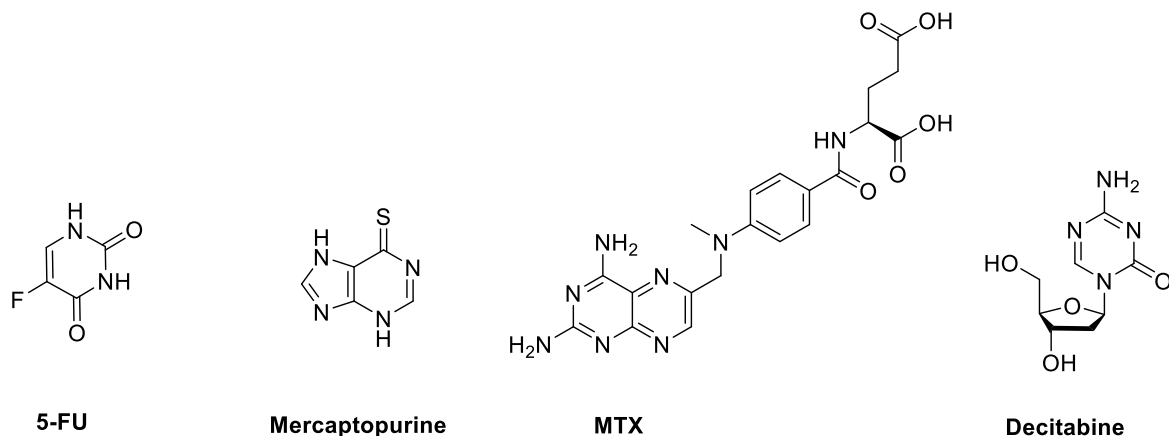


**Figure 6.** Structures of several antimetabolites drugs.

Antimetabolites can be used in the treatment of cancer because they interfere with DNA production and therefore with cell division and tumor growth because cancer cells divide more often than other cells, therefore inhibiting cell division will affect tumor cells more than other cells.

#### 1.2.4.2 Alkylating agents

The idea of using alkylating agents to treat cancer arose out of Edward Bell Krumbhaar, Indeed, Canadian soldiers who were victims of the combat gas (mustard gas) used in 1917 presented respiratory problems associated to disappearance of lymphocytes in the blood (lymphoid aplasia).<sup>12</sup>

Alkylating agents are able to link an alkyl group to the nitrogen atom (position 7) of guanine in DNA strands.<sup>13</sup> Cancer cells are more susceptible to DNA deterioration than normal cells and they proliferate faster and are therefore less able to correct mistakes made during the DNA replication. Alkylating agents are used to treat several cancers but present serious side effects on normal cells. This pharmacological class includes a very large number of substances and the most used are presented in figure 7.

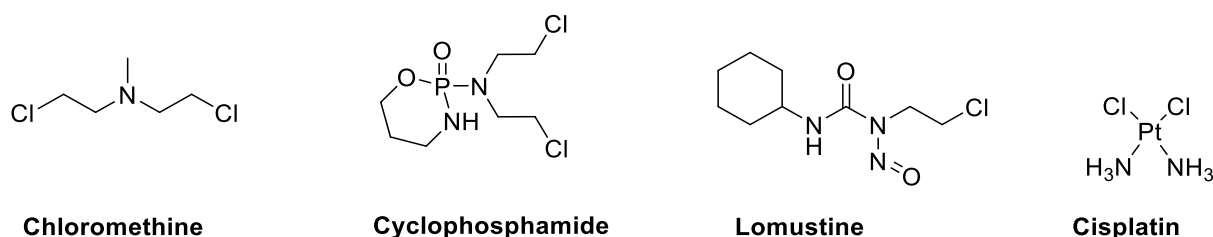


**Figure 7.** Structures of alkylating agent.

### 1.2.4.3 Antitumor antibiotics<sup>14</sup>

Topoisomerases are enzymes that cut and re-ligate a single strand of the DNA molecule. Their levels are much higher in tumor cells than in normal cells. They inhibit the re-ligation step of the two ends of the DNA strand, held by the enzyme, forming a complex at the DNA replication fork. They induce an arrest of cell division. These drugs act in synergy with platinum salts, alkylating drugs, ionizing radiation. The current products used in clinic are derivatives of camptothecin found in the ornamental plant *Camptotheca acuminata* found in China or doxorubicin which is a topoisomerase inhibitor and an intercalating agent produced by *Streptomyces* bacteria (figure 8).

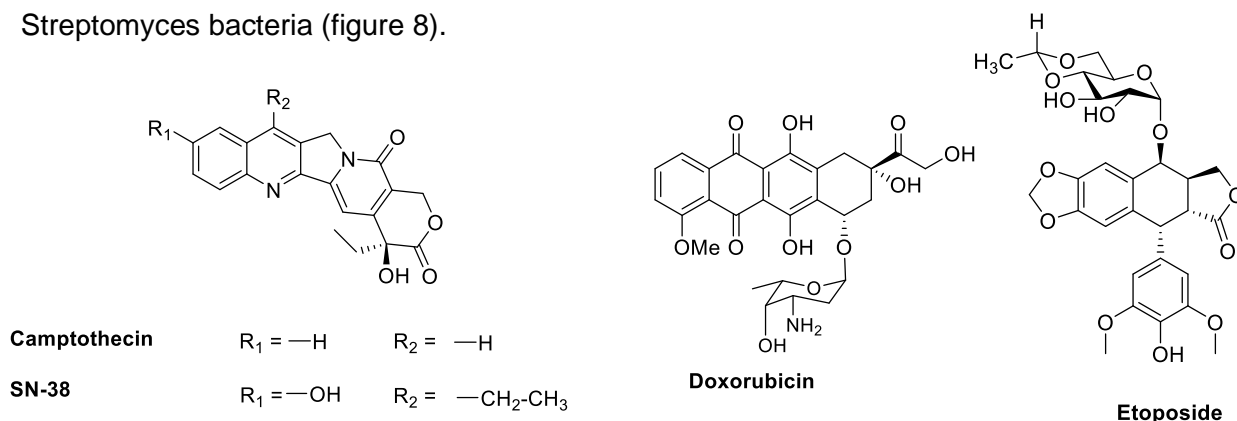


**Figure 8.** Structures of several antitumor antibiotics.

### 1.2.4.4 Mitotic inhibitors<sup>15</sup>

The common feature of spindle poisons is their binding to tubulin, which is part of the mitotic spindle and plays an important role in maintaining the cytoskeleton.<sup>15</sup> They disorganize the segregation of chromosomes at the time of mitosis and lead to the death of the cell. Several types of mitotic inhibitors can be distinguished according to their structure, their origin (often

natural) and their binding site on tubulin, resulting in various consequences on the microtubules.

- Periwinkle alkaloids or vinca alkaloids (vinblastine, vincristine, vindesine, vinorelbine, vinflunine) prevent microtubule polymerization and destabilize them.

- Taxanes (paclitaxel, derived from the Pacific yew *Taxus brevifolia*, docetaxel and cabazitaxel), on the other hand, are spindle stabilizers because they prevent spindle depolymerization and stimulate spindle polymerization.

- Dolastatin 10 is one of numerous potent cytotoxic natural products that have been isolated from the marine sea hare *Dolabella auricularia*. This drug has strong antiproliferative activity against murine PS leukemia cells by activating tubulin binding leading to lengthening cellular retention and is cytotoxic in vitro against several human cancer cell lines, such as melanoma, sarcoma, colorectal, and ovarian cancer.

These structures are represented in figure 9.

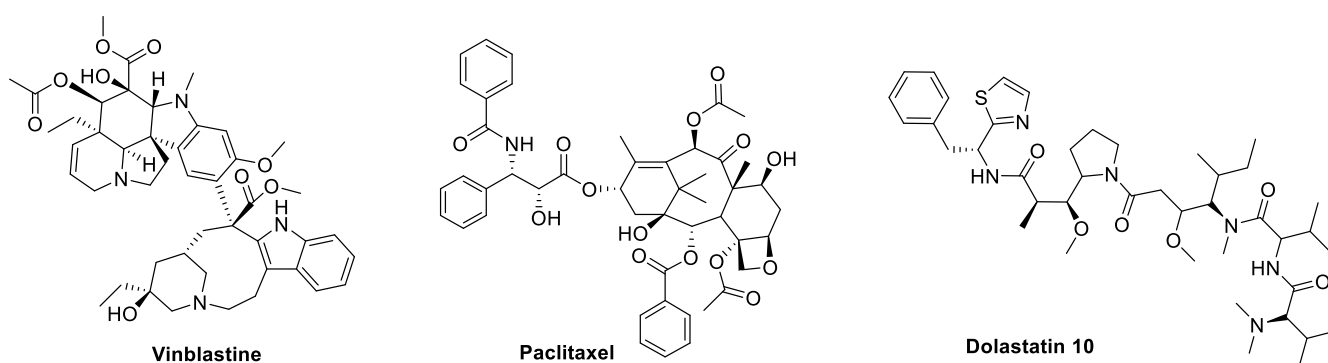


**Figure 9.** Structures of mitotic inhibitor drugs.

Overall, most clinically approved anticancer drugs are characterized by a narrow therapeutic window that results mainly from a high systemic toxicity of the drugs in combination with an evident lack of tumor selectivity.

## 2. Tumor targeted chemotherapy

The main problem of the cytotoxic agents is often their lack of cancer cells selectivity. When the drug is injected in the body, it diffuses within the body and operates in the tumor area to kill cancer cells, but normal cells are also damaged which generates many side effects like swelling, vomiting, nausea, hair loss etc. Thus, there is an urgent need for the development of

new and specific chemotherapies, capable of exploiting the differences between normal and tumor cells to increase the potency and decrease the dose and side effects (figure 10).

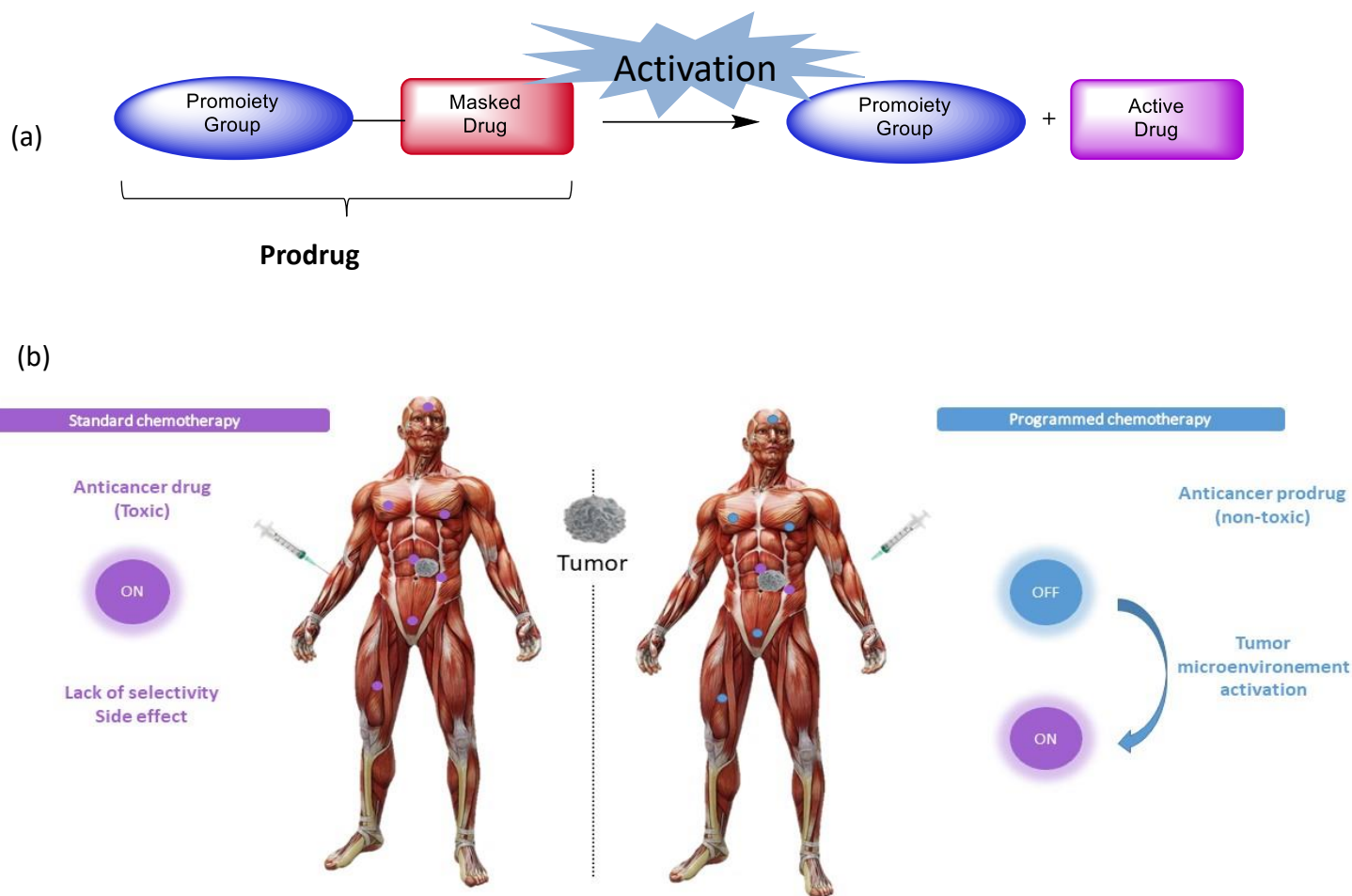


**Figure 10.** (a) General structure of a prodrug; (b) activation of the prodrug in the tumor area.

The prodrug strategy was initially introduced by Albert in 1958.<sup>16</sup> Prodrugs are activity-masked molecules designed to be activated *in vivo* by an enzymatic or a chemical reaction. In most cases, these molecules are covalent assemblies made of the active drug linked to a temporary moiety (figure 10a). The latter chemical unit confers new physicochemical properties to the entire entity optimizing its absorption, distribution, metabolism, excretion and toxicity (ADMET).<sup>17–19</sup> The prodrug strategy used in anticancer chemotherapy intends to deliver the active drug only at the tumor site in order to avoid deleterious side effects on normal tissues. This approach ideally ensures a high selectivity against targets and low toxicity, since drugs are liberated specifically at the tumor area, generally by enzymes strongly overexpressed at

the tumor site, by reactive oxygen species (ROS) or by hypoxia. Furthermore, the prodrug tactic remains faster and less expensive than the development of novel therapeutic agents with appropriate drug-like characteristics.<sup>20-22</sup>

The development of an antitumor prodrug mainly depends on 3 factors:

- **Tumor targeting:** It is important to distinguish the tumor specificity of cancerous tissue from healthy tissue in order to accumulate anticancer drug selectively and efficiently at the tumor site. The exploited targets used are found either in cancer cells or in the tumor microenvironment.
- **Controlled release:** The release of the active ingredient should take place only when in contact with the tumor area to avoid uncontrolled release of the drug throughout the body. Therefore, it is essential that the prodrug would be completely stable in the body and only breaks down under the stimulus associated to cancer cells via chemical or enzymatic release processes. In addition, the kinetics of activation of the prodrug and release of the active ingredient must be rapid to act specifically on cancer cells and not on healthy cells through diffusion.
- **Difference in activity between the prodrug and the drug:** The chemical grafting of an organic temporary group to a given drug is sometimes not sufficient to mask its pharmacological activity. It is therefore important to control that the biological inactivation of the prodrug is achieved.

## 2.1 Active targeting of cancer cells

### 2.1.1 Tumor cell targeting

Drug delivery in oncology is of particular interest owing to the narrow therapeutic window of anticancer agents. Cancer cells expressed on their surface particular receptors and antigens as shown in table 2. Medicinal chemists have therefore developed prodrugs composed of an antibody or a ligand coupled to an anticancer agent allowing targeting of cancer cells via ligand-receptor or antibody-antigen interactions. Cell surface targets can be classified as internalizing and non-internalizing systems. In non-internalizing systems, the drug conjugate has to be cleaved extracellularly, whereas in internalizing systems cleavage should occur intracellularly after endocytosis.<sup>23</sup>

	Receptors	Antigens
Vascular Receptors	Integrin ( $\alpha_v\beta_3$ , $\alpha_v\beta_5$ ) Nucleolin Aminopeptidase N Endoglin Vascular endothelial growth factor receptor (VEGF 1-4)	Cluster of differentiation (e.g CD20, CD33) Carcinoembryonic antigen Blood group carbohydrates Mucin type glycoproteins (MUC1, CanAg) Lewis Y, Lewis X Cancertesis antigens (CT7, MAGE-A3) Prostate-specific membrane antigen
Plasma proteine receptors	Low-density lipoprotein receptor	
Peptide receptors	Transferrin receptor Somatostatin receptor Bombesin receptor Neuropeptide Y receptors	
Receptors for growth factors and vitamins	Luteinizing-hormone-releasing-hormone receptor Folate receptors (FR- $\alpha$ , FR- $\beta$ , FR- $\gamma$ ) Epidermal growth factor receptors (e.g. EGF1, EGF2, Her2) Transforming growth factor receptor Fibroblast growth factor receptors	
Carbohydrate receptors	Asialoglycoprotein receptor Galectins (e.g. galectin 1, galectin 3) Selectins (e.g. E-selectin, P-selectin) Hyaluronic acid receptors (CD44, RHAMM, HACRLEC)	

**Table 2.** Examples of membrane-associated targets for prodrug therapy.<sup>23</sup>

Targeting the membrane receptors on the different type of cancers cells is a promising approach. This strategy is quite selective and may be tailored to a wide range of tumors by modulating the ligand or antibody in addition to the nature of the cytotoxic agent.

### **2.1.2 Antibody Drug Conjugates (ADCs)**

Many ADCs have been developed in the last 10 years (figure 11).

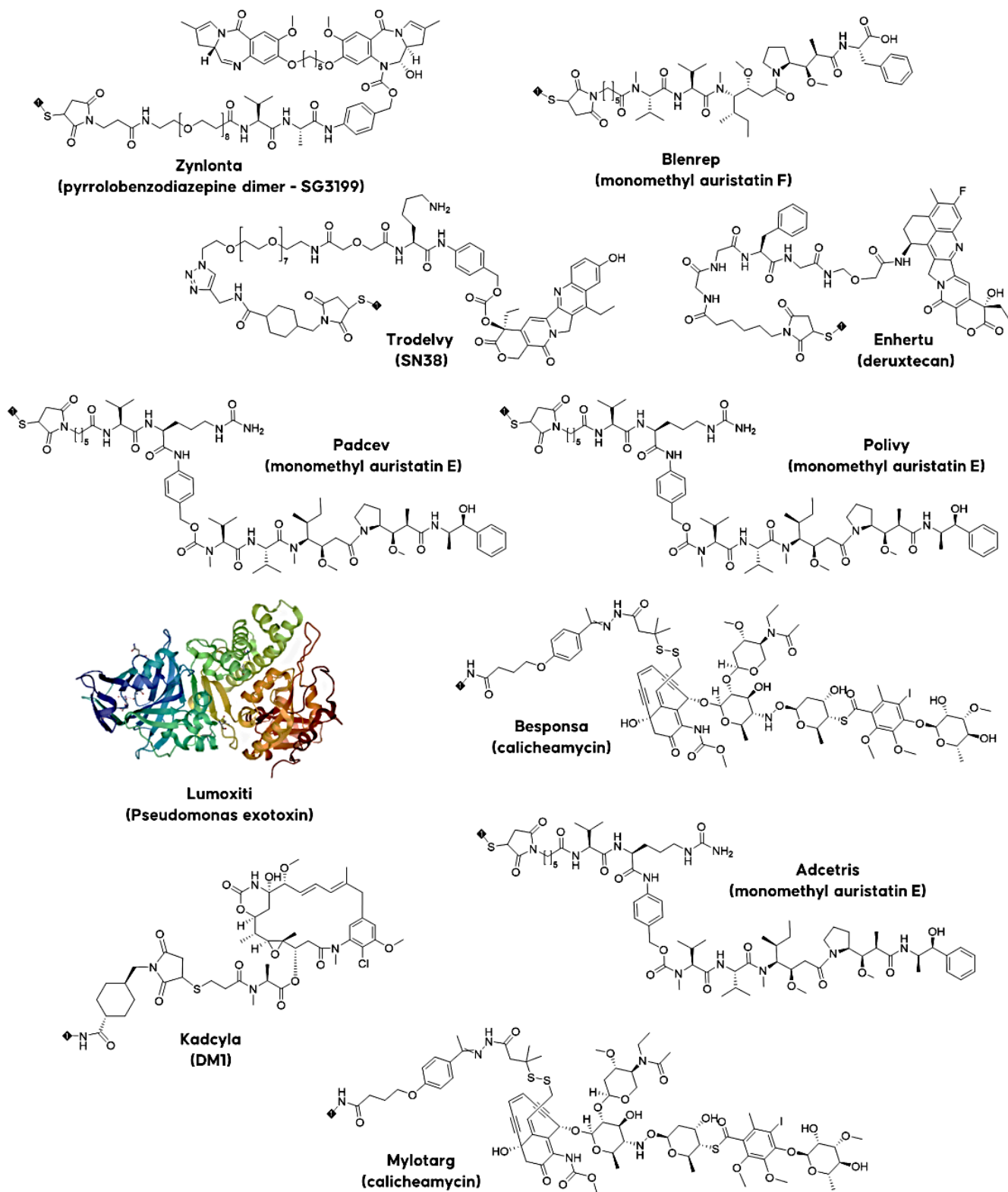


**Figure 11.** List of linker-payloads used in approved antibody-drug conjugates (as of September 2021).<sup>24</sup>

In 2009, only gemtuzumab ozogamicin, Mylotarg® (figure 12) was used clinically (approved by the US FDA in 2000, withdrawn in 2010 and approved again in 2017).<sup>25,26</sup> More than 80 others are currently in clinical trials.

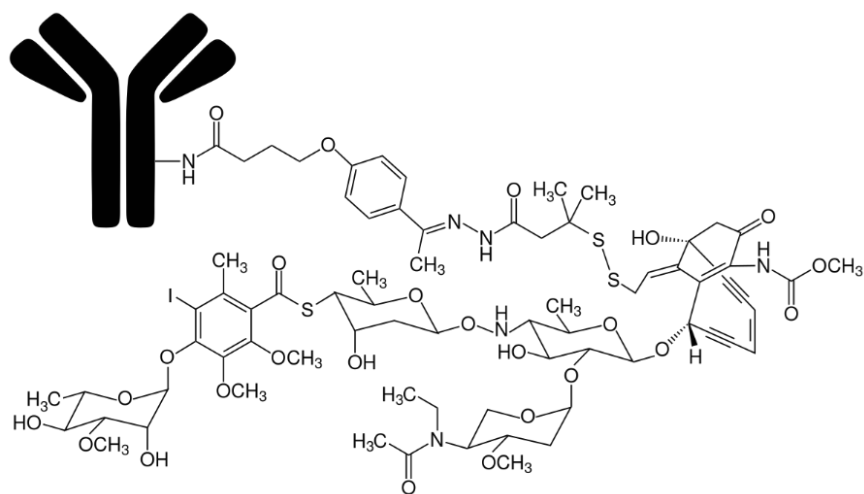
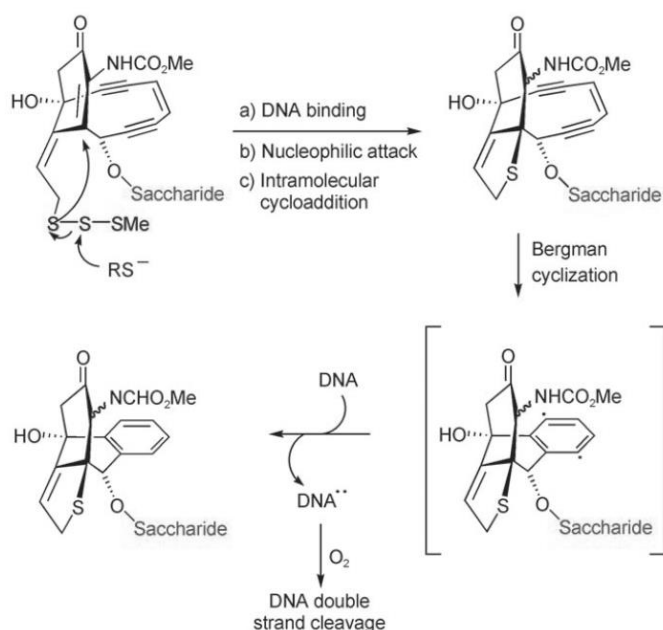


**Figure 12.** Structure of Mylotarg®.

Mylotarg® is an anti-CD33 humanized monoclonal antibody conjugated to calicheamicin. It represents an interesting option for patients over 60 years old with acute myelogenous leukemia.<sup>26</sup>

The potent DNA damaging agent calicheamicin was conjugated to a humanized monoclonal antibody that specifically binds to the CD33 cell surface antigen on acute myeloid leukemia cells. After internalization of the conjugate into the cancer cell by endocytosis, the drug is released by hydrolysis of the hydrazone bond in the acidic endosomes/lysosomes, the enediyne is then activated by reduction of the trisulfide bond (scheme 1).



**Scheme 1.** DNA-cleaving mechanism of calicheamicin  $\gamma 1$ .

After DNA binding, the trisulfide part is reduced by a thiol (e.g. glutathione) followed by intramolecular Michael addition of the thiolate to the adjacent  $\alpha,\beta$ -unsaturated ketone leading to the loss of the bridgehead double bond. The enediyne moiety thus cyclize by Bergman cyclization reaction to generate a diradical, which abstracts a hydrogen from DNA resulting in DNA cleavage.<sup>27</sup>

### 2.1.3 Small Molecule Drug Conjugates (SMDCs)

In lieu of an antibody or other macromolecules, the ligand-based prodrugs are made of the covalent assembly of a small molecule and a cytotoxic agent.<sup>28</sup> As observed for ADCs, the SMDC binds to the targeted receptor and the ligand-receptor is subsequently taken up by receptor-mediated endocytosis. Typical ligands are vitamins, peptides, or sugars. Folic acid is one of the mostly employed ligand for active tumor targeting. Interestingly, it was shown that folic acid conjugated to various drugs still present high affinity<sup>29–33</sup> for the overexpressed folate receptor of cancer cells.<sup>34–38</sup> Thus folate conjugated to camptothecin, doxorubicin, alkylating agents, platinum complexes, paclitaxel and 5-FU were studied.<sup>38–43</sup>

EC145, a conjugate of the Vinca alkaloid desacetylvinblastine monohydrazone coupled to folic acid was introduced by Leamon et al.<sup>45,46</sup> and evaluated in clinical phase I. The peptidic linker improved the water solubility of the conjugate whereas the disulfide bond was inserted in order to allow the drug release by reaction with glutathione in the endosomes. In vivo preclinical studies have shown that EC145 is better tolerated than the free drug in mice and moreover antitumor efficacy was stronger when using the conjugate (figure 13).

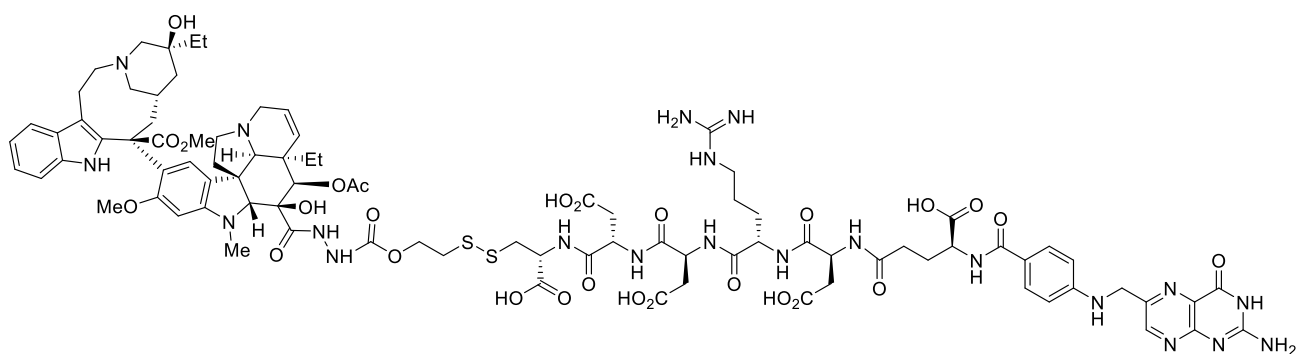


**Figure 13.** Structure of the folate–vinblastine prodrug EC145, containing desacetylvinblastine monohydrazide DAVLBH.

## 2.2 Metabolic particularities of cancer cells and tumor microenvironment for specific activation of prodrugs

Cancer cells are markedly different to cells from healthy tissues. In addition, the tumor microenvironment includes blood vessels, immune cells, fibroblasts, signaling molecules, such as chemokines, and the extracellular matrix displaying biochemical particularities. The biologic singularities of cancer cells and tumor microenvironment are therefore exploited in anticancer prodrug strategy in order to localize the delivery of the active drug at the tumor site. Abnormalities of the tumor environment has led to distinct strategies in cancer-responsive prodrug research. First, certain enzymes such as cathepsins are overexpressed in cancer cells and specific prodrugs were developed to target this characteristic.<sup>47–49</sup> Prodrugs capitalizing on the hypoxia of cancer cells inside solid tumors are also the object of intensive research.<sup>50–52</sup> Antitumor targeted-prodrugs responsive to the pronounced oxidative stress in cancer cells have been recently developed.<sup>53,54</sup>

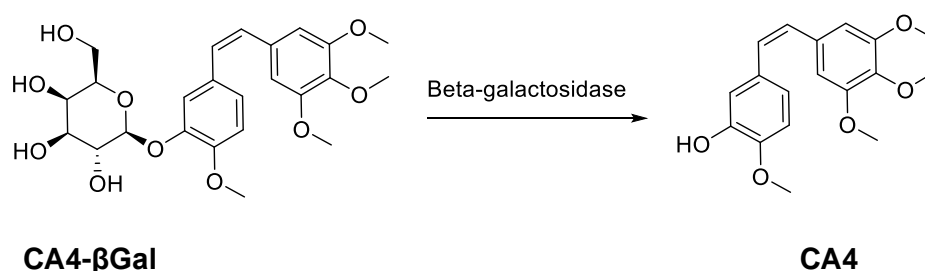
### 2.2.1 Drug release by enzymatic activation

The enzyme allowing activation of the prodrug must be naturally expressed or overexpressed in tumor cells. Activation of a prodrug can be carried out by tumor-associated enzymes such as proteases, glucuronidase, or carboxylesterases, which are expressed either intra- or extracellularly by cancer cells. Therefore, the use of a substrate recognized by the enzymatic site is an approach for tumor targeting. In the past, a great number of carrier-linked prodrugs have been developed with enzyme-specific substrates such as peptides or sugars. An overview of enzymes overexpressed by tumors and examples for respective substrates is given in table 3.

Enzymes	Functions	Substrate examples
Cathepsin B (EC 3.4.22.1) Cathepsin H (EC 3.4.22.16) Cathepsin L (EC 3.4.22.15)	Lysosomal degradation of proteins	Arg-Arg, Leu, Ala-Leu, Gly-Leu-Phe-Gly, Gly-Phe-Leu-Gly,Ala-Leu-Ala-Leu
Cathepsin D (EC 3.4.23.5)	Degradation of extracellular matrix	Phe-Ala-Ala-Phe(NO <sub>2</sub> )-Phe-Val-Leu-OM4P, Bz-Arg-Gly-Phe-Phe-Pro-4MβNA
Plasmin (EC 3.4.21.7)	Fibrinolysis, degradation of blood plasma proteins	D-Val-Leu-Lys,D-Ala-Phe-Lys,D-Ala-Trp-Lys
uPA (EC 3.4.21.73) tPA (EC 3.4.21.68)	Activation of plasmin formation	Gly-Gly-Gly-Arg-Arg Arg-Val
Prostate-specific antigen [PSA (EC 3.4.21.77)]	Liquefecation of semen	Mu-His-Ser-Ser-Lys-Leu-Gln-Leu, L-377,202
Matrix metalloproteases [MMP-2 (EC 3.4.24.24), MMP-9 (EC 3.4.24.35)]	Degradation of extracellular matrix and collagens	Ac-Pro-Leu-Gly-Leu, Ac-γE-Pro-Cit-Gly-Hof-Tyr-Leu, Gly-Pro-Leu-Gly-Ile-Ala-Gly-Gln
β-Gluconuronidase (EC3.2.1.31)	Hydrolysis of glucuronide moiety from proteins	Glucuronide moiety
Carboxylesterases [CES1/CES2 (EC 3.1.1.1)]	Hydrolysis or transesterification of drug xenobiotics	Ester or carbamate moieties

**Table 3.** Overview of enzymes that are overexpressed in tumors.

As shown in scheme 2, the Suzuki group developed a β-galactosidase-responsive prodrug composed of a galactose linked to the cytotoxic and antivasular Combretastatin A4 (CA4).<sup>55</sup>



**Scheme 2.** β-Galactosidase-responsive prodrug of CA4.

## **2.2.2 Drug release by chemical activation**

The various chemical activation processes exploited over the last few decades are based on the reactivity of certain functional groups in acidic pH ( $\approx 6.5-6.8$ )<sup>56</sup>, reducing environment (hypoxia) or oxidizing environment (ROS) characterizing cancer cells/tumors. Chemically activatable prodrugs must remain stable and inert under the physiological conditions encountered in healthy tissues.

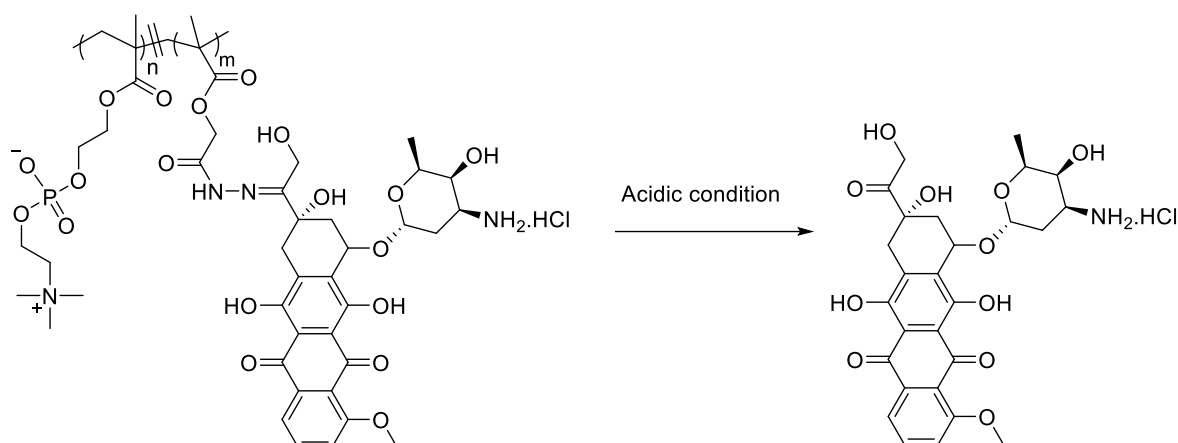
### **2.2.2.1 pH sensitive**

Acidic extracellular pH is a major feature of tumor tissue; extracellular acidification is considered to occur in the presence of lactic acid, which accumulates due to anaerobic glycolysis in hypoxic cancer cells; pentose phosphate pathway produces  $\text{CO}_2$ , which is then oxidized by the enzyme carbonic anhydrase (CA) leading to the increase of the proton concentration. An overview of pH sensitive linkers used in anticancer prodrug development is given in table 4.<sup>57</sup>

Linkers	Chemical structures	Therapeutics agents
Acetal		Diethylstilboestrol Doxorubicin
Ester		Bortezomib Doxorubicin
Hydrazone		Cisplatin Doxorubicin
Imine		Geldanamycin Gemcitabine Chromone Doxorubicin
Othoester		Paclitaxel
Oxime		Daunorubicin Doxorubicin Oligonucleotide
Phosphoramidate		Oligonucleotide
Vinyl ether		Oligonucleotide
$\beta$ -Thiopropionate		Oligonucleotide

**Table 4.** Overview of pH-sensitive linkers used in anticancer prodrug development.<sup>57</sup>

A pH-sensitive prodrug of doxorubicin was prepared by Chen et al.<sup>58</sup> The ability of the prodrug to release the cytotoxic in a weakly acidic medium was confirmed. Using in vitro cytotoxicity studies, it was shown that the pH-sensitive doxorubicin prodrug was able to accumulate in cancer tissues, therefore reducing nonspecific cytotoxicity associated with systemic administration of the free doxorubicin (scheme 3).<sup>58</sup>



**Scheme 3.** pH-Sensitive prodrug of doxorubicin.

### 2.2.2.2 Reducing environment (hypoxia sensitive prodrug)

Hypoxia corresponds to the situation of low concentration of oxygen in tissue in comparison with appropriate oxygen supply.<sup>59</sup> In solid tumors, hypoxia is essentially observed in the center of a tumor mass (100 - 150  $\mu\text{m}$ ) and gradually decrease with the distance to the oxygen supplying blood vessels (figure 14). This lack of oxygen resulting from reduced blood supply to the surrounding tissue is a common characteristic of solid tumors because of rapid cell growth.

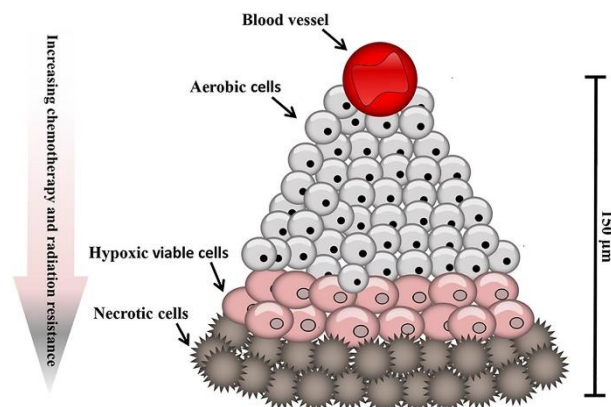
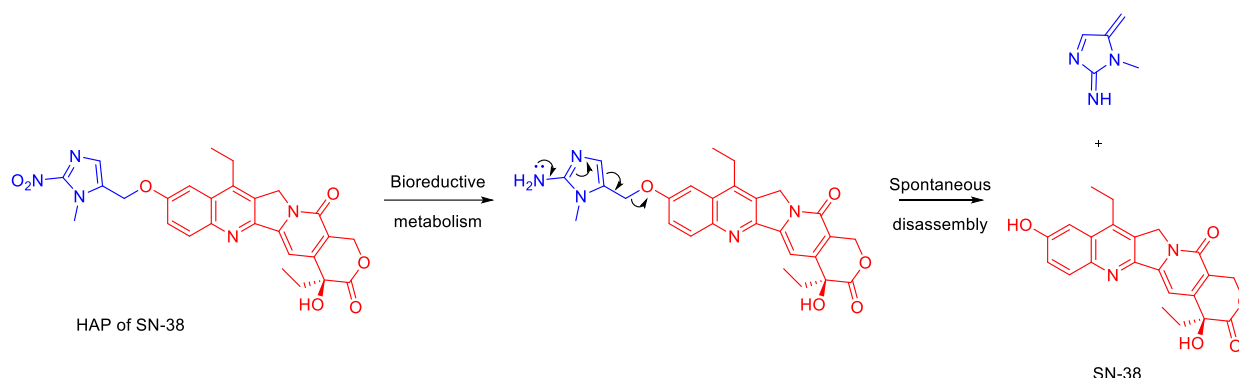


**Figure 14.** Hypoxia in a solid tumor.

Hypoxia in tumors is a predictor of both resistance to chemotherapy and of a metastatic/aggressive form of cancer, and as a result, development of cancer therapies which target hypoxia is of great importance. The strategy of hypoxia-activated prodrugs (HAPs) was then developed for the release of chemotherapeutic agents within hypoxic tumor regions. This targeting strategy is accomplished by attaching a hypoxia activated trigger (quinones, *N*-oxides, nitro-substituted aromatics and derivatives with a disulfide bridge) to a chemotherapeutic agent. Jin et al.<sup>60</sup> have prepared a hypoxia-activated prodrug of SN-38 by

conjugating a 2-nitroimidazol nucleus with SN-38 (scheme 4). This prodrug was designed to be activated by nitro reduction under hypoxia condition to release the drug in the tumor.



**Scheme 4.** Hypoxia-activated prodrug (HAP) of SN-38.

### 2.2.2.3 Oxidizing environment (ROS sensitive prodrug)

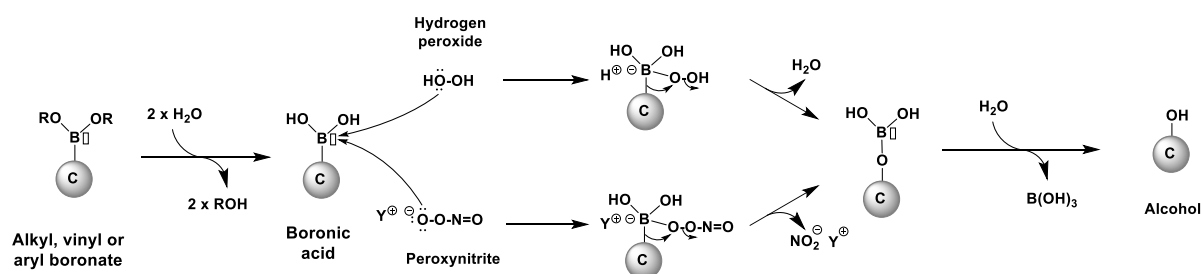
Biological studies of tumors have revealed that cancer cells have a higher degree of oxidative stress compared to healthy cells.<sup>61</sup> This stress is produced by deregulated and enhanced mitochondrial functions and cellular metabolism. Oxidative stress stimulates the tumor progression processes such as cell proliferation and angiogenesis. Cancer cells migration and neovascularization will ultimately lead to the dissemination and growth of cancer cells in metastatic sites. Macrophages have been described to promote the generation of oxidative stress of cancer cells through the secretion of molecular mediators.<sup>62</sup> These immune cells are primarily present around the tumor cells in order to eradicate them by both phagocytosis and production of oxygen-containing reactive molecules. Nonetheless, they will indirectly contribute to cancer progression.<sup>63</sup> These cellular events provide an increase of the oxygenated reactive molecules level in the tumor microenvironment.

These highly reactive molecules are composed of reactive oxygen species (ROS) and reactive nitrogen oxide species (RNOS).<sup>61</sup> Among ROS, superoxide anion ( $O_2^{\cdot-}$ ) is engendered from  $O_2$  via NADPH oxidase action and mitochondrial metabolism.  $O_2^{\cdot-}$  is subsequently converted to hydrogen peroxide ( $H_2O_2$ ) by superoxide dismutase (SOD) catalysis.  $H_2O_2$  further evolves into hypochlorous acid (HOCl) and hydroxyl radical ( $HO\cdot$ ). Among RNOS, nitric oxide ( $NO\cdot$ ) is produced by reaction of molecular oxygen and L-arginine catalyzed by nitric oxide synthases (NOSs).  $NO\cdot$  spontaneously reacts with  $O_2^{\cdot-}$  to form peroxynitrite/peroxinitrous acid ( $ONOO^-$  /  $ONOOH$ ). The latter species is unstable and generate hydroxyl radical and nitrogen dioxide radical ( $NO_2\cdot$ ).

Boronic acid (and ester) prodrugs targeting the overexpressed level of reactive oxygen species within tumor microenvironment represent a promising area for the discovery of new selective anticancer chemotherapy. This strategy that emerged only ten years ago is exponentially growing and could demonstrate its clinical usefulness in the near future. Herein, the previously described small-molecule and macromolecular anticancer prodrugs activated by carbon-boron oxidation are gathered. This chapter reports on the most interesting derivatives mentioned in the literature based on the *in vitro* and *in vivo* activity when available. Eventually, the pharmacological applicability of this strategy is discussed, in particular, the kinetic aspect of the prodrug oxidation and the selectivity of this reaction towards certain ROS from the tumor microenvironment are specified.

### 3. Boronic acid /boronate prodrugs

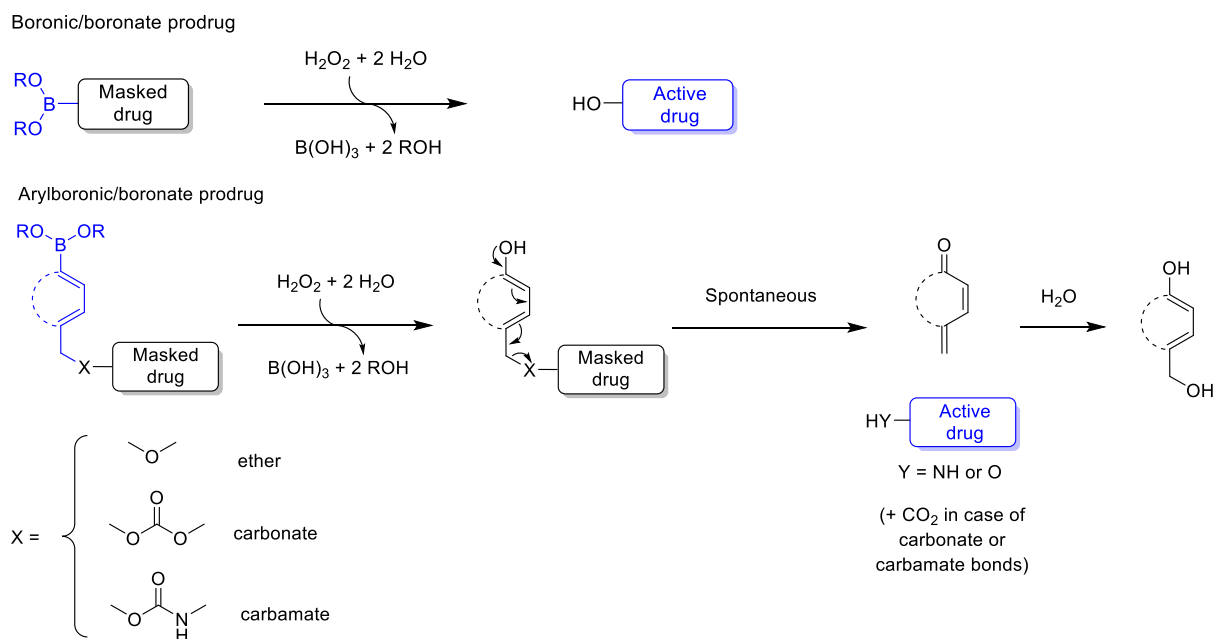
Boronic acids and their corresponding esters have been developed as temporary masking groups for drugs or probes specifically triggered by oxygen-containing reactive molecules.<sup>64–68</sup> In biological aqueous media, boronate esters are rapidly hydrolyzed into boronic acid.<sup>69</sup> Among the different reactive species, hydrogen peroxide, hypochlorite anion ( $\text{ClO}^-$ ) and peroxynitrite were shown to react with boronic acids and esters to further oxidize the carbon-boron bond to form an alcohol group.<sup>70</sup> In biological conditions, hypochlorite anion will almost exclusively react with cellular amines and thiols since the latter reactions will be faster than the oxidation of carbon-boron bonds. Nucleophilic oxygen of the reactive species will be able to attack the empty p orbital of the boron atom (scheme 5).<sup>71,72</sup> Carbon migration to oxygen further gives a borate that will be hydrolyzed to afford the corresponding alcohol and non-toxic boric acid.<sup>73</sup> At physiological pH, conversion by peroxynitrite is  $10^6$  times faster than the hydrogen peroxide-mediated oxidation likely due to the anionic form of peroxynitrite in comparison to neutral  $\text{H}_2\text{O}_2$ .<sup>70</sup>



**Scheme 5.** Mechanism of boronic acid oxidation into alcohol by either hydrogen peroxide or peroxynitrite.

The boronic/boronates functionalities were used as temporary moieties to either mask aliphatic alcohols,<sup>70,74</sup> enols<sup>75,76</sup> or aryl-alcohols.<sup>64,68</sup> The active effector can be connected to the

boronic/boronate groups directly or via self-immolative spacers.<sup>77,78</sup> The use of these spacers allows the bounding of different effectors through either their alcohol or amine functions generating ether, carbonate or carbamate bonds. The volume added by the spacer to the final entity contributes to a better masking of the biological activity. Oxidation of such spacer lead to the formation of an aryl-alcohol motif that will undergo spontaneous elimination leading to the release of an effector (scheme 6).



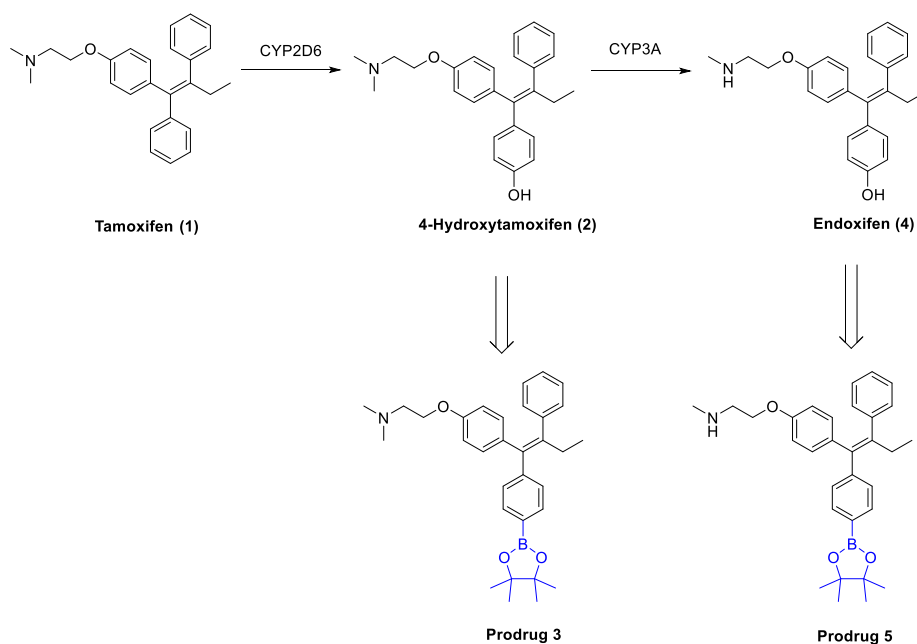
**Scheme 6.** Release of the active drug from boron-containing prodrug by either direct C-B bond oxidation or by oxidation and subsequent self-immolative process.

The strategy of boronic acid/boronate oxidation has been widely used for the emergence of many probes for tumor imaging and/or prodrugs with tumor targeting properties leading to the release of the parent drug. Herein, we comprehensively review the ROS responsive boronate prodrugs that were developed and evaluated as anticancer agents. In the next section, we gathered the different platforms used to construct the prodrug of interest: a majority of small molecules were found but a non-negligible amount of drug delivery-based polymeric matrix and nanoparticles were also described.

### 3.1 Small-molecule and macromolecular prodrugs

#### 3.1.1 Precursors of selective estrogen receptor modulators (SERM)

The selective estrogen receptor modulators have been developed to treat breast cancer tumors presenting the estrogen receptor.<sup>79</sup> Antiestrogens, such as tamoxifen **1**, bind to the hormone receptor and block the proliferation of the cancer cells. Moreover, tamoxifen **1** is a prodrug converted to both 4-hydroxytamoxifen **2** and endoxifen **4** by cytochrome P450 enzymes. The Wang group has therefore synthesized and evaluated boron-based prodrugs of 4-hydroxytamoxifen **2** and endoxifen **4** as potential anticancer agents (scheme 7).<sup>80-82</sup>



**Scheme 7.** Structures of 4-hydroxytamoxifen and endoxifen (oxidative metabolites of tamoxifen) and their prodrugs.

This strategy is indeed meaningful since these two active metabolites would be similarly obtained by oxidative cleavage of the boronic acid function of **3** and **5** in the tumor environment. In vitro cytotoxic activity of **3** and **5** was determined against MCF-7 and T47D, two breast cancer cell lines expressing the estrogen receptor. The prodrug **3** and its active metabolite 4-hydroxytamoxifen **2** were as active against a given cell line. 80% conversion of prodrug **3** to 4-hydroxytamoxifen **2** was observed in cell culture media and the cellular uptake of **3** was 4 times higher than 4-hydroxytamoxifen **2** in MCF-7 culture. Comparable in vitro observations were made for the prodrug/drug couple: **5**/endoxifen **4**. Growth inhibition of MCF-7 cancer xenografts in mice was similar for the prodrug **5** and the active metabolite endoxifen **4** at the optimal dose of 1 mg/kg. Metabolism and pharmacokinetic studies in mice showed that the

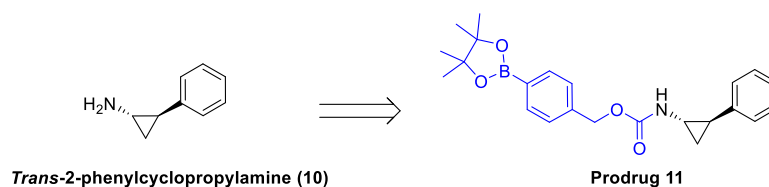


vorinostat **6** was determined in vitro and showed a partial recovery (~ 20%) of the drug activity after incubation.

Furthermore, Wang and colleagues prepared a prodrug **9** made of a benzene boronate nucleus branched to the hydroxamic acid moiety of belinostat **8** for the chemotherapy of solid tumors.<sup>85</sup> Belinostat **8** and **9** were tested in vitro against four cancer cell lines: A549 (lung carcinoma), HeLa (cervical cancer) and, MDA-MB-231 and MCF-7 (breast adenocarcinoma). Again, around 25% of the parent drug activity was recovered after incubation except for the MCF-7 cells where prodrug **9** displayed only 5% of the corresponding drug activity. Conversion of the prodrug **9** into belinostat **8** in MDA-MB-231 culture cell media was ~ 10% after 24h of incubation. The HDAC inhibitory activity of the prodrug **9** was then measured and was ten times lower than that of belinostat **8**. Altogether, these observations account for the noticeable difference of cancer cells viability between the drug and the prodrug. In vivo activity of prodrug **9** was compared to belinostat **8** in a MCF-7 xenograft model in mice at the dose of 10 mg/kg/day, a slight increase of efficacy was observed for **9** toward the free drug. The belinostat **8** concentration was twice higher in tumor tissue after prodrug **9** subcutaneous injection in contrast with the same injected dose of the parent drug. The higher efficacy of the prodrug is explained by the increased bioavailability of the benzene boronate precursor **9**. The plasmatic concentration in mice was quantified for both belinostat **8** and its prodrug **9**: 10 mg/kg were independently injected and after 3h, the concentration of belinostat **8** was 7-fold higher when using the prodrug **9**.<sup>87</sup> Moreover, study of **9** metabolism in liver S9 fraction clearly brought to light the role of the enzymatic metabolism (via cytochrome P450) in the conversion of the boronic acid function into the corresponding phenol leading to belinostat **8** through self-immolation.

### 3.1.2.2 Lysine-specific histone demethylase inhibitor

Among histone post-translational modifications, lysine methylation of histone governs the structure of chromatin and the methylation degree of histones is involved in cancer formation.<sup>88</sup> Lysine-specific histone demethylase inhibitor are not currently used in clinic but these molecules are studied for the development of anticancer epigenetic drugs. Engel et al.<sup>89</sup> have prepared a benzene boronate prodrug **11** of the promising histone demethylase inhibitor *trans*-2-phenylcyclopropylamine **10** (scheme 9).

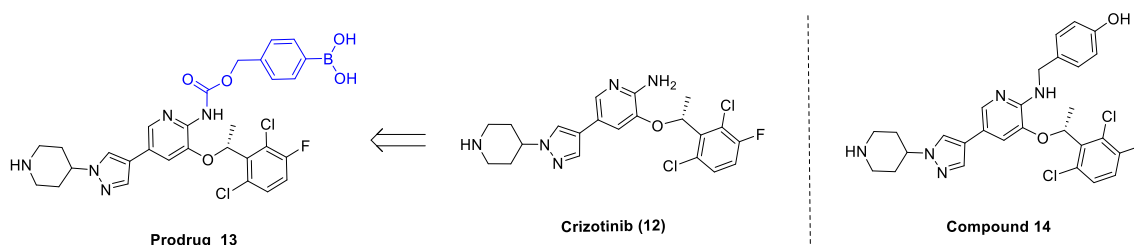


**Scheme 9.** Prodrug of *trans*-2-phenylcyclopropylamine.

Prodrug **11** was tested *in vitro* against glioblastoma U87 cells and primary glioblastoma cells, and healthy astrocytes. No activity was observed up to 300  $\mu\text{M}$  on healthy astrocytes while primary glioblastoma and U87 cells were impacted at 10  $\mu\text{M}$  and 1  $\mu\text{M}$  respectively. The authors also showed the impact of the quinone methide (formed from the benzene boronate promoiety) which reacts covalently with glutathione in cells reducing the intracellular concentration of this antioxidant (*vide infra*).

### 3.1.3 Precursor of tyrosine kinase inhibitors

Crizotinib **12** is a tyrosine kinase inhibitor developed to treat non-small cell lung cancers.<sup>90</sup> This drug however presents important side effects such as hepatotoxicity and neutropenia. These drawbacks prompted the Kowol group to prepare a benzene boronate prodrug **13** of this molecule in an attempt to selectively reach the cancer cells (scheme 10).<sup>90</sup>



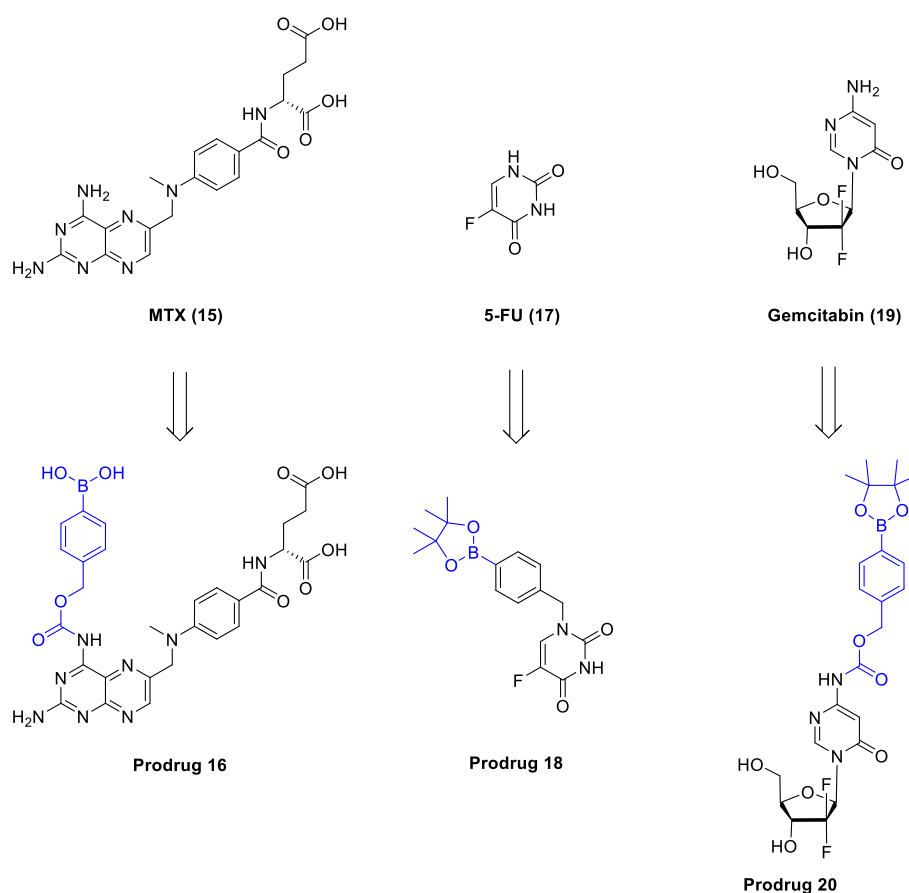
**Scheme 10.** Benzyloxycarbonyl prodrug of crizotinib and non-immolated metabolite **14**.

Three non-small cell lung cancer cell lines (H1993, RUMH and H2228) known to respond to crizotinib **12** were evaluated toward their production of ROS by flow cytometry using 2',7'-dichlorofluorescein diacetate. The *in vitro* ROS production of the H1993 cells was found to be twice as much as the two other cell lines. *In vitro* cytotoxicity assays showed that approximately 50% of free crizotinib **12** ( $\text{IC}_{50} \sim 3\text{-}15 \mu\text{M}$ ) activity was found with the prodrug **13**. Addition of  $\text{H}_2\text{O}_2$  prior to incubation with the different cell lines completely restored the activity of the original drug, except when in contact with H1993 cells where the activity remains surprisingly lower. The authors also observed that a stable non-immolated metabolite **14**, a *p*-

hydroxybenzyl adduct of crizotinib was as active as the free drug against all the tested cell lines pointing out that benzyl moiety is not sufficient to mask the drug activity in this case.

### 3.1.4 Precursors of antimetabolite drugs

Methotrexate (MTX) **15**, a potent inhibitor of the dihydrofolate reductase implied in the purine and pyrimidine synthesis, is used in clinic to treat cancer and autoimmune diseases. The Clausen group has described several benzene boronate prodrugs of methotrexate **15** originally developed for the treatment of rheumatoid arthritis (Scheme 11).<sup>91,92</sup>



**Scheme 11.** Prodrugs of MTX, 5-FU and gemcitabin.

Recently, the *in vitro* activity of the prodrug **16** (scheme 11) was reported on HL-60 (human leukemia cancer cell line), HeLa cancer cell line and HEK293 (human embryonic kidney cell line).<sup>47</sup> The HL-60 cells were shown to produce around ten times more ROS *in vitro* than of the HEK293 cells. However, prodrug **16** displayed close *in vitro* activity against the two latter cell lines ( $IC_{50} \sim 0.05 \mu M$ ), a growth inhibition decreased by a factor 2-4 in comparison with the free methotrexate **15**.

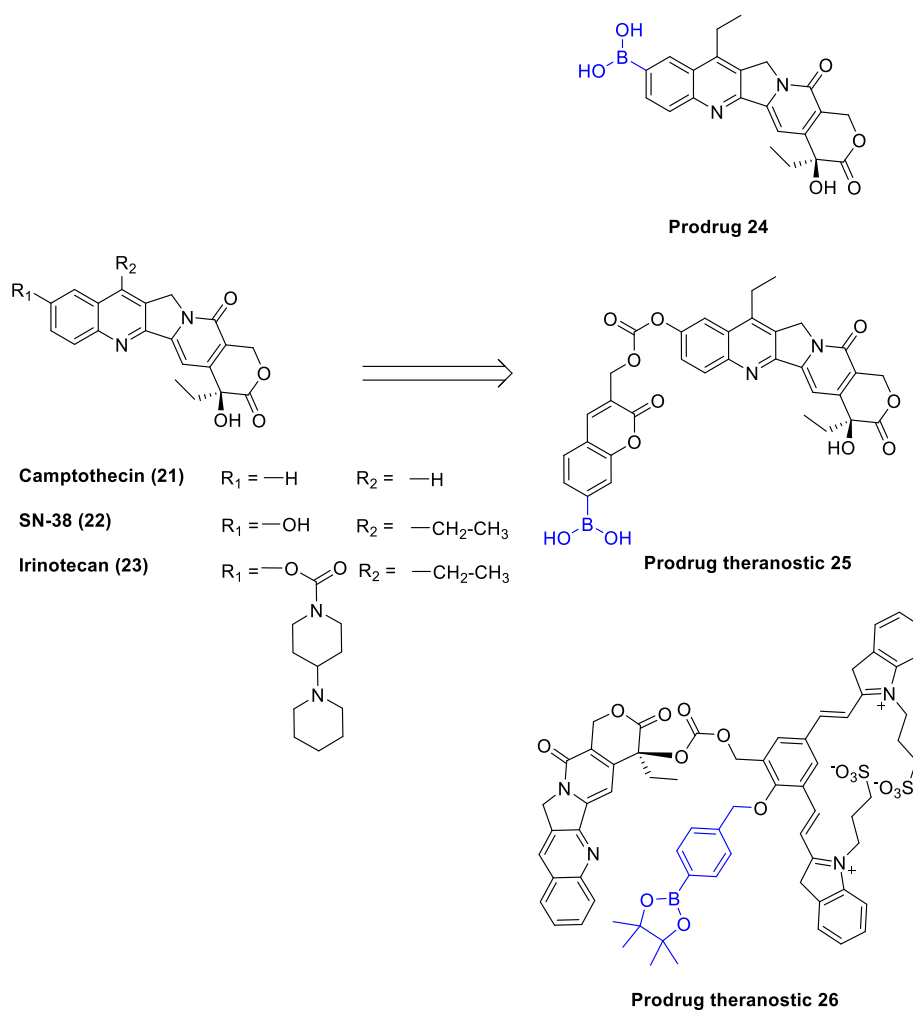
The antimetabolite 5-fluorouracil (5-FU) **17**, a widely used antitumor drug, presents several side effects such as myelosuppression and neurotoxicity. In order to reduce these drawbacks, the Xue group has developed the benzene boronate prodrug of 5-fluorouracil (scheme 11).<sup>93</sup> Boronate prodrug **18** and its corresponding boronic acid were tested in vitro against the 60 cancer cell lines from the National Cancer Institute. Prodrug **18** was more active against all cell lines than its boronic acid counterpart which is quite surprising since boronate esters are hydrolyzed into boronic acid in aqueous media (vide supra). Then, the authors particularly compared breast cancer cells MCF-7 to immortalized mouse embryonic epicardial cells MEC1. 5-Fluorouracil **17** was cytotoxic against two cell lines with an  $IC_{50}$  around 1  $\mu$ M whereas **18** had no effect against MEC1 up to a concentration of 100  $\mu$ M and was slightly active on the MCF-7 cancer cells ( $IC_{50}$  = 10-50  $\mu$ M). Aside from that, prodrug **18** showed a better drug safety profile than 5-fluorouracil **17** on wild-type C57BL/6 male mice.

Another nucleotide analog used in clinic, gemcitabin **19**, was linked to a benzene boronate moiety to build the prodrug **20** (scheme 11).<sup>94</sup> Gemcitabin **19** and prodrug **20** were evaluated in vitro against pancreatic cell lines: cancerous (PSN1 and BxPC3) and normal (NPEC). The  $H_2O_2$  level produced by each cell line was measured using the ROS-Glo™ assay which demonstrated a weakly higher production of ROS by the cancer cells. Gemcitabin **19** displayed an  $IC_{50}$  of 0.005-0.015  $\mu$ M against the three cell lines and prodrug **20** was around 20 times less active in each case. Nonetheless, prodrug **20** was able to retrieve the activity of gemcitabin **19** when ROS were artificially produced by the cancer cell lines via preliminary addition of 2-deoxy-D-glucose. In vivo activity was determined using PSN1 xenograft model in mice and showed a similar activity of both gemcitabin **19** and prodrug **20**. However, myelosuppression was lowered in mice treated with the prodrug **20** and the authors showed that concentration of the resulting gemcitabin **19** in bone marrow was reduced in comparison with the gemcitabin-treated group.

### 3.1.5 Precursors of cytotoxic drugs

#### 3.1.5.1 Camptothecin 21

Camptothecin **21** is a strongly cytotoxic natural product as a result of its topoisomerase I inhibitory activity. The 10-hydroxycamptothecin known as SN-38 **22**, is the toxic hydrolytic metabolite of the commercialized prodrug irinotecan **23**.<sup>95</sup> Thus, Lei et al.<sup>96</sup> prepared the oxidative prodrug **24** of SN-38 **22** by replacing the original phenol group into a boronic acid function (scheme 12).



**Scheme 12.** Prodrugs of camptothecin.

Prodrug **24** and the corresponding active metabolite SN-38 **22** were tested *in vitro* against six cancer cell lines: colon cancer cells HCT-15 and HT-29, breast cancer cells MCF-7 and MDA-MB-231 and, glioblastoma cells U87MG and U251. The activity of SN-38 **22** was fully restored upon incubation of **24** with the different cell lines ( $IC_{50}$  ranging from 0.01 to 5  $\mu M$ ). The authors observed that the conversion of **24** into SN-38 **22** in MCF-7 culture cell media was around 40% after 48h of incubation. Moreover, the topoisomerase I inhibitory evaluation of **24** showed that the boronic acid derivative was as potent as SN-38 **22**. These two latter observations therefore account for the good *in vitro* activity of **24** against this panel of cancer cells. Prodrug **24** was evaluated *in vivo* using U87MG cancer xenograft in mice and displayed a modest efficacy at 2 mg/kg in comparison with the reference irinotecan **23** (antitumor effect of 8% T/C with irinotecan vs. 28% T/C with **24**).

Theranostic boronate-based prodrugs of camptothecin were also prepared. In cancer chemotherapy, this approach combining therapy and diagnosis allows the visualization of the drug by imaging its localization within the organism. The Kim group prepared a prodrug **25**<sup>97</sup> able to release a fluorophore (a coumarin) and SN-38 **22** whereas the Shabat group developed a precursor **26** liberating a near-infrared cyanine fluorophore and camptothecin **21** (scheme 12).<sup>98</sup> Prodrug **25** and SN-38 **22** were evaluated in vitro against melanoma cells B16F10 and cervical cancer cells Hela. The prodrug **25** was able to restore around 60% of the SN-38 **22** activity on both cancer cells and a complete recovery was obtained when adding 100  $\mu\text{M}$  of  $\text{H}_2\text{O}_2$ . This latter observation was made at 100  $\mu\text{M}$  of tested compounds, a concentration way beyond the  $\text{IC}_{50}$  of SN-38 **22**. The authors treated a B16F10 melanoma xenograft in mice with **25** at 0.25 mg/kg or with a saline solution. Again, a relatively limited efficacy was observed with a slightly prolonged survival time (1-6 days) of the treated mice over the non-treated group. Regrettably, irinotecan **23** or the active ingredient SN-38 **22** were not evaluated in this in vivo study. In regards to the cyanine prodrug **26**, the activity against U87MG cells was first determined in vitro: the authors observed an  $\text{IC}_{50}$  of 0.25  $\mu\text{M}$  for the prodrug **26** whereas camptothecin **21** was ten times more active ( $\text{IC}_{50} = 0.02 \mu\text{M}$ ). Nonetheless, the pre-incubation of  $\text{H}_2\text{O}_2$  with **26** lead to the full release of camptothecin **21** and therefore the original  $\text{IC}_{50}$  of this free drug was re-established. In vivo imaging of the prodrug **26** using U87MG cancer xenograft in mice showed a precisely localized activation within the tumor after intratumoral administration. The fluorescence appeared only one minute after prodrug injection and the cyanine dye was still observable 6 hours after administration to the mice.

### 3.1.5.2 Doxorubicin **27**

Doxorubicin **27** is a cytotoxic natural product acting as DNA intercalating agent and topoisomerase II inhibitor (scheme 13). Although used in clinic as antitumor drug, important side effects such as cardiotoxicity were described.<sup>99</sup> Our group therefore prepared arylboronate-based prodrugs of doxorubicin by branching the free amine function of this drug.<sup>100</sup>



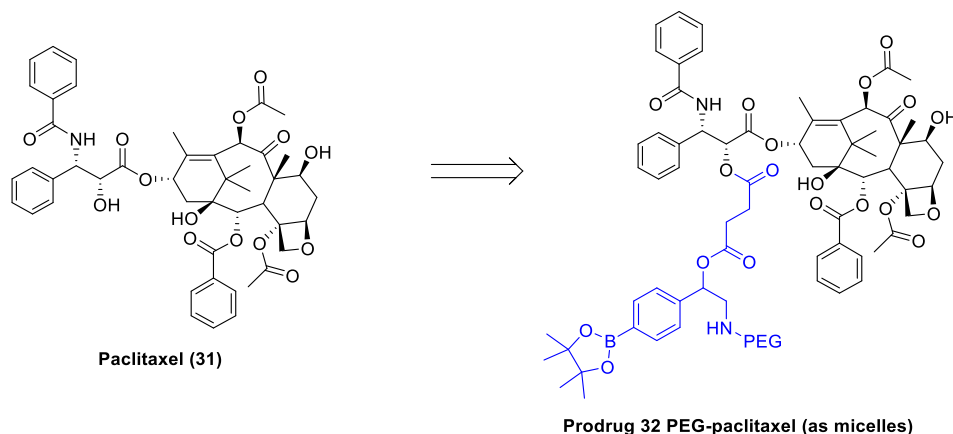
together with doxorubicin **27**,  $\beta$ -lapachone and **28** were evaluated in vitro against three breast cancer cell lines (4T1, MCF-7 and MCF-7 ADR, i.e resistant to doxorubicin) and against NIH/3T3 fibroblasts. Prodrug **28** was less active than doxorubicin **27** showing weak in vitro conversion of **28** into free drug against the four cell lines. Furthermore, the IC<sub>50</sub>s of doxorubicin **27**,  $\beta$ -lapachone and the loaded nanoparticles obtained were equals in every cases except with the resistant MCF-7 cells where the micelles and  $\beta$ -lapachone were 4-5 times more active. This last observation highlight the particular efficacy of the latter molecules against doxorubicin resistant cancer cells. In vivo pharmacokinetics assays showed that both bioavailability and tumor concentration of doxorubicin **27** is improved when the doxorubicin-containing polymeric micelles are injected to mice in comparison with the administration of free drug at the same dose. The different molecules were tested on a MCF-7 ADR tumor xenograft model by intravenous injections at 5 mg/kg. An important tumor regression was observed (~ 90%) when treated with doxorubicin **27** loaded nanoparticles which was higher than the free doxorubicin **27** (~ 50%) and prodrug **28** (~ 30%).

A theranostic prodrug **29** of doxorubicin was built based on a central benzenic self-immolative spacer able to release simultaneously the free drug and a fluorophore, a tetraphenylethene with aggregation-induced emission properties (scheme 13).<sup>102</sup> The construct **29** was evaluated in vitro on Hela cells that were first treated with 1-phorbol-12-myristate-13-acetate (PMA), an agent inducing the ROS production in cells. After incubation, fluorescence and cytotoxicity (IC<sub>50</sub> ~ 2  $\mu$ M) were observed in PMA-treated cells whereas no effect was detected on the PMA-free cells.

Organo-silica nanoparticles **30** displaying phenyl boronic moiety at their surface were prepared by the Shi group.<sup>103</sup> Doxorubicin was then covalently linked via its cis diol part to generate a boronate ester bond leading to nanoparticles covered with the drug (Scheme 19). These nanoparticles were designed to specifically release the doxorubicin within a tumor by ROS-mediated oxidation or by acidic cleavage of the boronate ester bond (due to particularly acidic pH in cancer cells). Hyaluronic acid was also coated at the surface of the nanoparticles in order to specifically target the CD44 receptor which is overexpressed at the surface of certain cancer cells. Efficient in vitro release of doxorubicin **27** was first demonstrated in presence of H<sub>2</sub>O<sub>2</sub> and then the particles were evaluated against Hep G2 cancer cells (CD44+++ ) and NIH/3T3 fibroblasts (CD44+). Nanoparticles **30** bearing hyaluronic acid and doxorubicin were: (i) more toxic against Hep G2 (IC<sub>50</sub> ~ 0.5  $\mu$ M) than their hyaluronic acid free counterparts (IC<sub>50</sub> = 2  $\mu$ M) and (ii) more active against Hep G2 than NIH/3T3 (IC<sub>50</sub> ~ 2  $\mu$ M).

### 3.1.5.3 Paclitaxel 31

Paclitaxel is an antitumor drug inhibiting microtubules depolymerization therefore blocking the mechanism of mitosis.<sup>104</sup> This form of the drug presently used suffers from several side effects and a micellar prodrug **32** built from conjugates “polyethylene glycol-benzene boronate-paclitaxel (scheme 14) was developed by Dong et al.<sup>105</sup>



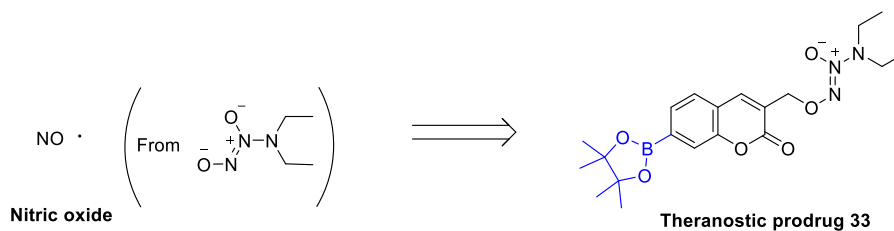
**Scheme 14.** Prodrug of paclitaxel.

Prodrug **32** was evaluated *in vitro* against breast cancer MCF-7 and U251 human glioma cells, the latter cell being less sensible to paclitaxel. Interestingly, prodrug **32** was three times more active than paclitaxel **31** against U251 cells when pre-incubation with PMA, the ROS inductor, was applied. A non-activatable analog of micellar prodrug **32** devoid of the boron trigger was also tested and showed significant cytotoxicity decreased by only a factor 5 in comparison with free paclitaxel **31**. This highlights the uncertain ability of the temporary promoiety, although very bulky, to clearly impair the paclitaxel activity. *In vivo*, a similar trend was observed on a MCF-7 xenograft tumor model in mice. Micelles **32** displayed the best activity with almost 90% of tumor inhibition attributable to its advantageous pharmacokinetics compared to paclitaxel **31** (~ 70% inhibition). Noticeably, the non-activatable prodrug was almost as active as paclitaxel **31** (~ 60% inhibition).

### 3.1.6 Precursor of nitric oxide

In cells, nitric oxide is an endogenous signaling molecule involved in several metabolic pathways. High concentration of nitric oxide usually lead to elevated formation of cytostatic peroxynitrite (*vide infra*). The Chakrapani group has prepared a theranostic precursor **33** of nitric oxide based on a self-immolative coumarin core linked to a nitrosohydroxylamine

(scheme 15).<sup>106</sup> The release of the latter moiety will spontaneously generate two molecules of nitric oxide.



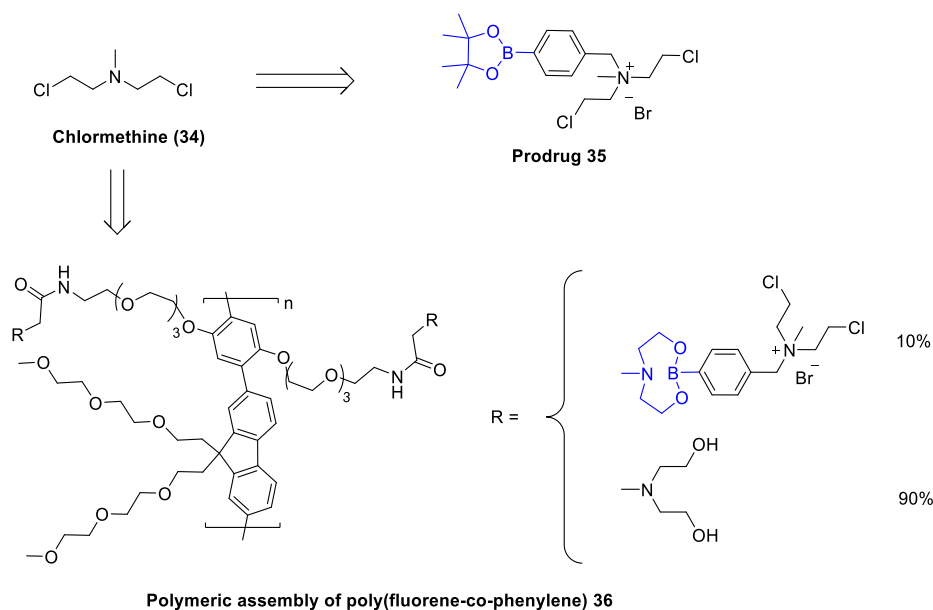
**Scheme 15.** Theranostic prodrug of nitric oxide.

Theranostic prodrug **33** was evaluated in vitro against MRC5 fibroblasts and three cancer cell lines: A549, HeLa, MDA-MB-231. Incubation with the cancer cells in particular with A549, showed greater conversion of **33** into turned-on coumarin and nitric oxide using fluorescence microscopy experiment. A similar activity was observed against all three cell lines ( $\text{IC}_{50} \sim 10 \mu\text{M}$ ) and a lower effect was noted on the MRC5 cells ( $\text{IC}_{50} \sim 25 \mu\text{M}$ ).

### 3.1.7 Precursors of DNA alkylating agents

#### 3.1.7.1 Nitrogen mustards

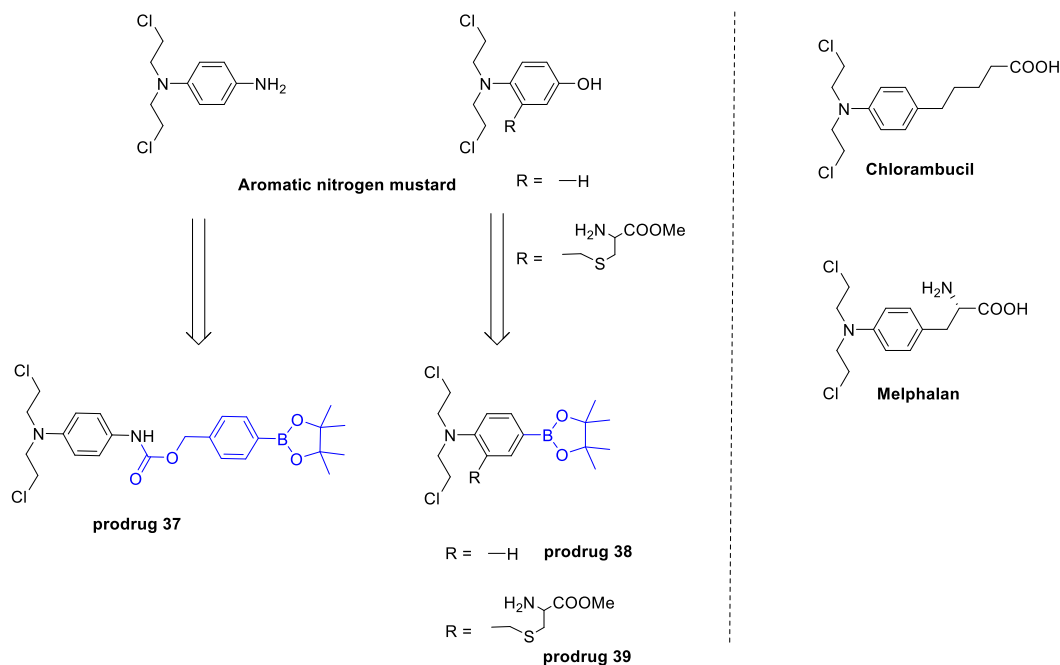
Nitrogen mustards are cytotoxic drugs reacting with DNA to form interstrand cross-links (ICLs). The Peng group designed and synthesized benzene boronate prodrugs of chlormethine **34** since this drug is weakly selective of cancer cells (scheme 16).<sup>107</sup>



**Scheme 16.** Prodrugs of chlormethine.

When linked to benzene boronate, chlormethine is not able to form the electrophilic aziridinium cycle strongly reacting with DNA. In vitro, prodrug **35** showed efficient ability to alkylate DNA in presence of H<sub>2</sub>O<sub>2</sub> and **35** was further evaluated against four cancer cells: leukemia cells SR, lung cancer cells NCI-H460, renal cancer cells SN12C and CAKI-1, and healthy lymphocytes. Prodrug **35** (with no added H<sub>2</sub>O<sub>2</sub>) was especially active against SR and NCI-H460 cells with 85-90% of growth inhibition at 10 μM while no activity was detected at this concentration on the normal lymphocytes. Rationally, the same activity for **35** and its corresponding free boronic acid was found in vitro against all cell lines. This benzene boronate prodrug of chlormethine **34** was further bonded to a polymeric assembly of poly(fluorene-co-phenylene) by Li et al.<sup>108</sup> The polymeric prodrug **36** (Scheme 22) can be considered as theranostic since the polymer backbone is fluorescent and was visualized into cells by imaging. The polymeric prodrug **36** was tested on HeLa and A549 cells, and globally, **36** displayed a similar level of cytotoxicity as prodrug **35** (i.e 80% of growth inhibition at 10 μM).

Using a closely related strategy as earlier, Peng and co-workers prepared boronate prodrugs of aromatic nitrogen mustards where the electron-withdrawing boronate function was either directly linked to the effector (**38** and **39**) or via a benzyl self-immolative spacer (**37**) (scheme 17).<sup>109,110</sup>

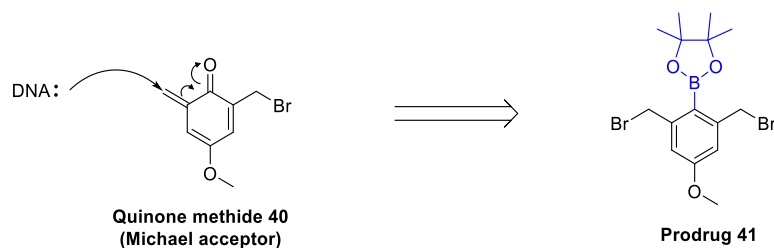


**Scheme 17.** Structures of chlorambucil, melphalan and the prodrugs of aromatic nitrogen mustard.

Amongst the synthesized prodrugs, prodrug **37** and **38** were the most active at forming ICLs and at inhibiting the panel of 60 cancer cells from the NCI. In particular,  $IC_{50}$ s of both prodrugs **37** and **38** were obtained below 1  $\mu$ M against SR and NCI-H460 cells. Analogs of prodrugs **38** bearing a substituent were synthesized to further optimize the antitumor activity of this series.<sup>111</sup> Prodrug **39** displaying a cysteinyl methyl ester motif was shown to enhance the water solubility and cell permeability. Moreover, **39** was more effective in vitro against MDA-MB-468 than **38** and the reference drugs chlorambucil and melphalan. Prodrug **39** was evaluated in vivo using MDA-MB-468 cancer xenograft in mice and displayed significantly reduced tumor growth compared to the vehicle with no side effects.

### 3.1.7.2 Quinone methides as alkylating agents

The Peng group also envisioned the generation of quinone methides as Michael acceptor for DNA strand (scheme 18).<sup>112–114</sup> Among several benzene boronate precursors, prodrug **41** was the most interesting of their series.



**Scheme 18.** Prodrug of quinone methide as Michael acceptor.

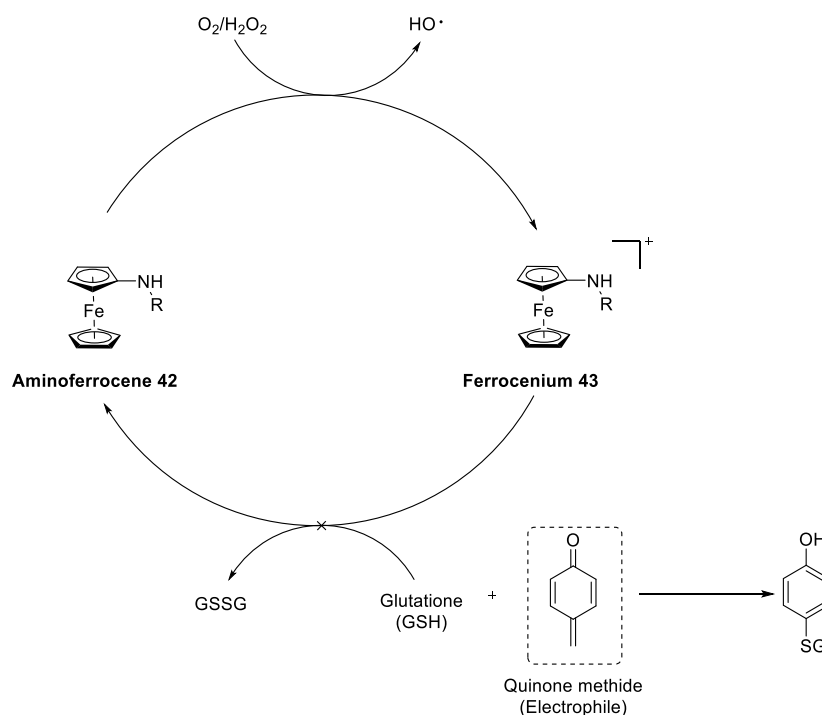
Prodrug **41** was able to form ICLs in presence of  $H_2O_2$  and its cytotoxicity was evaluated against the NCI cancer cells panel.  $IC_{50}$ s of **41** against several cancer cells was about 10-20  $\mu$ M which was significantly more active than chlorambucil and melphalan.

## 3.1.8 Precursors of ROS/RNOS amplifier/accumulator for oxidation therapy

### 3.1.8.1 Aminoferrocene

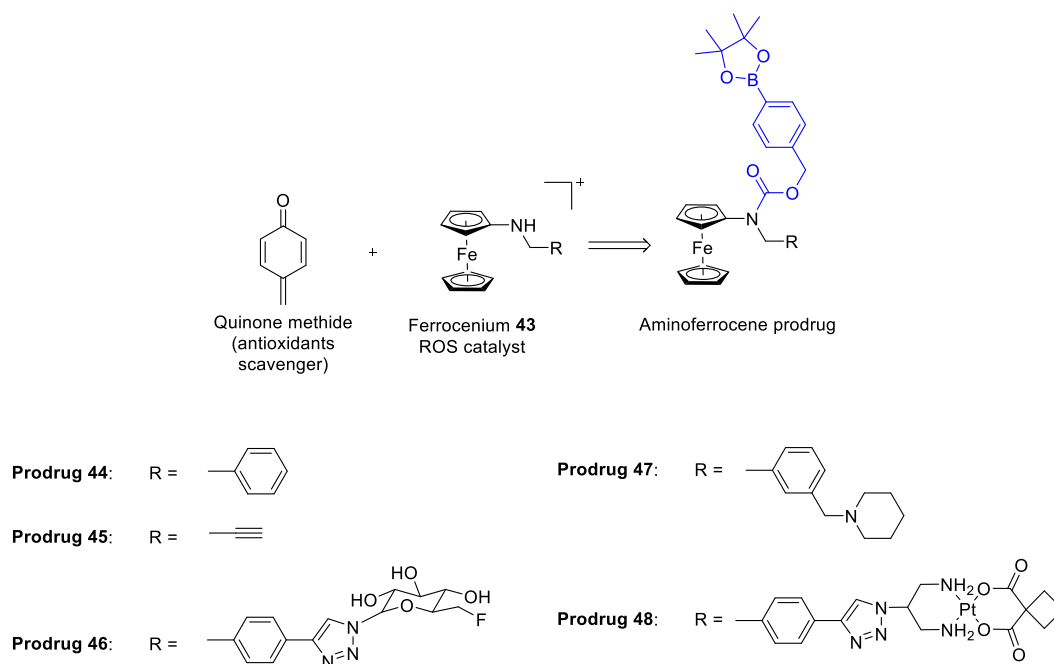
Over the last decade, the group of Mokhir has developed benzene boronate precursors of aminoferrocene.<sup>115–124</sup> These precursor were conceived to increase drastically ROS concentrations inside cancer cells leading ultimately to cell death, i.e oxidation therapy.<sup>125</sup> The released aminoferrocene **42** reacts with hydrogen peroxide or oxygen to afford both cytotoxic hydroxyl radical and ferrocenium ion **43** (scheme 19). These ROS are usually detoxified by

antioxidants such as glutathione but in this strategy, electrophilic quinone methide is also formed and acts as glutathione scavenger blocking this protective mechanism.



**Scheme 19.** Cycle for ROS amplification within tumor environment initiated by the presence of free aminoferrocene.

From a first series of aminoferrocene prodrugs,<sup>115</sup> the authors found that the prodrug **44** (Scheme 20) was the most efficient at both penetrating and amplifying ROS within HL-60 leukemia cells. This is attributable to the greater stability of the liberated *N*-benzylaminoferrocene and **44** was indeed the most cytotoxic prodrug against HL-60 ( $IC_{50} = 9 \mu M$ ) whereas no activity was found against healthy fibroblasts ( $IC_{50} > 100 \mu M$ ).



**Scheme 20.** Aminoferrocene prodrugs.

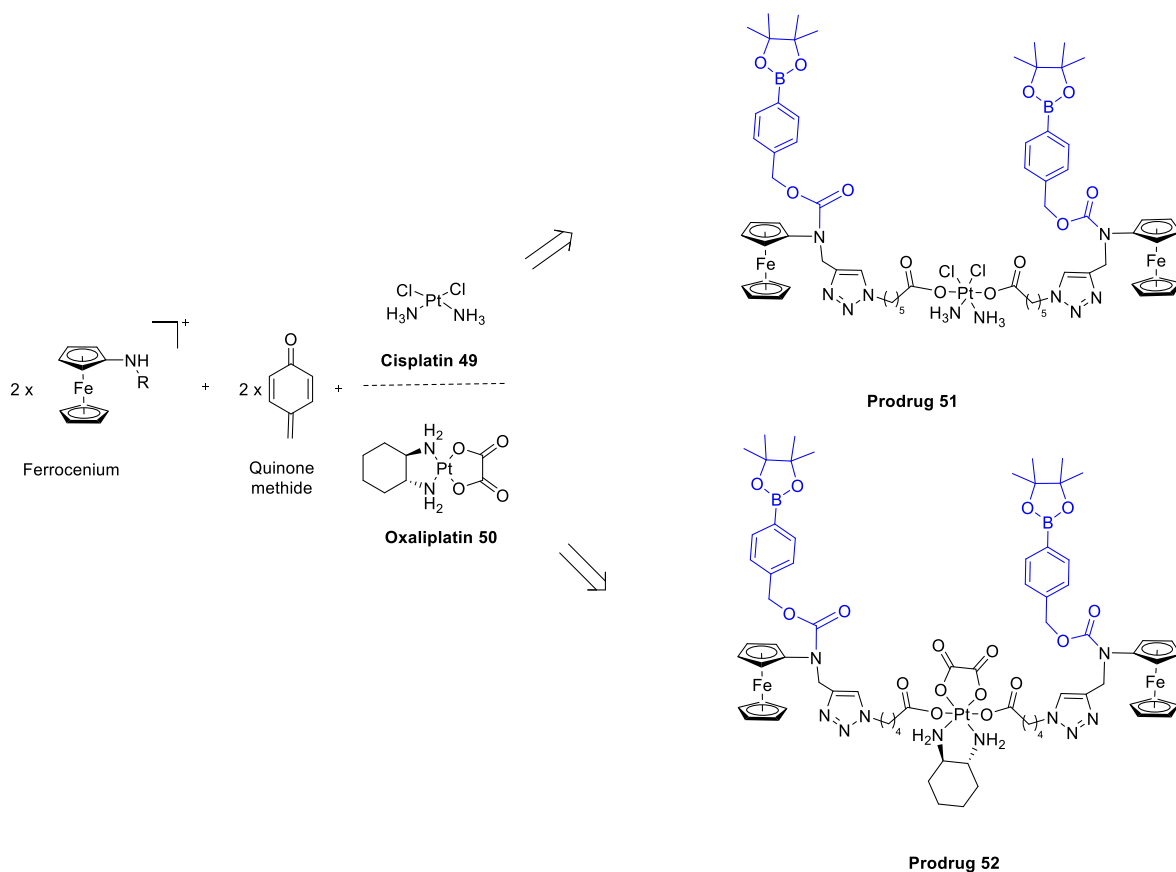
The authors further showed that the cytotoxicity was decreased when the ferrocene part was partly constituted of a cyclopentadiene carboxylic acid moiety.<sup>116</sup> Modification of the *N*-benzyl group by either introducing *ortho*- or *para*-substituent or replacement of the benzene ring by a pyridine nucleus was also counterproductive to the cytotoxicity on HL-60 cells.<sup>116,117</sup> Prodrug **44** was therefore selected for in vivo studies.<sup>117,118</sup> First, **44** was not toxic on healthy mice up to 6 mg/kg and **44** was further evaluated on L1210 leukemia xenografted mice. Six injections per day at 26  $\mu$ g/kg led to the extension of survival time (+ 30%) of the mice. The authors noted an increased oxidative stress in L1210 cancer cells recovered from treated animal.<sup>117</sup> Prodrug **44** was also evaluated on xenografts of human prostate adenocarcinoma in CBA mice in view of the high in vitro ROS production observed from prostate cancer cell lines. However, this latter in vivo assay showed a modest tumor mass reduction for the cohort treated with **44**.<sup>118</sup> Prodrug **44** was however described to aggregate in aqueous solution and new analogs were therefore designed in order to reduce this property. A *N*-propargyl prodrug **45** displaying lower hydrophobicity was indeed less susceptible to aggregation and was also shown to display in vitro cytotoxicity similar to that of **44**. Growth inhibition of Guerin's carcinoma in rat was observed when **45** was administrated intraperitoneally at a single dose of 30 mg/kg seven days after tumor transplantation.<sup>119</sup>

Aminoferrocene theranostic prodrugs (scheme 20) were then developed by branching benzene boronate precursors of aminoferrocene to a [<sup>18</sup>F]-fluoroglucose for positron emission tomography (PET).<sup>120</sup> Theranostic prodrug **46** had an in vitro cytotoxicity close to that of the

reference prodrug **44** (e.g. against HL-60,  $IC_{50}(\mathbf{46}) = 26 \mu\text{M}$  compared to  $IC_{50}(\mathbf{44}) \sim 10 \mu\text{M}$ ). The corresponding free boronic acid of **46** was injected in mice bearing two tumors: PC3 (human prostate cancer) and AR42J (rat pancreatic cancer). PET analysis showed a moderate localization of the tracer in both tumors but the measured radioactivity remain relatively stable in the tumors for 60 minutes in comparison with the healthy organs of the mice.

An organic moiety able to target the lysosome was alternatively added on the benzene boronate precursors of aminoferrocene.<sup>121</sup> The piperidine prodrug **47** (scheme 20) was prepared in order to obtain an ammonium form at physiological pH leading to lysosome trapping and accumulation. Biophysical properties of **47** were compared to the reference prodrug **44** and were shown significantly improved. In particular, the hydroxyl radical formation was more efficient from prodrug **47** and this was transcribed with the higher in vitro cytotoxicity observed for **47** than for **44** against several cancer cell lines (6 to 8 folds more active). The ability of prodrug **47** to disrupt lysosomal function was confirmed by a fluorescence imaging experiment. Prodrug **47** was evaluated in Nemeth-Kellner lymphoma xenograft mice model by intraperitoneal injection of eight doses of 40 mg/kg every two days for 15 days. The tumor weight of treated animals was reduced in comparison with the untreated cohort but the results were very contrasted.

These aminoferrocene precursors were further complexified by the increment of a platinum-based antineoplastic prodrug moiety (**48**, **51** and **52**) (scheme 20 and 21).<sup>122-124</sup>

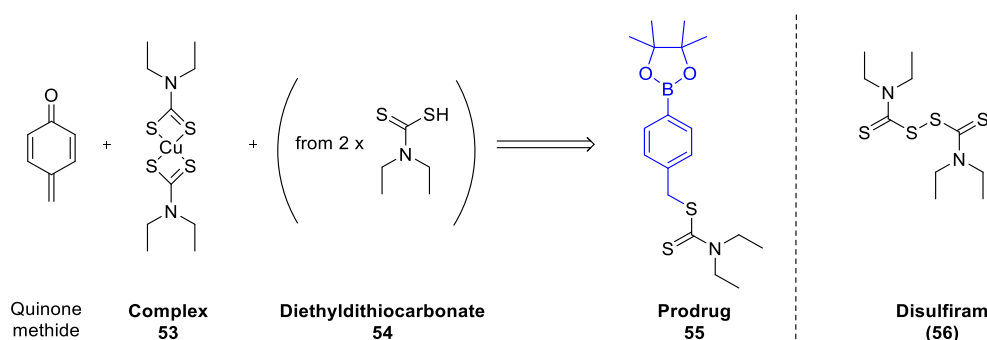


The bis “aminoferrocene-cisplatin” prodrug **51** was shown to effectively release cisplatin **49** after addition of  $\text{H}_2\text{O}_2$ , indeed, the free aminoferrocenes generated are able to transfer one electron that both reduces the metal complex into cisplatin and forms the activated ferrocenium. **51** was evaluated against normal fibroblasts HDFa, ovarian carcinoma cell line A2780 and the cisplatin resistant counterpart A2780cis cell line. Prodrug **51** was not toxic against the healthy fibroblasts while activity of free cisplatin **49** was fully recovered when A2780 cells were treated with **51** ( $\text{IC}_{50} \sim 2 \mu\text{M}$ ). Interestingly, the resistant A2780cis cells behaved differently: activity of prodrug **51** ( $\text{IC}_{50} = 6 \mu\text{M}$ ) was twice greater than cisplatin **49** ( $\text{IC}_{50} = 13 \mu\text{M}$ ). The authors revealed that prodrug **51** was not generating an aminoferrocene which strongly produces ROS but the activity of prodrug **51** was mostly due to the release of cisplatin **50** rather than the generally modest activity provided by ferrocenium. The oxaliplatin prodrug **52** was built with the same scaffold used for cisplatin prodrug **51** (Scheme 21).<sup>123</sup> In construct **52**, the spacer between the ferrocene and the platinum-based drug was truncated ( $\text{C}_4$  in lieu of  $\text{C}_5$ ) in order to facilitate the intramolecular electron transfer within these two moieties. Prodrug **52** was indeed more active than **51** against both ovarian cancer cell lines in vitro :  $\text{IC}_{50}$  (A2780) =  $0.4 \mu\text{M}$  and  $\text{IC}_{50}$  (A2780cis) =  $0.7 \mu\text{M}$ . Analog **52** followed the trend described for

prodrug **51** in view of the stronger activity (over free cisplatin **49**) displayed by the free drug oxaliplatin **50** :  $IC_{50}$  (A2780) = 0.9  $\mu$ M and  $IC_{50}$  (A2780cis) = 3  $\mu$ M. The authors further synthesized a mono-“carboplatin-aminoferrocene” prodrug **48** (scheme 20).<sup>124</sup> Accumulation of **48** in the mitochondria of A2780 cancer cells was demonstrated using the mitochondrial tracker rhodamine R123 and it was assumed that this uptake was due to the release of a delocalized lipophilic cation: the generated ferrocenium. In vitro activity of **48** was then determined against the three aforementioned cell lines and adopted the tendency observed for cisplatin prodrug **51** but to a weaker extent.

### 3.1.8.2 Diethyldithiocarbamate **54**

Diethyldithiocarbamate **54** is a metabolite of disulfiram **56**, a drug used in clinic to treat chronic alcoholism and recently, copper complex of diethyldithiocarbamate **53** was shown to have anticancer activity.<sup>126</sup> The formation of this complex **53** generates ROS in the cancer cells and the Pu group prepared a prodrug **55** capitalizing on the ROS amplification due to both formation of the latter complex and a quinone methide (Scheme 22).<sup>127</sup>

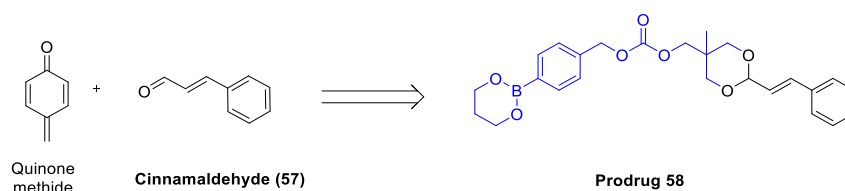


**Scheme 22.** Structures of disulfiram and the prodrug of diethyldithiocarbamate.

Prodrug **55** was tested against 4T1 breast cancer cells in vitro : In the presence of the nontoxic concentration of copper (1  $\mu$ M), activity was six times more potent on cancer cells ( $IC_{50}$  = 1  $\mu$ M) than on normal fibroblasts NIH3T3 ( $IC_{50}$  = 6  $\mu$ M). This difference of activity could be explained by the high ROS production of 4T1 which was essentially due to the diethyldithiocarbamate copper complex formation and minimally as a result of quinone methide generation. In vivo testing was made on a 4T1 xenograft mice and the most potent result was obtained using a co-injection of copper gluconate at 1.5 mg/kg with **55** at 37 mg/kg. Applying this protocol, a decrease of 80% of the tumors volume was observed in comparison to the inactive vehicle or copper gluconate alone.

### 3.1.8.3 Cinnamaldehyde 57

Cinnamaldehyde **57** is a natural product found in cinnamon essential oil and used as food flavoring. This aldehyde was shown to amplify ROS in cancer cells but this action is very limited on healthy cells. Poor bioavailability of cinnamaldehyde **57** has prevented its application in clinic and therefore this compound was a good candidate for prodrug development. Thus, the Lee group has prepared a benzene boronate prodrug of cinnamaldehyde **58** (scheme 23).<sup>128</sup>

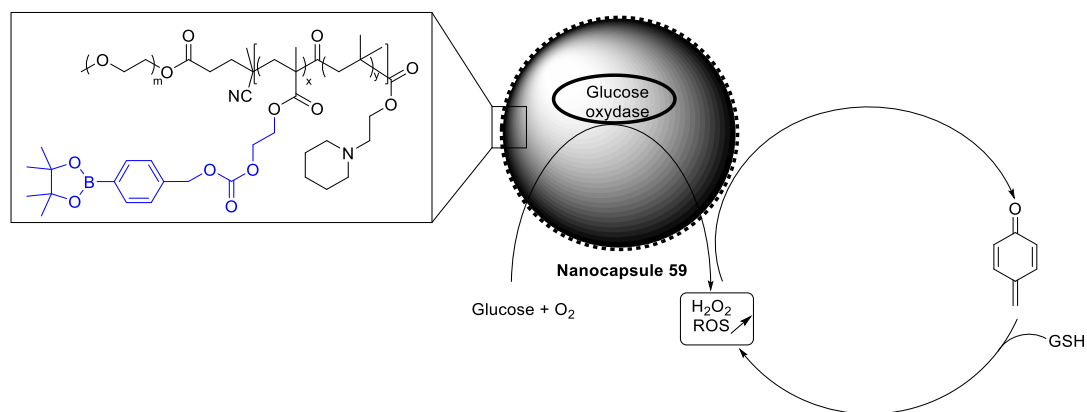


**Scheme 23.** Prodrug of cinnamaldehyde.

Under oxidative conditions, this prodrug **58** will generate a quinone methide able to covalently trap antioxidants leading to ROS accumulation in cells. Moreover, a molecule of cinnamaldehyde **57** will be released under acidic conditions found in cancer cells and then enhanced the already high level of ROS. The authors first evaluated the ability of **58** to lower the glutathione level in three cell lines: prostate cancer DU145, colon cancer SW620 and fibroblasts NIH3T3. Only the DU145 cells were responsive to **58** and presented a reduction of around 50% of intracellular glutathione concentration. Cytotoxicity of prodrug **58** was weak against the three cell lines and DU145 cells were more affected ( $IC_{50} = 48 \mu M$ ) than the NIH3T3 fibroblasts ( $IC_{50} = 182 \mu M$ ). A tumor xenograft mouse model of DU145 cells was used to evaluate the in vivo antitumor effect of **58** and camptothecin **21** as reference drug. Seven injections every 3 days of either **58** or camptothecin **21** at 2 mg/kg showed the same tumor volume reduction (~ 75 %). Prodrug **58** was more active than control compound cinnamaldehyde **57** or a quinone methide generator alone.

### 3.1.8.4 Glucose oxidase

The glucose oxidase enzyme catalyze the reaction of glucose and oxygen into gluconolactone and hydrogen peroxide. This enzyme can therefore generate ROS from two compounds naturally abundant in cells. To capitalize on this, Li et al.<sup>129</sup> have prepared nanocapsules **59** able to entrap glucose oxidase (scheme 24).



**Scheme 24.** Nanocapsules loaded with glucose oxidase for the amplification of ROS within the tumor microenvironment.

The shell of the capsule was made of a diblock copolymer of PEG and polymethacrylate grafted with benzene boronate and piperidine moieties. Protonation of piperidine in the acidic tumor environment increases the permeability of the nanocapsule and allows the entry of glucose which lead to the strong production of H<sub>2</sub>O<sub>2</sub>. This enhanced level of hydrogen peroxide further reinforces the oxidation of the benzene boronate part into glutathione scavenger quinone methide. The authors verified that this dual acting nanoconstruct was operational in vitro by measuring H<sub>2</sub>O<sub>2</sub> production and quinone methide formation. Mice bearing lung carcinoma A549 were treated with nanocapsule **59** and showed complete inhibition of tumor growth in comparison with either glucose oxidase or empty nanocapsule alone.

### 3.2 Pharmacological relevance

In this section, the strategy of boron-containing prodrugs responsive to oxidative stress is discussed in regards to its potential to reach the market as effective cancer treatment. Indeed, boronic acid/boronate prodrug have been largely evaluated in animal models but no clinical trials have been started with any of these molecules so far.

Nonetheless, the potential of these constructs is strong considering that several drugs containing a boronic acid function, are already on the market.<sup>73,130</sup> Moreover, the development of boron-containing classical drug remains a dynamic area of research.<sup>131</sup> In terms of drug delivery, the boronic acid function is particularly relevant since it allows facilitated internalization in cancer cells.<sup>132,133</sup> The reversible formation of ester bonds between boronic acid and the diol of saccharides ensure this membrane crossing. Precisely, high affinity

between boronic acids and the glyocalix of cancer cells lead to the selective uptake of the molecules bearing this moiety.

Furthermore, to improve the strategy of the small-molecule prodrugs, the kinetic of prodrug conversion must be considered. At the tumor site, activation of boron-containing prodrugs by ROS can either occur extra- or intracellularly. As the system is not closed, the liberated drug will then freely diffuse around the tumor ( $\sim 10^{-3}$  mm<sup>3</sup>; a mass of around 1,000 cancer cells) and that will influence the concentration profile of the drug. Scission of the prodrugs should arise locally to preserve an efficient dose of the liberated drugs within the tumor. In view of the diffusion coefficient of small molecules ( $10^{-10}$  m<sup>2</sup>.s<sup>-1</sup>) and considering the aforementioned tumor volume, oxidation of precursors into drugs should last approximately 2 minutes in order to maintain the concentration of the free drugs equal to that of the corresponding prodrugs. When the prodrug conversion implies an additional self-immolative step, the complete process must not exceed the latter duration.

The reaction of boron-containing prodrug with the ROS species is bimolecular and the rate will therefore depend on the concentration of both reactants:  $v = k[\text{prodrug}][\text{ROS}]$ . The concentration of the prodrug is mostly guided by the dose injected to the biologic system but levels of peroxynitrite and hydrogen peroxide is dictated by the living organism. Specific activation in the tumor microenvironment can occur since the concentrations of peroxynitrite and hydrogen peroxide are strongly increased in comparison with healthy tissues. Cellular concentration of peroxynitrite can reach 50-100  $\mu\text{M}$  in pathological conditions whereas a basal concentration of 0.1-1  $\mu\text{M}$  was estimated in healthy cells.<sup>134,135</sup> Physiological hydrogen peroxide is produced at a steady-state concentration of 0.1-1  $\mu\text{M}$  which rises to 10-100  $\mu\text{M}$  in malignant organs.<sup>136,137</sup>

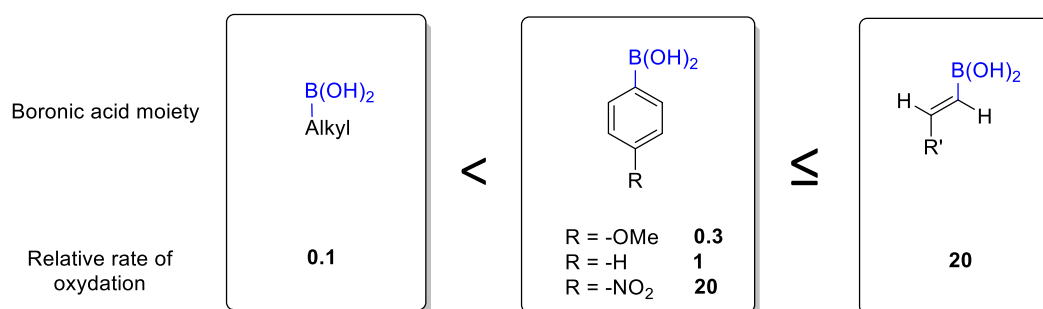
In this activation strategy, two parameters must be taken into account: the half-life of each ROS in vivo and the rate constant associated to a ROS and a particular prodrug structure.

As mentioned earlier, at physiological pH, oxidation of the carbon-boron bond by peroxynitrite is  $10^6$  faster than that obtained with hydrogen peroxide: e.g. conversion of phenylboronic acid to phenol occurred with rate constant of  $1 \times 10^6$  M<sup>-1</sup>.s<sup>-1</sup> with peroxynitrite and approximately  $1-2$  M<sup>-1</sup>.s<sup>-1</sup> with hydrogen peroxide.<sup>25</sup> In vivo, peroxynitrite has a half-life of  $\sim 10$  ms and reacts preponderantly but reversibly with carbon dioxide (1-2 mM) to form nitrosoperoxocarbonate anion (ONOO<sub>2</sub><sup>-</sup>) at a rate constant of  $0.5 \times 10^5$  M<sup>-1</sup>.s<sup>-1</sup>. As opposed to hypochlorite anion which react faster with biomolecules than boronate/boronic acid in vivo, peroxynitrite is able to oxidize the carbon-boron bond due to the rapid kinetic of this reaction over the addition of carbon dioxide.

In biological systems, hydrogen peroxide also reacts with biomolecules such as amino acids and metals (free or inside metallo-enzymes). Consequently, its half-life in cells is ~ 1 ms. The reaction with the thiol group of cysteine residues was described as the fastest physiological transformation of hydrogen peroxide with a rate constant up to  $10^6 \text{ M}^{-1} \cdot \text{s}^{-1}$ .<sup>138,139</sup>

Given the differences of reactivity of both involved oxidative species, peroxyxynitrite is likely to be the main actor for the conversion of these prodrugs into the corresponding free drugs. In view of the short half-life of oxidative species, increasing the rate constant of this oxidation reaction should result to a greater number of available peroxyxynitrite molecules that can react with the boronic acid prodrug. This would lead to a better yield of prodrug transformation at the tumor site and then improve the chance of treatment efficacy. Notably, the structure of the prodrug will also greatly affect the kinetic of oxidation in regards of the ROS involved in the reaction. The possibility of modulating the prodrug scaffold in favor of a faster reactivity toward ROS is crucial and can be operated by medicinal chemists.

In term of structure-kinetic studies of boronic acids conversion into alcohols, we noted that aliphatic boronic acids are 10 times slower than benzene boronic acids (scheme 25).<sup>70</sup>



**Scheme 25.** Relative rate of C-B bonds oxidation of alkyl, benzyl and vinyl boronic acid derivatives.

The oxidation kinetic of benzene boronic acids is dependent of the substitutions of the aromatic nucleus.<sup>69,75</sup> Adding a strongly electron-withdrawing substituent such as a nitro group at the *para* position of the ring increased the oxidation rate by 20-fold whereas an electron-donating methoxy group at the same position divided this rate by a factor of three. Although electron-withdrawing group substitution of the benzenic ring lead to a faster formation of the quinone methide intermediate, this latter modification also cause a dramatic reduction of the kinetic of the following self-immolation step.<sup>77</sup> Therefore, no substitution of benzene boronate nucleus as self-immolative promoiety can be envisioned to increase the global rate of the oxidation/disassembly steps of such constructs.

The vinyl boronic acid group was also shown to release an effector through oxidation and subsequent self-immolation process.<sup>75,76,140</sup> The oxidation of the vinyl boronic acid motif was 20 times more rapid than that of the equivalent unsubstituted benzene boronic acid group.<sup>75</sup> This difference of reactivity could be attributed to a faster self-immolation step since the  $\pi$  electrons of the double bond are not delocalized within a benzene nucleus and therefore available for the elimination reaction. Moreover, the empty p-orbital of the boron in vinyl boronic acid motif is less hindered than in the benzenic equivalent leading to an easiest access of the nucleophilic oxidative species. Eventually, this motif could be further engineered to potentially increase the global rate of effector release.

With the condition that an average drug concentration of 10  $\mu\text{M}$  is required within the tumor of around  $10^{-3} \text{ mm}^3$ , the rate of the reaction ( $v = k[\text{prodrug}][\text{ROS}]$ ) should not fall below 10  $\mu\text{M}$  per 2 minutes which is about  $0.1 \mu\text{M}\cdot\text{s}^{-1}$  (total conversion inside the tumor). Given the concentration of peroxynitrite ( $\sim 10 \mu\text{M}$ ; the most reactive ROS) in cancer cells, only prodrugs oxidized at rate constant ( $k$ ) higher than  $10^3 \text{ M}^{-1}\cdot\text{s}^{-1}$  would be effective. Nonetheless, due to the short half-life of peroxynitrite ( $\sim 10 \text{ ms}$ ), we estimate that the reaction of the latter oxidant with a particular boronic acid prodrug should react at a rate constant superior to  $10^7 \text{ M}^{-1}\cdot\text{s}^{-1}$  in order to afford 10  $\mu\text{M}$  of drug localized at the tumor site. In light of this short physiological half-life, targeting mitochondria is a relevant strategy in order to efficiently reach the cellular ROS. Such vectorized prodrug containing a delocalized lipophilic cation was already developed by the Mokhir group.<sup>124</sup>

In regards of the aforementioned boronic acid promoieties, we noticed that the quinone methide species generated from benzene boronates were not strongly cytotoxic but very efficient at scavenging antioxidants.<sup>89,115,128,129</sup> Remarkably, it was occasionally reported that the boronic promoiety was not completely masking the pharmacological activity of the branched drug.<sup>45,60</sup> This suggests that the attachment of a benzene boronic acid promoiety to a drug do not provoke the automatic discontinuation of the bioactivity. Furthermore, the nominal boronic acid function is often used in this reviewed prodrug strategy and it was recently proposed that the latter function could be used as a bioisoster of a hydroxyl group. Some successful drug analogs were indeed developed by the Wang group<sup>141–143</sup> that formerly developed boronic acid-containing prodrugs (vide supra).

The same group showed that boronic acid prodrug were also activated by the cytochromes P450.<sup>87</sup> Thus, the benzene boronic promoiety could even be employed for the development of several types of prodrug allowing the prolonged release of any drug for the treatment of any disease.<sup>144</sup> Consequently, this activation could compete with the expected oxidation by the ROS of cancer-targeting boronic acid prodrugs within the tumor microenvironment. It is

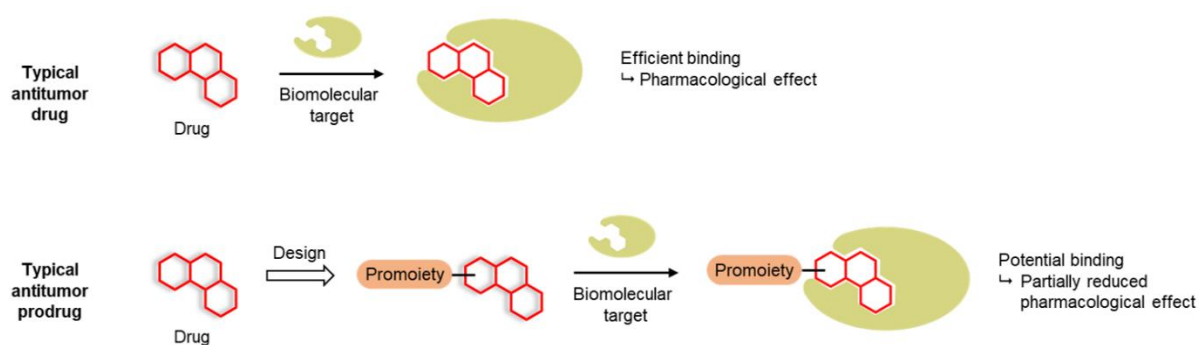
important to note, however, that unlike a direct chemical reaction between an oxidant and a boronic acid molecule, the reaction of the latter function with the cytochromes P450 is an enzymatic reaction. This implies the entrance of the prodrug into the active site before oxidation of the C-B bond. In order to develop boronic acid prodrugs specifically targeting tumors, their oxidation by cytochromes P450 should be evaluated. In case of unwanted interaction, modulation of the structural core of the boronic acid promoiety should be therefore considered to impede the prodrug access to the catalytic sites of the cytochromes P450.

### 3.3 Conclusion

This chapter reports on the different small-molecule, polymeric and nanoparticle-based prodrugs activated through oxidation of intrinsic carbon-boron bonds by ROS from tumor environment. Since we published this chapter as a review, two articles reported the development of boronic acid based anticancer prodrugs of evodiamine<sup>145</sup> and melatoninine.<sup>143</sup> The literature reveals several constructs with interesting activity and until now, none of these prodrugs have entered into clinical trial. In view of the in vivo data, this prodrug strategy is promising for the treatment of several tumors such as leukemia, breast and pancreatic cancers which produce high concentrations of ROS. Chemical system leading to both ROS amplification and anticancer agent delivery were particularly effective. In order to obtain a ROS-activated boronic acid prodrug with a great therapeutic potential, it would be beneficial to develop a structure which could both intensify the ROS level within cancer cells and ensure rapid release of a drug by virtue of a rapid C-B oxidation.

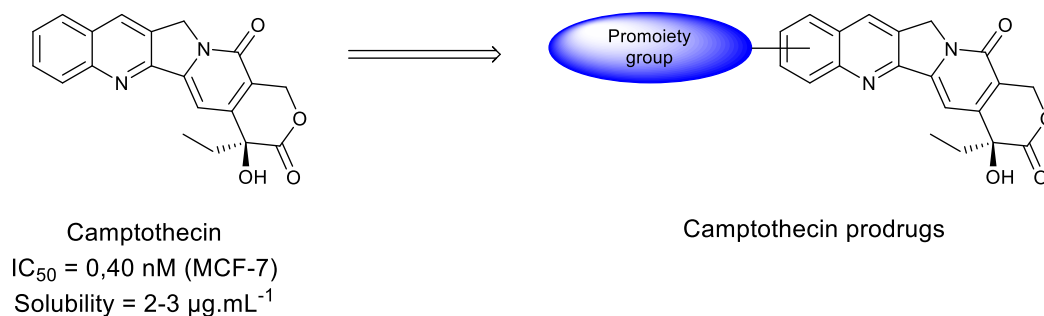
## **Chapter 2: Thesis project**

In cancer chemotherapy, the prodrug strategy has risen as the cytotoxic drugs available in clinic often present similar toxicity towards both cancer and normal cells. Many research groups have made significant efforts in the development of innovative antitumor prodrug but the typical prodrug approach remains the branching of an organic promoiety to antitumor drugs in order to mask their original activity (scheme 26).<sup>20,142,146–149</sup> Subsequently, masked drugs are therefore liberated at the tumor site as a result of modified cancer cell metabolism. One major drawback in this prodrug strategy is often the poor ability of the promoiety (regardless of its size) to clearly impair the pharmacological activity of the expected masked drug (e.g. the prodrug can nearly bind as tight as the free drug to the biological target).<sup>150–153</sup>



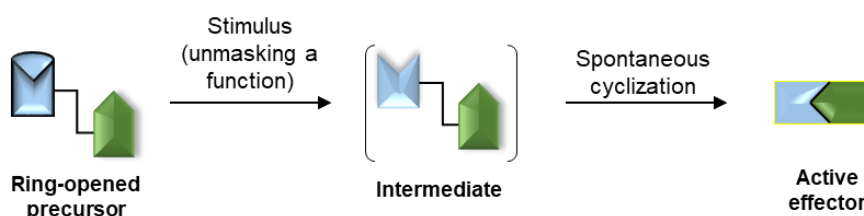
**Scheme 26.** Antitumor drug and cancer-targeting prodrug strategies. (a) Typical antitumor drug binds to its biological target inducing a pharmacological effect. (b) Typical prodrug for cancer-targeted therapy is constituted of an existing drug linked to a bioresponsive promoiety. Frequently, the assembly can be almost as pharmacologically active as the free drug owing to the preserved binding to the biological target.

As significant example, the natural product camptothecin is not used in clinic due to its strong general toxicity, lack of selectivity and low solubility. These problems have led researchers to develop camptothecin prodrugs based on conjugates of promoieties associated to hydroxy-camptothecin.<sup>154,155</sup> However, pharmacological activity was reduced by a factor 10 to 50 which is not sufficient to prevent the cytotoxic effect on healthy cells (Scheme 27).



**Scheme 27.** General structure of camptothecin prodrugs.

In the literature, the enediynes are natural products that cyclize spontaneously into cytotoxic antibiotics (scheme 1).<sup>156–159</sup> Moreover, this scaffold is the sole described as able to afford cytotoxic agents after internal cyclization. Conjugation of these molecules to antibodies lead to the development of the antibody-drug conjugates Mylotarg® and Besponsa® used in clinic to treat cancer.<sup>160</sup> Furthermore, precursors of coumarins relying on an intramolecular cyclization to eventually generate the fluorophore were also studied.<sup>161–163</sup> In this thesis, we intend to adapt this feature by establishing chemist-made precursors of antitumor agents operating analogously: (i) no branched organic promoiety is used but masked reactive functions are rather inserted; (ii) the proposed prodrug is not a drug linked to a hindered moiety but a synthetic precursor of the drug that will need an in-cell cyclization step to produce the final drug (scheme 28).

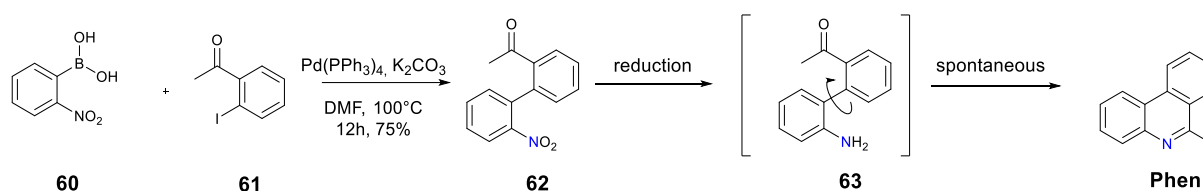


**Scheme 28.** Generation of anticancer agents from ring-opened precursors through bioorthogonal cyclization.

The prodrug is made of a relatively flexible precursor of the final drug, in order to strongly reduce the possibility of prodrug potency in respect to the free drug. In this approach, the prodrug displays lower molecular mass in comparison to classic prodrugs, a favorable characteristic for both crossing biological membranes and complying with the Lipinski's rule of 5.

The phenanthridines present large and planar structures which are frequently encountered features of intercalating agents and topo isomerase I inhibitors. Moreover, phenanthridines are

not used in clinic due to their general toxicity,<sup>164–166</sup> and are therefore candidates of choice to explore this strategy. In this context, we first envisioned to prepare ring-opened precursors of phenanthridine (scheme 29). Starting from a biaryl precursor, we proposed a cyclization by imination that would generate the nitrogen-containing central ring of the aromatic phenanthridine **Phen**. We then designed a biaryl derivative containing a nitro and a ketone functions to test the ability of this precursor to spontaneously cyclize. The final step of formation of the phenanthridine would be then possible via spontaneous intramolecular cyclization due to entropic favorability as the driving force. Using the commercially available nitrophenylboronic acid **60** and the iodoacetophenone **61**, we were able to efficiently obtain the needed precursor **62** in one step by palladium catalyzed coupling. In order to initiate the expected cyclization reaction, we reduced the nitro by hydrogenation at 37°C in presence of Raney nickel. This reaction was carried out in organic solvent and then in cell medium.

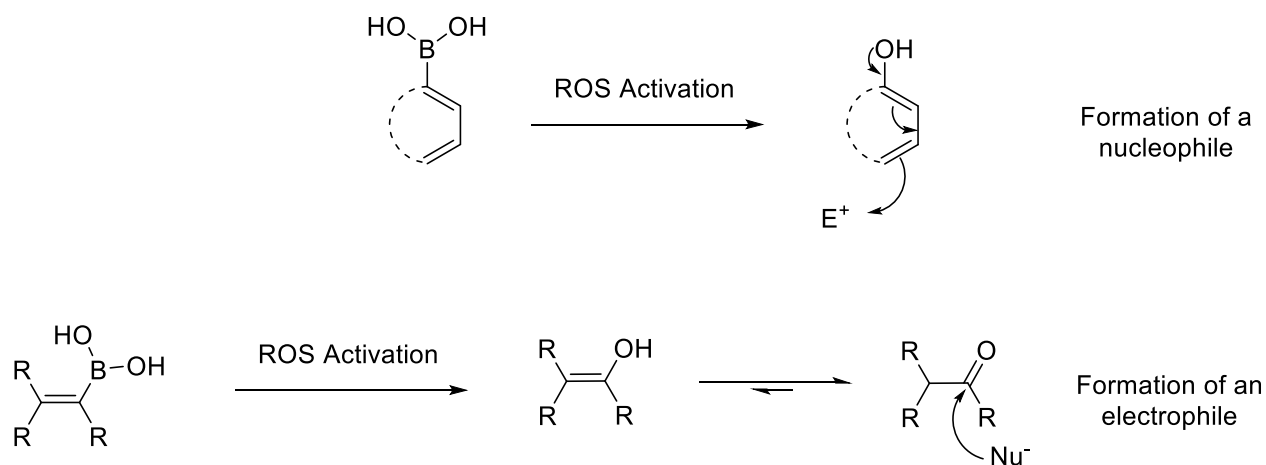


**Scheme 29.** A nitro-biaryl derivative was chemically reduced to afford its corresponding aniline that spontaneously generated the aromatic phenanthridine.

By following the reaction by TLC, we monitored the rapid formation of the cyclic compound whereas no observation of the aniline intermediate was possible by this method. Interestingly, the formed phenanthridine was fluorescent and it would be therefore straightforward to develop a strategy to measure the kinetic of phenanthridine assembly. Two steps are involved in this process: first the nitroreduction and the subsequent imination of the ketone function by the newly formed aniline. The kinetics of the whole process must be fast in order to rapidly form the final compound once the reaction is triggered. This is of particular importance when developing prodrugs. Indeed, in an open system, molecular motion affects the concentration profiles. Hence, co-localizing product liberation with precursor activation at the concentration of the non-activated precursor (a much sought after goal in the prodrug design) is kinetically constrained: the fastest activation and self-assembly chemistry must be therefore found.

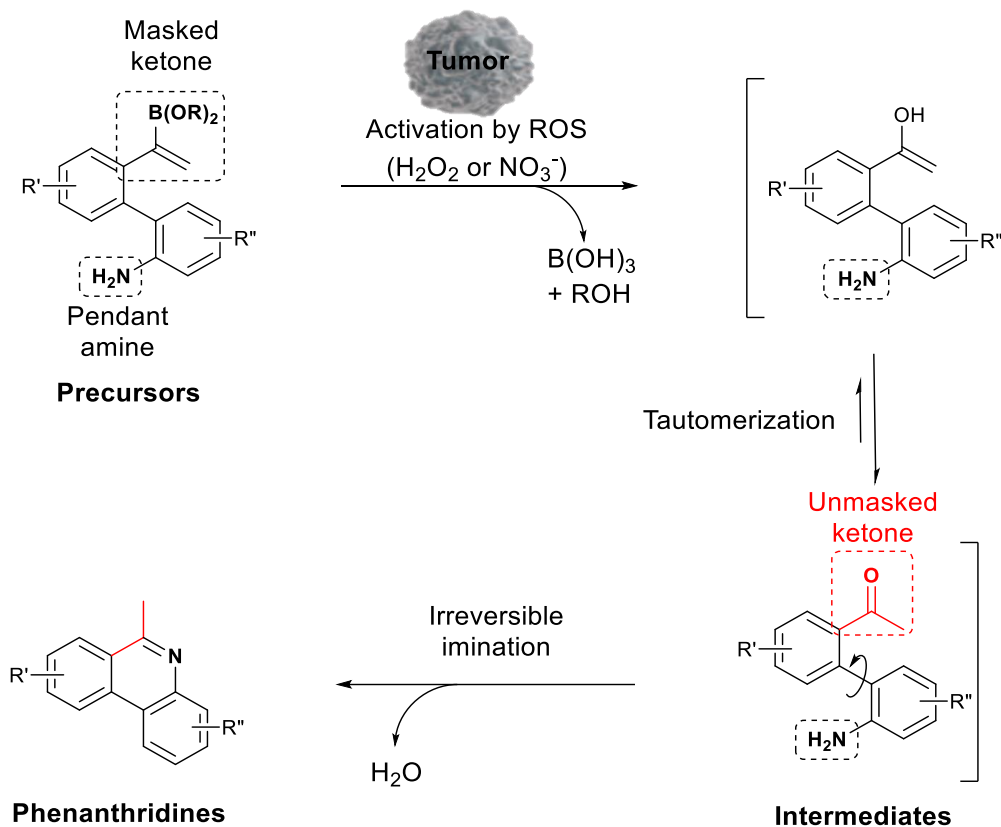
As discussed in chapter 1, the reactive oxygen species (hydrogen peroxide or peroxyinitrite) overproduction in cancer cells is a common way of anticancer prodrug activation. Boronic acid precursors are oxidized into corresponding alcohols and these precursors were largely designed to generate phenols (scheme 30). However, vinyl boronic precursors were less studied, in particular, the goal of generating a ketone function starting from such motif was not

previously described. Indeed, in the presence of ROS, the vinyl boronic acid would be transformed into an enol moiety tautomerizing into its keto equivalent.



**Scheme 30.** Strategy to generate either an electrophile or a nucleophile from boronic acids. In the presence of ROS, delocalization of  $\pi$  electrons can generate a nucleophile starting from arylboronic acid or an electrophile can be generated from a vinylboronic acid by transformation into enol tautomerizing into ketone.

Due to the strong interest of Raphaël Labruere's group in boronic acid-containing prodrugs, we decided to focus our strategy toward insertion of a vinyl boronic acid motif into our precursor scaffold. The designed prodrugs of phenanthridine would thus contain one masked ketone (vinyl boronic acid motif). Once the ketone is selectively unmasked in the tumor microenvironment, this latter group would react with a pendant amine function to build up an imine bond finally shaping the non-hydrolysable phenanthridine scaffold (scheme 31).

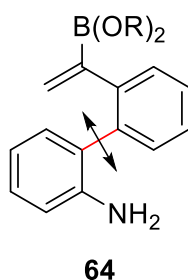


**Scheme 31.** Generation of anticancer agents from ring-opened precursors through bioorthogonal cyclization. In lieu of the chemical modification of the existing drug, the ring-opened antitumor prodrug displaying a spatial structure markedly distinct from the drug is designed to cyclize in cancer cells to finally synthesize the antitumor agent. Interaction of this prodrug with the biological target is extremely unlikely.

**Chapter 3: Preparation of the  
model biaryl precursor ProPhen  
and kinetics of transformation  
into the 6-methylphenanthridine  
Phen**

## 1.Synthesis of biaryl precursor ProPhen

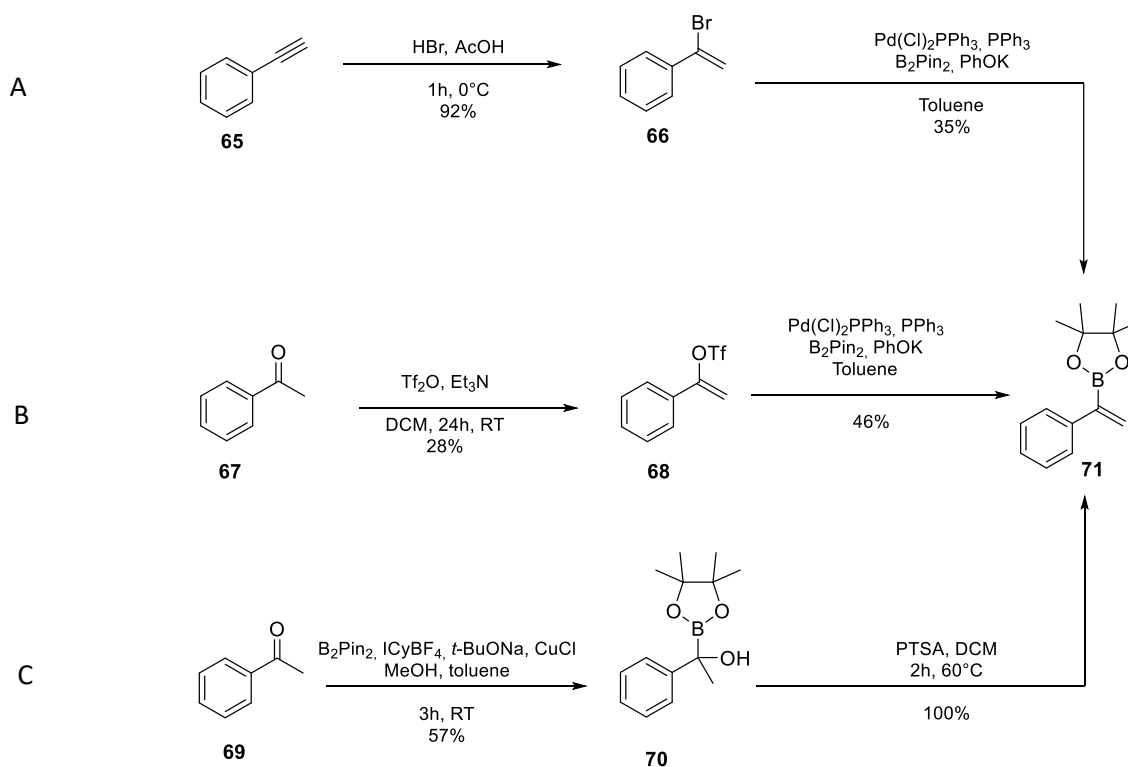
In our strategy for the preparation of the biaryl precursor **ProPhen** (able to generate phenanthridine **Phen** after activation), we envisioned the synthesis of each aryl moiety bearing the appropriate substituents and subsequent bonding of these two units by a palladium catalyzed coupling reaction (Scheme 32).



**Scheme 32.** Disconnection envisioned for the preparation of **ProPhen**.

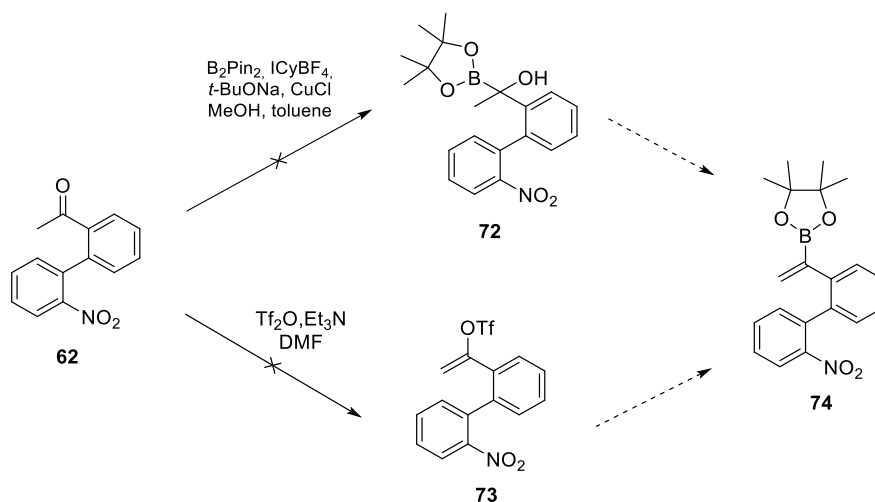
We first investigated the possible synthetic pathways to generate 1-phenylvinylboronic motif from phenylacetylene **65** (synthetic pathway **A**) or from acetophenone (synthetic pathway **B** and **C**) (Scheme 33).

- The synthetic pathway **A** allowed to obtain the vinyl boronate in two steps from phenylacetylene **65**: the first step consisted to the  $\alpha$ -bromination of phenylacetylene using the protocol of Dong et al.<sup>167</sup> with HBr in acetic acid as solvent to generate a mixture of  $\alpha$ -bromo styrene **66** in 92% yield. The  $\alpha$ -bromo styrene was engaged in boron-bromide exchange using the method of Miyaura et al.<sup>168</sup> to afford the vinyl boronate motif **71** in a global yield of 32%.
- The synthetic pathway **B** also provided the vinyl boronate **71** in two steps starting from acetophenone **67**: the first step consisted in the enol formation which was trapped using  $\text{Tf}_2\text{O}$ ,  $\text{Et}_3\text{N}$  in DCM during 24h at RT to give the triflate **68** in 28% yield. The triflate group was exchanged into boronate pinacol ester group with the method of Miyaura et al.<sup>168</sup> to give vinyl boronate motif **71** in a global yield of 13%.
- In the synthetic pathway **C**,  $\alpha$ -boryl alcohol **70** was prepared from acetophenone **69** according to the procedure involving bis(pinacolato)diboron, 1,3-bis(cyclohexyl)imidazolium tetrafluoroborate ( $\text{ICyBF}_4$ ),  $t\text{-BuONa}$  and  $\text{CuCl}$  by Hanna et al.<sup>74</sup> Subsequent dehydration reaction with  $p$ -toluenesulfonic acid (PTSA) gave vinyl boronate **71** in a global yield of 57%.



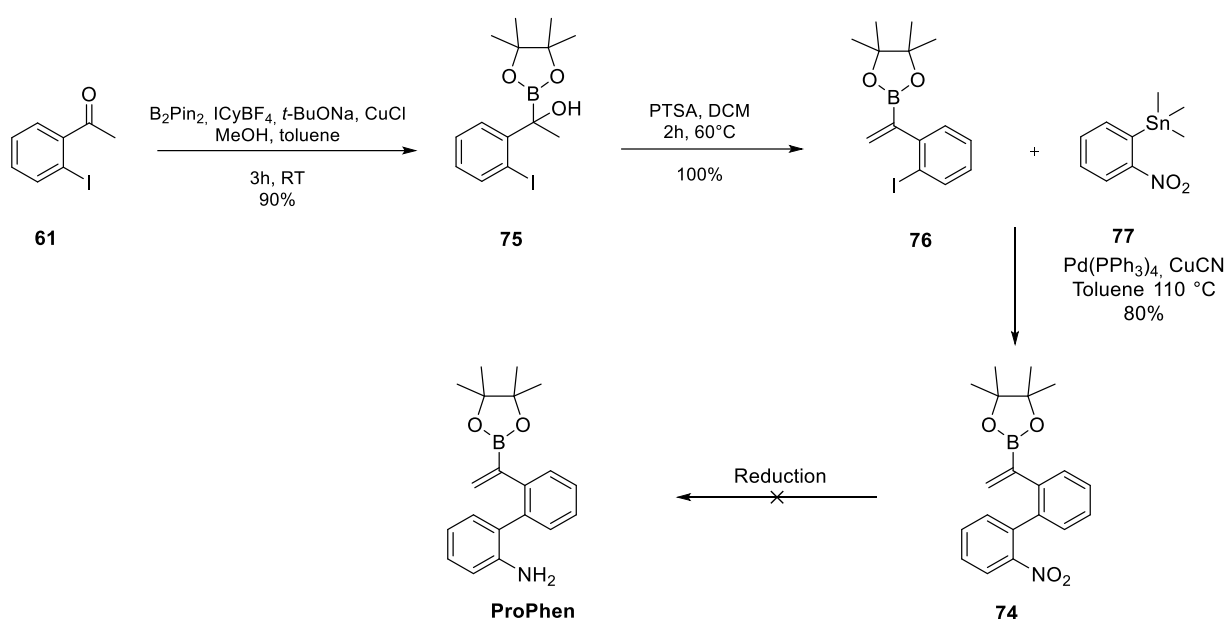
**Scheme 33.** Synthetic pathway to generate vinyl boronate **71**.

At this stage, we decided to exploit the biaryl **62** prepared as the model precursor of this project as it displays the appropriate ketone function and a nitrobenzene moiety that could be further reduced into aniline (scheme 29 and 34). We first attempted to prepare the corresponding  $\alpha$ -boryl alcohol **72** using the protocol developed by Hanna et al.<sup>74</sup> but we surprisingly observed the direct formation of the phenanthridine compound **Phen**. The second synthetic pathway consisted in the generation of the vinyl triflate derivate **73** using  $\text{Tf}_2\text{O}$  but this route was also unsuccessful.



**Scheme 34.** Synthetic pathway to generate biaryl **74**.

We then returned to our initial strategy of preparing separately both aryl moieties in order to couple these molecules in the end of the reaction. Vinyl boronate **76** was then prepared in a two-step procedure: (i) starting from iodoacetophenone **61**,  $\alpha$ -boryl alcohol **75** was obtained in excellent yield using the protocol developed by Hanna et al.<sup>74</sup> involving bis(pinacolato)diboron, 1,3-bis(cyclohexyl)imidazolium tetrafluoroborate (ICyBF<sub>4</sub>), *t*-BuONa and CuCl; (ii) Subsequent dehydration in presence of PTSA for 2 hours afforded alkene **76** in quantitative yield. Formation of biaryl **74** was achieved via a Stille coupling of the vinyl boronate **76** and (2-nitrophenyl)stannane **77** using Pd(PPh<sub>3</sub>)<sub>4</sub>, CuCN in toluene at 110°C overnight without observable traces of Suzuki homo-coupling reaction (scheme 35).



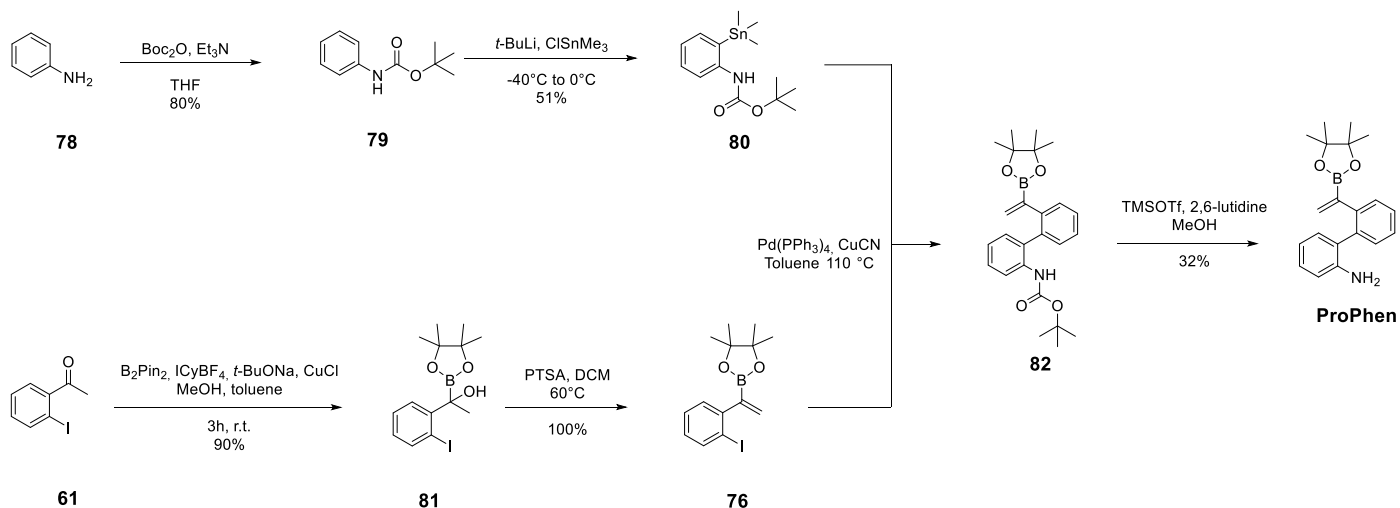
**Scheme 35.** Synthetic pathway to generate **ProPhen**.

The last step to produce **ProPhen** would be then the nitro-reduction under the conditions described in Table 5. Unfortunately, none of the employed conditions for the reduction of the nitro group afforded **ProPhen**. Again, we only obtained **Phen** as observed by TLC.

	Conditions	Results
1	Zn, NH <sub>4</sub> Cl, EtOH	<b>Phen</b>
2	Zn, NH <sub>4</sub> Cl, AcOH	<b>Phen</b>
3	Fe, AcOH	<b>Phen</b>
4	H <sub>2</sub> , Raney nickel	<b>Phen</b>

**Table 5.** Conditions used for the reduction of the nitro group.

We therefore decided to replace the nitrobenzene used in the previous synthetic scheme by a protected aniline (Scheme 36). *N*-Boc aniline **78** was treated with *t*-BuLi leading to an *ortho*-lithiated intermediate which was directly reacted with trimethyltin chloride to afford stannane **80** in 51% yield. Formation of biaryl **82** was achieved via a Stille coupling reaction with **76**. Again, we observed a total selectivity for the Stille reaction. Eventually, removal of the Boc protecting group afforded the precursor **ProPhen** in 32% yield over two steps.



**Scheme 36.** Synthetic pathway to precursors **ProPhen**.

In order to study the cyclization of precursor **ProPhen**, the corresponding product 6-methylphenanthridine **Phen** previously prepared (scheme 29) of this reaction was used as a reference product.

## 2. Cyclization analysis of ProPhen into Phen by <sup>1</sup>H NMR

Ability of precursor **ProPhen** to cyclize was first monitored by <sup>1</sup>H NMR spectroscopy in a mixture of CD<sub>3</sub>CN and deuterated PBS buffer (pH 8) using hydrogen peroxide as oxidizing agent triggering the 6-methylphenanthridine **Phen** formation. By comparing both <sup>1</sup>H NMR spectra of precursor **ProPhen** and 6-methylphenanthridine **Phen**, in particular the disappearance of the gem-hydrogens signal over time, we observed the direct conversion of precursor **ProPhen** into **Phen** (figure 15).

H<sub>2</sub>O<sub>2</sub>-mediated oxidation of the vinyl boronate moiety of **ProPhen** was followed by <sup>1</sup>H NMR performed with a Bruker avance II (<sup>1</sup>H at 600 MHz). The NMR spectrometer was programmed to acquire a spectrum of 16 scans (1 minute, 44 seconds) with a relaxation time of 2 seconds to ensure accurate integration values. Between two acquisitions, we have a timeout of two minutes (total between two acquisition = 3 minutes, 44 seconds).

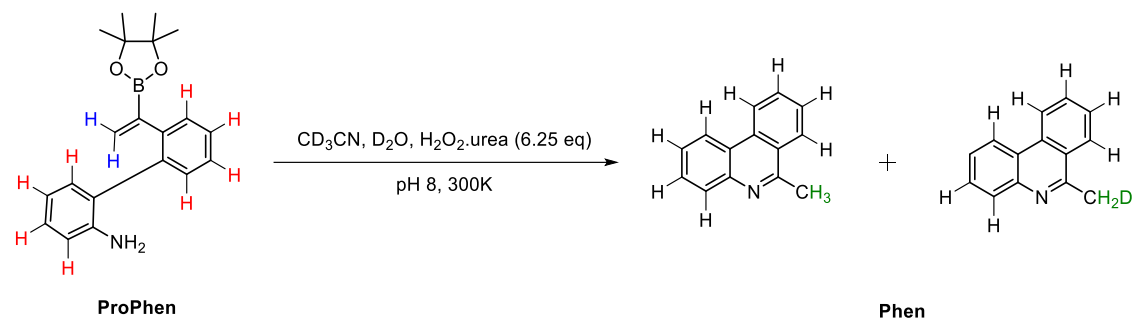
We followed the protocol described by Hanna et al.<sup>74</sup> to carry out this experiment: **ProPhen** (3.9 mg, 0.012 mmol) was dissolved in CD<sub>3</sub>CN (475 μL) then D<sub>2</sub>O (50 μL) followed by pH 8 phosphate buffer (25 μL, 0.1 M, D<sub>2</sub>O) were added. The resulting solution was transferred into a NMR tube and the oxidation was monitored at 300 K. An initial <sup>1</sup>H NMR spectra before addition of H<sub>2</sub>O<sub>2</sub>.urea was acquired to obtain the baseline of integration values. The NMR sample was treated with a solution of H<sub>2</sub>O<sub>2</sub>.urea (3.0 M, 25 μL, 6.25 equivalents), and mixing was achieved by shaking the NMR tube three times. The final concentration of **ProPhen** was 20 mM and the final concentration of H<sub>2</sub>O<sub>2</sub> was 125 mM.

In this experiment, the spectral window (8.50-0 ppm) was not large enough to encompass all of the <sup>1</sup>H NMR signals of **Phen** and among the eight aromatic protons, only six are shown (figure 15). The reaction of **ProPhen** into **Phen** can however be observed by: the disappearance of the vinyl (blue) and aromatic (red) protons signals of **ProPhen** at 6.00-5.75 ppm and 7.50-6.55 ppm respectively; the appearance of the 6-methyl (green) and six of the aromatic (black) protons signals of **Phen** at 2.95 ppm and 8.50-7.55 ppm respectively.

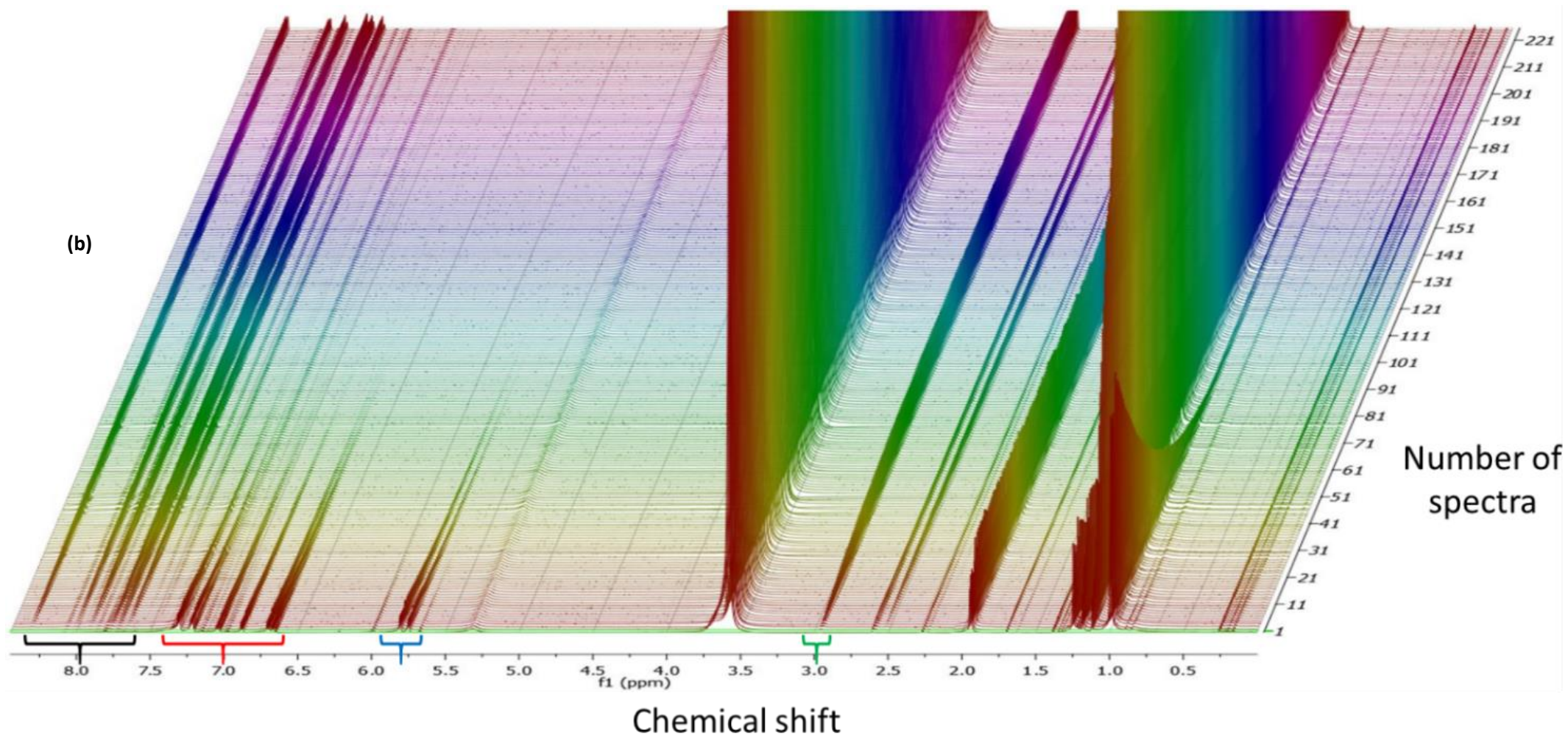
During cyclization, we observed deuterium incorporation into the methyl of **Phen**. After oxidation of the C-B bond of **ProPhen**, the subsequent hydrolysis of the C-OB bond generated two enols: one bearing a proton and the other one bearing a deuterium cation. We detected the methyl CH<sub>3</sub> as a singlet at 2.96 ppm and the CH<sub>2</sub>D as a typical triplet at 2.94 ppm which respectively integrate for ≈ 1 and ≈ 2 protons (figure 15). Therefore, the final mixture is composed of **Phen** (1/3) and its deuterated isotope (2/3). HRMS analysis confirmed the

presence of deuterated **Phen** (ESI<sup>+</sup>, m/z calculated for C<sub>14</sub>H<sub>11</sub>DN, [M+H]<sup>+</sup>: 195.1027, found: 195.1024).

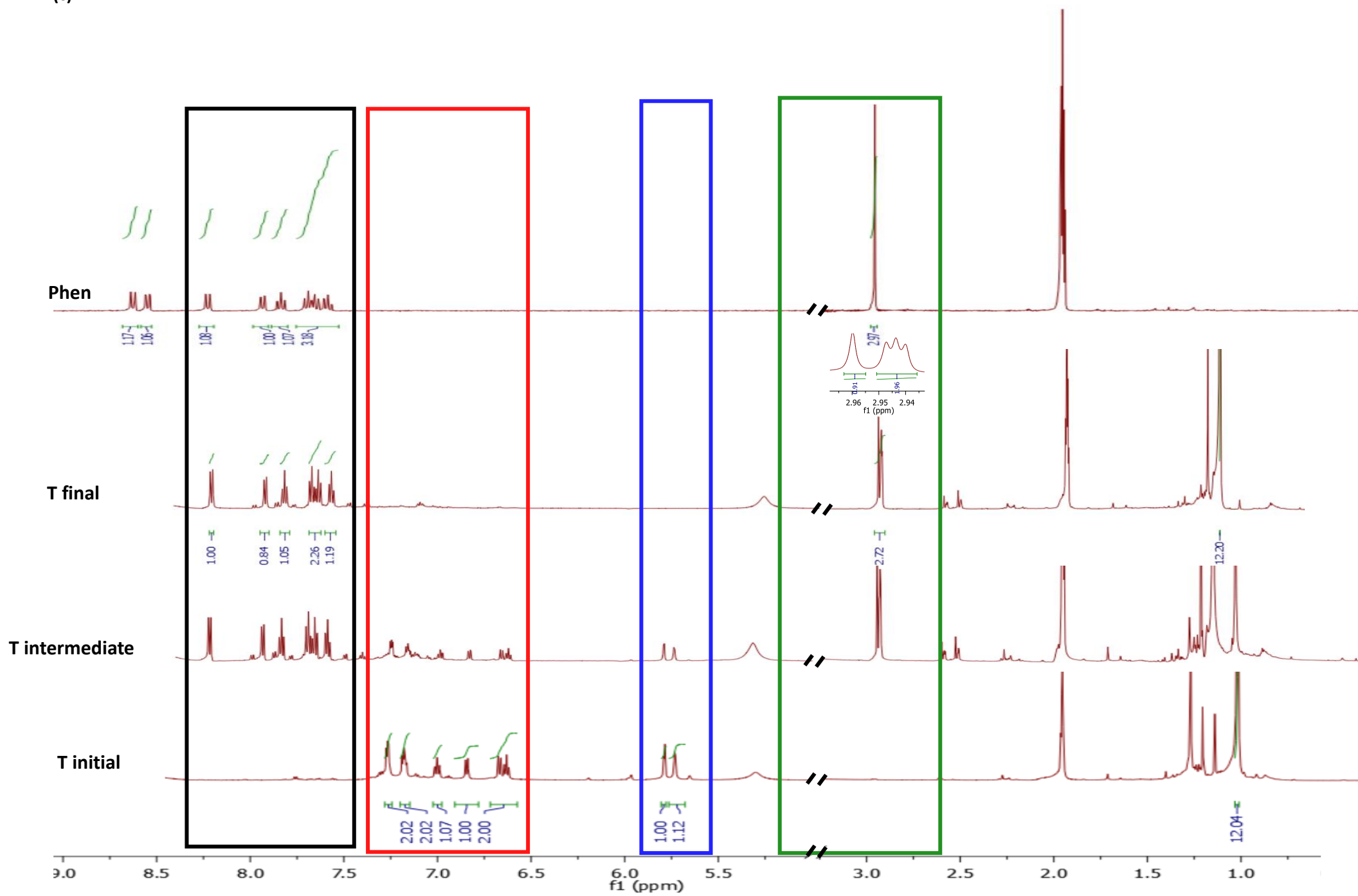
(a)



(b)



(c)



(d)

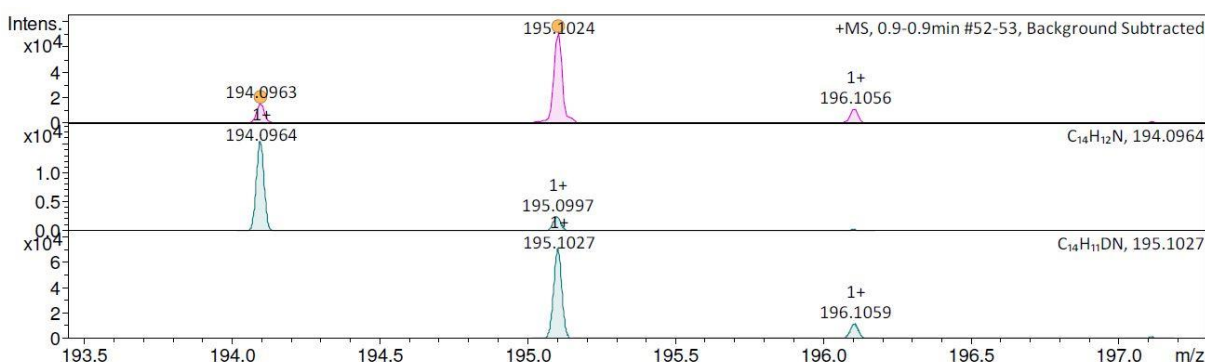
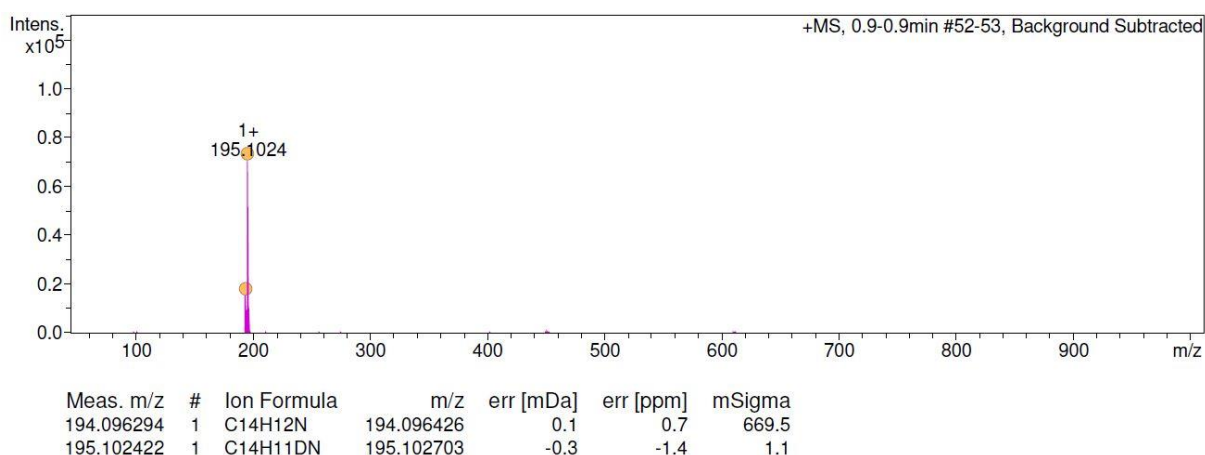


**Figure 15.** Oxidation of **ProPhen** into **Phen** and its deuterated isotope with 6.25 equivalents of  $\text{H}_2\text{O}_2$ . **a:** Chemical reaction and structures; **b:** Alignment of  $^1\text{H}$  NMR spectra recorded every two minutes; **c:** Extraction of initial, intermediate (#50), final spectra and **Phen**; **d:** Mass spectrum of the mixture at the end of the reaction.

### 3. Kinetic analysis of phenanthridine cyclization from open biaryl precursor

Then, we launched the accurate determination of the kinetic constants of both oxidation and cyclization reactions and, advantageously, phenanthridine **Phen** is fluorescent as opposed to its precursor **ProPhen**.

The absorption spectra of **ProPhen** and **Phen** were measured in a solvent mixture:  $\text{CH}_3\text{CN}:\text{PBS buffer}:\text{DMSO}$  48.5:48.5:1 v/v/v. at  $T = 298\text{ K}$  in figure 16.

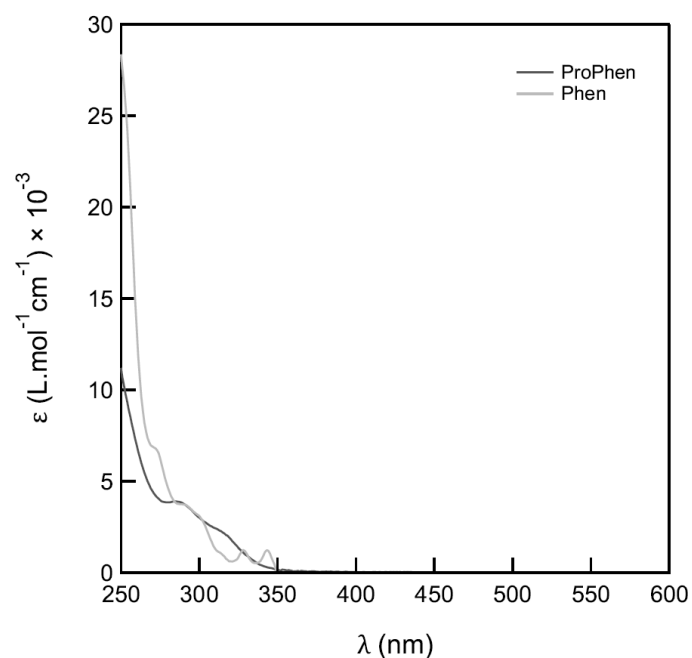


**Figure 16.** Absorption spectra of **ProPhen** (black) and **Phen** (grey).

At the excitation wavelength (300 nm) subsequently used in our kinetic experiments, the phenanthridine **Phen** would be the only species able to fluoresce under the illumination conditions used for the cuvette experiment. The emission spectra upon one-photon excitation of **ProPhen** and **Phen** upon illuminating at  $\lambda_{\text{exc}} = 300$  nm were recorded (figure 17). Solutions for fluorescence measurements were adjusted to concentrations such that the absorption maximum was below 0.15 at the excitation wavelength.

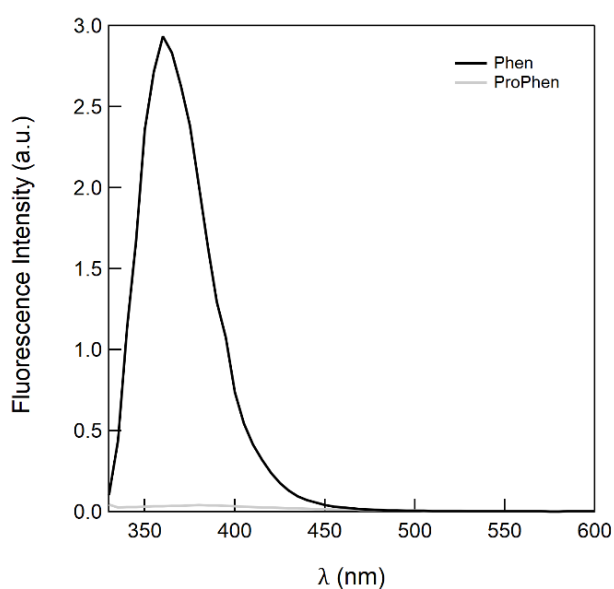
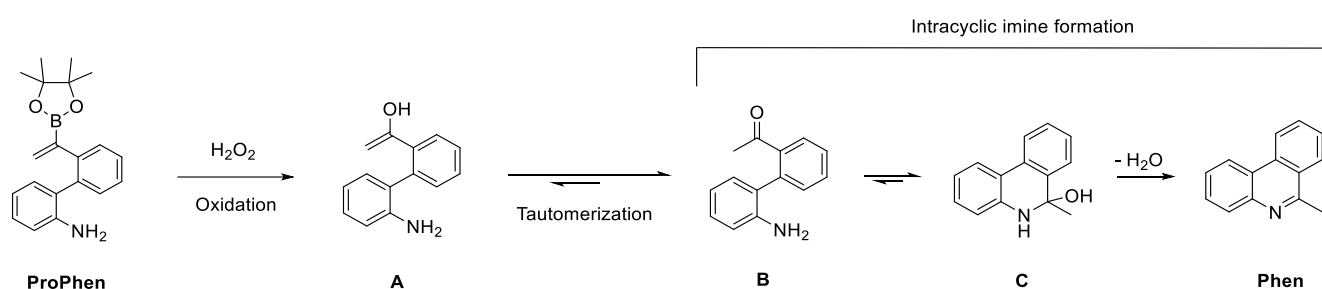


**Figure 17.** Emission spectra of **ProPhen** (grey) and **Phen** (black) upon illuminating at  $\lambda_{\text{exc}} = 300$  nm.

### 3.1 ProPhen oxidation and subsequent cyclization into Phen

The kinetic analysis of the phenanthridine assembly following oxidation of the C-B bond, tautomerization and subsequent imination has been performed and validated stepwise. We analyzed the most general kinetic scheme relevant for the open precursors. The kinetic analysis of oxidation-cyclization was performed using **ProPhen** conversion into **Phen** in presence of hydrogen peroxide (scheme 37).

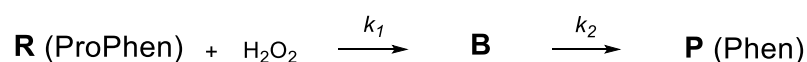


**Scheme 37.** ProPhen conversion into Phen with H<sub>2</sub>O<sub>2</sub> as oxidizing agent.

The oxidative cleavage of the boronate ester moiety initiates the cascade of reactions. The enol tautomerizes into its keto counterpart that subsequently undergoes an intramolecular imine formation by reaction with the pending aniline group. Note that the intermediate **C** leads to a stable aromatized phenanthridine.

### 3.2 Theoretical model

The tautomerization reaction is expected to occur below the millisecond time scale.[6] A fast equilibrium is also assumed for the attack of aniline on the keto group of the acetophenone. Therefore, it is relevant to analyze the formation of **Phen** from **ProPhen** via the cascade of two reactions shown in scheme 38.



**Scheme 38.** Reduced kinetic model for the conversion of ProPhen into Phen with H<sub>2</sub>O<sub>2</sub> as oxidant.

The set of differential equations governing the evolution of the concentration in the species shown in scheme 37 is given in Eqs.(1-3):

$$\frac{dR}{dt} = -\kappa_1 R \quad (1)$$

$$\frac{dB}{dt} = \kappa_1 R - k_2 B \quad (2)$$

$$\frac{dP}{dt} = k_2 B \quad (3)$$

with the additional conservation law

$$R_0 = R + B + P \quad (4)$$

since the system is closed. In Eqs. (1-4), R and P respectively designate **ProPhen** and **Phen**, and  $k_1 = \kappa_1[\text{H}_2\text{O}_2]$  where the concentration  $[\text{H}_2\text{O}_2]$  is assumed to be constant since  $\text{H}_2\text{O}_2$  is in excess of the R, B, and P species.

In the most general case, the rate constants  $\kappa_1$  and  $k_2$  are different and the solutions of Eqs.(1-3) are given in Eqs.(5-7):

$$\frac{R(t)}{R_0} = e^{-\kappa_1 t} \quad (5)$$

$$\frac{B(t)}{R_0} = \frac{\kappa_1}{k_2 - \kappa_1} (e^{-\kappa_1 t} - e^{-k_2 t}) \quad (6)$$

$$\frac{P(t)}{R_0} = 1 - \frac{k_2 e^{-\kappa_1 t} - \kappa_1 e^{-k_2 t}}{k_2 - \kappa_1} \quad (7)$$

In the case  $k_2 \gg k_1$ , this set of equations transforms into Eqs.(8-10) at  $t \gg 1/k_2$ .

$$\frac{R(t)}{R_0} = e^{-\kappa_1 t} \quad (8)$$

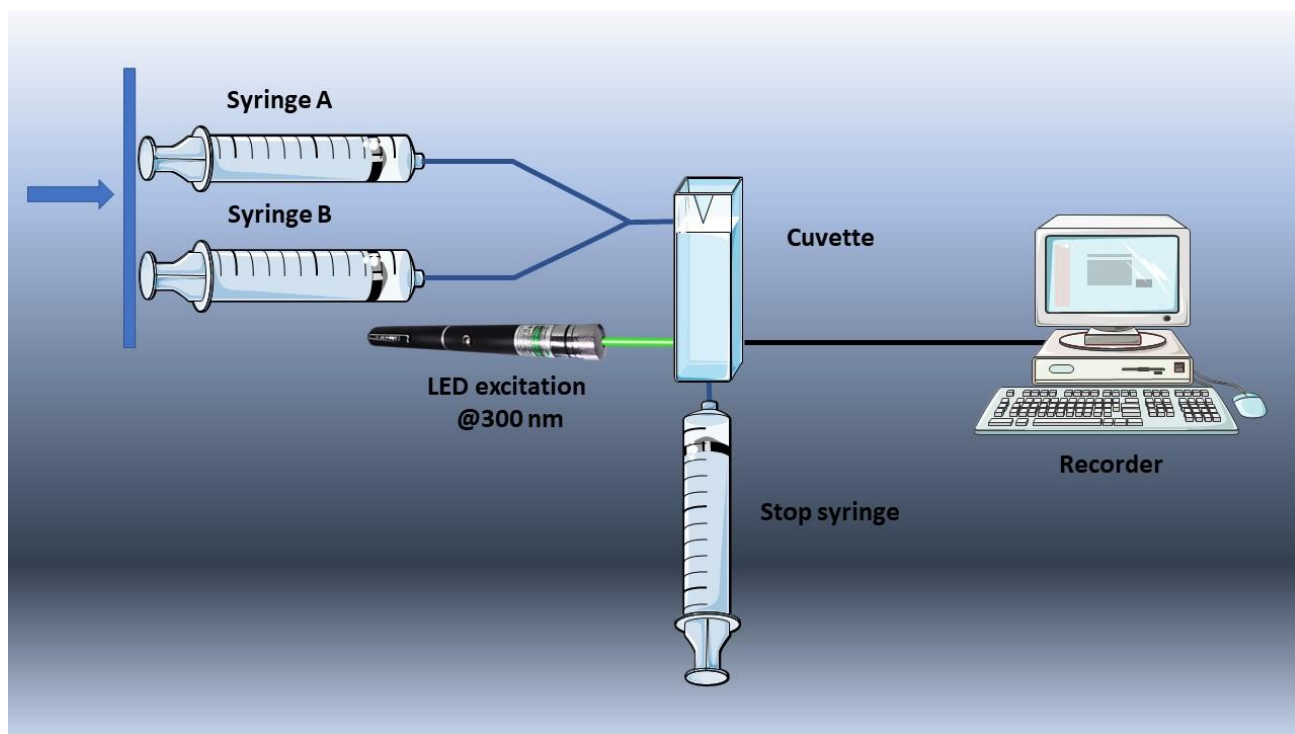
$$\frac{B(t)}{R_0} \approx 0 \quad (9)$$

$$\frac{P(t)}{R_0} = 1 - e^{-\kappa_1 t} \quad (10)$$

### 3.3 Experimental result

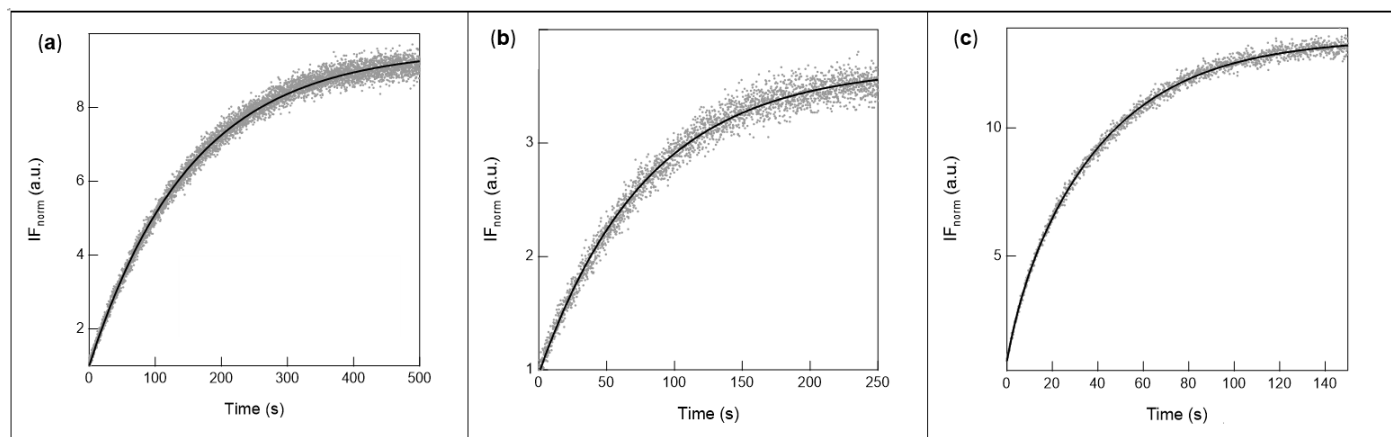
For this study, we devised a stopped-flow fluorescence spectrometry experiment (scheme 39) to analyze the kinetics of **Phen** formation initiated by hydrogen peroxide addition to precursor **ProPhen**.

The syringe A contains **ProPhen** and syringe B contains a solution of  $\text{H}_2\text{O}_2$  at different concentrations. The solutions A and B were injected at the same time in the cuvette. With our equipment, the temporal resolution reaches 10 ms.



**Scheme 39.** Stopped flow method.

With this method, we recorded the temporal evolution of the fluorescence signal from a  $0.5 \mu\text{M}$  solution of **ProPhen** in PBS:DMSO 99:1 v:v (pH 7.4) at  $25^\circ\text{C}$  with various  $\text{H}_2\text{O}_2$  concentrations to rely on a global fit to extract the kinetic constants (Figure 18).



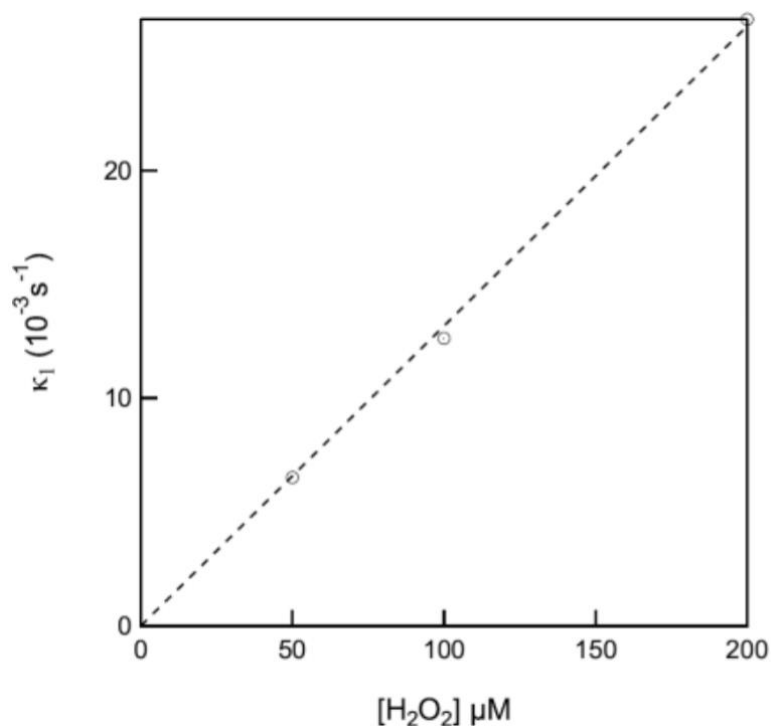
**Figure 18.** Temporal evolution of the fluorescence emission at  $\lambda_{em} = 365$  nm of a  $0.5 \mu\text{M}$  **ProPhen** solution upon addition of  $\text{H}_2\text{O}_2$  at various concentrations at 298 K: **a:**  $50 \mu\text{M}$ ; **b:**  $100 \mu\text{M}$ ; **c:**  $200 \mu\text{M}$ . Grey dots: experimental data; black solid line: fit with Eq. 11. From the fits, we retrieved  $\kappa_1$  values equal to  $6.5 \times 10^{-3} \pm 2.1 \times 10^{-5}$ ,  $1.26 \times 10^{-2} \pm 9 \times 10^{-5}$ , and  $2.6 \times 10^{-2} \pm 1.0 \times 10^{-4} \text{ s}^{-1}$  at 50, 100 and 200  $\mu\text{M}$   $\text{H}_2\text{O}_2$  at 298 K. Solvent: PBS buffer:DMSO 99:1 v/v (pH 7.4). T = 298 K.

Figure 18 displays the temporal evolution of the fluorescence emission originating from adding various concentrations of  $\text{H}_2\text{O}_2$  to a continuously illuminated  $0.5 \mu\text{M}$  solution of **ProPhen** at 298K using the stopped-flow apparatus. As anticipated, an increase of fluorescence emission was observed, which is associated to the formation of the fluorescent phenanthridine **Phen**.

For a total absorbance lower than 0.15 (as in the present series of experiments), fluorescence emission is proportional to the sum of the contributions of the fluorescent components, which are individually proportional to their respective concentrations. By neglecting the contributions of non-absorbing and non-emissive species, we derived:

$$I_F^P(t) = \alpha Q_P P(t) \quad (11)$$

The temporal evolution of the fluorescence signal was satisfactorily adjusted with Eqs. (10,11). In particular, the relevance of Eq.(10) suggests to be in a kinetic regime such that acquisition is performed with  $t \gg 1/k_2$ . Since we used a 100 Hz acquisition frequency, we deduced  $k_2 \gg 10^2 \text{ s}^{-1}$ .



**Figure 19.** Dependence of  $k_1$  on  $\text{H}_2\text{O}_2$  concentration. Solvent: PBS buffer:DMSO 99:1 v/v (pH 7.4).  $T = 298 \text{ K}$ .

As we monitor the steps occurring beyond the millisecond, we reduced the preceding reactive scheme from three to two steps considering that tautomerization reactions typically occur at the sub-millisecond time scale.<sup>169</sup> In the corresponding reduced scheme, the rate constant  $k_1$  was associated to oxidation of the C-B bond whereas  $k_2$  refers to the cyclization step. Satisfactory fits (figures 18 and 19) were obtained and we analyzed the dependence of  $k_1$  on the  $\text{H}_2\text{O}_2$  concentration, which led us to retrieve  $k_1 \sim 130 \text{ M}^{-1}\cdot\text{s}^{-1}$ . This value indicates a rate of oxidation by hydrogen peroxide of the vinyl boronate ester motif enhanced by a factor  $10^2$  in comparison with the intensively studied benzene boronate esters ( $1\text{-}2 \text{ M}^{-1}\cdot\text{s}^{-1}$ ).<sup>170</sup> Then, we extracted  $k_2 > 10^2 \text{ s}^{-1}$  which represent a time of assembly ( $\tau_2 = 1/k_2$ ) below **10 ms**.

# **Chapter 4: Preparation of 6-methylphenanthridines and identification of the cytotoxic ToxPhen**

## 1. Introduction

Phenanthridines are an important class of heterocyclic compounds that have attracted much attention due to their medicinal importance (figure 20).<sup>171–173</sup> Indeed, molecules containing the phenanthridine motif were the subject of numerous studies as antitumor agents,<sup>165,174,175</sup> antiparasitic agents, and antibacterial agents.<sup>176</sup> The mode of action of these alkaloids is characterized by their potency as topoisomerase I inhibitors and DNA intercalating agents. Furthermore, ethidium bromide (figure 20) is a widely used fluorescent markers of both DNA and RNA and was also studied for its potential pharmacological activity but its mutagenic property interrupted further study. As of today, no phenanthridines are currently used in clinic due to the general toxicity observed for these structures.

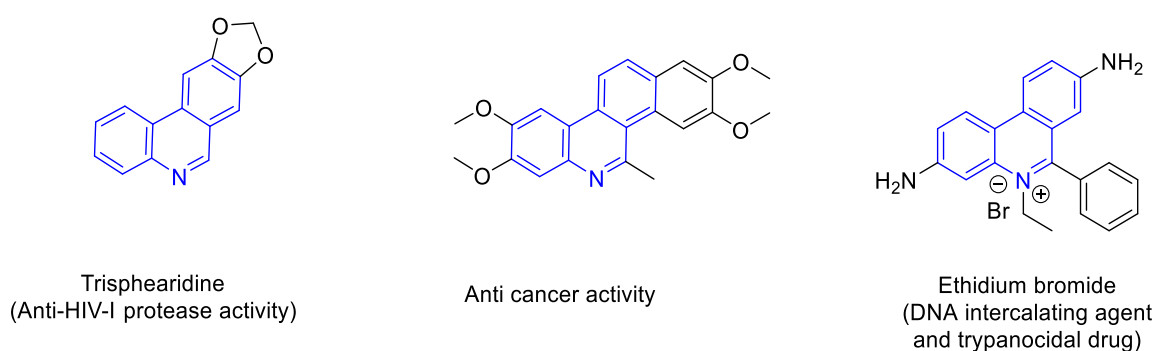


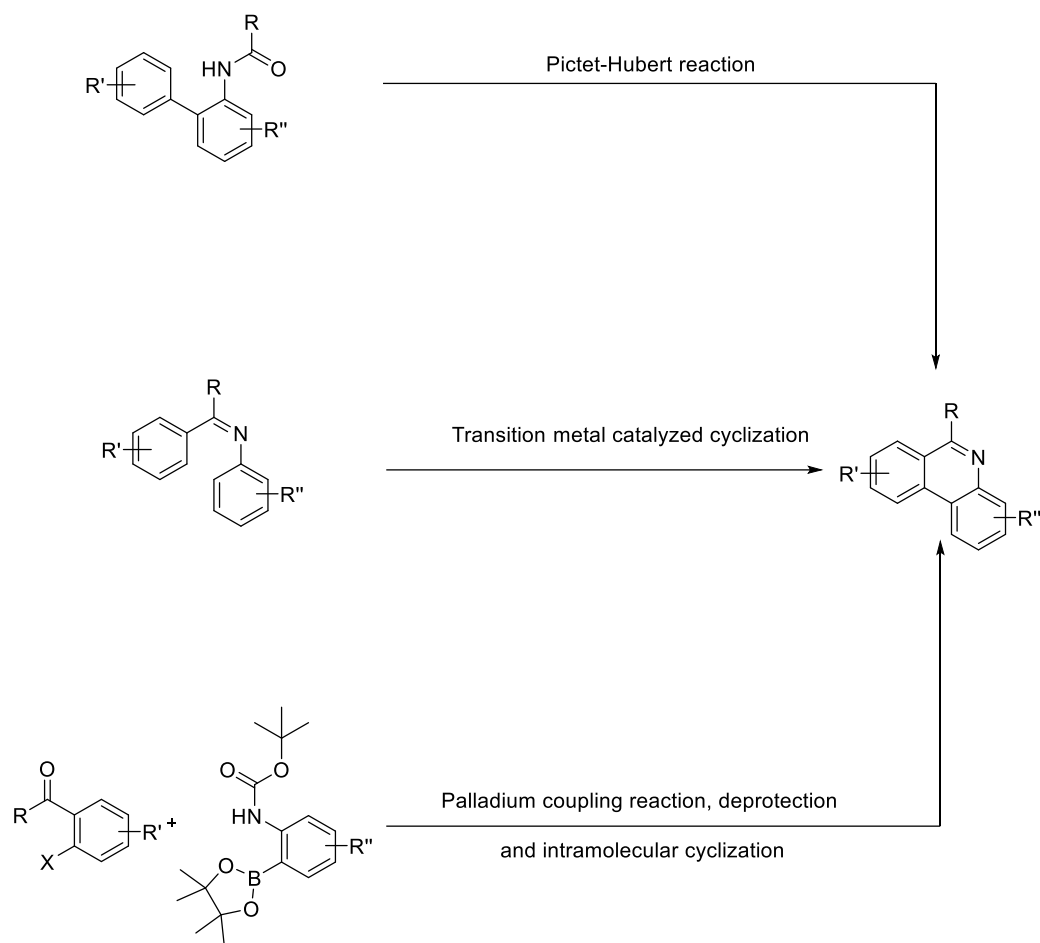
**Figure 20.** Bioactive phenanthridines.

As seen in chapter 2 and 3, in our strategy, only 6-methylphenanthridine derivatives can be produced as potential drug based on the internal imination reaction between an aniline and an acetophenone. In order to identify a toxic 6-methylphenanthridine, we decided to prepare several derivatives bearing various substituents and evaluate their cytotoxic activity against KB 3.1 cells, a cancer cell line frequently used to ascertain the activity of phenanthridines.<sup>175,177,178</sup>

## 2. Synthesis

Due to their versatile applications, the development of new methodologies for the preparation of substituted phenanthridines was the subject of vigorous research (scheme 40). The Pictet-Hubert reaction is carried out at high temperatures which has limited the application of this method for the preparation of variously substituted phenanthridines<sup>179,180</sup>. Other approaches to synthesize phenanthridines have been developed using transition metal,<sup>181–184</sup> cycloaddition,<sup>185–187</sup> and intramolecular cyclization.<sup>188–192</sup> Recently, Ge et al. have developed a

one pot synthesis of phenanthridine via a Suzuki palladium coupling followed by a *N*-Boc deprotection and intramolecular cyclization by imination (scheme 40).<sup>193</sup>



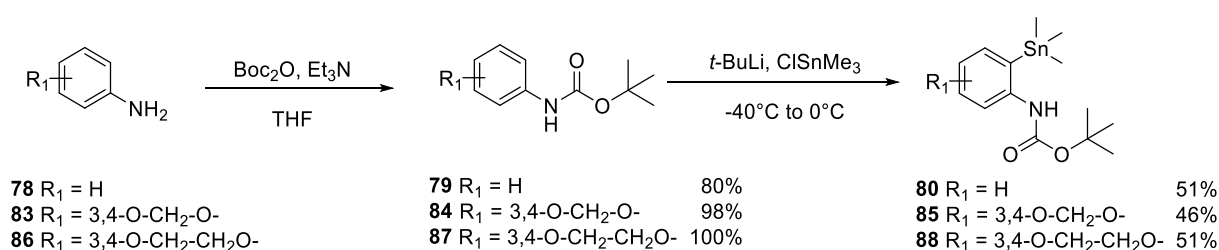
**Scheme 40.** Methods to generate phenanthridine derivatives.

We then became interested in that straightforward method for the generation of 6-methylphenanthridines. In our strategy, the prodrug is bearing a vinyl boronate moiety and the preparation of our phenanthridine prodrugs cannot rely on a Suzuki reaction. We therefore decided to adapt this method using a Stille coupling for the synthesis of the biaryl bond (scheme 41). The choice of the 6-methylphenanthridines substituents in this study was mainly guided by the abundant reported cytotoxicity results from the LaVoie group.<sup>165,174,175,177,178</sup> In particular, benzannulated phenanthridines and/or the presence of alkoxy substituents were found as efficient features for anti-proliferative activity. Moreover, the di-*ortho*-substitution of the aryl building blocks of the Stille reaction was ruled out in order to enable the biaryl bond formation.



**Scheme 41.** Retrosynthetic analysis for the synthesis of 6-methylphenanthridines.

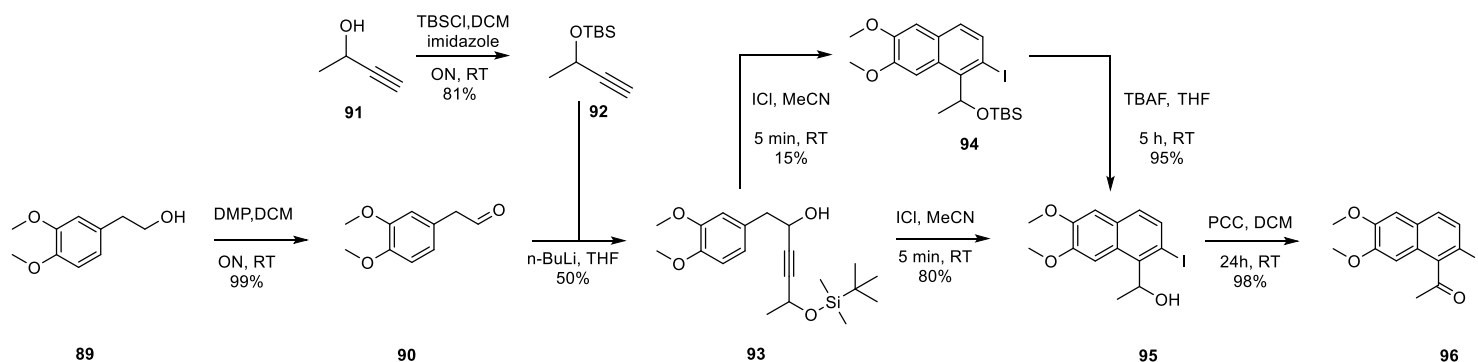
First, we synthesized the phenyl stannane building blocks **80**, **85** and **88** in two steps starting from the commercial anilines **78**, **83** and **86** (scheme 42). *N*-Boc anilines **79**, **84** and **87** were prepared in very good yield using Boc<sub>2</sub>O in THF at room temperature overnight. An *ortho*-lithiation was then carried out with *t*-BuLi followed by the addition of SnMe<sub>3</sub>Cl in freshly distilled diethyl ether to afford the protected stannanes **80**, **85** and **88** in good yield.



**Scheme 42.** Reaction pathway to phenyl stannane building blocks.

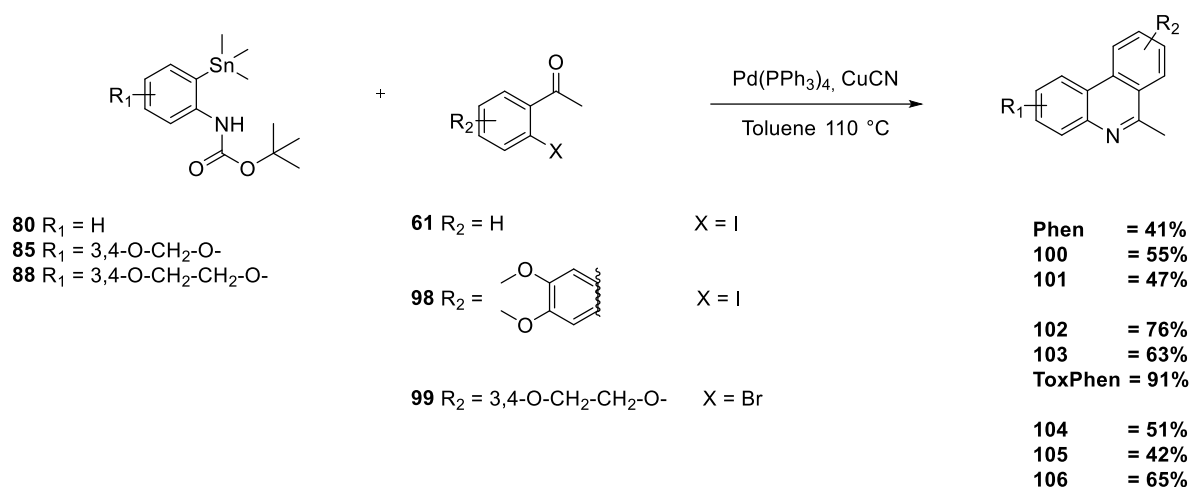
In regards to the acetophenone building blocks, the iodoacetophenone **61** and bromo-(ethylenedioxy)acetophenone **99** are commercially available except **96** which was prepared according to a convergent synthesis starting from 3,4-dimethoxyphenethyl alcohol **89** (scheme 43). The primary alcohol of **89** was oxidized with Dess-Martin periodinane reagent in dry dichloromethane to give the aldehyde **90** in excellent yield. **92** was obtained from 3-butyne-2-ol **91** which was protected with a *tert*-butyldimethylsilyl (TBS) group in 81% yield. Terminal alkyne **92** was deprotonated with *n*-BuLi in dry THF and nucleophilic addition was then performed onto compound **90** to provide alcohol **93** in 50% yield.

According to a described procedure,<sup>194</sup> the next step consisted in the iodocyclization of **93** in the presence of ICl during 5 min resulting in the formation of two products: compound **95** as unprotected iodo-naphthalene and compound **94** as TBS-protected iodo-naphthalene in 80% and 15% yield respectively. The unprotected iodo-naphthalene **95** was directly formed as HCl and H<sub>2</sub>O were generated during the reaction. The TBS group of the iodo-naphthalene **94** was finally cleaved using TFAB in THF in 95% yield. In this latter sequence, deprotected iodo-naphthalene **95** was thus obtained in 95% yield. Oxidation of the alcohol group of **95** with PCC in dry DCM at room temperature during 24h gave compound **96** in almost quantitative yield. The synthesis of ketone **96** was then achieved in 5 steps with 32% overall yield.



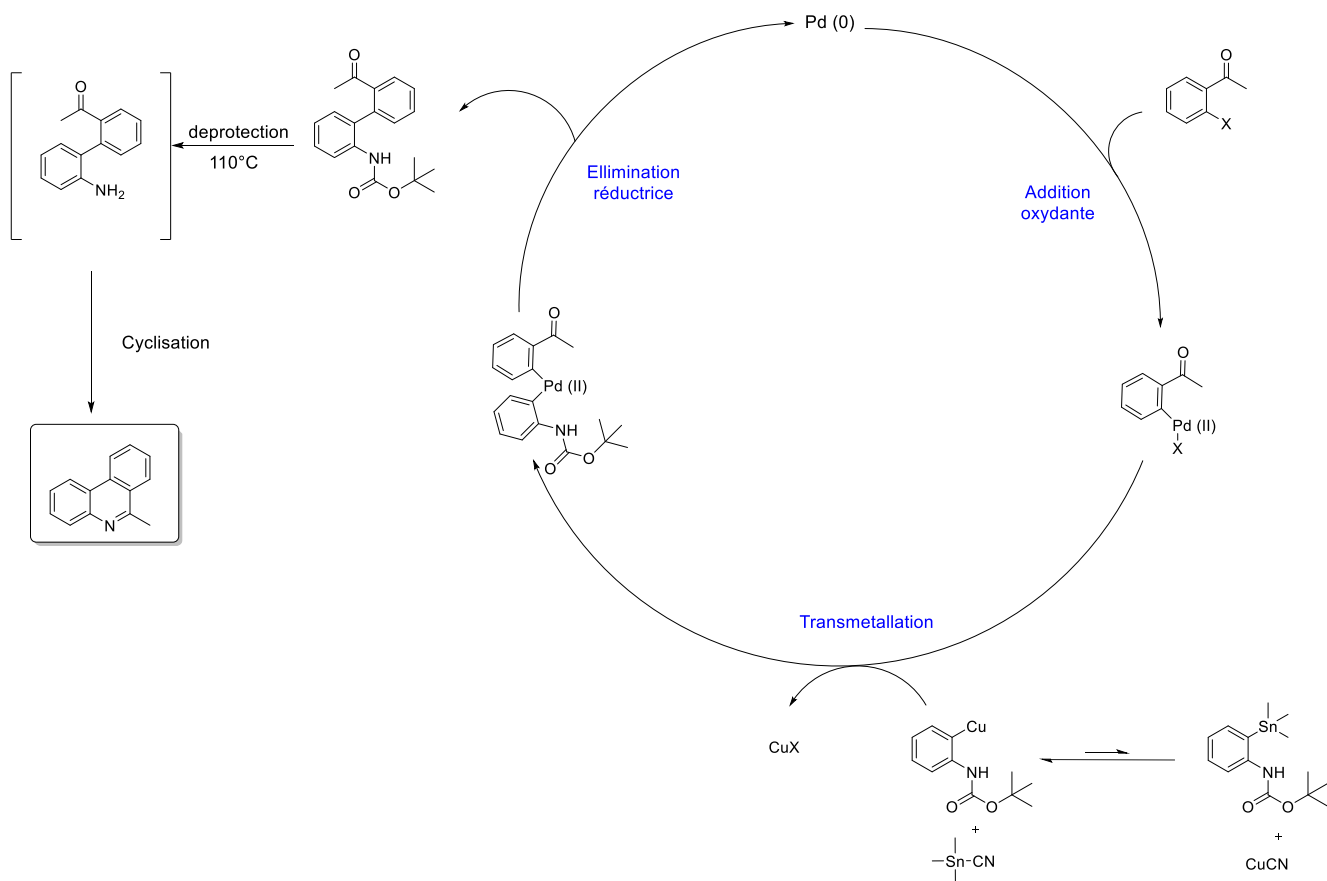
**Scheme 43.** Synthetic pathway to generate building block **96**.

The 6-methyl phenanthridines were then prepared via a three-step sequence of reaction in one pot (scheme 44): (i) biaryl coupling using Pd(PPh<sub>3</sub>)<sub>4</sub>, CuCN in freshly distilled toluene at 110°C during 24h under argon; (ii) Thermolytic deprotection of the *N*-Boc group due to the high temperature of the reaction; (iii) spontaneous cyclization by imination. In the first few hours of the reaction, we observed the formation of the biaryl with the protected amine. In order to allow the reaction to go to completion and therefore increase the yield of phenanthridine formation, the reaction must be maintained for 24 hours at 110°C.



**Scheme 44.** 6-methyl phenanthridines synthesized by one pot reaction.

In scheme 45, we detailed the different steps of this synthesis. First, a phenyl stannane undergoes a tin-copper exchange reaction.<sup>195</sup> The resulting intermediate and a 2-halogenoacetophenone will then react following a classical catalytic cycle of the Stille reaction. Then, the Boc group will be removed by thermolysis<sup>196</sup> and subsequent intramolecular cyclization between the aniline and the ketone will finally afford the 6-methylphenanthridine.

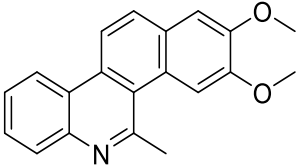
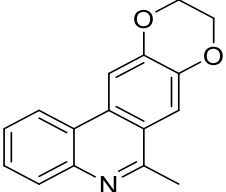
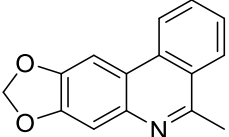
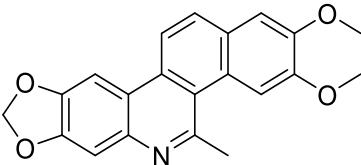
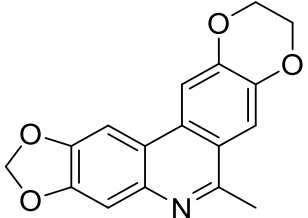
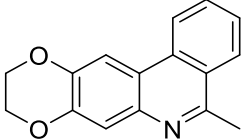
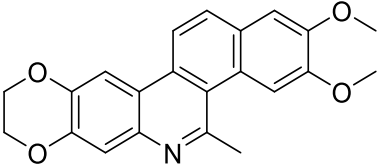
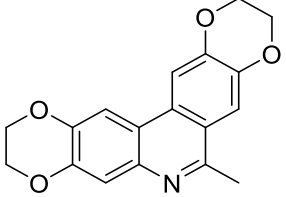


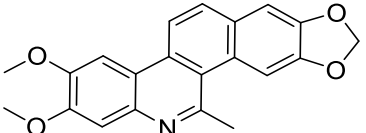
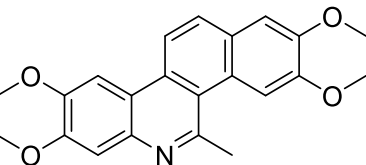
**Scheme 45.** Catalytic cycle and subsequent reactions to generate 6-methylphenanthridine one pot.

Nine different 6-methylphenanthridines were synthesized according to this method and two reportedly cytotoxic 6-methylphenanthridines **107** and **108** were also prepared using the procedure described.<sup>174</sup>

### 3. Cytotoxicity

The in vitro cytotoxicity ( $IC_{50}$ ) of the eleven 6-methylphenanthridines were evaluated on human papillomavirus-related endocervical adenocarcinoma (KB 3.1) cells, a well responsive cell line toward the activity of phenanthridines. The results are depicted in table 6.

Name	Compounds	IC <sub>50</sub>
Phen		> 50 μM
100		≈ 10 μM
101		≈ 50 μM
102		> 50 μM
103		> 10 μM
ToxPhen		670 ± 50 nM (≈ 0.7 μM)
104		≈ 50 μM
105		3.6 ± 0.1 μM
106		6.3 ± 0.4 μM

107		> 50 $\mu$ M
108		> 50 $\mu$ M

**Table 6.** Biological activity of 6-methylphenanthridines against KB 3.1 cancer cells.

We first observed that the unsubstituted 6-methylphenanthridine **Phen** was completely inactive up to 50  $\mu$ M which was the maximum concentration not exceeding **Phen** solubility limit in the assay conditions. Addition of one supplementary cycle to the latter scaffold was achieved employing either a methylenedioxy bridge **100**, an ethylenedioxy motif (**101** and **104**) or a dimethoxybenzene nucleus (**100**) but resulted in no improvement of the antiproliferative activity.

We then evaluated the two phenanthridines **107** and **108** previously reported as moderately cytotoxic but we were not able to retrieve the same level of activity whether it be on the same cell line with the methylenedioxy **107**: compare  $IC_{50}$  (KB 3.1) = 12  $\mu$ M<sup>175</sup> with  $IC_{50}$  (KB 3.1) > 50  $\mu$ M or a different cell line with **108**: compare  $IC_{50}$  (CPT-K5) = 11  $\mu$ M<sup>174</sup> with  $IC_{50}$  (KB 3.1) > 50  $\mu$ M. In our optimized protocol for the determination of cytotoxicity on KB 3.1 cell, we incubated the different compounds with the cells for three days instead of the four days mentioned in the described procedure<sup>174,175</sup> and we assume that this shorter duration of exposure to the tested compounds decreases the observed activity. In regards to **107**, isomer **103** where both the methylenedioxy motif and the dimethoxy substituents are placed on the opposite side of the phenanthridine scaffold is also inactive. However, phenanthridines **ToxPhen**, **104** and **106** substituted on both sides with at least one ethylenedioxy moiety were all cytotoxic. Interestingly, replacement of the methylenedioxy motif in **103** by an ethylenedioxy group in **105** lead to an increase of the activity. Nonetheless, it is the reverse modification from **106** ( $IC_{50} \approx 6 \mu$ M) that produced the most cytotoxic phenanthridine **ToxPhen** of this series with an activity enhanced by a factor 10 ( $IC_{50} \approx 0.7 \mu$ M). This phenanthridine has been therefore selected for the preparation of the corresponding ring-opened biaryl prodrug.

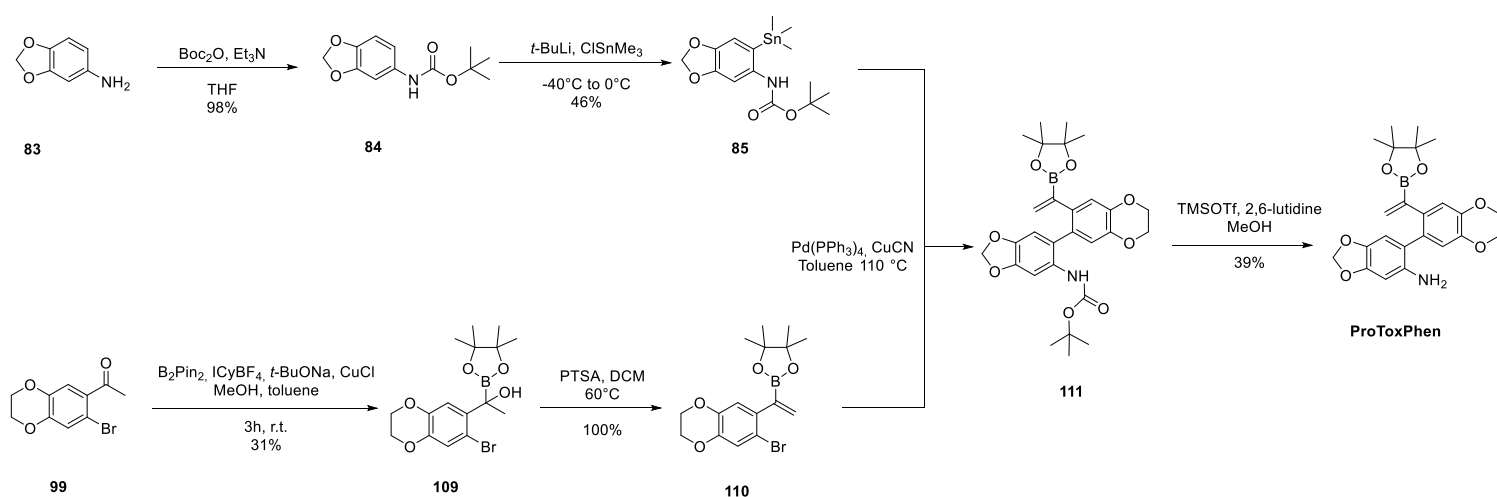
# **Chapter 5: Preparation of the biaryl precursor of ToxPhen and in-cell studies of cyclization**

Having identified a fast-cyclizing scaffold for spontaneous phenanthridine generation, we next examined the feasibility of using such reaction to generate a cytotoxic phenanthridine within tumor tissue. Beforehand, several 6-methylphenanthridines have been tested against KB cancer cells. We chose the most cytotoxic phenanthridine **ToxPhen** of our series displaying two alkoxy groups: a methylene dioxy and an ethylene dioxy.

The biaryl precursor of **ToxPhen** which we named **ProToxPhen** was thus designed based on the **ProPhen** scaffold.

## 1. Synthesis of ProToxPhen

The prodrug **ProToxPhen** of phenanthridine **ToxPhen** was prepared (scheme 46) following the same synthetic pathway devised for unsubstituted precursor **ProPhen**.



**Scheme 46.** Synthetic pathway to precursors **ProToxPhen**.

*N*-Boc methylenedioxyaniline **83** was treated with *t*-BuLi leading to an *ortho*-lithiated intermediate **84** which was directly reacted with trimethyltin chloride to afford stannane **85** in 46% yield. Vinyl boronate **110** was then prepared in a two-step procedure: (i) starting from 2'-bromo-4',5'-(ethylenedioxy)acetophenone **99**,  $\alpha$ -boryl alcohol **109** was obtained in excellent yield using the protocol developed by Hanna et al<sup>74</sup> involving bis(pinacolato)diboron, 1,3-bis(cyclohexyl)imidazolium tetrafluoroborate (ICyBF<sub>4</sub>), *t*-BuONa and CuCl; (ii) Subsequent dehydration in presence of *p*-toluenesulfonic acid (PTSA) for 2 hours afforded alkene **110** in quantitative yield. Formation of biaryl **111** was achieved via a Stille coupling reaction using Pd(PPh<sub>3</sub>)<sub>4</sub> and CuCN in toluene heated under reflux. Moreover, we observed a total selectivity

for the Stille reaction and no traces of Suzuki homocoupling reaction. Eventually, removal of the Boc protecting group afforded the precursor **ProToxPhen** in 39% yield over two steps.

## 2. Cytotoxicity experiments on KB 3.1 human cancer cells

### 2.1 In vitro cell-proliferation assays

The antitumoral activity of **ProToxPhen** was evaluated on KB cells using the same procedure devised for the cytotoxicity determination of the phenanthridines in chapter 4.

The cytotoxic activity of **ProToxPhen** was then compared to the one obtained with **ToxPhen** (figure 21).

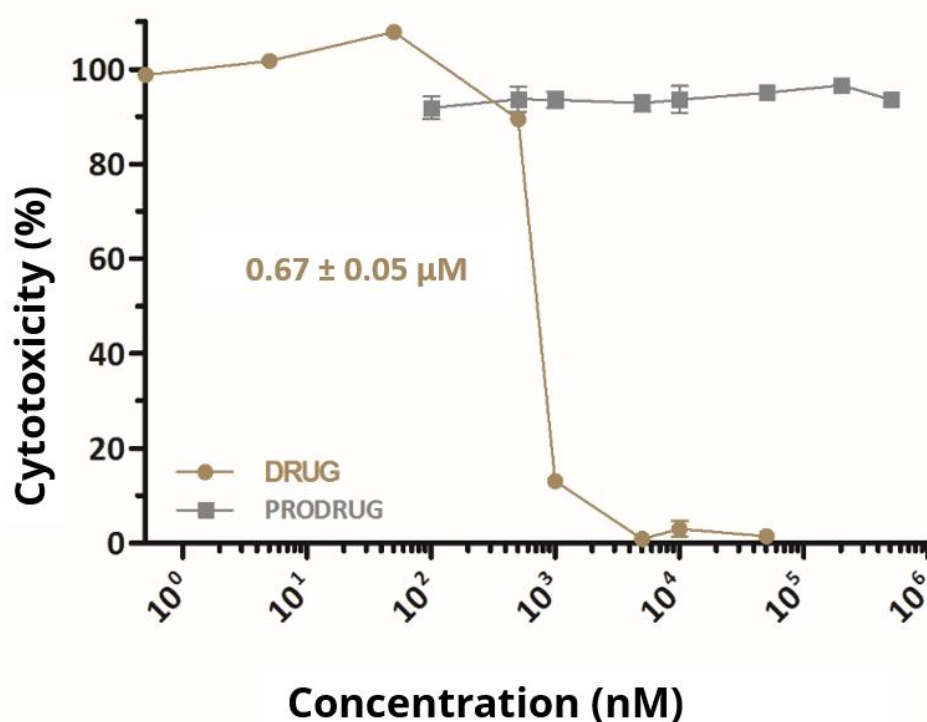


**Figure 21.** Cytotoxicity of **ProToxPhen** and **ToxPhen** on KB 3.1 cancer cells.

We observed that biaryl prodrug **ProToxPhen** activity was significantly decreased by a factor superior to 700 ( $IC_{50} > 500 \mu M$ ): considered as completely inactive in comparison to the corresponding drug **ToxPhen** ( $IC_{50} \approx 0.7 \mu M$ ).

Furthermore, the cytotoxic activity of **ProToxPhen** and **ToxPhen** was then investigated using a KB 3.1 spheroid, a 3D model of in vivo tumors<sup>197</sup>. In a round-bottom 96-well plate, 1,000 cells (100  $\mu L$ ) were seeded with 100  $\mu L$  of each compound at different concentrations (from 50  $\mu M$

to 0.05 nM for the **ProToxPhen** compound and from 500  $\mu\text{M}$  to 100 nM for the **ToxPhen** compound) and incubated at 37 °C in presence of 5%  $\text{CO}_2$  and under 95% hygrometry. After 72h, the formed KB spheroids were observed using an optical microscope (Olympus CK 2) and their morphology were imaged with a digital camera (Moticam 1000 1.3MP Live resolution) mounted on the optical microscope. The pictures were then normalized using Image J software (figure 22).

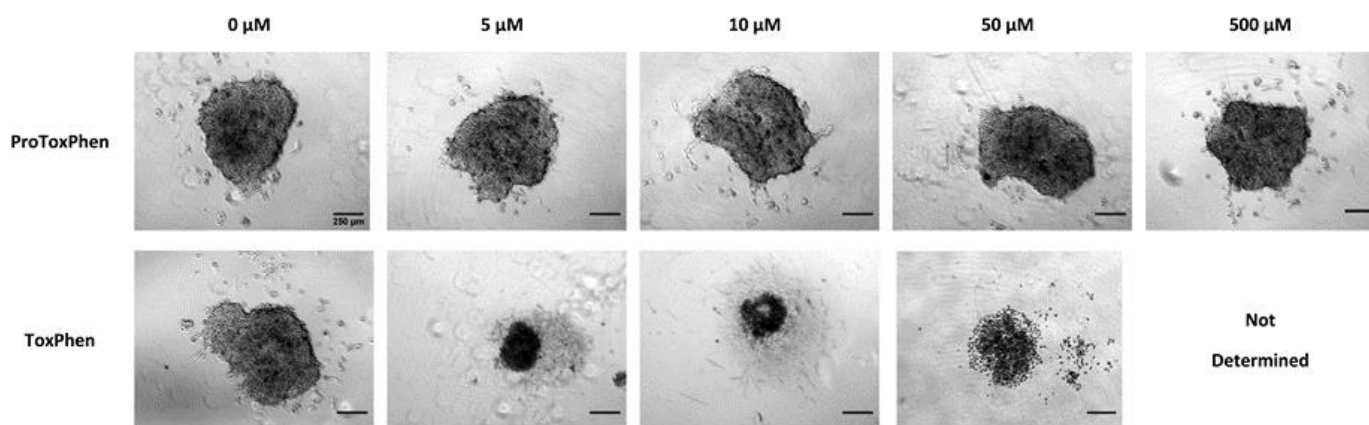


**Figure 22.** Cytotoxicity on KB spheroids in function of the tested compounds at several increasing concentrations (scale bar: 250  $\mu\text{m}$ ).

We observed that biaryl prodrug **ProToxPhen** have no activity at 500  $\mu\text{M}$  in comparison to the corresponding drug **ToxPhen** active at 5  $\mu\text{M}$ .

### 3. Conformational analysis

Such difference of pharmacological activity was expected as **ProToxPhen** displays a non-planar structure over the completely planar phenanthridine **ToxPhen**. The dihedral angle of **ProToxPhen** was then calculated from MM2 energy minimization which a dihedral angle of  $40^\circ$  ( $47.18 \text{ kcal.mol}^{-1}$ ) whereas **ToxPhen** was completely planar as expected. These data are in agreement with the reported optimal dihedral angle (ca.  $43^\circ$ ) obtained on the elementary biphenyl from MP2 calculations.<sup>198</sup> Such twist engenders a significant variation in the 3D structure of the biaryl in comparison to the phenanthridine scaffold. The molecular geometry of the open precursor is therefore drastically different from the cytotoxic phenanthridine **ToxPhen** (figure 23).

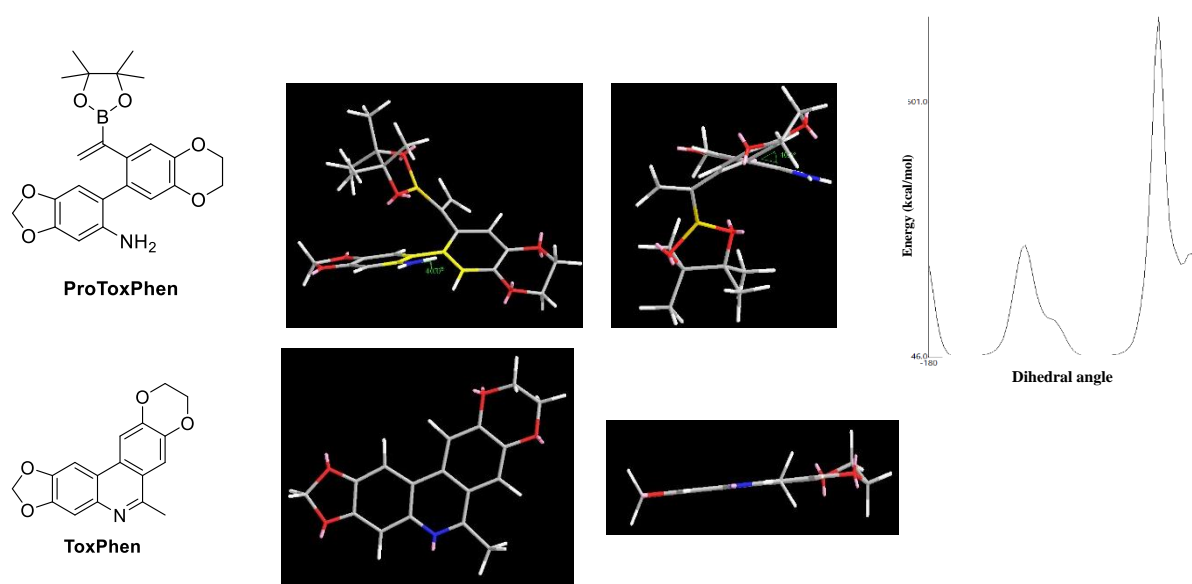


**Figure 23.** Optimized 3D representations of **ProToxPhen** and **ToxPhen** and relative conformation energy diagrams as a function of dihedral angle of **ProToxPhen**.

### 4. Live-cell imaging experiments

Modification of cell and nuclear morphologies induced by our lead compound **ToxPhen** was then observed by fluorescence microscopy.<sup>199,200</sup> We transfected U2OS cells with H2B-mCherry, a nuclear fluorescent protein marker and further monitored the shape evolution of the nucleus and whole-cell in presence of **ToxPhen** at different time intervals. To investigate the cytotoxicity of **ToxPhen**, the U2OS-H2B-mCherry cell and nuclear morphologies were observed by epifluorescence microscopy (excitation 580 nm, emission 628 nm) in presence of  $150 \mu\text{M}$  of **ToxPhen** in DPBS solution at different time intervals.

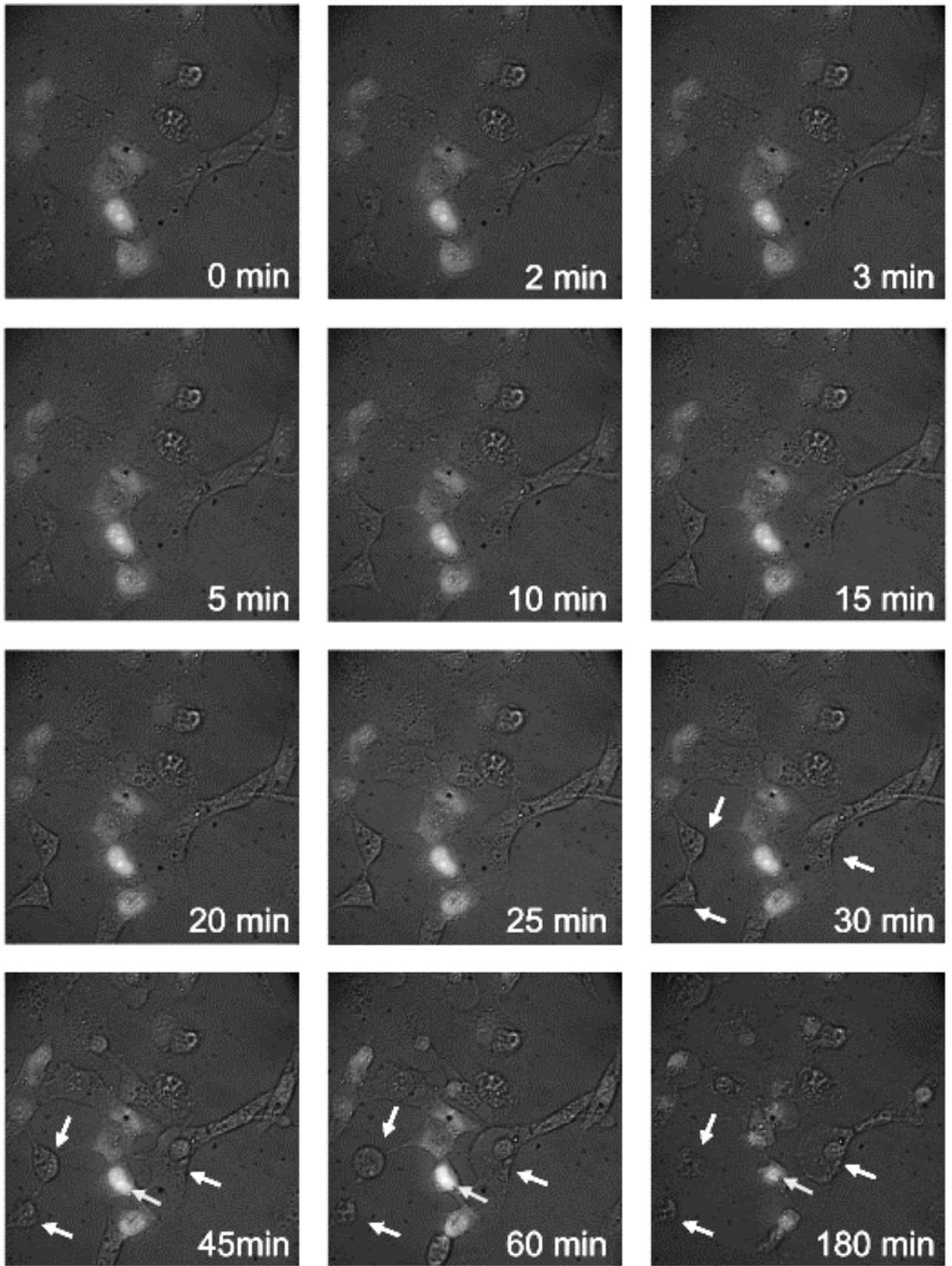


**Figure 24.** Bright field and fluorescence (mCherry channel) microscopy images (50x magnification) of U2OS cells treated with **ToxPhen** at 150 μM.

As depicted in figure 24, cell shrinkage, loss of cell–cell contact, and membrane blebbing is observed after treatment with **ToxPhen** (150  $\mu\text{M}$ ). An enhanced effect was detected after 45, 60 and 180 min incubation (white arrows). Nuclear fragmentation was also observed after 180 min of incubation (grey arrows). These whole-cell and nuclear deformations are induced by **ToxPhen** and have been pointed out to be characteristic features of cell apoptosis<sup>199,200</sup>. For this experience, we used a home-built epifluorescence microscopy set-up.

## 5. Kinetic analysis of ProToxPhen conversion into ToxPhen within KB 3.1 spheroids by video microscopy

The absorption spectra of **ProToxPhen** and **ToxPhen** were measured in a solvent mixture:  $\text{CH}_3\text{CN}:\text{PBS buffer}:\text{DMSO}$  48.5:48.5:1 v/v/v. at  $T = 298\text{ K}$  in figure 25.

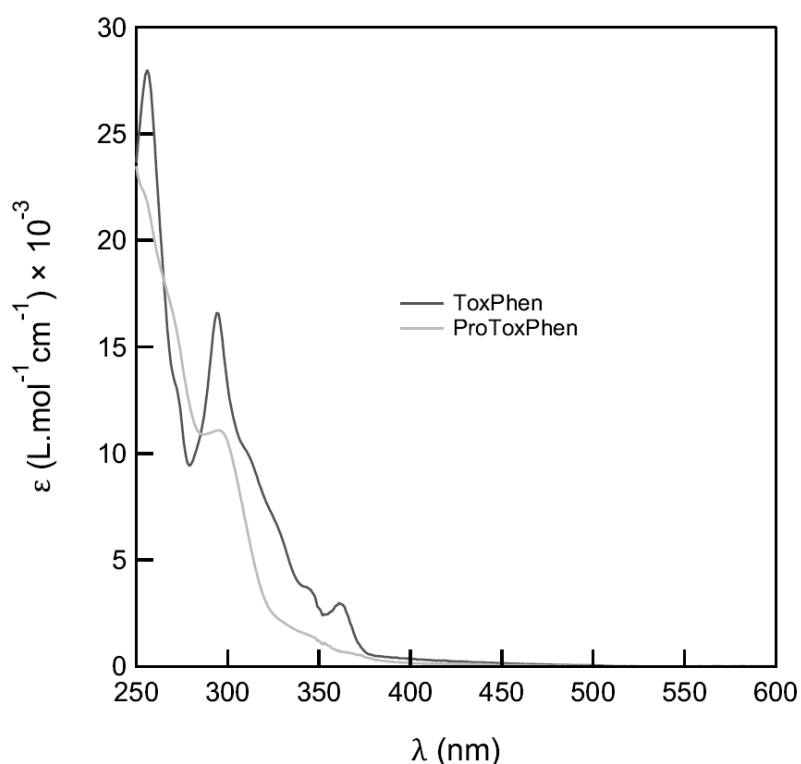


**Figure 25.** Absorption spectra of **ProToxPhen** (grey) and **ToxPhen** (black).  $\text{CH}_3\text{CN}:\text{PBS}$  buffer: $\text{DMSO}$  48.5:48.5:1 v/v/v.  $T = 298\text{ K}$ .

At the excitation wavelength (365 nm) the phenanthridine **ToxPhen** would be the only species able to fluoresce under the illumination conditions used for the in-cell kinetic experiment (see figure 26)

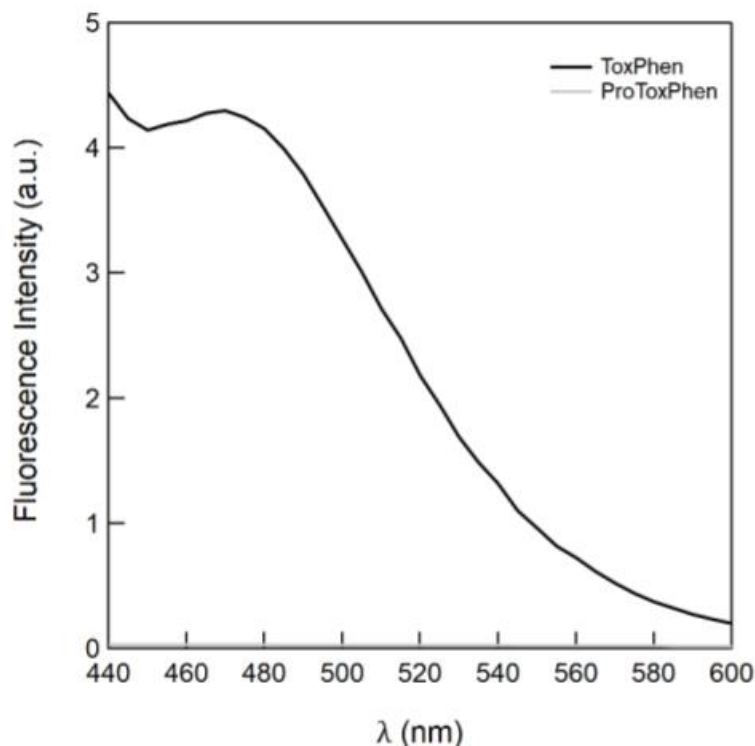


**Figure 26.** Emission spectra of **ProToxPhen** (gray) and **ToxPhen** (black) upon illuminating at  $\lambda_{exc} = 365$  nm.

- A preliminary study of the cyclization of **ProToxPhen** into **ToxPhen** was carried out in presence of KB 3.1 cells. A calibration curve using a set of standard samples of known **ToxPhen** concentrations (1% DMSO in DMEM) was assessed by reading its fluorescence intensity at  $\lambda_{exc} = 365$  nm,  $\lambda_{em} = 440$  nm with spectrofluorometer microplate reader. First, the cyclization of 50  $\mu$ M of **ProToxPhen** was performed in 1% DMSO in DMEM with 50 equivalents of  $H_2O_2$ .urea and afforded the 6-methylphenanthridine **ToxPhen** in quantitative yield. The presence of **ToxPhen** was further confirmed by HRMS. This reaction was then performed in-cell using KB 3.1 cells. In a 6-well plate, 100 000 cells/well were seeded and incubated at 37 °C in presence of 5 %  $CO_2$  and under 95 % hygrometry. After 15 h, 50  $\mu$ M of **ProToxPhen** were added (sixplicate) and further incubated for 30 minutes. The wells were treated with 50 equivalents of  $H_2O_2$ .urea and after a 6h incubation period under the same conditions, each well was sonicated three times during 5 s and 100  $\mu$ L of the supernatant was transferred in a 96-well black plate. Using the Tecan 34 microplate reader, we observed that the yield of cyclization was also quantitative indicating no cross reaction in presence of KB 3.1 cells during the generation of **ToxPhen** (figure 27).

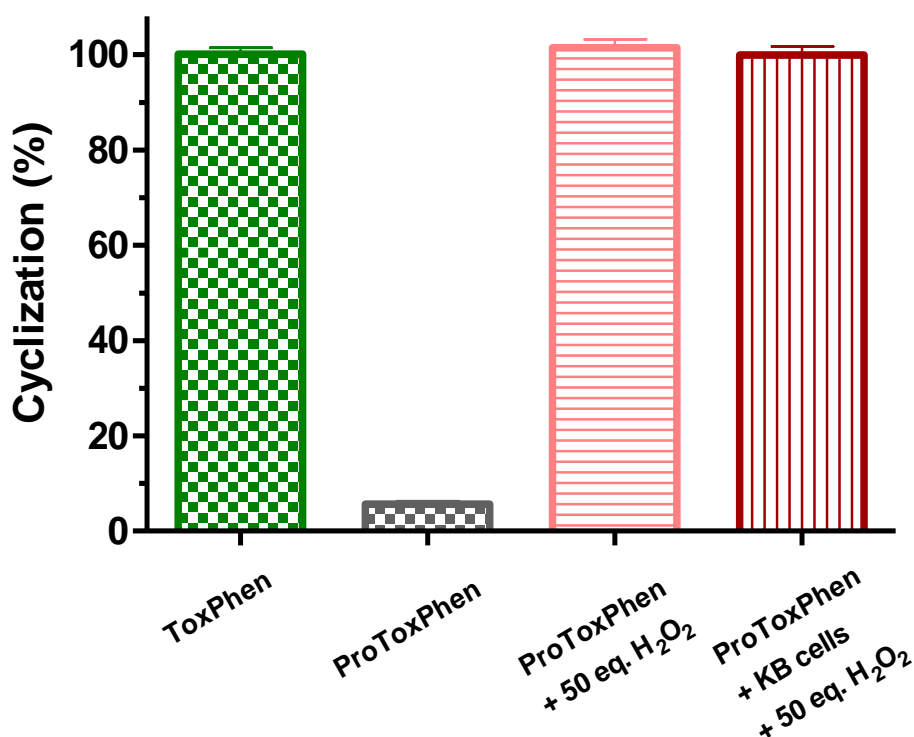
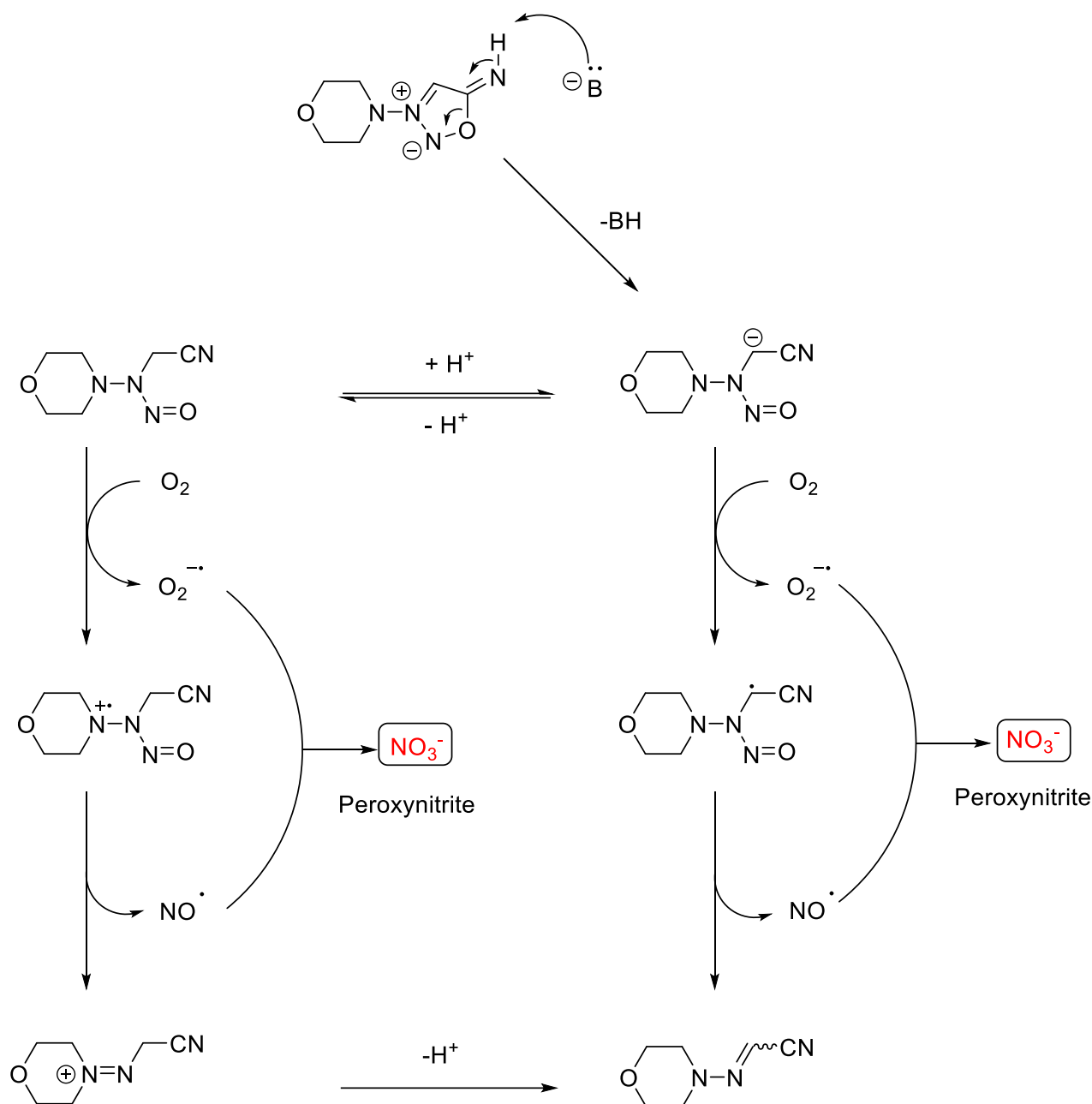


**Figure 27.** Percentage of cyclization of **ProToxPhen** (green) into **ToxPhen** upon addition of DMEM alone (grey) or 50 equivalents of H<sub>2</sub>O<sub>2</sub>.urea in DMEM (salmon) or 50 equivalents of H<sub>2</sub>O<sub>2</sub>.urea in presence of KB 3.1 (burgundy).

We then achieved the accurate determination of the prodrug conversion kinetics within KB spheroids. KB cells were incubated for three days in a 150  $\mu$ M solution of **ProToxPhen** in DMEM:DMSO 99:1 v:v in order to form observable spheroids. The spheroids were washed with PBS and deposited on a 35 mm glass circular round microscope slide. The prodrug oxidation was then triggered by peroxyntirite, a powerful oxidant of the C-B bond having a physiological half-life ten times higher than that of hydrogen peroxide.<sup>153</sup> The peroxyntirite was generated from the decomposition of 3-morpholinosydnonimine (SIN-1, scheme 47).<sup>201</sup>



**Scheme 47.** Decomposition of 3-morpholinosydnimine into peroxynitrite.<sup>201</sup>

To initiate the reaction, a 2 mM solution of peroxynitrite generator 3-morpholinosydnimine (SIN-1)<sup>202</sup> leading to peroxynitrite production rate of ca. 30  $\mu\text{M}\cdot\text{min}^{-1}$  in PBS was added onto the **ProToxPhen** containing cells. This continual flux mimics the tumor microenvironment where peroxynitrite production is estimated at ca. 50  $\mu\text{M}\cdot\text{min}^{-1}$  essentially supplied by tumor cells and tumor-associated macrophages<sup>135,203</sup>. Considering the rapid decomposition of peroxynitrite in cells (ca. 1.5  $\text{s}^{-1}$ ),<sup>202</sup> we calculated a steady-state peroxynitrite concentration of ca. 0.3  $\mu\text{M}$  in our experiment. Moreover, peroxynitrite was shown to rapidly diffuse through cell membranes (< 10 ms).<sup>204</sup> The in-cell kinetic of cyclisation of **ProToxPhen** in **ToxPhen** was studied using homemade epi-fluorescence microscopy using KB 3.1 spheroid models. In a

round-bottom 96-well plate, 500 cells were seeded in a 150  $\mu\text{M}$  **ProToxPhen** solution (200  $\mu\text{L}$ , DMEM) and incubated at 37  $^{\circ}\text{C}$  in presence of 5 %  $\text{CO}_2$  and under 95 % hygrometry. After 3 days, the formed KB spheroids were observed using an optical microscope. 100  $\mu\text{L}$  of media were aspirated and the spheroids were washed twice with PBS (100  $\mu\text{L}$ ). The spheroid was then aspirated (20  $\mu\text{L}$ ) and deposited on a 35 mm glass circular round microscope slide. 20  $\mu\text{L}$  of SIN-1 (4 mM) in PBS was dropped on the spheroid to initiate the cyclization kinetic. Using a homemade epi-fluorescence microscope, we observed **ToxPhen** fluorescence emission in real time at 440 nm upon illumination at 365 nm (figure 28 and 29). This experiment was carried out in triplicates. We observed the same cyclization behavior among several cell populations and different spheroids. No cyclization was observed outside the living cells showing the absence of prodrug leakage over the time scale of our experiments.

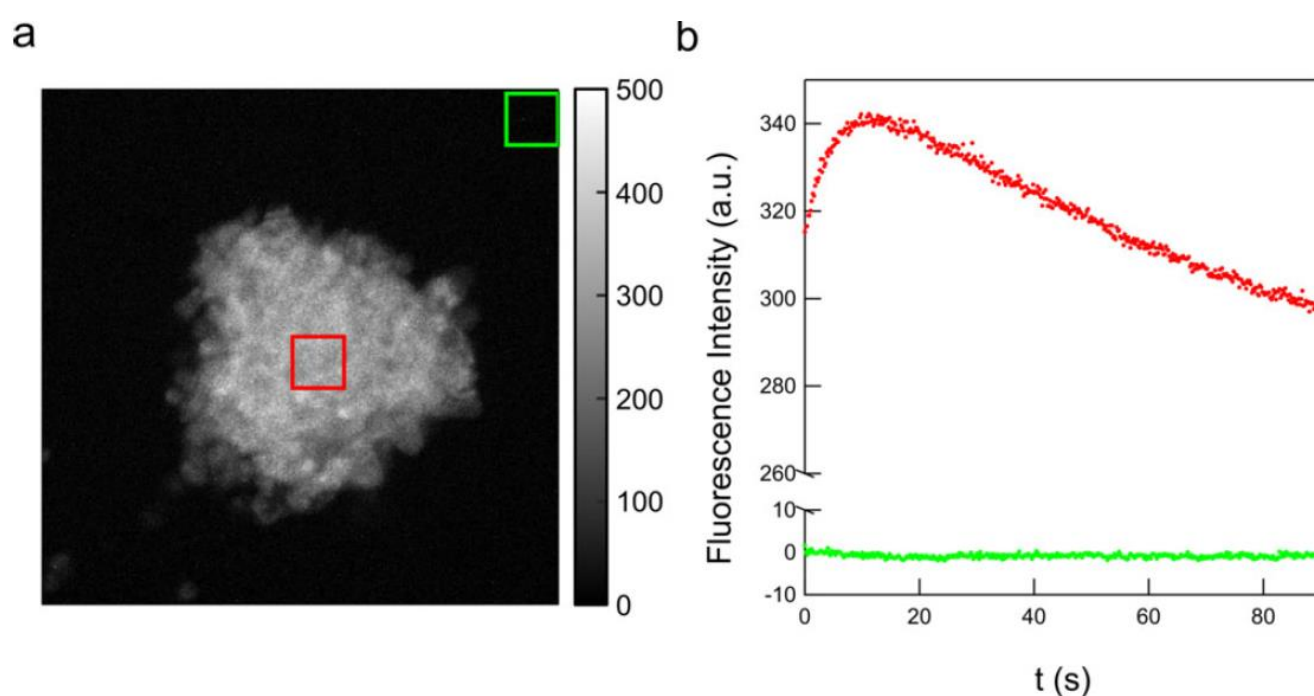


**Figure 28.** In-spheroid kinetic of cyclisation of **ProToxPhen** into **ToxPhen** studied by epifluorescence microscopy. (a) Image of the spheroid at time  $t = 5$  s after SIN-1 (2 mM) was added to initiate the generation of **ToxPhen** from **ProToxPhen**; (b) Time evolution of the average fluorescence intensity following the addition of SIN-1. Signal extracted from regions of interest inside (red) and outside (green) the spheroid. Solvent: 100 mM PBS pH 7.4 buffer/DMSO 99:1 (v:v).  $T = 37^{\circ}\text{C}$ .

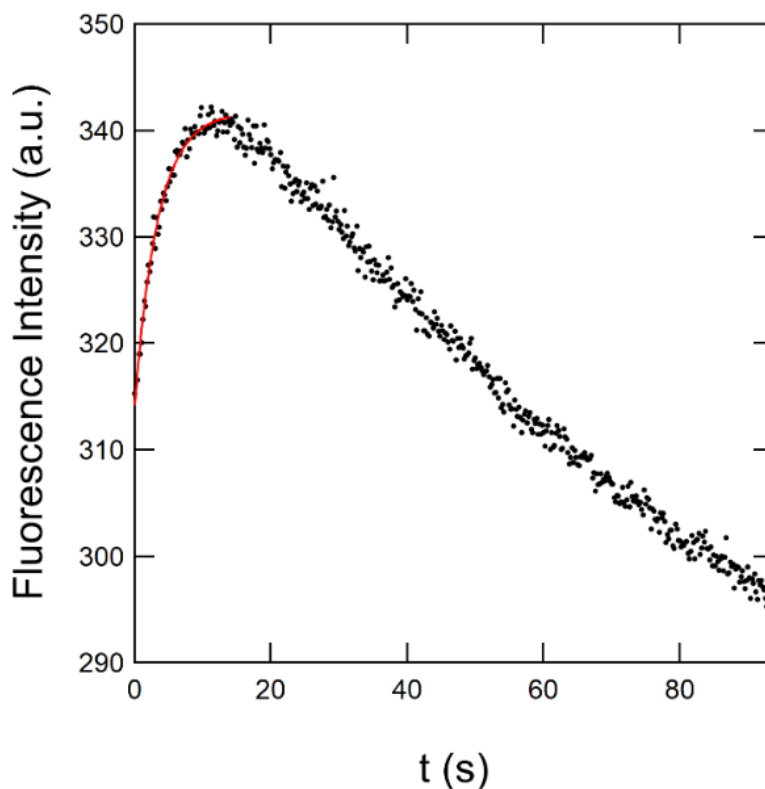


**Figure 29.** Temporal evolution of the fluorescence emission at  $\lambda_{em} = 440$  nm of a  $150 \mu\text{M}$  **ProToxPhen** solution upon addition of SIN-1 ( $2 \text{ mM}$ ). Black dots: experimental data; red solid line: fit with Eq. 11. From the fits, we retrieved  $\tau = 3.5$  s. Solvent: PBS buffer (pH 7.4).  $T = 298\text{K}$ .

The kinetics of **ToxPhen** formation within KB cells was analyzed as mentioned in chapter 3. The temporal evolution of the fluorescence signal (figure 29) was satisfactorily adjusted with Eq. (10,11) and yielded  $k_2 \gg 10^2 \cdot \text{s}^{-1}$  in agreement with the value found in vitro. Next, we derived the rate constant of oxidation  $k_1 = 1.8 \cdot 10^4 \text{ M}^{-1} \cdot \text{s}^{-1}$  which is  $10^2$  times faster than the reaction with hydrogen peroxide. A sluggish decrease in fluorescence was subsequently observed as expected from unbalancing production of **ToxPhen** with its diffusion out of the cells (figures 29 and 30).

The decrease in fluorescence after generation of **ToxPhen** was observed at similar rate in both an isolated cell (green) and the whole spheroid (red). We assume that this drop originates from diffusion of **ToxPhen** out of the cells.

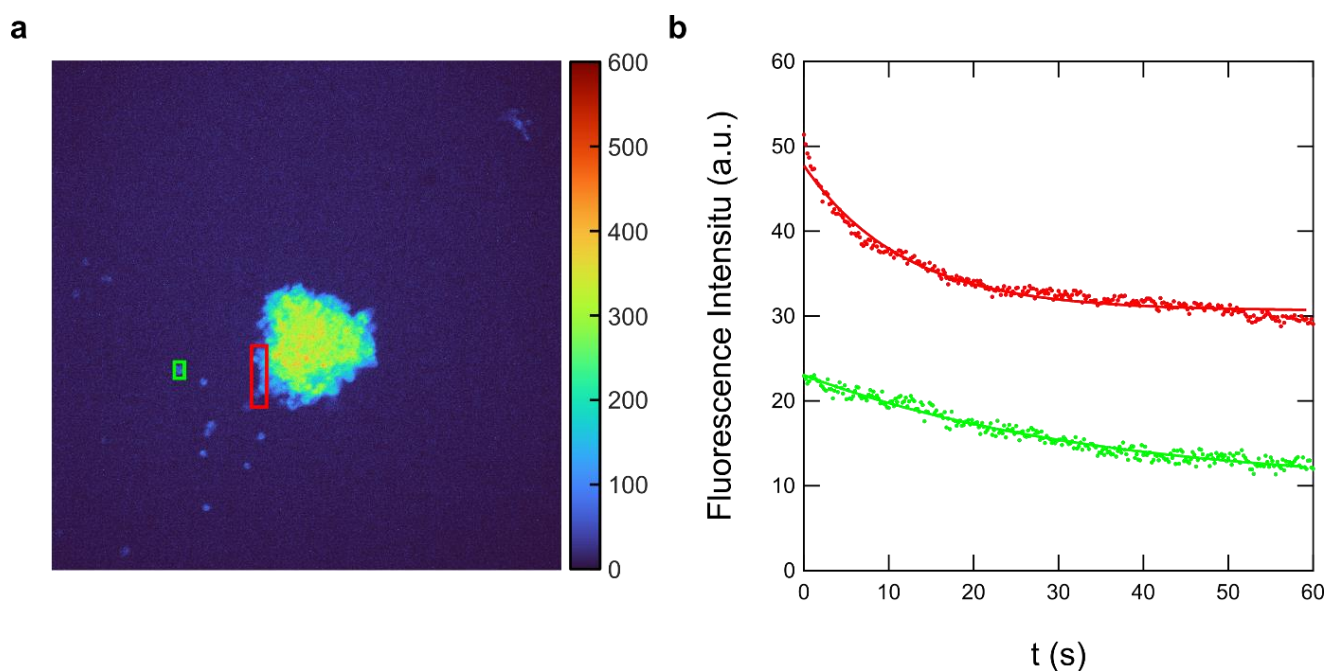


**Figure 30.** In-spheroid kinetics of cyclisation of 150  $\mu\text{M}$  of **ProToxPhen** into **ToxPhen** studied by epifluorescence microscopy. **(a):** Image of the spheroid at  $t = 0$  s (corresponding to  $t = 20$  s after SIN-1 (2 mM) addition). **(b):** Time evolution of the average fluorescence intensity following the addition of SIN-1. Signal extracted from regions of interest at the edge of the spheroid (red) and in an isolated cell (green). Red and green dots: experimental data; red and green solid lines: fit with simple mono-exponential equation. From the fits, we retrieved  $\tau = 11.8$  s (red, edge of the spheroid) and  $\tau = 13.3$  s (green, isolated cell). Solvent: 100 mM PBS pH 7.4 buffer/DMSO 99:1 (v:v).  $T = 298$  K.

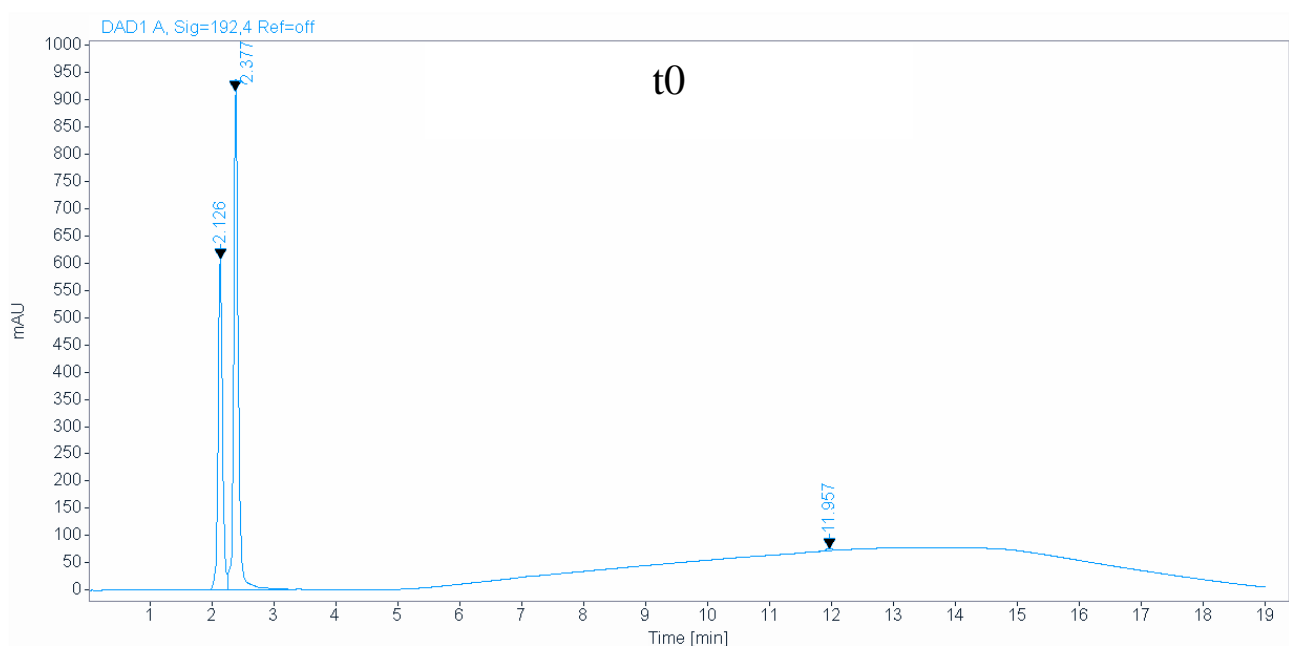
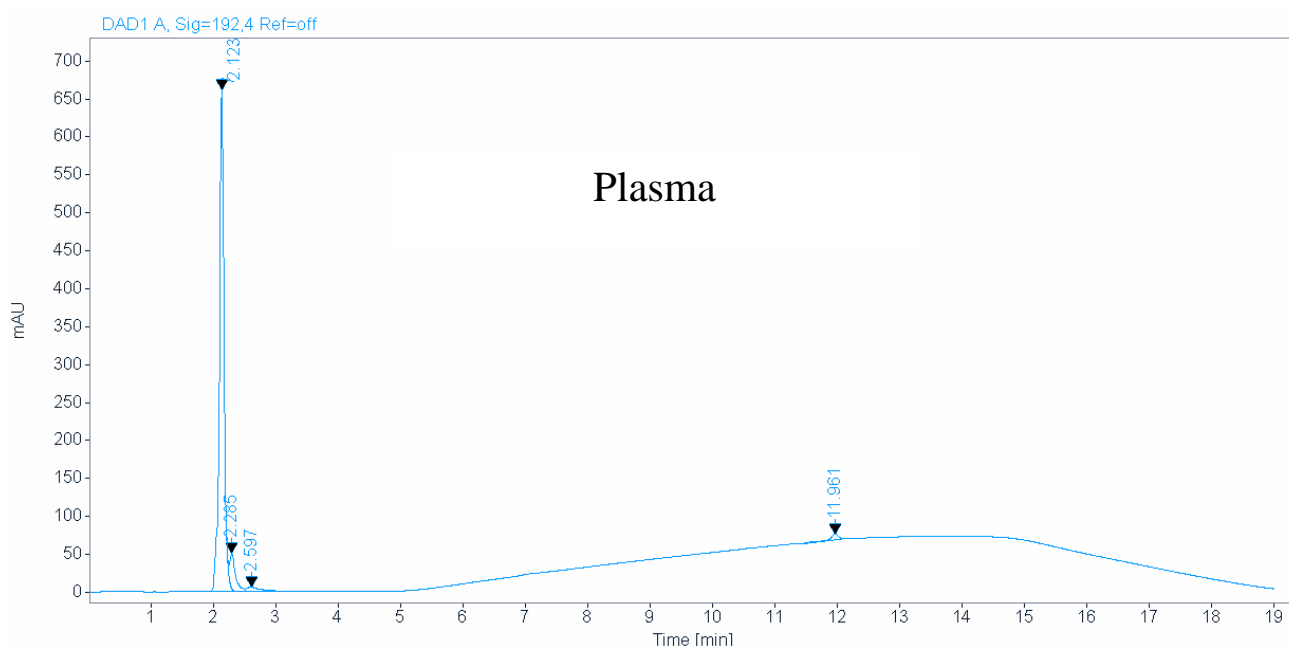
An effective **ProToxPhen** concentration of 10  $\mu\text{M}$  at the tumor would generate an equal steady-state concentration of **ToxPhen** at the tumor site in light of the prompt activation cyclization of the prodrug. This point is fundamental since a too long prodrug conversion would lead to diffusion and cause a drop of the drug concentration at the tumor and its presence far away from the tumor site. Furthermore, the selectivity towards the tumor microenvironment is expected as the production rate of peroxyxynitrite in healthy cells (ca.  $0.1 \mu\text{M}\cdot\text{min}^{-1}$ )<sup>135</sup> is  $10^2$  times slower than the flux found in the pathological condition.

## 6. Plasma stability of ProToxPhen

Rat plasma (Sigma-Aldrich) was reconstituted with deionized water to a final volume of 1 mL. 1 mL of PBS buffer at pH 7.5 was then added to the freshly prepared plasma. **ProToxPhen** solutions at 10  $\mu\text{M}$  were prepared (100  $\mu\text{L}$ ) in the mixture described above and were incubated at 37°C at different time interval ( $t_0$ , 2h, 6h, 24h and 72h). Each sample were then extracted under vigorous mixing with 300  $\mu\text{L}$  of LCMS grade acetonitrile. After centrifugation at 4,000 rpm for 2 min, the supernatant was filtered before being analyzed by LCMS.

Analyses were performed on Agilent 1260 Infinity II LC System coupled to an Agilent mass spectrometry MS SQ 6120 (ESI/Q). UV detection was primarily made at 280 nm. Elutions were performed using a Luna® C18 column (5 µm; 4.6 x 250 mm). Mobile phases consisted of solution A: acetonitrile and solution B: water. The column was eluted with a gradient linearly increasing from 40 to 80% of solution A during 19 minutes. The flow rate was 1 mL/min.

HPLC analysis revealed one major compound with a retention time of 2.37 min (see the chromatograms below, figure 31).



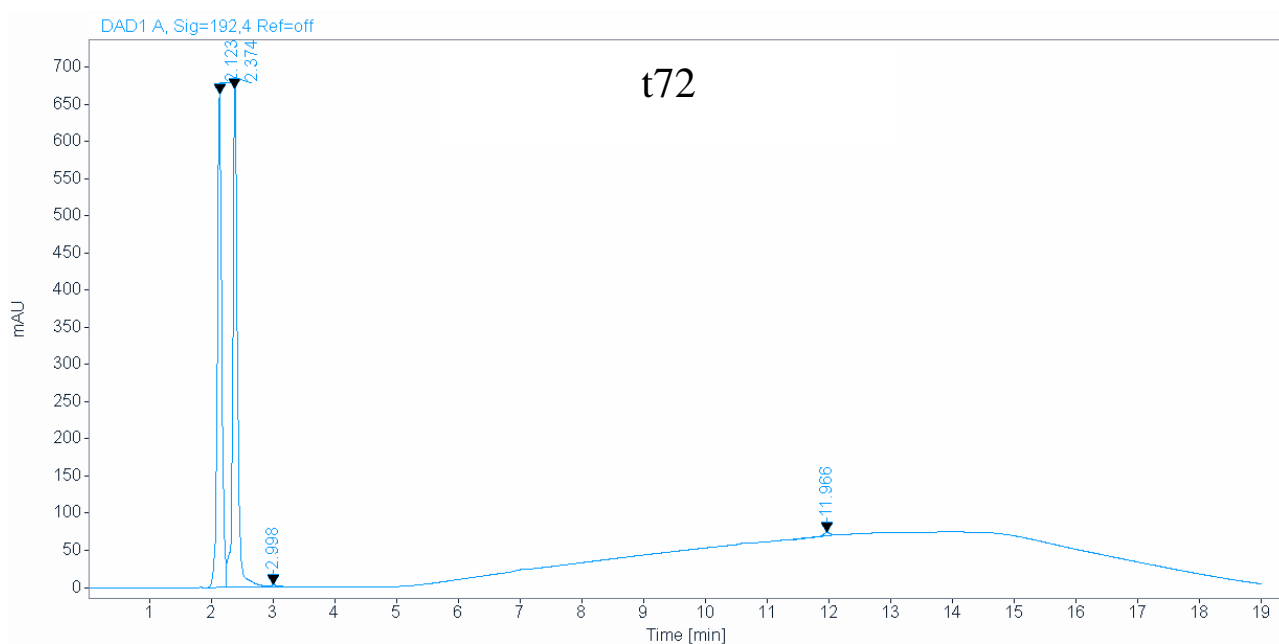
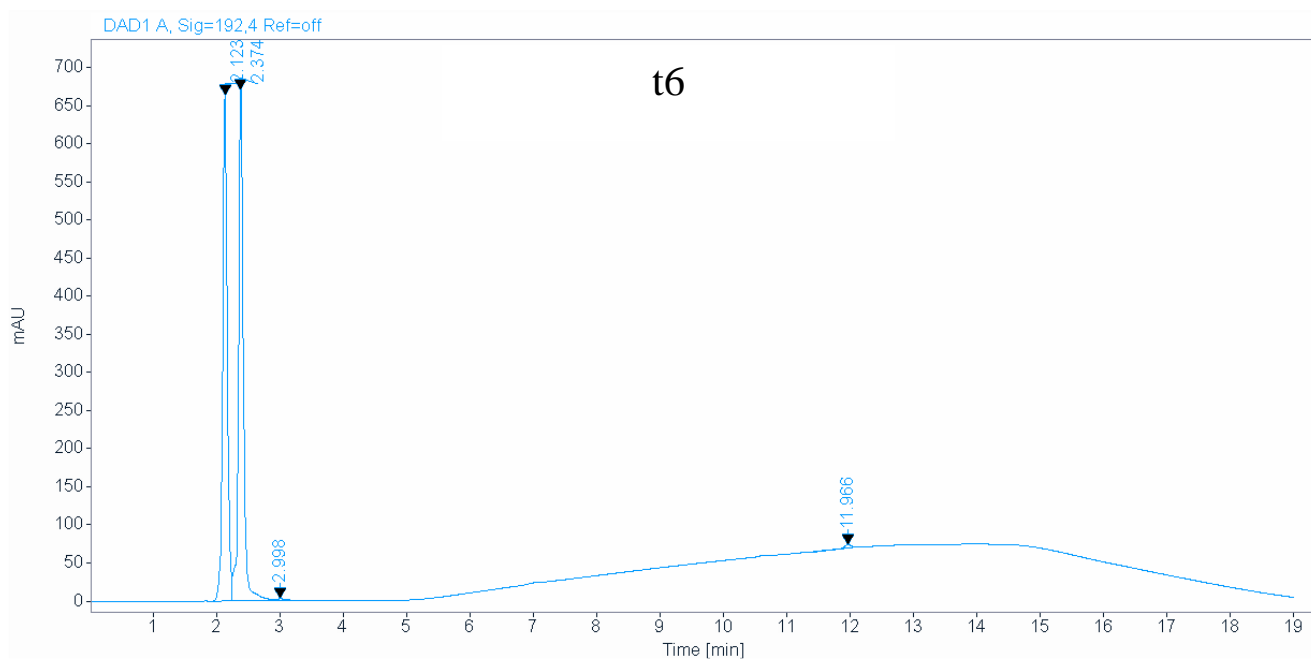


**Figure 31. Plasma stability of ProToxPhen.**

This compound was present at t0 and remained stable up to 72h of incubation in the plasma (area under curve  $\approx$  60% in all cases) associated to no appearance of metabolites. This compound with  $m/z = 342$  was analyzed as the corresponding free boronic acid of the parent **ProToxPhen** structure (figure 32). Samples at t0 and 72h were further subjected to HRMS analysis (ESI<sup>+</sup>,  $m/z$  calculated for C<sub>17</sub>H<sub>17</sub>BNO<sub>6</sub>, [M+H]<sup>+</sup>: 342.1146, found: 342.1139) confirming the presence of the hydrolyzed counterpart of **ProToxPhen** even when no incubation with plasma was performed. As expected, hydrolysis of boronate ester into corresponding boronic acid was very fast<sup>69</sup> in aqueous media and interestingly the obtained boronic acid was highly stable in plasma.

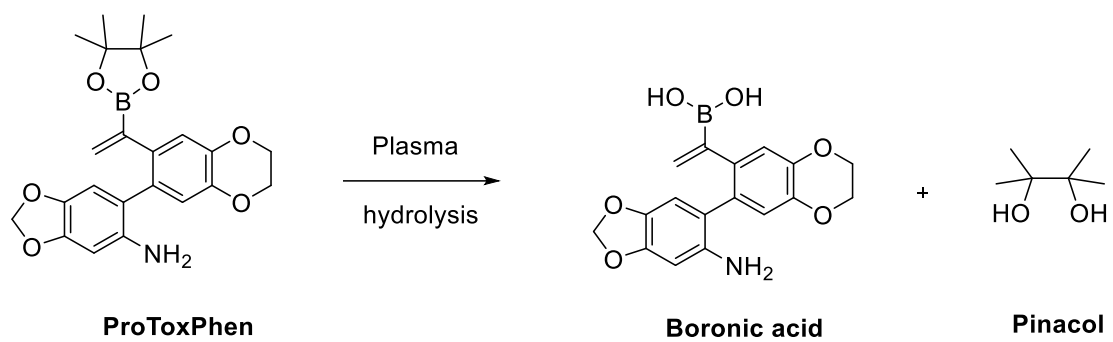


**Figure 32.** Conversion of **ProToxPhen** into its **Boronic acid** counterpart via ester hydrolysis.

## Conclusion and perspectives

The objective of this dissertation in chemical biology was the development of a novel approach in the design of antitumor prodrugs. Inspired by the bioorthogonal chemistry field and previous data observed in our group, we have described a methodology for the preparation of inactive antitumor prodrugs. These prodrugs were built as ring-opened precursors of the drugs that will cyclize within tumors upon cancer cell-specific stimuli in contrast to the conventional grafting of a bulky temporary moiety hardly inactivating the drug.

After a general introduction about cancer and the different treatments available in clinic, a bibliographic work on anticancer boronic acid/boronate-containing prodrugs responsive to oxidative stress from the tumor microenvironment was carried out in chapter 1. We selected the phenanthridines as drug model for the implementation of our strategy. We then developed a biaryl precursor of phenanthridine bearing both an aniline and a vinyl boronate ester motif able to get oxidized by hydrogen peroxide or peroxyxynitrite to afford a ketone function. We first measured the kinetics of oxidation and observed that the rate of oxidation of our vinyl boronate ester motif was oxidized  $10^2$  times faster than the benzene boronate ester moiety. In spite of the presence of a poorly nucleophilic aniline, a spontaneous and fast cyclization of our precursors was measured by virtue of both the geometry of their biaryl scaffolds and the final formation of a six-membered aromatic nucleus. Common imines are rapidly hydrolyzed under physiological conditions and, oxime and hydrazone bonds were introduced to prohibit the reversibility of the former link but these reactions display sluggish kinetics. In this work, the generated imine is inserted in an aromatic ring conferring high stability toward hydrolysis of the newly formed bond. We then devised a new method for the one pot preparation of 6-methylphenanthridines and then synthesized several derivatives. The most cytotoxic was selected, the corresponding prodrug was then prepared and we observed that this prodrug was completely devoid of cytotoxicity. Indeed, the radically different structures geometry of the prodrug toward that of the drug induced a vast change of cytotoxic activity. Using this prodrug, we recorded a very fast cyclization (3.5 s) into the phenanthridine counterpart within tumor spheroids under tumor microenvironment conditions.

New bioorthogonal reactions are constantly investigated in order to either improve existing reactions (i.e. rate constant modifications) or solely access to more complex applications. Thus, this system based on fast cyclization by biorthogonal imination could be expanded to other platforms integrating other types of (i) chemical switch to trigger the reaction and (ii) in vivo-compatible synthetic steps. The design of such programmed "cycl'in-cell" precursors may find applications in the development of new tools for imaging aside from prodrugs involved in several pathologies.

# Experimental part

## 1. Biology

### 1.1 Cell culture

Human papillomavirus-related endocervical adenocarcinoma cell line (KB 3.1) cells were grown in DMEM (Dulbecco's Modified Eagle Medium) supplemented with 10% of fetal calf serum (FCS) and 100 U/mL penicillin and 100 µg/mL streptomycin (Invitrogen) in a 5% CO<sub>2</sub> and 95% hygrometry environment at 37 °C.

U2OS cells were grown at 37°C in a 5% CO<sub>2</sub> atmosphere in McCoy's 5A medium complemented with 9% fetal bovine serum (FBS). Cells were transiently transfected with Genejuice (Merck) according to the manufacturer's protocol. Cells were seeded into Ibidi culture slides and incubated at 37 °C in presence of 5 % CO<sub>2</sub> and under 95 % hygrometry. Cells were washed with Dulbecco's phosphate-buffered saline (DPBS) prior to microscopy imaging.

### 1.2 Cytotoxicity experiments on KB 3.1 human cancer cells

#### 1.2.1 In vitro cell-proliferation assay (2D)

The cytotoxic activity phenanthridines was investigated using the MTS (3-(4,5-dimethylthiazol-2-yl)-5-(3-carboxymethoxyphenyl)-2-(4-sulfophenyl)-2*H*-tetrazolium) method (Promega). 7.10<sup>3</sup> KB 3.1 cells (100 µL) were seeded in 96-well plates with 100 µL of each compound at different concentrations (from 50 µM to 0.05 nM for **ToxPhen** compound and from 500 µM to 100 nM for the **ProToxPhen** compound) and incubated at 37 °C in presence of 5 % CO<sub>2</sub> and under 95 % hygrometry. After 72 h, the media was aspirated and 100 µL of a MTS solution (10% in media) were added in each well. After a 3 h incubation period at 37 °C in presence 5% CO<sub>2</sub> and 95% hygrometry, the optical density was measured at 490 nm wavelength using a microplate reader (Infinite M200 Pro, Tecan trading AG, Switzerland). Untreated cells were used as control. Each concentration was tested in six replicates and the experiment was fulfilled in triplicates. The concentration inhibiting 50% of the cell proliferation (IC<sub>50</sub>) was determined using GraphPad Prism software (GraphPad Software Inc, San Diego, CA, USA).

#### 1.2.2 In vitro 3D tumor spheroid viability assay

The cytotoxic activity of **ProToxPhen** and **ToxPhen** was investigated using a KB 3.1 spheroid model. In a round-bottom 96-well plate, 1 000 cells (100 µL) were seeded with 100 µL of each compound at different concentrations (from 50 µM to 0.05 nM for the **ProToxPhen** compound

and from 500  $\mu\text{M}$  to 100 nM for the **ProToxPhen** compound) and incubated at 37 °C in presence of 5%  $\text{CO}_2$  and under 95% hygrometry.

After 72h, the formed KB spheroids were observed using an optical microscope (Olympus CK 2) and their morphology were imaged with a digital camera (Moticam 1000 1.3MP Live resolution) mounted on the optical microscope. The pictures were then normalized using Image J software.

## 2. Photophysical analyses

### 2.1 UV-visible absorption

UV-Vis absorption spectra were recorded in 1 cm  $\times$  1 cm quartz cuvettes (Hellma) on a diode array UV-Vis spectrophotometer (Evolution array, Thermo Scientific) at 293 K. The molar absorption coefficients were extracted while checking the validity of the Beer-Lambert law.

### 2.2 Epifluorescence spectroscopy

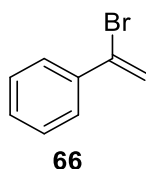
Photon Technology International QuantaMaster QM-1 spectrofluorimeter (PTI, Monmouth Junction, NJ) equipped with a Peltier cell holder (TLC50, Quantum Northwest, Shoreline, WA) was used.

### 2.3 Epifluorescence microscopy

We used a home-built epifluorescence microscopy set-up. The samples were illuminated using a NCSU033B LED (Nichia Corp., Tokushima, Japan) filtered at  $365 \pm 40$  nm (Chroma Technology, Bellows Falls, VT) and a LXZ1-PL02 LED (Lumileds, Schipol, Netherlands) filtered at  $585 \pm 10$  nm as light sources. The LEDs were supplied by a LED driver (LEDD1B, Thorlabs Inc, Newton, NJ). A lens (ACL2520U; Thorlabs,  $f = 20$  mm) and were placed just after each diode to collimate the light source. A dichroic mirror (T425LPXR, Chroma, Bellows Falls, VT; or a FF505-606-Di01, Semrock, Rochester, NY for excitation at 585 nm) and a second pair of lenses were used to focus the light at the back focal plane of the objective. Fluorescence images at  $440 \pm 20$  nm (HQ 440/40x; Chroma Technology) or at  $628 \pm 16$  (FF628-32, Semrock) were acquired with a 50 $\times$  MPLFLN (NA 0.8, Olympus Corporation, Tokyo, Japan) with a Luca-R CCD camera (Andor Technology, Belfast, UK).

### 3. Chemistry

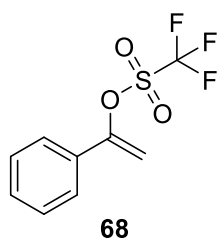
All chemical reagents were of analytical grade, obtained from Acros, Alfa Aesar, or Aldrich, and used without further purification. Solvents were obtained from SDS or VWR-Prolabo. Dichloromethane (DCM) was freshly distilled under  $\text{CaH}_2$  and used immediately. Tetrahydrofuran (THF) was freshly distilled under sodium and used immediately. Toluene was freshly distilled under  $\text{CaH}_2$  and used immediately. Flash chromatography was performed using silica gel (35–70  $\mu\text{m}$ , Merck). Evaporation of solutions was performed under reduced pressure at temperature below 40 °C using rotary evaporator. Analytical TLC was performed using Silica Gel 60 F254 pre-coated aluminum plates (Merck). Spots were visualized by treatment with phosphomolybdic acid (PMA) revelator (for molecules containing boron atom) followed by heating and/or by absorbance/emission under UV light at 254 or 360 nm, or diode or  $\text{KMnO}_4$  on silica. NMR spectra were collected on Bruker DPX 250 ( $^1\text{H}$  at 250 MHz and  $^{13}\text{C}$  at 62.5 MHz), AV 300 ( $^1\text{H}$  at 300 MHz and  $^{13}\text{C}$  at 75 MHz and  $^{11}\text{B}$  at 96 MHz) or AV 360 ( $^1\text{H}$  at 360 MHz and  $^{13}\text{C}$  at 90 MHz) spectrometers and analyzed using MestReNova software. Chemical shifts are reported in ppm ( $\delta$ ) and coupling constants in Hz (J). NMR spectra were performed in  $\text{CDCl}_3$ ,  $(\text{CD}_3)_2\text{SO}$ ,  $\text{CD}_3\text{CN}$  or  $\text{D}_2\text{O}$ . High-resolution mass spectrometry (HRMS) analyses were performed by electrospray with positive or negative ( $\text{ESI}^+$  or  $\text{ESI}^-$ ).



**Compound 66.** To a flask containing a magnetic stir bar was added phenylacetylene **65** (1.02 g, 10.0 mmol, 1.0 eq). Then HBr (1.8 mL, 11.0 mmol, 1.1 eq, 33% in acetic acid) was added dropwise at 0 °C and the solution was stirred for 1 h at room temperature. Then, the reaction mixture was cooled to 0 °C and 20 mL of saturated aqueous solution of NaHCO<sub>3</sub> was added. This solution was extracted with DCM (3 x 20 mL) and the combined organic phases were dried with Na<sub>2</sub>SO<sub>4</sub>. The solvent was evaporated to afford the crude product which was purified by flash chromatography on silica gel (cyclohexane:EtOAc = 95:5 to 70:30) to give the expected product (1.68 g, 92%) as a dark brown oil.

<sup>1</sup>H NMR (300 MHz, CDCl<sub>3</sub>) δ = 7.89–7.84 (m, 2H), 7.45–7.38 (m, 3H), 5.86 (d, J = 2.0 Hz, 1 H), 6.19 (d, J = 2.0 Hz, 1 H).

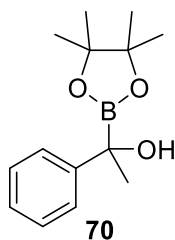
The spectral data are similar to those reported in: *Angewandte Chemie International Edition* **2021**, *60* (4), 2160–2164.



**Compound 68.** To a solution of acetophenone **67** (100 mg, 0.84 mmol, 1 eq) in 3 mL of dry DCM at 0°C was added Et<sub>3</sub>N (176 μL, 1.04 mmol, 1.25 eq). The mixture was stirred at 0°C during 15 min and Tf<sub>2</sub>O (174 μL, 1.26 mmol, 1.5 eq) was then added dropwise. The mixture was stirred at r.t. overnight and the solvent was removed under reduced pressure. The crude product was purified by flash chromatography (cyclohexane:EtOAc = 95:5 to 60:40) to give the expected product (59 mg, 28%) as a colorless oil.

<sup>1</sup>H NMR (400 MHz, CDCl<sub>3</sub>) δ 7.60-7.20 (m, 5H), 5.50 (d, J = 2 Hz, 2H).

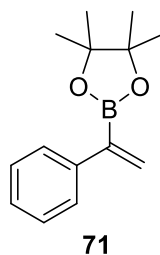
The spectral data are similar to those reported in: *Journal of Heterocyclic Chemistry* **1988**, 25 (4), 1237–1241.



**Compound 70.** To a flame-dried 100 mL round-bottom flask containing a stir bar was added bis(pinacolato)diboron (3.16 g, 12.5 mmol, 1.5 eq), 1,3-bis(cyclohexyl)imidazolium tetrafluoroborate (266 mg, 0.83 mmol, 0.1 eq), *t*-BuONa (160 mg, 1.6 mmol, 0.2 eq), and CuCl (164 mg, 1.6 mmol, 0.2 eq). 60 mL of toluene were added, the flask was sealed, and the reaction was stirred for 30 min. Benzophenone **69** (1 g, 8.3 mmol, 1 eq) was then added via a syringe followed immediately by MeOH (672  $\mu$ L, 16.6 mmol, 2 eq) addition. After 24 h, the mixture was loaded directly onto a short pad of silica gel pretreated with DCM. The pad was thoroughly washed with Et<sub>2</sub>O and the filtrate was evaporated under reduced pressure. The resulting residue was purified by flash chromatography on silica gel (cyclohexane:EtOAc = 95:5 to 70:30) to give the expected product (1.16 g, 57%) as a light yellow oil.

<sup>1</sup>H NMR (300 MHz, CDCl<sub>3</sub>)  $\delta$  7.48-7.22 (m, 5H), 1.65 (s, 3H), 1.25 (s, 12H).

<sup>13</sup>C NMR (75 MHz, CDCl<sub>3</sub>)  $\delta$  140.92, 129.30, 127.12, 126.45, 97.63, 84.54, 83.48, 26.89, 25.06, 17.16.



**Synthetic pathway A & B.** To a solution of  $\text{PdCl}_2(\text{PPh}_3)_2$  (0.03 eq),  $\text{PPh}_3$  (0.06 eq),  $\text{B}_2(\text{Pin})_2$  (1.1 eq),  $\text{PhOK}$  (1.5 eq) in 2.3 mL of toluene was added **66** or **68** (1 eq). The solution was stirred under Ar at 50°C during 4h and at 100°C during 3h. Water was added, the aqueous layer was extracted with EtOAc, washed with brine, dried with  $\text{MgSO}_4$ , and concentrated under reduced pressure. The crude was purified by flash chromatography on silica gel (cylcohexane-EtOAc = 100:0 to 90:10) to give the expected product as a colorless oil.

Reaction followed by TLC (revelation:  $\text{I}_2$  and PMA)

Yield from synthetic pathway **A** = 35%

Yield from synthetic pathway **B** = 46%

### Synthetic pathway C

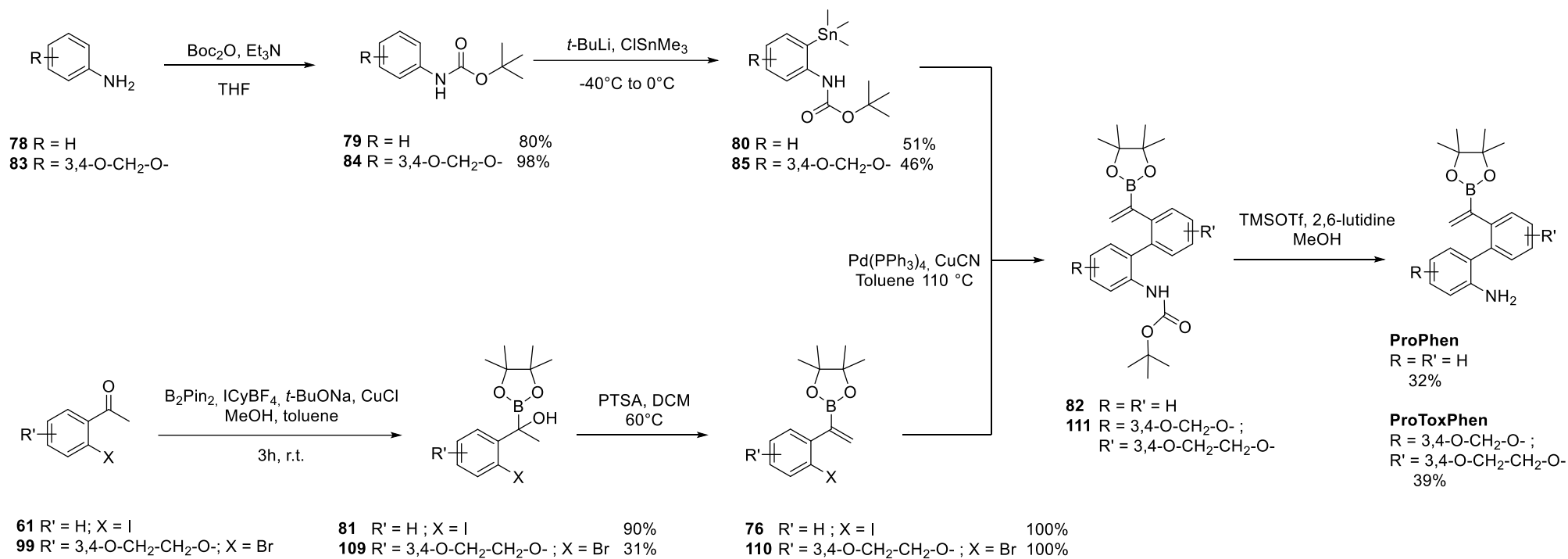
To a solution of **70** (248 g, 1 mmol, 1 eq) in 20 mL of toluene was added *p*-toluenesulfonic acid (525 mg, 3 mmol, 3 eq). The mixture was heated at 60°C during 2 h. 50 mL of a saturated aqueous solution of  $\text{Na}_2\text{CO}_3$  was added and the aqueous layer was extracted with EtOAc (3 x 50 mL). The organic phases were combined, washed with brine, dried with  $\text{MgSO}_4$  and concentrated under reduced pressure to give the expected product (230 mg, 100%) as a colorless oil. (No further purification was needed)

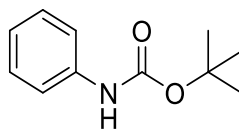
Yield from synthetic pathway **C** = 100%

$^1\text{H}$  NMR (300 MHz,  $\text{CDCl}_3$ )  $\delta$  7.46 – 7.35 (m, 2H), 7.21 (m, 3H), 6.00 (d,  $J = 3.5$  Hz, 2H), 1.25 (s, 12H).

$^{13}\text{C}$  NMR (75 MHz,  $\text{CDCl}_3$ )  $\delta$  141.36, 130.91, 128.16, 127.15, 126.99, 83.76, 77.00, 24.77.

$^{11}\text{B}$  NMR (160.4 MHz,  $\text{CDCl}_3$ ):  $\delta$  30.2.



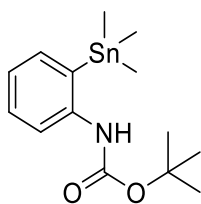


**79**

**Compound 79.** To a solution of aniline **78** (300 mg, 3.2 mmol, 1.0 eq) in 65 mL of THF was added triethylamine (850  $\mu$ L, 6.4 mmol, 2.0 eq) and Boc<sub>2</sub>O (700 mg, 3.2 mmol, 1.0 eq). The mixture was then stirred at r.t. overnight. When the reaction was complete (checked by TLC), the THF was removed by evaporation and the mixture was poured into water (10 mL). The residual water phase was extracted with EtOAc (3 x 30 mL) and dried over Na<sub>2</sub>SO<sub>4</sub>. Removal of solvent under reduced pressure gave a crude product that was purified by flash chromatography (cyclohexane: EtOAc = 3:1) to afford the expected product (490 mg, 80%) as a white powder.

<sup>1</sup>H NMR (360 MHz, CDCl<sub>3</sub>)  $\delta$  7.40 – 7.26 (m, 3H), 7.07 – 7.00 (m, 2H), 6.36 (s, 1H), 1.52 (s, 9H).

The spectral data are similar to those reported in: *J. Org. Chem.* **1988**, 53, 6138-6139.

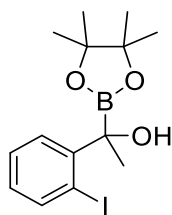


80

**Compound 80.** *N*-Boc-aniline (**79**) (100 mg, 0.52 mmol, 1.0 eq) was placed in an oven-dried round-bottom flask and dissolved in 1 mL of dry Et<sub>2</sub>O. The solution was cooled to -40 °C under an Ar atmosphere. *t*-BuLi (1.7 M in pentane, 647 μL, 1.1 mmol, 2.1 eq) was added via a syringe pump over 30 min, during which the mixture became homogenous, and the resulting solution was stirred at 0 °C for 3 h. The reaction mixture was further cooled to -78 °C, treated with a solution of Me<sub>3</sub>SnCl (104 mg, 0.52 mmol, 1.0 eq) in 1 mL of Et<sub>2</sub>O and stirred at 0 °C for 6 h. The reaction mixture was quenched with saturated aqueous NaHCO<sub>3</sub> solution (5 mL) at 0 °C. The organic phase was extracted with Et<sub>2</sub>O (2 x 30 mL) and then washed with brine (50 mL). The combined organic layers were dried over Na<sub>2</sub>SO<sub>4</sub> and concentrated under reduced pressure. Flash chromatography using neutral alumina pre-washed with a 40:4:1 mixture of cyclohexane:Et<sub>3</sub>N:EtOAc and eluted with a 20:1 mixture of cyclohexane:EtOAc gave the expected product (94 mg, 51%) as a colorless oil.

<sup>1</sup>H NMR (250 MHz, CDCl<sub>3</sub>) δ 7.52 (d, *J* = 8.2 Hz, 1H), 7.40 (dd, *J* = 7.2, 1.5 Hz, 1H), 7.32 (td, *J* = 7.7, 1.7 Hz, 1H), 7.12 (td, *J* = 7.3, 1.1 Hz, 1H), 6.28 (s, 1H), 1.51 (s, 9H), 0.34 (s, 9H).

The spectral data are similar to those reported in: *J. Org. Chem.* **1988**, 53, 6138-6139.



**81**

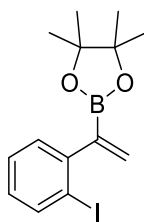
**Compound 81.** To a flame-dried 50 mL round-bottom flask containing a stir bar was added bis(pinacolato)diboron (1.52 g, 6.0 mmol, 1.5 eq), 1,3-bis(cyclohexyl)imidazolium tetrafluoroborate (128 mg, 0.4 mmol, 0.1 eq), *t*-BuONa (77 mg, 0.8 mmol, 0.2 eq), and CuCl (79 mg, 0.8 mmol, 0.2 eq). 30 mL of Toluene was added, the flask was sealed, and the reaction was stirred for 30 min. Iodobenzophenone **61** (1 g, 4.0 mmol, 1 eq) was added via a syringe followed immediately by MeOH (342  $\mu$ L, 8 mmol, 2 eq) addition. After 24 h, the mixture was loaded directly onto a short pad of silica gel pretreated with DCM. The pad was thoroughly washed with Et<sub>2</sub>O and the filtrate was evaporated under reduced pressure. The resulting residue was purified by flash chromatography (cyclohexane:EtOAc = 95:5 to 70:30) to give the expected product (1.12 g, 75%) as a light yellow oil. TLC conditions: eluent (cyclohexane:EtOAc = 80:20); R<sub>f</sub> = 0.71; revelation by PMA.

<sup>1</sup>H NMR (300 MHz, CDCl<sub>3</sub>)  $\delta$  7.82 (dd, *J* = 7.8, 1.3 Hz, 1H), 7.57 (dd, *J* = 7.9, 1.7 Hz, 1H), 7.36 (td, *J* = 7.6, 1.3 Hz, 1H), 6.93 (td, *J* = 7.6, 1.3 Hz, 1H), 2.26 (s, 1H), 1.67 (s, 3H), 1.33 (s, 12H).

<sup>13</sup>C NMR (75 MHz, CDCl<sub>3</sub>)  $\delta$  148.62, 140.42, 128.56, 128.34, 126.45, 97.63, 84.54, 83.48, 26.89, 25.06.

<sup>11</sup>B NMR (96 MHz, CDCl<sub>3</sub>)  $\delta$  31.47.

HRMS (ESI<sup>+</sup>): *m/z* Calcd for C<sub>14</sub>H<sub>20</sub>BO<sub>3</sub> + Na, [M+Na]<sup>+</sup>: 397.0445, found [M+Na]<sup>+</sup>: 397.0421.



76

**Compound 76.** To a solution of **81** (1.5 g, 4 mmol, 1 eq) in 80 mL of toluene was added *p*-toluenesulfonic acid (2.1 g, 12 mmol, 3 eq). The mixture was heated at 60°C during 2 h. 50 mL of a Na<sub>2</sub>CO<sub>3</sub> saturated aqueous solution was added and the aqueous layer was extracted with EtOAc (3x50 mL). The organic phases were combined, washed with brine, dried with MgSO<sub>4</sub> and concentrated under reduced pressure to give the expected product (1.41 g, 100%) as a colorless oil.

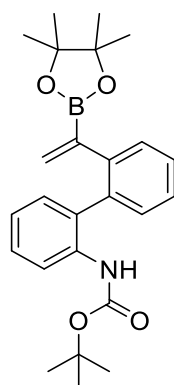
TLC conditions: eluent (cyclohexane:EtOAc = 70:30); R<sub>f</sub> = 0.78.

<sup>1</sup>H NMR (360 MHz, CDCl<sub>3</sub>) δ 7.80 (dd, *J* = 7.6, 1.3 Hz, 1H), 7.31 (td, *J* = 7.6, 1.3 Hz, 1H), 7.18 (dd, *J* = 7.6, 1.8 Hz, 1H), 6.93 (td, *J* = 7.6, 1.3 Hz, 1H), 6.12 (d, *J* = 3.3 Hz, 1H), 5.73 (d, *J* = 3.3 Hz, 1H), 1.32 (s, 12H).

<sup>13</sup>C NMR (91 MHz, CDCl<sub>3</sub>) δ 147.77, 138.38, 132.74, 128.78, 128.34, 128.25, 98.62, 83.94, 24.90.

<sup>11</sup>B NMR (96 MHz, CDCl<sub>3</sub>) δ 29.67.

HRMS (ESI<sup>+</sup>): *m/z* Calcd for C<sub>14</sub>H<sub>18</sub>BIO<sub>2</sub> + H, [M+H]<sup>+</sup>: 357.0522, found: 357.0519.



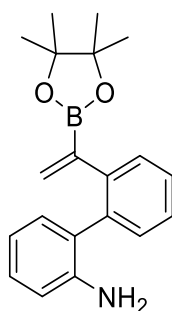
**82**

**Compound 82.** To a flame-dried 25 mL round-bottom flask containing a stir bar was added **81** (222 mg, 0.66 mmol, 1.1 eq), **76** (210 mg, 0.6 mmol, 1 eq), Pd(PPh<sub>3</sub>)<sub>4</sub> (14 mg, 0.012 mmol, 0.02 eq) and CuCN (10 mg, 0.12 mmol, 0.2 eq) and the mixture was refluxed in 6.5 mL of toluene under argon for 1h. The mixture was quenched with EtOAc, filtered through a pad of celite which was thoroughly washed with EtOAc. The filtrate was then concentrated under reduced pressure to give a crude product that was engaged in the next step without further purification.

TLC conditions: eluent (cyclohexane:EtOAc = 80:20); R<sub>f</sub> = 0.75.

HRMS (ESI<sup>+</sup>): m/z Calcd for = C<sub>25</sub>H<sub>32</sub>BNO<sub>4</sub> + H, [M+H]<sup>+</sup>: 422.2502, found: 422.2501.

HRMS (ESI<sup>+</sup>): m/z Calcd for C<sub>25</sub>H<sub>32</sub>BNO<sub>4</sub> + Na, [M+Na]<sup>+</sup>: 444.2322, found: 444.2321.



**ProPhen**

**ProPhen.** To a solution of Boc derivative **82** (50 mg, 0.12 mmol, 1.0 eq) in 1 mL of dry dichloromethane was added 2,6-lutidine (162  $\mu$ L, 1.4 mmol, 12 eq) and TMSOTf (128  $\mu$ L, 0.71 mmol, 6 eq) at r.t. and under Ar atmosphere. The solution was stirred for 1h30 before water (10 mL) was added. The resulting mixture was diluted with CH<sub>2</sub>Cl<sub>2</sub> (50 mL) and stirred vigorously for 15 min. The organic phase was separated, washed with water and brine, dried over MgSO<sub>4</sub> and concentrated on a rotary evaporator. The crude product was purified by flash chromatography (cyclohexane:EtOAc = 70:30) followed by purification by PTLC (cyclohexane:EtOAc = 70:30) to give the expected product (12 mg, 32%) as a brown power.

<sup>1</sup>H NMR (300 MHz, CDCl<sub>3</sub>)  $\delta$  7.32 (s, 4H), 7.14 – 6.98 (m, 2H), 6.81 – 6.66 (m, 2H), 5.98 (d, J = 3.0 Hz, 1H), 5.86 (d, J = 3.0 Hz, 1H), 1.04 (s, 6H), 1.02 (s, 6H).

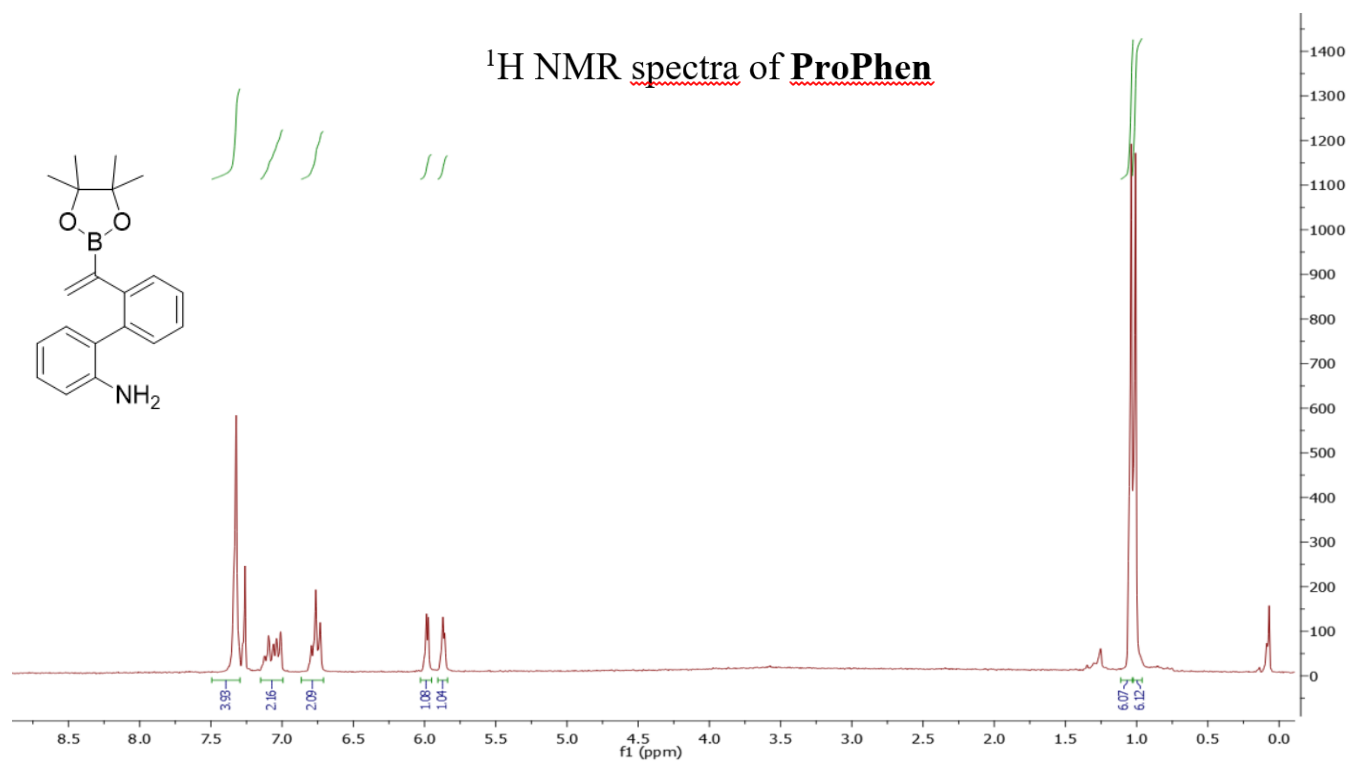
<sup>13</sup>C NMR (75 MHz, CDCl<sub>3</sub>)  $\delta$  144.10, 142.30, 137.08, 132.18, 131.87, 130.39, 129.28, 128.25, 127.59, 127.20, 118.07, 115.68, 83.45, 24.77, 24.45.

<sup>11</sup>B NMR (96 MHz, CDCl<sub>3</sub>)  $\delta$  29.99.

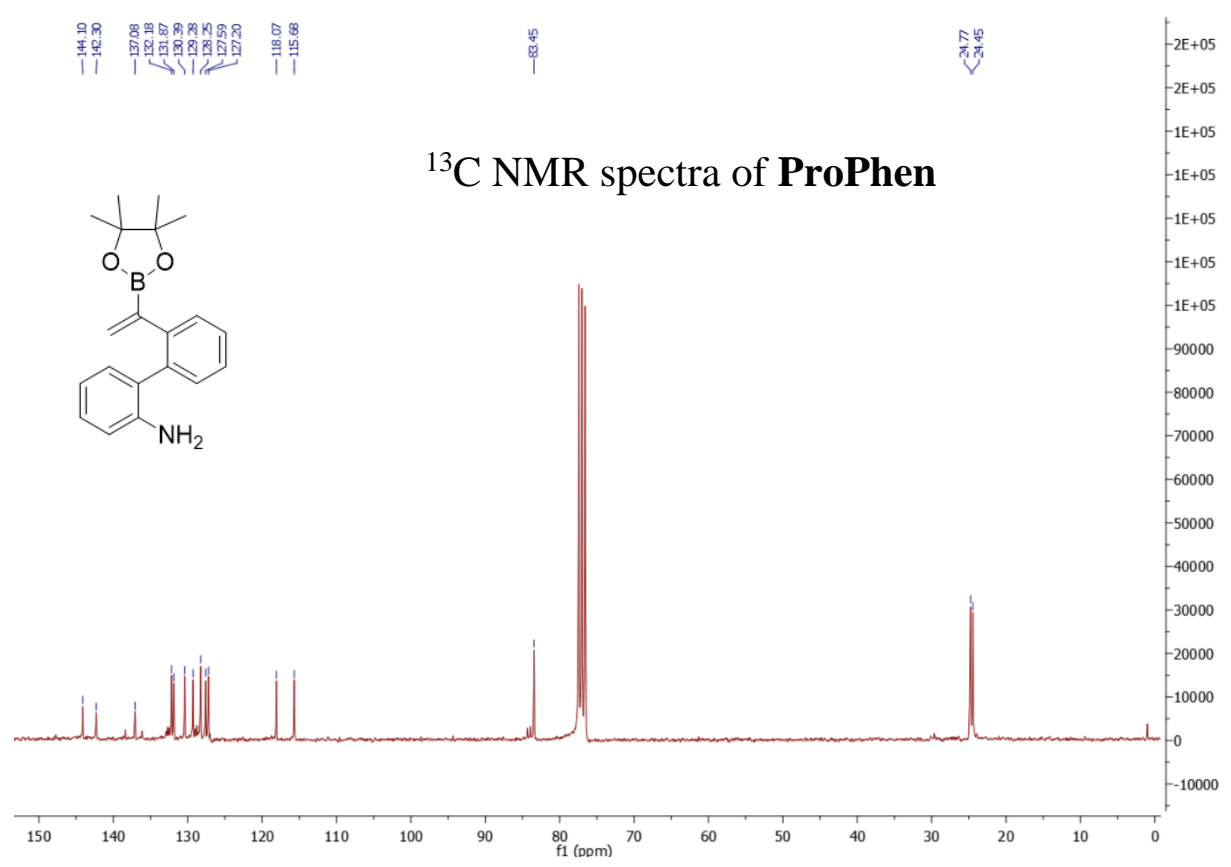
HRMS (ESI<sup>+</sup>): m/z Calcd for = C<sub>20</sub>H<sub>24</sub>BNO<sub>2</sub> + H, [M+H]<sup>+</sup>: 322.1976, found: 322.1966.

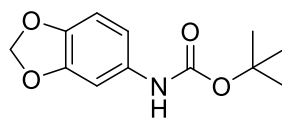
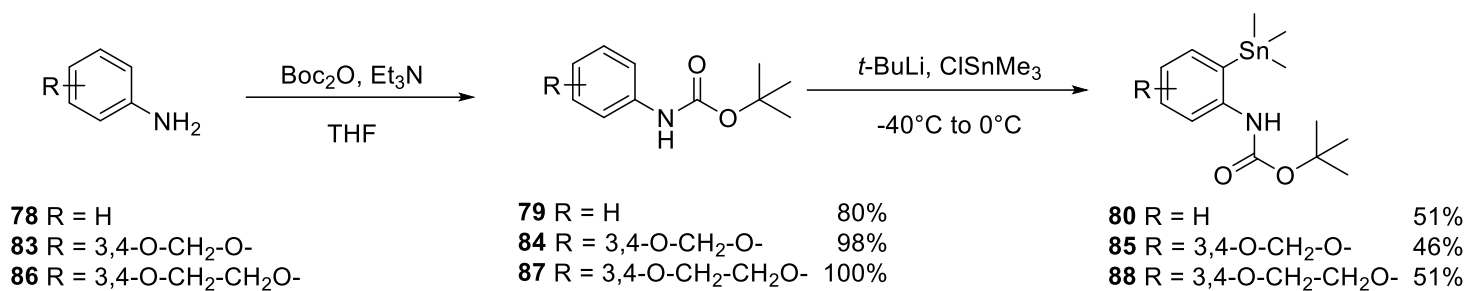
HRMS (ESI<sup>+</sup>): m/z Calcd for C<sub>20</sub>H<sub>24</sub>BNO<sub>2</sub> + Na, [M+Na]<sup>+</sup>: 344.1797, found: 344.1781.

### <sup>1</sup>H NMR spectra of ProPhen



### <sup>13</sup>C NMR spectra of ProPhen



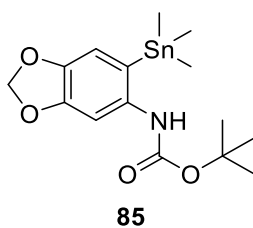


**84**

**Compound 84.** To a solution of 3,4-methylenedioxyaniline **83** (300 mg, 2.19 mmol, 1 eq) in 45 mL of THF was added triethylamine (581  $\mu$ L, 4.4 mmol, 2 eq) and Boc<sub>2</sub>O (478 mg, 2.19 mmol, 1 eq). Then the mixture was stirred at r.t overnight. When the reaction was complete (checked by TLC), the THF was removed under reduced pressure and the resulting mixture was poured onto water (10 mL). The aqueous mixture was extracted with EtOAc (3 x 30 mL) and dried over Na<sub>2</sub>SO<sub>4</sub>. Removal of solvents under reduced pressure gave a crude product that was purified by flash chromatography (cyclohexane:EtOAc = 3:1) to give the expected product (507 mg, 98%) as a white powder

<sup>1</sup>H NMR (360 MHz, CDCl<sub>3</sub>)  $\delta$  7.03 (bs, 1H), 6.74 – 6.67 (m, 1H), 6.67 – 6.57 (m, 1H), 6.37 (bs, 1H), 5.91 (s, 2H), 1.50 (s, 9H).

The spectral data are similar to those reported in: *Eur. J. Org. Chem.* **2010**, 3704–3710.

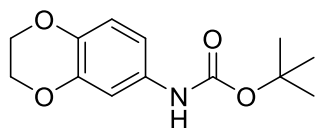


**Compound 85.** *N*-Boc-3,4-methylenedioxyaniline **84** (100 mg, 0.42 mmol, 1.0 eq) was placed in an oven-dried round-bottom flask and dissolved in 1 mL of dry Et<sub>2</sub>O. The solution was cooled to -40 °C under an Ar atmosphere. *t*-BuLi (1.7 M in pentane, 524 μL, 0.89 mmol, 2.1 eq) was added via a syringe pump over 30 min, during which the mixture became homogenous, and the resulting solution was stirred at 0 °C for 3 h. The reaction mixture was further cooled to -78 °C and Me<sub>3</sub>SnCl (84 mg, 0.42 mmol, 1.0 eq) in 1 mL of Et<sub>2</sub>O solution was added and the reaction was stirred at 0 °C for 6 h. The reaction mixture was quenched with saturated NaHCO<sub>3</sub> aqueous solution (5 mL) at 0 °C. The organic phase were extracted with Et<sub>2</sub>O (2 x 30 mL) and washed with brine (50 mL). The combined organic phases were dried over Na<sub>2</sub>SO<sub>4</sub> and concentrated under reduced pressure. Flash chromatography using neutral alumina pre-washed with a 40:4:1 mixture of hexane:Et<sub>3</sub>N:EtOAc and eluted with 20:1 mixture of hexane:EtOAc gave the expected product (77 mg, 46%) as a yellow oil.

<sup>1</sup>H NMR (250 MHz, CDCl<sub>3</sub>) δ 7.52 (d, *J* = 8.2 Hz, 1H), 7.40 (dd, *J* = 7.2, 1.5 Hz, 1H), 7.32 (td, *J* = 7.7, 1.7 Hz, 1H), 7.17 – 7.08 (m, 1H), 6.29 (s, 1H), 1.51 (s, 9H), 0.34 (s, 9H).

<sup>13</sup>C NMR (91 MHz, CDCl<sub>3</sub>) δ 154.42, 153.38, 143.20, 136.44, 108.53, 100.23, 89.64, 80.13, 28.33, -7.85.

HRMS (ESI<sup>+</sup>): *m/z* Calcd for C<sub>15</sub>H<sub>23</sub>NO<sub>4</sub>Sn + Na, [M+Na]<sup>+</sup>: 424.0541, found: 424.0544.



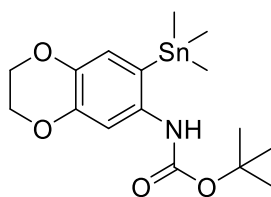
**87**

**Compound 87.** To a solution of 1,4-benzodioxan-6-amine **86** (2.3 g, 20 mmol, 1 eq) in 200 mL of THF was added triethylamine (5.57 mL, 40 mmol, 2 eq) and Boc<sub>2</sub>O (4.4 g, 20 mmol, 1 eq). The mixture was then stirred at RT overnight. When the reaction was complete (checked by TLC), the THF was removed by evaporation under reduced pressure and the crude product was purified by flash chromatography (cyclohexane:EtOAc = 7:3) to afford the expected product (5.0 g, 100%) as a yellow powder.

<sup>1</sup>H NMR (300 MHz, CDCl<sub>3</sub>) δ 6.95 (s, 1H), 6.76-6.74 (m, 2H), 6.49 (s, 1H), 4.20 (s, 4H), 1.48 (s, 9H).

<sup>13</sup>C NMR (75 MHz, CDCl<sub>3</sub>) δ 152.93, 143.41, 139.60, 132.05, 117.02, 112.29, 108.43, 80.14, 64.34, 64.13, 28.24, 26.79.

HRMS (ESI<sup>+</sup>): m/z Calcd for C<sub>13</sub>H<sub>17</sub>NO<sub>4</sub> + Na, [M+Na]<sup>+</sup>: 274.1049, found: 274.1044



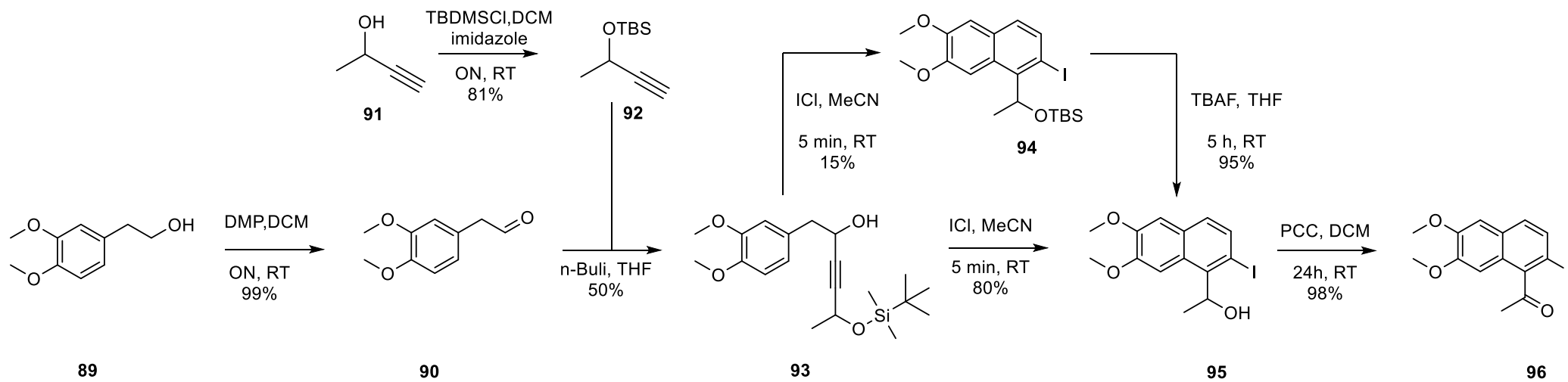
**88**

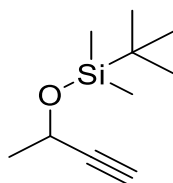
**Compound 88.** Amine **87** (1.5 g, 6 mmol, 1.0 eq) was placed in an oven dried round bottomed-flask and dissolved in 15 mL of dry Et<sub>2</sub>O. The solution was cooled to - 40 °C under an Ar atmosphere. *t*-BuLi (1.7 M in pentane, 7.3 mL, 12.5 mmol, 2.1 eq) was added via a syringe pump over 30 min, during which the mixture became homogenous, and the resulting solution was stirred at 0 °C for 3 h. The reaction mixture was further cooled to - 78 °C, treated with Me<sub>3</sub>SnCl (1.19 g, 6 mmol, 1.0 eq) in a solution of 9 mL of Et<sub>2</sub>O, and stirred at 0 °C for 6 h. The reaction mixture was quenched with saturated aqueous NaHCO<sub>3</sub> solution (60 mL) at 0 °C. The organic phases were extracted with Et<sub>2</sub>O (30 mL x 2) and washed with brine (50 mL). The combined organic layers were dried over Na<sub>2</sub>SO<sub>4</sub> and concentrated under reduced pressure. Column chromatography using neutral alumina pre-washed with a 40:4:1 mixture of hexane/Et<sub>3</sub>N/EtOAc, eluted with 20:1 mixture of Hex/EtOAc gave the expected product (1.26 g, 51%) as a yellow solid.

<sup>1</sup>H NMR (360 MHz, CDCl<sub>3</sub>) δ 7.12 – 6.89 (m, 1H), 6.82 – 6.76 (m, 1H), 6.32 (s, 1H), 4.19 (s, 4H), 1.49 (s, 9H), 0.34 (s, 9H).

<sup>13</sup>C NMR (91 MHz, CDCl<sub>3</sub>) δ 154.08, 146.78, 140.13, 136.25, 117.96, 79.66, 64.49, 63.89, 28.25, 26.73, -7.18.

HRMS (ESI<sup>+</sup>): *m/z* Calcd for C<sub>16</sub>H<sub>25</sub>NO<sub>4</sub>Sn + Na, [M+Na]<sup>+</sup>: 438.0700, found: 437.0722.



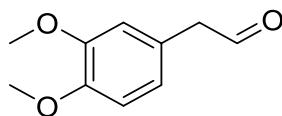


**92**

**Compound 92.** To a solution of but-3-yn-2-ol **91** (10 g, 143 mmol, 1 eq) in anhydrous DCM (0.5 M) were added TBDMSCl (28.0 g, 186 mmol, 1.3 eq) and imidazole (12.3 g, 186 mmol, 1.3 eq) at 0°C under argon. The resulting mixture was warmed to room temperature and stirred at the same temperature overnight. Then, the reaction mixture was treated with saturated aqueous NH<sub>4</sub>Cl and extracted with EtOAc, washed with water and brine, dried over MgSO<sub>4</sub>, and concentrated under reduced pressure to give 21.3 g (81%) of silylated ether.

<sup>1</sup>H NMR (250 MHz, CDCl<sub>3</sub>): δ = 4.51 (qd, *J* = 6.6, 2.1 Hz, 1H), 2.37 (d, *J* = 2.0 Hz, 1H), 1.42 (d, *J* = 6.6 Hz, 3H), 0.90 (s, 9H), 0.13 (s, 3H), 0.12 (s, 3H).

The spectral data are similar to those reported in: *J. Am. Chem. Soc.* **2004**, 126, 16553-16558.



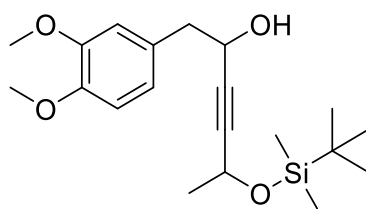
**90**

**Compound 90.** To a solution of 2-(3,4-dimethoxyphenyl)ethanol **89** (4.0 g, 11.0 mmol, 1 eq) in 100 mL dichloromethane was added Dess-Martin reagent (11.2 g, 13.2 mmol, 1.2 eq). The mixture was stirred at r.t. overnight. The suspension was filtered and the solid was rinsed with dichloromethane. The filtrate was concentrated under reduced pressure to give the expected product that was engaged in the next step without further purification.

<sup>1</sup>H NMR (360 MHz, CDCl<sub>3</sub>) δ 9.71 (t, *J* = 2.4 Hz, 1H), 6.85 (d, *J* = 8.1 Hz, 1H), 6.76 (dt, *J* = 8.1, 2.0 Hz, 1H), 6.69 (d, *J* = 2.0 Hz, 1H), 3.86 (s, 6H), 3.61 (d, *J* = 2.4 Hz, 2H).

<sup>13</sup>C NMR (91 MHz, CDCl<sub>3</sub>) δ 199.40, 149.22, 148.30, 124.11, 121.74, 112.50, 111.50, 55.84, 55.77, 49.98.

The spectral data are similar to those reported in: *Monatshefte für Chemie*, 2004, 135, 1289-1295.



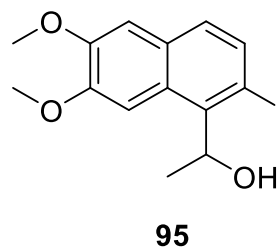
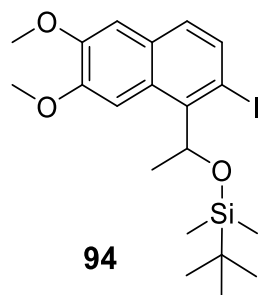
**93**

**Compound 93.** To a solution of **92** (6.8 g, 37 mmol, 2 eq) in 50 mL of anhydrous THF was added *n*-BuLi 2.5 M (14.8 mL, 37 mmol, 2 eq) at 0°C under Ar atmosphere. The resulting solution was stirred at the same temperature for 1 h. Then **90** (3.31 g, 18 mmol, 1 eq) in 11 mL of THF was added dropwise by syringe. The reaction mixture was kept under the inert atmosphere and stirred for 16 h while it warmed up to ambient temperature. The mixture was then quenched by adding saturated aqueous NH<sub>4</sub>Cl and extracted twice with EtOAc. The combined organic fractions were dried over MgSO<sub>4</sub> and concentrated under vacuum to yield the crude product, which was purified by flash chromatography on silica gel (cyclohexane:EtOAc = 95:5 to 60:40) to give 3.30 g (50%) of expected product.

<sup>1</sup>H NMR (300 MHz, CDCl<sub>3</sub>) δ 6.80-6.82 (m, 3H), 4.65 – 4.40 (m, 2H), 3.88 (s, 3H), 3.86 (s, 3H), 3.00 – 2.85 (m, 2H), 1.38 (d, J = 6.5 Hz, 3H), 0.92 – 0.86 (m, 9H), 0.12 – 0.06 (m, 6H).

<sup>13</sup>C NMR (75 MHz, CDCl<sub>3</sub>) δ 148.82, 148.03, 129.30, 121.79, 112.95, 111.18, 88.23, 83.44, 63.26, 63.13, 58.94, 55.83, 43.57, 25.78, 25.38, -4.60, -4.95.

HRMS (ESI<sup>+</sup>): m/z Calcd for C<sub>20</sub>H<sub>32</sub>O<sub>4</sub>Si + Na, [M+Na]<sup>+</sup>: 387.1962, found: 387.1949.



**Compounds 94 and 95.** To a solution of **93** (3.30 g, 9.1 mmol 1 eq) in 70 mL of dry MeCN was added NaHCO<sub>3</sub> (1.53 g, 18.2 mmol, 2 eq). The solution was stirred for 1 min at room temperature then ICl (2.95 g 18.2 mmol, 2 eq) in 10 mL of dry CH<sub>3</sub>CN was added dropwise. The reaction mixture was stirred at room temperature during 5 min. The reaction mixture was then diluted with 100 mL of EtOAc and washed with 50 mL of saturated aqueous Na<sub>2</sub>S<sub>2</sub>O<sub>3</sub>. The organic layer was separated, and the aqueous layer was extracted three time with 30 mL of EtOAc. The combined organic layers were dried over MgSO<sub>4</sub> and filtered. The solvent was evaporated under reduced pressure and the crude product was purified by flash chromatography on silica gel (cyclohexane:EtOAc = 95:5 to 60:40) to give 641 mg of **94** (15%) and 2.76 g (85%) of **95**.

#### Compound **94**:

<sup>1</sup>H NMR (300 MHz, CDCl<sub>3</sub>) δ 8.53 (s, 1H), 7.85 (d, *J* = 8.6 Hz, 1H), 7.47 – 7.39 (m, 1H), 7.21 (s, 1H), 5.80 (q, *J* = 6.6 Hz, 1H), 4.17 (s, 3H), 4.16 (s, 3H), 1.80 (d, *J* = 6.6 Hz, 3H), 1.04 (s, 9H), 0.28 (s, 3H), 0.10 (s, 3H).

<sup>13</sup>C NMR (75 MHz, CDCl<sub>3</sub>) δ 149.24, 148.21, 140.63, 134.58, 130.69, 127.69, 127.46, 106.58, 105.96, 94.38, 79.09, 55.70, 26.90, 25.86, 23.29, -4.76, -4.97.

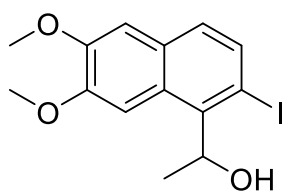
HRMS (ESI<sup>+</sup>): *m/z* Calcd for C<sub>20</sub>H<sub>29</sub>I<sub>3</sub>O<sub>3</sub>Si + Na, [M+Na]<sup>+</sup>: 495.0822, found: 495.0805.

#### Compound **95**:

<sup>1</sup>H NMR (360 MHz, CDCl<sub>3</sub>) δ 8.22 (s, 1H), 7.63 (d, *J* = 8.6 Hz, 1H), 7.18 (dd, *J* = 11.3, 5.6 Hz, 1H), 6.98 (s, 1H), 5.67 (q, *J* = 6.7 Hz, 1H), 3.94 (s, 3H), 3.92 (s, 3H), 1.63 (d, *J* = 6.8 Hz, 3H).

<sup>13</sup>C NMR (91 MHz, CDCl<sub>3</sub>) δ 149.39, 148.63, 139.59, 134.77, 130.72, 128.07, 127.28, 106.90, 104.93, 78.30, 55.89, 55.75, 21.63.

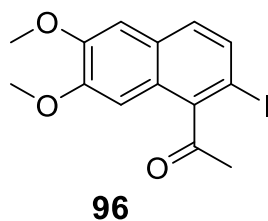
HRMS (ESI<sup>+</sup>): *m/z* Calcd for C<sub>14</sub>H<sub>15</sub>I<sub>3</sub>O<sub>3</sub> + Na, [M+Na]<sup>+</sup>: 380.9963, found: 380.9956.



**95**

#### Compound 95 (from 94).

To a solution of **94** (500 mg, 1.0 mmol, 1 eq) in dry THF was added TBAF (1.1 mmol, 1.1 mL, 1.0 M in THF, 1.1 eq) and the reaction was stirred at r.t. during 5 h. Water (20 mL) was added and the mixture was extracted with EtOAc (2 x 20 mL). The combined organic layers were dried over MgSO<sub>4</sub>. The solvent was removed under reduced pressure and the crude product was purified by flash chromatography on silica gel (cyclohexane:EtOAc = 95:5 to 60:40) to give 340 mg of **95** (95%).



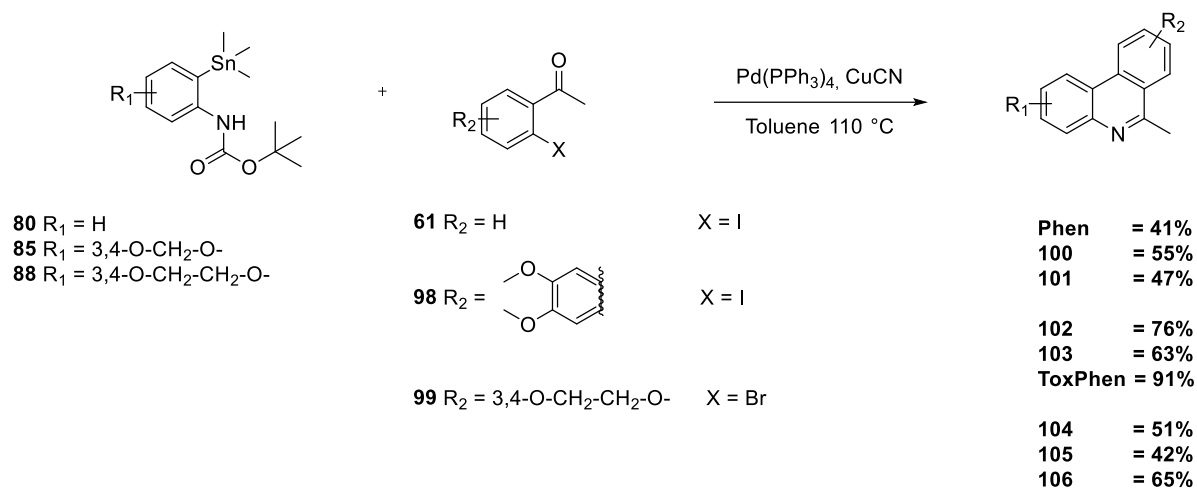
**Compound 96.** To a solution of compound **95** (1.50 g, 4.2 mmol, 1 eq) in 60 mL of dry DCM was added PCC (4.5 g, 21 mmol, 5 eq). The dark solution was stirred at r.t. during 24h. 50 mL of Et<sub>2</sub>O was added, and the suspension was filtered under celite. The pad of celite was washed with DCM and the filtrate was concentrated under reduced pressure. The crude product was purified by flash chromatography on silica gel (cyclohexane:EtOAc = 95:5 to 60:40) to give 1.46 g (98%) of expected product as an orange powder.

<sup>1</sup>H NMR (300 MHz, CDCl<sub>3</sub>) δ 7.64 (d, *J* = 8.6 Hz, 1H), 7.39 (d, *J* = 8.6 Hz, 1H), 7.08 (s, *J* = 5.6 Hz, 1H), 6.80 (s, 1H), 3.98 (s, 3H), 3.93 (s, 3H), 2.70 (s, 3H).

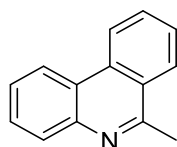
<sup>13</sup>C NMR (75 MHz, CDCl<sub>3</sub>) δ 206.52, 150.59, 150.07, 143.10, 133.37, 128.66, 128.49, 125.63, 106.67, 102.71, 56.4, 28.05.

HRMS (ESI<sup>+</sup>): *m/z* Calcd for C<sub>14</sub>H<sub>13</sub>I O<sub>3</sub> + H, [M+H]<sup>+</sup>: 356.9987, found: 356.9975.

HRMS (ESI<sup>+</sup>): *m/z* Calcd for C<sub>14</sub>H<sub>13</sub>I O<sub>3</sub> + Na, [M+Na]<sup>+</sup>: 378.9801, found: 378.9801.



**6-methylphenanthridines “Phen/ToxPhen/100-106”.** To a flame-dried round-bottom flask containing a stir bar was added the **acetophenone derivatives** (1.1 eq), the **phenyl stannane derivatives** (1 eq),  $\text{Pd(PPh}_3)_4$  (0.02 eq) and  $\text{CuCN}$  (0.2 eq). 4 mL of dry toluene was then added and the solution was refluxed during 24 h. The mixture was filtered through a pad of celite and the filtrate was concentrated under reduced pressure. The crude product was purified by flash chromatography on silica gel (cyclohexane:EtOAc = 9:1 to 6:4) to give the expected product.



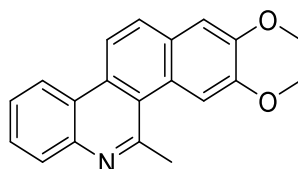
**Phen**

$^1\text{H}$  NMR (300 MHz,  $\text{CDCl}_3$ )  $\delta$  7.79 (s, 1H), 7.65 (s, 1H), 7.59 (s, 1H), 7.43 (bs, 1H), 6.10 (s, 2H), 4.41 (m, 4H), 2.90 (s, 3H).

$^{13}\text{C}$  NMR (75 MHz,  $\text{CDCl}_3$ )  $\delta$  155.36, 148.54, 147.26, 143.43, 128.60, 120.94, 118.99, 112.87, 108.51, 107.05, 101.52, 100.76, 99.21, 97.72, 64.72, 64.40, 26.79.

HRMS (ESI<sup>+</sup>):  $m/z$  Calcd for  $\text{C}_{14}\text{H}_{11}\text{N} + \text{H}$ ,  $[\text{M}+\text{H}]^+$ : 194.0929, found: 194.0964.

Yield = 41%



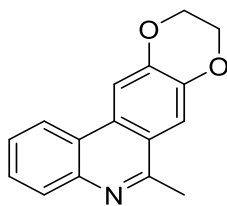
**100**

$^1\text{H}$  NMR (400 MHz,  $\text{CDCl}_3$ )  $\delta$  8.59 (d,  $J = 8.2$  Hz, 1H), 8.51 (d,  $J = 8.9$  Hz, 1H), 8.32 (s, 1H), 8.16 (d,  $J = 8.1$  Hz, 1H), 8.03 (d,  $J = 8.8$  Hz, 1H), 7.76 (t,  $J = 7.4$  Hz, 1H), 7.66 (t,  $J = 7.5$  Hz, 1H), 7.34 (s, 1H), 4.14 (s, 3H), 4.10 (s, 3H), 3.47 (s, 3H).

$^{13}\text{C}$  NMR (101 MHz,  $\text{CDCl}_3$ )  $\delta$  156.66, 149.34, 148.97, 143.30, 132.66, 130.77, 129.14, 128.72, 128.46, 126.21, 125.78, 123.71, 122.61, 122.32, 118.62, 108.24, 108.11, 56.02, 55.92, 31.22.

HRMS (ESI<sup>+</sup>):  $m/z$  Calcd for  $\text{C}_{20}\text{H}_{17}\text{NO}_2 + \text{H}$ ,  $[\text{M}+\text{H}]^+$ : 296.0917, found: 296.0913.

Yield = 55%



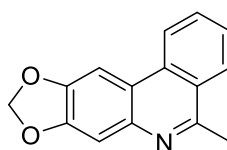
**101**

$^1\text{H}$  NMR (400 MHz,  $\text{CDCl}_3$ )  $\delta$  8.32 (d,  $J = 8.1$  Hz, 1H), 8.04 (d,  $J = 8.1$  Hz, 1H), 7.99 (s, 1H), 7.63 (s, 1H), 7.53 (dd,  $J = 19.4, 12.2$  Hz, 1H), 7.26 (dt,  $J = 15.1, 7.2$  Hz, 1H), 4.53 – 4.35 (m, 4H), 2.93 (s, 3H).

$^{13}\text{C}$  NMR (91 MHz,  $\text{CDCl}_3$ )  $\delta$  157.65, 147.10, 143.95, 142.98, 129.13, 128.36, 127.88, 126.04, 123.47, 121.74, 121.69, 113.27, 109.08, 64.69, 64.40, 23.35.

HRMS (ESI<sup>+</sup>):  $m/z$  Calcd for  $\text{C}_{16}\text{H}_{13}\text{NO}_2 + \text{H}$ ,  $[\text{M}+\text{H}]^+$ : 252.1019, found: 252.1018.

Yield = 47%



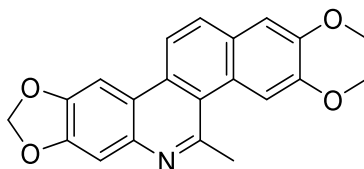
**102**

$^1\text{H}$  NMR (300 MHz,  $\text{CDCl}_3$ )  $\delta$  8.43 (d,  $J = 8.3$  Hz, 1H), 8.20 (d,  $J = 8.2$  Hz, 1H), 7.81 (t,  $J = 7.7$  Hz, 1H), 7.65 (t,  $J = 7.6$  Hz, 1H), 7.50 (s, 1H), 7.28 (s, 1H), 6.15 (s, 2H), 3.03 (s, 3H).

$^{13}\text{C}$  NMR (75 MHz,  $\text{CDCl}_3$ )  $\delta$  156.57, 149.16, 147.58, 140.87, 132.62, 130.16, 126.52, 126.40, 125.06, 122.08, 119.46, 107.18, 101.67, 99.35, 22.99.

HRMS (ESI<sup>+</sup>):  $m/z$  Calcd for  $\text{C}_{15}\text{H}_{11}\text{NO}_2 + \text{H}$ ,  $[\text{M}+\text{H}]^+$ : 238.0863, found: 238.0859.

Yield = 76%



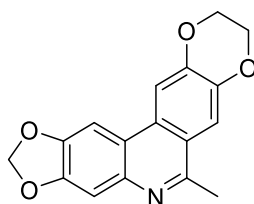
**103**

$^1\text{H}$  NMR (360 MHz,  $\text{CDCl}_3$ )  $\delta$  8.90 (d,  $J = 8.9$  Hz, 1H), 8.30 (s, 1H), 7.99 (d,  $J = 8.9$  Hz, 1H), 7.71 (d,  $J = 8.6$  Hz, 1H), 7.42 – 7.30 (m, 2H), 6.29 (s, 2H), 4.12 (s, 3H), 4.08 (s, 3H), 3.39 (s, 3H).

$^{13}\text{C}$  NMR (91 MHz,  $\text{CDCl}_3$ )  $\delta$  154.83, 149.14, 149.02, 144.60, 141.82, 139.93, 130.71, 130.13, 129.35, 125.36, 122.78, 122.67, 122.23, 111.49, 110.93, 107.95, 107.87, 101.66, 55.98, 55.90, 31.08.

HRMS (ESI<sup>+</sup>):  $m/z$  Calcd for  $\text{C}_{21}\text{H}_{17}\text{NO}_4 + \text{H}$ ,  $[\text{M}+\text{H}]^+$ : 348.1235, found: 348.1219.

Yield = 63%



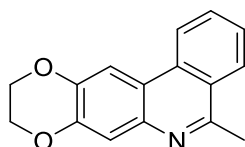
**ToxPhen**

$^1\text{H}$  NMR (300 MHz,  $\text{CDCl}_3$ )  $\delta$  7.79 (s, 1H), 7.65 (s, 1H), 7.59 (s, 1H), 7.43 (s, 1H), 6.10 (s, 2H), 4.41 (m, 4H), 2.90 (s, 3H).

$^{13}\text{C}$  NMR (75 MHz,  $\text{CDCl}_3$ )  $\delta$  155.36, 148.54, 147.26, 143.43, 128.60, 120.94, 118.99, 112.87, 108.51, 107.05, 101.52, 100.76, 99.21, 97.72, 64.72, 64.40, 26.79.

HRMS (ESI<sup>+</sup>):  $m/z$  Calcd for  $\text{C}_{17}\text{H}_{13}\text{NO}_4 + \text{H}$ ,  $[\text{M}+\text{H}]^+$ : 296.0917, found: 296.0913.

Yield = 91%



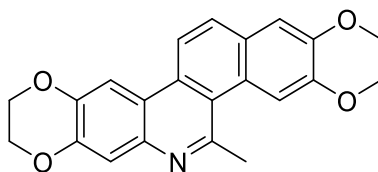
**104**

$^1\text{H}$  NMR (360 MHz,  $\text{CDCl}_3$ )  $\delta$  9.40 (dd,  $J = 8.6, 0.6$  Hz, 1H), 8.13 (dd,  $J = 8.2, 1.0$  Hz, 1H), 7.79 – 7.54 (m, 3H), 7.26 – 7.15 (m, 1H), 4.53 – 4.32 (m, 4H), 2.92 (s, 3H).

$^{13}\text{C}$  NMR (91 MHz,  $\text{CDCl}_3$ )  $\delta$  156.81, 141.06, 140.44, 139.94, 132.13, 129.87, 128.14, 126.84, 126.30, 125.96, 122.37, 119.01, 114.93, 64.30, 63.91, 23.26.

HRMS (ESI<sup>+</sup>):  $m/z$  Calcd for  $\text{C}_{16}\text{H}_{13}\text{NO}_2 + \text{H}$ ,  $[\text{M}+\text{H}]^+$ : 252.1019, found: 252.1018.

Yield = 51%



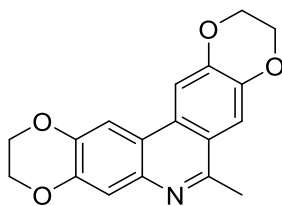
**105**

$^1\text{H}$  NMR (360 MHz,  $\text{CDCl}_3$ )  $\delta$  7.59 (d,  $J = 8.6$  Hz, 1H), 7.33 (t,  $J = 9.2$  Hz, 1H), 7.19 (s, 1H), 7.02 (s, 1H), 6.74 (s, 1H), 6.70 (s, 1H), 4.20 – 4.08 (m, 4H), 3.93 (s, 3H), 3.87 (s, 3H), 2.65 (s, 3H).

$^{13}\text{C}$  NMR (91 MHz,  $\text{CDCl}_3$ )  $\delta$  150.60, 150.09, 143.52, 143.12, 139.51, 133.41, 132.04, 128.68, 128.52, 125.65, 117.13, 112.34, 108.47, 106.68, 102.72, 84.79, 64.43, 64.22, 55.97, 55.92, 31.43.

HRMS (ESI<sup>+</sup>):  $m/z$  Calcd for  $\text{C}_{22}\text{H}_{19}\text{NO}_4 + \text{H}$ ,  $[\text{M}+\text{H}]^+$ : 362.1386, found: 362.1373.

Yield = 42%



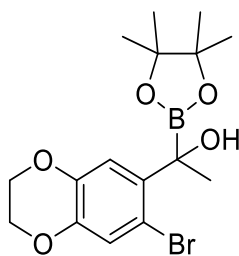
**106**

$^1\text{H}$  NMR (360 MHz,  $\text{CDCl}_3$ )  $\delta$  7.57 (s, 1H), 7.47 – 7.29 (m, 1H), 7.27 – 7.08 (m, 1H), 6.86 – 6.48 (m, 1H), 4.55 – 3.95 (m, 8H), 1.36 (s, 3H).

$^{13}\text{C}$  NMR (75 MHz,  $\text{CDCl}_3$ )  $\delta$  155.58, 153.31, 143.31, 143.09, 139.79, 133.62, 129.68, 124.30, 120.33, 118.73, 116.81, 115.26, 112.86, 65.08, 64.29, 63.92, 63.22, 28.29.

HRMS (ESI<sup>+</sup>):  $m/z$  Calcd for  $\text{C}_{18}\text{H}_{15}\text{NO}_4 + \text{H}$ ,  $[\text{M}+\text{H}]^+$ : 310.1073, found: 310.1063.

Yield = 65%



**109**

**Compound 109.** To a flame-dried 50 mL round-bottom flask containing a stir bar was added bis(pinacolato)diboron (1.47 g, 5.8 mmol, 1.5 eq), 1,3-bis(cyclohexyl)imidazolium tetrafluoroborate (125 mg, 0.39 mmol, 0.1 eq), *t*-BuONa (75 mg, 0.78 mmol, 0.2 eq), and CuCl (77 mg, 0.78 mmol, 0.2 eq). Then 10 mL of toluene was added, the flask was sealed and the reaction was stirred for 30 min. Compound **99** (1 g, 3.9 mmol, 1 eq) was added via a syringe followed immediately by MeOH (342  $\mu$ L, 8 mmol, 2 eq) addition. After 3 h, the mixture was loaded directly onto a short pad of silica gel pretreated with DCM. The pad was thoroughly washed with Et<sub>2</sub>O and the filtrate was evaporated under reduced pressure. The resulting residue was purified by flash chromatography on silica gel (cyclohexane:EtOAc = 95:5 to 60:40) to give the expected product (470 mg, 31%) of expected product as a colorless oil.

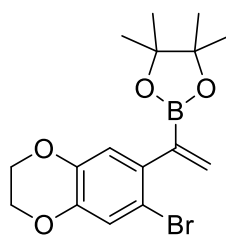
TLC condition: eluent (cyclohexane:EtOAc = 8:2); R<sub>f</sub> = 0.51.

<sup>1</sup>H NMR (300 MHz, CDCl<sub>3</sub>)  $\delta$  7.10 (s, 1H), 7.04 (s, 1H), 4.22 (s, 4H), 2.28 (s, 1H), 1.42 (s, 3H), 1.30 (s, 12H).

<sup>13</sup>C NMR (63 MHz, CDCl<sub>3</sub>)  $\delta$  142.93, 142.89, 138.74, 121.37, 115.53, 112.77, 84.44, 83.10, 64.33, 64.27, 26.89, 25.00, 24.83, 24.73, 24.53.

<sup>11</sup>B NMR (96 MHz, CDCl<sub>3</sub>)  $\delta$  30.74.

HRMS (ESI<sup>+</sup>): *m/z* Calcd for C<sub>16</sub>H<sub>22</sub>BBro<sub>5</sub> + Na, [M+Na]<sup>+</sup>: 407.0638, found: 407.0629.



**110**

**Compound 110.** To a solution of **109** (470 mg, 1.22 mmol, 1 eq) in toluene (40 mL) was added *p*-toluenesulfonic acid (630 mg, 3.66 mmol, 3 eq). The mixture was heated at 60°C for 3 h. 5 mL of a Na<sub>2</sub>CO<sub>3</sub> saturated aqueous solution was added and the aqueous layer was extracted with EtOAc (3x20 mL). The organic phases were combined, washed with brine, dried with MgSO<sub>4</sub> and concentrated under reduced pressure to give the expected product (447 mg, 100%) as a white solid.

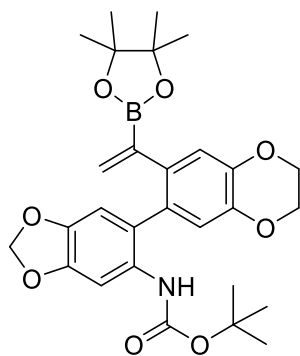
<sup>1</sup>H NMR (400 MHz, CDCl<sub>3</sub>) δ 7.04 (s, 1H), 6.75 (s, 1H), 6.03 (d, *J* = 3.3 Hz, 1H), 5.75 (d, *J* = 3.3 Hz, 1H), 4.22 (s, 4H), 1.30 (s, 12H).

<sup>13</sup>C NMR (96 MHz, CDCl<sub>3</sub>) δ 128.88, 128.64, 123.74, 120.11, 111.04, 109.06, 105.34, 82.37, 67.03, 66.98, 36.22, 36.04.

<sup>11</sup>B NMR (96 MHz, CDCl<sub>3</sub>) δ 29.60.

HRMS (ESI<sup>+</sup>): *m/z* Calcd for C<sub>16</sub>H<sub>20</sub>BBro<sub>4</sub> + H, [M+H]<sup>+</sup>: 367.0716, found: 367.0698.

HRMS (ESI<sup>+</sup>): *m/z* Calcd for C<sub>16</sub>H<sub>20</sub>BBro<sub>4</sub> + NH<sub>4</sub>, [M+NH<sub>4</sub>]<sup>+</sup>: 384.0979, found: 384.0964.

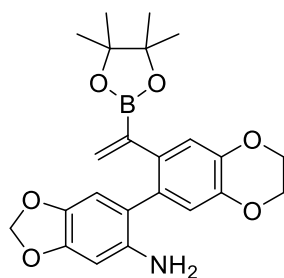


111

**Compound 111.** To a flame-dried 5 mL round-bottom flask containing a stir bar was added **85** (67 mg, 0.17 mmol, 1.1 eq), **110** (56 mg, 0.15 mmol, 1 eq), Pd(PPh<sub>3</sub>)<sub>4</sub> (3.5 mg, 0.0036 mmol, 0.02 eq) and CuCN (2.7 mg, 0.036 mmol, 0.2 eq) and the mixture was refluxed in 4 mL of toluene under argon for 14h. The mixture was quenched with EtOAc, filtered through a pad of celite which was thoroughly washed with EtOAc. The filtrate was then concentrated under reduced pressure to give a crude product that was engaged in the next step without further purification.

HRMS (ESI<sup>+</sup>): m/z Calcd for = C<sub>28</sub>H<sub>34</sub>BNO<sub>8</sub> + H, [M+H]<sup>+</sup>: 524.2455, found: 524.2441.

HRMS (ESI<sup>+</sup>): m/z Calcd for C<sub>28</sub>H<sub>34</sub>BNO<sub>8</sub> + Na, [M+Na]<sup>+</sup>: 546.2257, found: 546.2274.



**ProToxPhen**

**ProToxPhen.** To a solution of Boc derivative **111** (13 mg, 0.025 mmol, 1.0 eq) in 1 mL of dry dichloromethane was added 2,6-lutidine (35  $\mu$ L, 0.30 mmol, 12 eq) and TMSOTf (27  $\mu$ L, 0.15 mmol, 6.0 eq) at r.t. and under Ar atmosphere. The solution was stirred for 1h30 before water (10 mL) was added. The resulting mixture was diluted with  $\text{CH}_2\text{Cl}_2$  (50 mL) and stirred vigorously for 15 min. The organic phase was separated, washed with water and brine, dried over  $\text{MgSO}_4$  and concentrated on a rotary evaporator. The crude product was purified by flash chromatography (cyclohexane:EtOAc = 70:30) followed by purification by PTLC (cyclohexane:EtOAc = 70:30) to give the expected product (4.1 mg, 39%) as a brown powder.

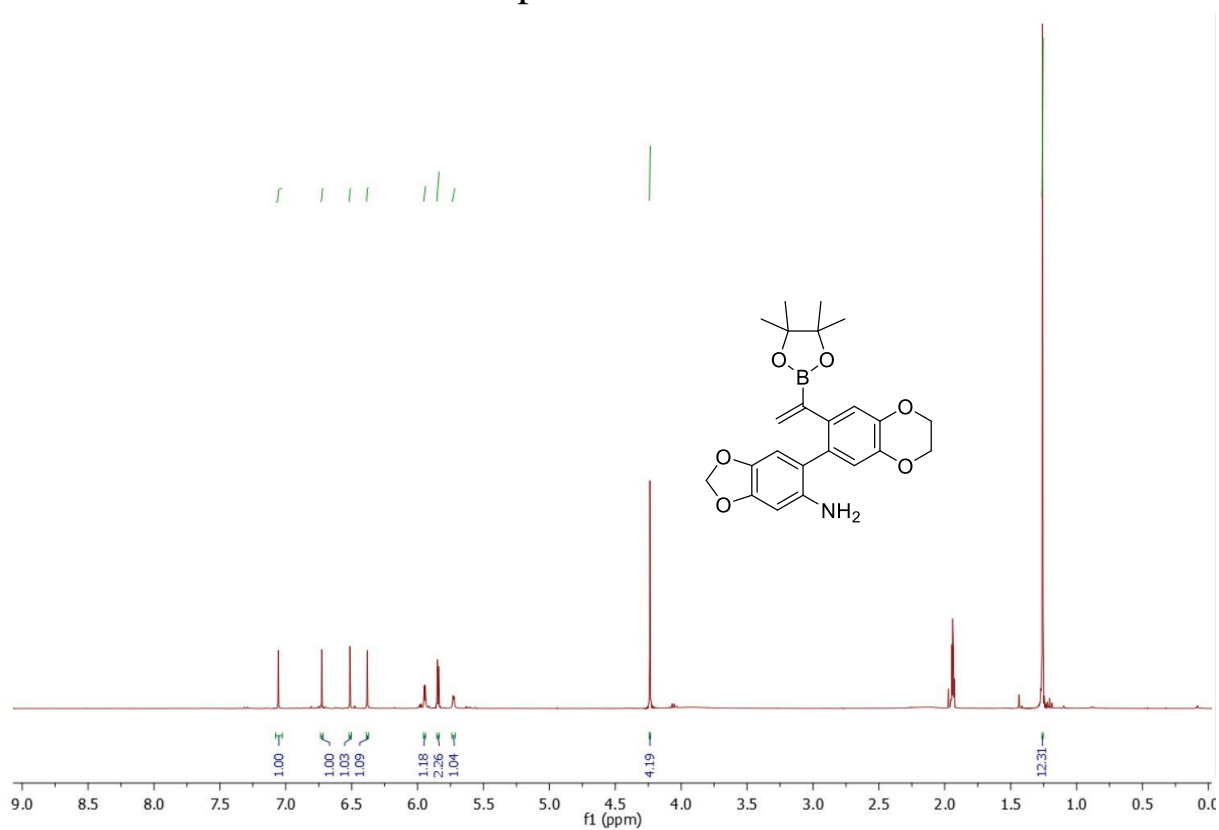
$^1\text{H}$  NMR (360 MHz,  $\text{CD}_3\text{CN}$ )  $\delta$  7.08 (s, 1H), 6.90 (s, 1H), 6.84 (s, 1H), 6.76 (s, 1H), 6.10 – 5.98 (m, 2H), 5.98 (d,  $J$  = 3.2 Hz, 1H), 5.76 (d,  $J$  = 2.9 Hz, 1H), 4.27 (s, 4H), 1.29 (s, 12H).

$^{13}\text{C}$  NMR (91 MHz,  $\text{CD}_3\text{CN}$ )  $\delta$  149.21, 146.40, 144.47, 144.19, 137.49, 132.43, 120.86, 118.58, 113.53, 111.66, 103.27, 103.17, 84.77, 65.29, 65.23, 25.05.

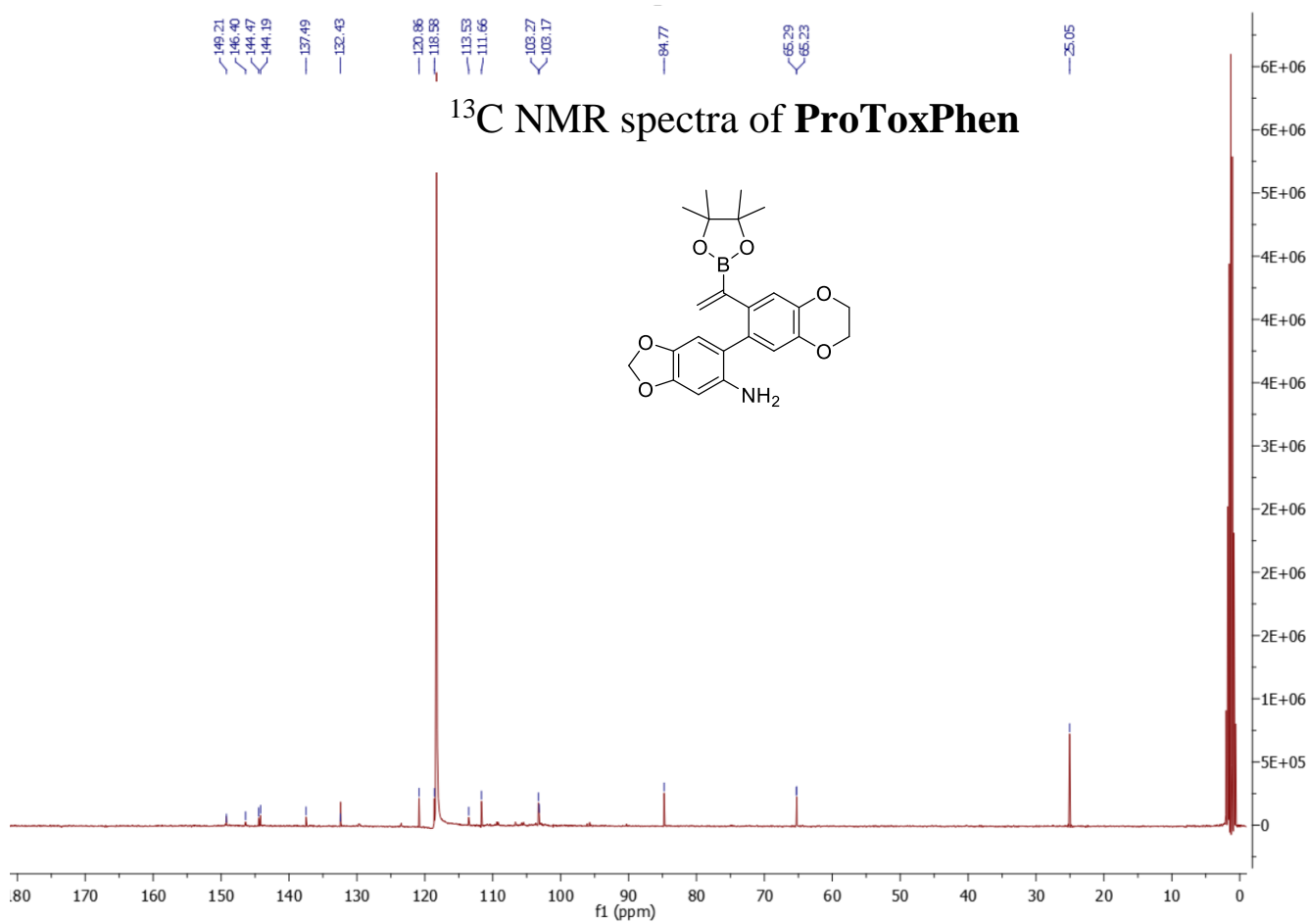
$^{11}\text{B}$  NMR (96 MHz,  $\text{CD}_3\text{CN}$ )  $\delta$  32.78.

HRMS (ESI $^+$ ):  $m/z$  Calcd for =  $\text{C}_{23}\text{H}_{26}\text{BNO}_6 + \text{H}$ ,  $[\text{M}+\text{H}]^+$ : 424.1930, found: 424.1912.

# <sup>1</sup>H NMR spectra of ProToxPhen



# <sup>13</sup>C NMR spectra of ProToxPhen



# Bibliography

- (1) Cancer <https://www.who.int/fr/news-room/fact-sheets/detail/cancer> (accessed 2021 -09 -09).
- (2) Seyfried, T. N.; Huysentruyt, L. C. On the Origin of Cancer Metastasis. *Crit Rev Oncog* **2013**, *18* (1–2), 43–73.
- (3) Cancer today <http://gco.iarc.fr/today/home> (accessed 2021 -11 -05).
- (4) MacMahon, B.; Cole, P.; Lin, T. M.; Lowe, C. R.; Mirra, A. P.; Ravnihar, B.; Salber, E. J.; Valaoras, V. G.; Yuasa, S. Age at First Birth and Breast Cancer Risk. *Bull World Health Organ* **1970**, *43* (2), 209–221.
- (5) Institut National Du Cancer - Accueil <https://www.e-cancer.fr/> (accessed 2021 -09 -09).
- (6) Cancers <https://www.santepubliquefrance.fr/maladies-et-traumatismes/cancers> (accessed 2021 -11 -05).
- (7) Baskar, R.; Dai, J.; Wenlong, N.; Yeo, R.; Yeoh, K.-W. Biological Response of Cancer Cells to Radiation Treatment. *Front Mol Biosci* **2014**, *1*, 24. <https://doi.org/10.3389/fmolb.2014.00024>.
- (8) Ozsaran, Z.; Yalman, D.; Yürüt, V.; Aras, A.; Ozsaran, A.; Hanhan, M.; Haydaroğlu, A. Radiochemotherapy for Patients with Locally Advanced Cervical Cancer: Early Results. *Eur J Gynaecol Oncol* **2003**, *24* (2), 191–194.
- (9) How Immunotherapy Is Used to Treat Cancer <https://www.cancer.org/treatment/treatments-and-side-effects/treatment-types/immunotherapy/what-is-immunotherapy.html> (accessed 2021 -11 -05).
- (10) Chemotherapy <https://www.gustaveroussy.fr/fr/chimiotherapie> (accessed 2021 -11 -05).
- (11) InfoCancer - ARCAGY - GINECO – Traitements – Traitements systémiques – Chimiothérapie – Les médicaments - Les antimétabolites <http://www.arcagy.org/infocancer/traitement-du-cancer/traitements-systemiques/chimiotherapie/les-medicaments/les-antimetabolites.html/> (accessed 2021 -11 -05).
- (12) Lewisite, I. of M. (US) C. on the S. of the H. E. of M. G. and; Pechura, C. M.; Rall, D. P. *Other Physiological Effects of Mustard Agents and Lewisite*; National Academies Press (US), 1993.
- (13) List of Alkylating agents <https://www.drugs.com/drug-class/alkylating-agents.html> (accessed 2021 -11 -05).
- (14) Antineoplastic Antibiotic - an overview | ScienceDirect Topics <https://www.sciencedirect.com/topics/medicine-and-dentistry/antineoplastic-antibiotic> (accessed 2021 -11 -05).
- (15) Mitotic Inhibitors - an overview | ScienceDirect Topics <https://www.sciencedirect.com/topics/neuroscience/mitotic-inhibitors> (accessed 2021 -11 -05).
- (16) Albert, A. Chemical Aspects of Selective Toxicity. *Nature* **1958**, *182* (4633), 421–423. <https://doi.org/10.1038/182421a0>.
- (17) Rautio, J.; Kumpulainen, H.; Heimbach, T.; Oliyai, R.; Oh, D.; Järvinen, T.; Savolainen, J. Prodrugs: Design and Clinical Applications. *Nat Rev Drug Discov* **2008**, *7* (3), 255–270. <https://doi.org/10.1038/nrd2468>.
- (18) Huttunen, K. M.; Raunio, H.; Rautio, J. Prodrugs--from Serendipity to Rational Design. *Pharmacological reviews* **2011**, *63* (3), 750–771. <https://doi.org/10.1124/pr.110.003459>.
- (19) Rautio, J.; Meanwell, N. A.; Di, L.; Hageman, M. J. The Expanding Role of Prodrugs in Contemporary Drug Design and Development. *Nature reviews. Drug discovery* **2018**, *17* (8), 559–587. <https://doi.org/10.1038/nrd.2018.46>.
- (20) Denny, W. A. Prodrug Strategies in Cancer Therapy. *European journal of medicinal chemistry* **2001**, *36* (7–8), 577–595. [https://doi.org/10.1016/s0223-5234\(01\)01253-3](https://doi.org/10.1016/s0223-5234(01)01253-3).
- (21) Zhang, X.; Li, X.; You, Q.; Zhang, X. Prodrug Strategy for Cancer Cell-Specific Targeting: A Recent Overview. *European journal of medicinal chemistry* **2017**, *139*, 542–563. <https://doi.org/10.1016/j.ejmech.2017.08.010>.

- (22) Taresco, V.; Alexander, C.; Singh, N.; Pearce, A. K. Stimuli-Responsive Prodrug Chemistries for Drug Delivery. *Adv Ther-Germany* **2018**, *1* (4), 1800030. <https://doi.org/10.1002/Adtp.201800030>.
- (23) Kratz, F.; Müller, I. A.; Ryppa, C.; Warnecke, A. Prodrug Strategies in Anticancer Chemotherapy. *ChemMedChem* **2008**, *3* (1), 20–53. <https://doi.org/10.1002/cmdc.200700159>.
- (24) Drug Hunter | discover together <https://drughunter.com/> (accessed 2021 -11 -05).
- (25) Research, C. for D. E. and. FDA Approves Gemtuzumab Ozogamicin for CD33-Positive AML in Pediatric Patients. *FDA* **2020**.
- (26) Pfizer Receives FDA Approval for MYLOTARG™ (gemtuzumab ozogamicin) | Pfizer [https://www.pfizer.com/news/press-release/press-release-detail/pfizer\\_receives\\_fda\\_approval\\_for\\_mylotarg\\_gemtuzumab\\_ozogamicin](https://www.pfizer.com/news/press-release/press-release-detail/pfizer_receives_fda_approval_for_mylotarg_gemtuzumab_ozogamicin) (accessed 2021 -11 -05).
- (27) Elmroth, K.; Nygren, J.; Mårtensson, S.; Ismail, I.; Hammarsten, O. Cleavage of Cellular DNA by Calicheamicin  $\Gamma$ 1. *DNA repair* **2003**, *2*, 363–374. [https://doi.org/10.1016/S1568-7864\(02\)00235-5](https://doi.org/10.1016/S1568-7864(02)00235-5).
- (28) Cazzamalli, S.; Dal Corso, A.; Widmayer, F.; Neri, D. Chemically Defined Antibody– and Small Molecule–Drug Conjugates for in Vivo Tumor Targeting Applications: A Comparative Analysis. *J. Am. Chem. Soc.* **2018**, *140* (5), 1617–1621. <https://doi.org/10.1021/jacs.7b13361>.
- (29) Lu, Y.; Segal, E.; Leamon, C. P.; Low, P. S. Folate Receptor-Targeted Immunotherapy of Cancer: Mechanism and Therapeutic Potential. *Adv Drug Deliv Rev* **2004**, *56* (8), 1161–1176. <https://doi.org/10.1016/j.addr.2004.01.009>.
- (30) Pohl, J.; Bertram, B.; Hilgard, P.; Nowrousian, M. R.; Stüben, J.; Wiessler, M. D-19575--a Sugar-Linked Isophosphoramidate Mustard Derivative Exploiting Transmembrane Glucose Transport. *Cancer Chemother Pharmacol* **1995**, *35* (5), 364–370. <https://doi.org/10.1007/s002800050248>.
- (31) McHugh, M.; Cheng, Y. C. Demonstration of a High Affinity Folate Binder in Human Cell Membranes and Its Characterization in Cultured Human KB Cells. *J Biol Chem* **1979**, *254* (22), 11312–11318.
- (32) Antony, A. C. The Biological Chemistry of Folate Receptors. *Blood* **1992**, *79* (11), 2807–2820.
- (33) Antony, A. C. Folate Receptors. *Annu Rev Nutr* **1996**, *16*, 501–521. <https://doi.org/10.1146/annurev.nu.16.070196.002441>.
- (34) Dixon, K. H.; Mulligan, T.; Chung, K. N.; Elwood, P. C.; Cowan, K. H. Effects of Folate Receptor Expression Following Stable Transfection into Wild Type and Methotrexate Transport-Deficient ZR-75-1 Human Breast Cancer Cells. *J Biol Chem* **1992**, *267* (33), 24140–24147.
- (35) Ross, J. F.; Chaudhuri, P. K.; Ratnam, M. Differential Regulation of Folate Receptor Isoforms in Normal and Malignant Tissues in Vivo and in Established Cell Lines. Physiologic and Clinical Implications. *Cancer* **1994**, *73* (9), 2432–2443. [https://doi.org/10.1002/1097-0142\(19940501\)73:9<2432::aid-cncr2820730929>3.0.co;2-s](https://doi.org/10.1002/1097-0142(19940501)73:9<2432::aid-cncr2820730929>3.0.co;2-s).
- (36) Holm, J.; Hansen, S. I.; Høier-Madsen, M.; Helkjaer, P. E.; Nichols, C. W. Folate Receptors in Malignant and Benign Tissues of Human Female Genital Tract. *Biosci Rep* **1997**, *17* (4), 415–427. <https://doi.org/10.1023/a:1027313502270>.
- (37) Franklin, W. A.; Waintrub, M.; Edwards, D.; Christensen, K.; Prendegrast, P.; Woods, J.; Bunn, P. A.; Kolhouse, J. F. New Anti-Lung-Cancer Antibody Cluster 12 Reacts with Human Folate Receptors Present on Adenocarcinoma. *Int J Cancer Suppl* **1994**, *8*, 89–95. <https://doi.org/10.1002/ijc.2910570719>.
- (38) Campbell, I. G.; Jones, T. A.; Foulkes, W. D.; Trowsdale, J. Folate-Binding Protein Is a Marker for Ovarian Cancer. *Cancer Res* **1991**, *51* (19), 5329–5338.
- (39) Henne, W. A.; Doorneweerd, D. D.; Hilgenbrink, A. R.; Kularatne, S. A.; Low, P. S. Synthesis and Activity of a Folate Peptide Camptothecin Prodrug. *Bioorg Med Chem Lett* **2006**, *16* (20), 5350–5355. <https://doi.org/10.1016/j.bmcl.2006.07.076>.
- (40) Liu, J.; Kolar, C.; Lawson, T. A.; Gmeiner, W. H. Targeted Drug Delivery to Chemoresistant Cells: Folic Acid Derivatization of FdUMP[10] Enhances Cytotoxicity toward 5-FU-Resistant Human

- Colorectal Tumor Cells. *J Org Chem* **2001**, *66* (17), 5655–5663. <https://doi.org/10.1021/jo005757n>.
- (41) Lee, J. W.; Lu, J. Y.; Low, P. S.; Fuchs, P. L. Synthesis and Evaluation of Taxol-Folic Acid Conjugates as Targeted Antineoplastics. *Bioorg Med Chem* **2002**, *10* (7), 2397–2414. [https://doi.org/10.1016/s0968-0896\(02\)00019-6](https://doi.org/10.1016/s0968-0896(02)00019-6).
- (42) Bae, Y.; Jang, W.-D.; Nishiyama, N.; Fukushima, S.; Kataoka, K. Multifunctional Polymeric Micelles with Folate-Mediated Cancer Cell Targeting and PH-Triggered Drug Releasing Properties for Active Intracellular Drug Delivery. *Mol Biosyst* **2005**, *1* (3), 242–250. <https://doi.org/10.1039/b500266d>.
- (43) Steinberg, G.; Borch, R. F. Synthesis and Evaluation of Pteric Acid-Conjugated Nitroheterocyclic Phosphoramidates as Folate Receptor-Targeted Alkylating Agents. *J Med Chem* **2001**, *44* (1), 69–73. <https://doi.org/10.1021/jm000306g>.
- (44) Leamon, C. P.; Reddy, J. A.; Vlahov, I. R.; Vetzal, M.; Parker, N.; Nicoson, J. S.; Xu, L.-C.; Westrick, E. Synthesis and Biological Evaluation of EC72: A New Folate-Targeted Chemotherapeutic. *Bioconjug Chem* **2005**, *16* (4), 803–811. <https://doi.org/10.1021/bc049709b>.
- (45) Reddy, J. A.; Dorton, R.; Westrick, E.; Dawson, A.; Smith, T.; Xu, L.-C.; Vetzal, M.; Kleindl, P.; Vlahov, I. R.; Leamon, C. P. Preclinical Evaluation of EC145, a Folate-Vinca Alkaloid Conjugate. *Cancer Res* **2007**, *67* (9), 4434–4442. <https://doi.org/10.1158/0008-5472.CAN-07-0033>.
- (46) Vlahov, I. R.; Santhapuram, H. K. R.; Kleindl, P. J.; Howard, S. J.; Stanford, K. M.; Leamon, C. P. Design and Regioselective Synthesis of a New Generation of Targeted Chemotherapeutics. Part 1: EC145, a Folic Acid Conjugate of Desacetylvincristine Monohydrazone. *Bioorg Med Chem Lett* **2006**, *16* (19), 5093–5096. <https://doi.org/10.1016/j.bmcl.2006.07.030>.
- (47) Bildstein, L.; Dubernet, C.; Couvreur, P. Prodrug-Based Intracellular Delivery of Anticancer Agents. *Advanced drug delivery reviews* **2011**, *63* (1–2), 3–23. <https://doi.org/10.1016/j.addr.2010.12.005>.
- (48) Walther, R.; Rautio, J.; Zelikin, A. N. Prodrugs in Medicinal Chemistry and Enzyme Prodrug Therapies. *Advanced drug delivery reviews* **2017**, *118*, 65–77. <https://doi.org/10.1016/j.addr.2017.06.013>.
- (49) Hamada, Y. Recent Progress in Prodrug Design Strategies Based on Generally Applicable Modifications. *Bioorganic & medicinal chemistry letters* **2017**, *27* (8), 1627–1632. <https://doi.org/10.1016/j.bmcl.2017.02.075>.
- (50) Brown, J. M.; Wilson, W. R. Exploiting Tumour Hypoxia in Cancer Treatment. *Nature reviews. Cancer* **2004**, *4* (6), 437–447. <https://doi.org/10.1038/nrc1367>.
- (51) Wilson, W. R.; Hay, M. P. Targeting Hypoxia in Cancer Therapy. *Nature reviews. Cancer* **2011**, *11* (6), 393–410. <https://doi.org/10.1038/nrc3064>.
- (52) Sharma, A.; Arambula, J. F.; Koo, S.; Kumar, R.; Singh, H.; Sessler, J. L.; Kim, J. S. Hypoxia-Targeted Drug Delivery. *Chemical Society reviews* **2019**, *48* (3), 771–813. <https://doi.org/10.1039/c8cs00304a>.
- (53) Trachootham, D.; Alexandre, J.; Huang, P. Targeting Cancer Cells by ROS-Mediated Mechanisms: A Radical Therapeutic Approach? *Nature reviews. Drug discovery* **2009**, *8* (7), 579–591. <https://doi.org/10.1038/nrd2803>.
- (54) Yan, K.-C.; Sedgwick, A. C.; Zang, Y.; Chen, G.-R.; He, X.-P.; Li, J.; Yoon, J.; James, T. D. Sensors, Imaging Agents, and Theranostics to Help Understand and Treat Reactive Oxygen Species Related Diseases. *Small Methods* **2019**, *3* (7), 1900013. <https://doi.org/10.1002/smt.201900013>.
- (55) Doura, T.; Takahashi, K.; Ogra, Y.; Suzuki, N. Combretastatin A4- $\beta$ -Galactosyl Conjugates for Ovarian Cancer Prodrug Monotherapy. *ACS Med. Chem. Lett.* **2017**, *8* (2), 211–214. <https://doi.org/10.1021/acsmchemlett.6b00427>.
- (56) Neri, D.; Supuran, C. T. Interfering with PH Regulation in Tumours as a Therapeutic Strategy. *Nat Rev Drug Discov* **2011**, *10* (10), 767–777. <https://doi.org/10.1038/nrd3554>.

- (57) Patel, M.; Law, B. *Activation Approaches on Delivery of Imaging and Therapeutic Agents*; 2014; p 731. [https://doi.org/10.1007/978-1-4471-4372-7\\_26](https://doi.org/10.1007/978-1-4471-4372-7_26).
- (58) Chen, X.; Parelkar, S. S.; Hency, E.; Schneider, S.; Emrick, T. PolyMPC–Doxorubicin Prodrugs. *Bioconjugate Chem.* **2012**, *23* (9), 1753–1763. <https://doi.org/10.1021/bc200667s>.
- (59) Al Tameemi, W.; Dale, T. P.; Al-Jumaily, R. M. K.; Forsyth, N. R. Hypoxia-Modified Cancer Cell Metabolism. *Frontiers in Cell and Developmental Biology* **2019**, *7*, 4. <https://doi.org/10.3389/fcell.2019.00004>.
- (60) Jin, C.; Zhang, Q.; Lu, W. Synthesis and Biological Evaluation of Hypoxia-Activated Prodrugs of SN-38. *European Journal of Medicinal Chemistry* **2017**, *132*, 135–141. <https://doi.org/10.1016/j.ejmech.2017.03.040>.
- (61) Liou, G. Y.; Storz, P. Reactive Oxygen Species in Cancer. *Free radical research* **2010**, *44* (5), 479–496. <https://doi.org/10.3109/10715761003667554>.
- (62) Tan, H. Y.; Wang, N. The Reactive Oxygen Species in Macrophage Polarization: Reflecting Its Dual Role in Progression and Treatment of Human Diseases. **2016**, *2016*, 2795090. <https://doi.org/10.1155/2016/2795090>.
- (63) Qian, B. Z.; Pollard, J. W. Macrophage Diversity Enhances Tumor Progression and Metastasis. *Cell* **2010**, *141* (1), 39–51. <https://doi.org/10.1016/j.cell.2010.03.014>.
- (64) Peng, X.; Gandhi, V. ROS-Activated Anticancer Prodrugs: A New Strategy for Tumor-Specific Damage. *Therapeutic delivery* **2012**, *3* (7), 823–833. <https://doi.org/10.4155/tde.12.61>.
- (65) Peiró Cadahía, J.; Previtali, V. Prodrug Strategies for Targeted Therapy Triggered by Reactive Oxygen Species. **2019**, *10* (9), 1531–1549. <https://doi.org/10.1039/c9md00169g>.
- (66) Ye, H.; Zhou, Y.; Liu, X.; Chen, Y.; Duan, S.; Zhu, R.; Liu, Y. Recent Advances on Reactive Oxygen Species-Responsive Delivery and Diagnosis System. **2019**, *20* (7), 2441–2463. <https://doi.org/10.1021/acs.biomac.9b00628>.
- (67) Antonio, J. P. M.; Russo, R.; Carvalho, C. P.; Cal, P.; Gois, P. M. P. Boronic Acids as Building Blocks for the Construction of Therapeutically Useful Bioconjugates. *Chemical Society reviews* **2019**, *48* (13), 3513–3536. <https://doi.org/10.1039/c9cs00184k>.
- (68) Andina, D.; Leroux, J. C.; Luciani, P. Ratiometric Fluorescent Probes for the Detection of Reactive Oxygen Species. *Chemistry* **2017**, *23* (55), 13549–13573. <https://doi.org/10.1002/chem.201702458>.
- (69) Cao, S.; Christiansen, R.; Peng, X. Substituent Effects on Oxidation-Induced Formation of Quinone Methides from Arylboronic Ester Precursors. *Chemistry (Weinheim an der Bergstrasse, Germany)* **2013**, *19* (27), 9050–9058. <https://doi.org/10.1002/chem.201300539>.
- (70) Zielonka, J.; Sikora, A.; Hardy, M.; Joseph, J.; Dranka, B. P.; Kalyanaraman, B. Boronate Probes as Diagnostic Tools for Real Time Monitoring of Peroxynitrite and Hydroperoxides. *Chemical research in toxicology* **2012**, *25* (9), 1793–1799. <https://doi.org/10.1021/tx300164j>.
- (71) Sikora, A.; Zielonka, J.; Lopez, M.; Joseph, J.; Kalyanaraman, B. Direct Oxidation of Boronates by Peroxynitrite: Mechanism and Implications in Fluorescence Imaging of Peroxynitrite. *Free radical biology & medicine* **2009**, *47* (10), 1401–1407. <https://doi.org/10.1016/j.freeradbiomed.2009.08.006>.
- (72) Sikora, A.; Zielonka, J.; Lopez, M.; Dybala-Defratyka, A.; Joseph, J.; Marcinek, A.; Kalyanaraman, B. Reaction between Peroxynitrite and Boronates: EPR Spin-Trapping, HPLC Analyses, and Quantum Mechanical Study of the Free Radical Pathway. *Chemical research in toxicology* **2011**, *24* (5), 687–697. <https://doi.org/10.1021/tx100439a>.
- (73) Baker, S. J.; Ding, C. Z.; Akama, T.; Zhang, Y. K.; Hernandez, V.; Xia, Y. Therapeutic Potential of Boron-Containing Compounds. *Future medicinal chemistry* **2009**, *1* (7), 1275–1288. <https://doi.org/10.4155/fmc.09.71>.
- (74) Hanna, R. D.; Naro, Y.; Deiters, A.; Floreancig, P. E. Alcohol, Aldehyde, and Ketone Liberation and Intracellular Cargo Release through Peroxide-Mediated  $\alpha$ -Boryl Ether Fragmentation. *Journal of the American Chemical Society* **2016**, *138* (40), 13353–13360. <https://doi.org/10.1021/jacs.6b07890>.

- (75) Mosey, R. A.; Floreancig, P. E. Versatile Approach to  $\alpha$ -Alkoxy Carbamate Synthesis and Stimulus-Responsive Alcohol Release. *Organic & biomolecular chemistry* **2012**, *10* (39), 7980–7985. <https://doi.org/10.1039/c2ob26571k>.
- (76) Brooks, A. D.; Mohapatra, H.; Phillips, S. T. Design, Synthesis, and Characterization of Small-Molecule Reagents That Cooperatively Provide Dual Readouts for Triaging and, When Necessary, Quantifying Point-of-Need Enzyme Assays. *The Journal of organic chemistry* **2015**, *80* (21), 10437–10445. <https://doi.org/10.1021/acs.joc.5b02013>.
- (77) Alouane, A.; Labruere, R.; Le Saux, T.; Schmidt, F.; Jullien, L. Self-Immolative Spacers: Kinetic Aspects, Structure-Property Relationships, and Applications. *Angewandte Chemie* **2015**, *54* (26), 7492–7509. <https://doi.org/10.1002/anie.201500088>.
- (78) Gisbert-Garzarán, M.; Manzano, M.; Vallet-Regí, M. Self-Immolative Chemistry in Nanomedicine. *Chemical Engineering Journal* **2018**, *340*, 24–31. <https://doi.org/10.1016/j.cej.2017.12.098>.
- (79) Patel, H. K.; Bihani, T. Selective Estrogen Receptor Modulators (SERMs) and Selective Estrogen Receptor Degradable (SERDs) in Cancer Treatment. *Pharmacology & therapeutics* **2018**, *186*, 1–24. <https://doi.org/10.1016/j.pharmthera.2017.12.012>.
- (80) Jiang, Q.; Zhong, Q.; Zhang, Q.; Zheng, S.; Wang, G. Boron-Based 4-Hydroxytamoxifen Bioisosteres for Treatment of de Novo Tamoxifen Resistant Breast Cancer. *ACS medicinal chemistry letters* **2012**, *3* (5), 392–396. <https://doi.org/10.1021/ml3000287>.
- (81) Zhang, C.; Zhong, Q.; Zhang, Q.; Zheng, S.; Miele, L.; Wang, G. Boronic Prodrug of Endoxifen as an Effective Hormone Therapy for Breast Cancer. *Breast cancer research and treatment* **2015**, *152* (2), 283–291. <https://doi.org/10.1007/s10549-015-3461-9>.
- (82) Zhong, Q.; Zhang, C.; Zhang, Q.; Miele, L.; Zheng, S.; Wang, G. Boronic Prodrug of 4-Hydroxytamoxifen Is More Efficacious than Tamoxifen with Enhanced Bioavailability Independent of CYP2D6 Status. *BMC Cancer* **2015**, *15* (1), 625. <https://doi.org/10.1186/s12885-015-1621-2>.
- (83) Manal, M.; Chandrasekar, M. J.; Gomathi Priya, J.; Nanjan, M. J. Inhibitors of Histone Deacetylase as Antitumor Agents: A Critical Review. *Bioorganic chemistry* **2016**, *67*, 18–42. <https://doi.org/10.1016/j.bioorg.2016.05.005>.
- (84) Liao, Y.; Xu, L.; Ou, S.; Edwards, H.; Luedtke, D.; Ge, Y.; Qin, Z. H<sub>2</sub>O<sub>2</sub>/Peroxynitrite-Activated Hydroxamic Acid HDAC Inhibitor Prodrugs Show Antileukemic Activities against AML Cells. *ACS medicinal chemistry letters* **2018**, *9* (7), 635–640. <https://doi.org/10.1021/acsmchemlett.8b00057>.
- (85) Zheng, S.; Guo, S.; Zhong, Q.; Zhang, C.; Liu, J.; Yang, L.; Zhang, Q.; Wang, G. Biocompatible Boron-Containing Prodrugs of Belinostat for the Potential Treatment of Solid Tumors. *ACS medicinal chemistry letters* **2018**, *9* (2), 149–154. <https://doi.org/10.1021/acsmchemlett.7b00504>.
- (86) Hole, P. S.; Zabkiewicz, J.; Munje, C.; Newton, Z.; Pearn, L.; White, P.; Marquez, N.; Hills, R. K.; Burnett, A. K.; Tonks, A.; Darley, R. L. Overproduction of NOX-Derived ROS in AML Promotes Proliferation and Is Associated with Defective Oxidative Stress Signaling. *Blood* **2013**, *122* (19), 3322–3330. <https://doi.org/10.1182/blood-2013-04-491944>.
- (87) Zhang, C.; Guo, S.; Zhong, Q.; Zhang, Q.; Hossain, A.; Zheng, S. Metabolism and Pharmacokinetic Study of the Boron-Containing Prodrug of Belinostat (ZL277), a Pan HDAC Inhibitor with Enhanced Bioavailability. **2019**, *12* (4). <https://doi.org/10.3390/ph12040180>.
- (88) Varier, R. A.; Timmers, H. T. Histone Lysine Methylation and Demethylation Pathways in Cancer. *Biochimica et biophysica acta* **2011**, *1815* (1), 75–89. <https://doi.org/10.1016/j.bbcan.2010.10.002>.
- (89) Engel, M.; Gee, Y. S. Novel Dual-Action Prodrug Triggers Apoptosis in Glioblastoma Cells by Releasing a Glutathione Quencher and Lysine-Specific Histone Demethylase 1A Inhibitor. **2019**, *149* (4), 535–550. <https://doi.org/10.1111/jnc.14655>.

- (90) Bielec, B.; Poetsch, I.; Ahmed, E.; Heffeter, P.; Keppler, B. K.; Kowol, C. R. Reactive Oxygen Species (ROS)-Sensitive Prodrugs of the Tyrosine Kinase Inhibitor Crizotinib. *Molecules* **2020**, *25* (5). <https://doi.org/10.3390/molecules25051149>.
- (91) Peiró Cadahía, J.; Bondebjerg, J.; Hansen, C. A.; Previtali, V.; Hansen, A. E.; Andresen, T. L.; Clausen, M. H. Synthesis and Evaluation of Hydrogen Peroxide Sensitive Prodrugs of Methotrexate and Aminopterin for the Treatment of Rheumatoid Arthritis. **2018**, *61* (8), 3503–3515. <https://doi.org/10.1021/acs.jmedchem.7b01775>.
- (92) Previtali, V.; Petrovic, K.; Peiró Cadahía, J.; Troelsen, N. S.; Clausen, M. H. Auxiliary in Vitro and in Vivo Biological Evaluation of Hydrogen Peroxide Sensitive Prodrugs of Methotrexate and Aminopterin for the Treatment of Rheumatoid Arthritis. *Bioorganic & medicinal chemistry* **2020**, *28* (2), 115247. <https://doi.org/10.1016/j.bmc.2019.115247>.
- (93) Ai, Y.; Obianom, O. N.; Kuser, M.; Li, Y.; Shu, Y.; Xue, F. Enhanced Tumor Selectivity of 5-Fluorouracil Using a Reactive Oxygen Species-Activated Prodrug Approach. *ACS medicinal chemistry letters* **2019**, *10* (1), 127–131. <https://doi.org/10.1021/acsmchemlett.8b00539>.
- (94) Matsushita, K.; Okuda, T. A Hydrogen Peroxide Activatable Gemcitabine Prodrug for the Selective Treatment of Pancreatic Ductal Adenocarcinoma. **2019**, *14* (15), 1384–1391. <https://doi.org/10.1002/cmdc.201900324>.
- (95) Rothenberg, M. L. Irinotecan (CPT-11): Recent Developments and Future Directions--Colorectal Cancer and Beyond. *The oncologist* **2001**, *6* (1), 66–80. <https://doi.org/10.1634/theoncologist.6-1-66>.
- (96) Wang, L.; Xie, S.; Ma, L.; Chen, Y.; Lu, W. 10-Boronic Acid Substituted Camptothecin as Prodrug of SN-38. *European journal of medicinal chemistry* **2016**, *116*, 84–89. <https://doi.org/10.1016/j.ejmech.2016.03.063>.
- (97) Kim, E. J.; Bhuniya, S.; Lee, H.; Kim, H. M.; Cheong, C.; Maiti, S.; Hong, K. S.; Kim, J. S. An Activatable Prodrug for the Treatment of Metastatic Tumors. *Journal of the American Chemical Society* **2014**, *136* (39), 13888–13894. <https://doi.org/10.1021/ja5077684>.
- (98) Redy-Keisar, O.; Ferber, S.; Satchi-Fainaro, R.; Shabat, D. NIR Fluorogenic Dye as a Modular Platform for Prodrug Assembly: Real-Time in Vivo Monitoring of Drug Release. *ChemMedChem* **2015**, *10* (6), 999–1007. <https://doi.org/10.1002/cmdc.201500060>.
- (99) Octavia, Y.; Tocchetti, C. G.; Gabrielson, K. L.; Janssens, S.; Crijns, H. J.; Moens, A. L. Doxorubicin-Induced Cardiomyopathy: From Molecular Mechanisms to Therapeutic Strategies. *Journal of molecular and cellular cardiology* **2012**, *52* (6), 1213–1225. <https://doi.org/10.1016/j.yjmcc.2012.03.006>.
- (100) Skarbek, C.; Serra, S.; Maslah, H.; Rascol, E.; Labruère, R. Arylboronate Prodrugs of Doxorubicin as Promising Chemotherapy for Pancreatic Cancer. *Bioorganic Chemistry* **2019**, *91*, 103158. <https://doi.org/10.1016/j.bioorg.2019.103158>.
- (101) Ye, M.; Han, Y.; Tang, J.; Piao, Y.; Liu, X.; Zhou, Z.; Gao, J.; Rao, J.; Shen, Y. A Tumor-Specific Cascade Amplification Drug Release Nanoparticle for Overcoming Multidrug Resistance in Cancers. *Advanced materials (Deerfield Beach, Fla.)* **2017**, *29* (38). <https://doi.org/10.1002/adma.201702342>.
- (102) Gao, X.; Cao, J.; Song, Y.; Shu, X.; Liu, J.; Sun, J. Z.; Liu, B.; Tang, B. Z. A Unimolecular Theranostic System with H<sub>2</sub>O<sub>2</sub>-Specific Response and AIE-Activity for Doxorubicin Releasing and Real-Time Tracking in Living Cells. *RSC Advances* **2018**, *8* (20), 10975–10979. <https://doi.org/10.1039/C8RA01185K>.
- (103) Xu, Y.; Shi, W. H(2) O(2) -Responsive Organosilica-Doxorubicin Nanoparticles for Targeted Imaging and Killing of Cancer Cells Based on a Synthesized Silane-Borate Precursor. **2019**, *14* (11), 1079–1085. <https://doi.org/10.1002/cmdc.201900142>.
- (104) Blagosklonny, M. V.; Fojo, T. Molecular Effects of Paclitaxel: Myths and Reality (a Critical Review). *International journal of cancer* **1999**, *83* (2), 151–156. [https://doi.org/10.1002/\(sici\)1097-0215\(19991008\)83:2<151::aid-ijc1>3.0.co;2-5](https://doi.org/10.1002/(sici)1097-0215(19991008)83:2<151::aid-ijc1>3.0.co;2-5).
- (105) Dong, C.; Zhou, Q.; Xiang, J.; Liu, F.; Zhou, Z.; Shen, Y. Self-Assembly of Oxidation-Responsive Polyethylene Glycol-Paclitaxel Prodrug for Cancer Chemotherapy. *Journal of controlled*

- release: official journal of the Controlled Release Society* **2020**, *321*, 529–539. <https://doi.org/10.1016/j.jconrel.2020.02.038>.
- (106) Ravikumar, G.; Bagheri, M.; Saini, D. K.; Chakrapani, H. A Small Molecule for TheraNOstic Targeting of Cancer Cells. *Chemical communications (Cambridge, England)* **2017**, *53* (100), 13352–13355. <https://doi.org/10.1039/c7cc08526e>.
- (107) Kuang, Y.; Balakrishnan, K.; Gandhi, V.; Peng, X. Hydrogen Peroxide Inducible DNA Cross-Linking Agents: Targeted Anticancer Prodrugs. *Journal of the American Chemical Society* **2011**, *133* (48), 19278–19281. <https://doi.org/10.1021/ja2073824>.
- (108) Li, M.; Li, S.; Chen, H.; Hu, R.; Liu, L.; Lv, F.; Wang, S. Preparation of Conjugated Polymer Grafted with H<sub>2</sub>O<sub>2</sub>-Sensitive Prodrug for Cell Imaging and Tumor Cell Killing. *ACS applied materials & interfaces* **2016**, *8* (1), 42–46. <https://doi.org/10.1021/acsami.5b11846>.
- (109) Chen, W.; Han, Y.; Peng, X. Aromatic Nitrogen Mustard-Based Prodrugs: Activity, Selectivity, and the Mechanism of DNA Cross-Linking. *Chemistry – A European Journal* **2014**, *20* (24), 7410–7418. <https://doi.org/10.1002/chem.201400090>.
- (110) Chen, W.; Balakrishnan, K.; Kuang, Y.; Han, Y.; Fu, M.; Gandhi, V.; Peng, X. Reactive Oxygen Species (ROS) Inducible DNA Cross-Linking Agents and Their Effect on Cancer Cells and Normal Lymphocytes. *Journal of medicinal chemistry* **2014**, *57* (11), 4498–4510. <https://doi.org/10.1021/jm401349g>.
- (111) Chen, W.; Fan, H.; Balakrishnan, K.; Wang, Y.; Sun, H.; Fan, Y.; Gandhi, V.; Arnold, L. A. Discovery and Optimization of Novel Hydrogen Peroxide Activated Aromatic Nitrogen Mustard Derivatives as Highly Potent Anticancer Agents. **2018**, *61* (20), 9132–9145. <https://doi.org/10.1021/acs.jmedchem.8b00559>.
- (112) Cao, S.; Wang, Y.; Peng, X. ROS-Inducible DNA Cross-Linking Agent as a New Anticancer Prodrug Building Block. *Chemistry (Weinheim an der Bergstrasse, Germany)* **2012**, *18* (13), 3850–3854. <https://doi.org/10.1002/chem.201200075>.
- (113) Cao, S.; Wang, Y.; Peng, X. The Leaving Group Strongly Affects H<sub>2</sub>O<sub>2</sub>-Induced DNA Cross-Linking by Arylboronates. *The Journal of organic chemistry* **2014**, *79* (2), 501–508. <https://doi.org/10.1021/jo401901x>.
- (114) Wang, Y.; Fan, H.; Balakrishnan, K.; Lin, Z.; Cao, S.; Chen, W.; Fan, Y.; Guthrie, Q. A.; Sun, H.; Teske, K. A.; Gandhi, V.; Arnold, L. A.; Peng, X. Hydrogen Peroxide Activated Quinone Methide Precursors with Enhanced DNA Cross-Linking Capability and Cytotoxicity towards Cancer Cells. *European journal of medicinal chemistry* **2017**, *133*, 197–207. <https://doi.org/10.1016/j.ejmech.2017.03.041>.
- (115) Hagen, H.; Marzenell, P.; Jentsch, E.; Wenz, F.; Veldwijk, M. R.; Mokhir, A. Aminoferrocene-Based Prodrugs Activated by Reactive Oxygen Species. *Journal of medicinal chemistry* **2012**, *55* (2), 924–934. <https://doi.org/10.1021/jm2014937>.
- (116) Marzenell, P.; Hagen, H.; Sellner, L.; Zenz, T.; Grinyte, R.; Pavlov, V.; Daum, S.; Mokhir, A. Aminoferrocene-Based Prodrugs and Their Effects on Human Normal and Cancer Cells as Well as Bacterial Cells. *Journal of medicinal chemistry* **2013**, *56* (17), 6935–6944. <https://doi.org/10.1021/jm400754c>.
- (117) Daum, S.; Chekhun, V. F.; Todor, I. N.; Lukianova, N. Y.; Shvets, Y. V.; Sellner, L.; Putzker, K.; Lewis, J.; Zenz, T.; de Graaf, I. A.; Groothuis, G. M.; Casini, A.; Zozulia, O.; Hampel, F.; Mokhir, A. Improved Synthesis of N-Benzylaminoferrocene-Based Prodrugs and Evaluation of Their Toxicity and Antileukemic Activity. *Journal of medicinal chemistry* **2015**, *58* (4), 2015–2024. <https://doi.org/10.1021/jm5019548>.
- (118) Schikora, M.; Reznikov, A.; Chaykovskaya, L.; Sachinska, O.; Polyakova, L.; Mokhir, A. Activity of Aminoferrocene-Based Prodrugs against Prostate Cancer. *Bioorganic & medicinal chemistry letters* **2015**, *25* (17), 3447–3450. <https://doi.org/10.1016/j.bmcl.2015.07.013>.
- (119) Daum, S.; Babiy, S.; Konovalova, H.; Hofer, W.; Shtemenko, A.; Shtemenko, N.; Janko, C.; Alexiou, C.; Mokhir, A. Tuning the Structure of Aminoferrocene-Based Anticancer Prodrugs to Prevent Their Aggregation in Aqueous Solution. *Journal of inorganic biochemistry* **2018**, *178*, 9–17. <https://doi.org/10.1016/j.jinorgbio.2017.08.038>.

- (120) Daum, S.; Toms, J.; Reshetnikov, V.; Özkan, H. G.; Hampel, F.; Maschauer, S.; Hakimioun, A.; Beierlein, F.; Sellner, L.; Schmitt, M.; Prante, O. Identification of Boronic Acid Derivatives as an Active Form of N-Alkylaminoferrocene-Based Anticancer Prodrugs and Their Radiolabeling with (18)F. *2019*, *30* (4), 1077–1086. <https://doi.org/10.1021/acs.bioconjchem.9b00019>.
- (121) Daum, S.; Reshetnikov, M. S. V.; Sisa, M.; Dumych, T.; Lootsik, M. D.; Bilyy, R.; Bila, E.; Janko, C.; Alexiou, C.; Herrmann, M.; Sellner, L.; Mokhir, A. Lysosome-Targeting Amplifiers of Reactive Oxygen Species as Anticancer Prodrugs. *Angewandte Chemie International Edition* **2017**, *56* (49), 15545–15549. <https://doi.org/10.1002/anie.201706585>.
- (122) Reshetnikov, V.; Daum, S.; Mokhir, A. Cancer-Specific, Intracellular, Reductive Activation of Anticancer Pt(IV) Prodrugs. *Chemistry (Weinheim an der Bergstrasse, Germany)* **2017**, *23* (24), 5678–5681. <https://doi.org/10.1002/chem.201701192>.
- (123) Reshetnikov, V.; Arkhypov, A.; Julakanti, P. R.; Mokhir, A. A Cancer Specific Oxaliplatin-Releasing Pt(IV)-Prodrug. *Dalton transactions (Cambridge, England : 2003)* **2018**, *47* (19), 6679–6682. <https://doi.org/10.1039/c8dt01458b>.
- (124) Reshetnikov, V.; Daum, S.; Janko, C.; Karawacka, W.; Tietze, R.; Alexiou, C.; Paryzhak, S.; Dumych, T.; Bilyy, R.; Tripal, P.; Schmid, B.; Palmisano, R.; Mokhir, A. ROS-Responsive N-Alkylaminoferrocenes for Cancer-Cell-Specific Targeting of Mitochondria. **2018**, *57* (37), 11943–11946. <https://doi.org/10.1002/anie.201805955>.
- (125) Fang, J.; Nakamura, H.; Iyer, A. K. Tumor-Targeted Induction of Oxystress for Cancer Therapy. *Journal of drug targeting* **2007**, *15* (7–8), 475–486. <https://doi.org/10.1080/10611860701498286>.
- (126) Viola-Rhenals, M.; Patel, K. R.; Jaimes-Santamaria, L.; Wu, G.; Liu, J.; Dou, Q. P. Recent Advances in Antabuse (Disulfiram): The Importance of Its Metal-Binding Ability to Its Anticancer Activity. *Current medicinal chemistry* **2018**, *25* (4), 506–524. <https://doi.org/10.2174/0929867324666171023161121>.
- (127) Pan, Q.; Zhang, B.; Peng, X.; Wan, S.; Luo, K.; Gao, W.; Pu, Y.; He, B. A Dithiocarbamate-Based H(2)O(2)-Responsive Prodrug for Combinational Chemotherapy and Oxidative Stress Amplification Therapy. *Chemical communications (Cambridge, England)* **2019**, *55* (92), 13896–13899. <https://doi.org/10.1039/c9cc05438c>.
- (128) Noh, J.; Kwon, B.; Han, E.; Park, M.; Yang, W.; Cho, W.; Yoo, W.; Khang, G.; Lee, D. Amplification of Oxidative Stress by a Dual Stimuli-Responsive Hybrid Drug Enhances Cancer Cell Death. *Nature communications* **2015**, *6*, 6907. <https://doi.org/10.1038/ncomms7907>.
- (129) Li, J.; Dirisala, A.; Ge, Z.; Wang, Y.; Yin, W.; Ke, W.; Toh, K.; Xie, J.; Matsumoto, Y.; Anraku, Y.; Osada, K.; Kataoka, K. Therapeutic Vesicular Nanoreactors with Tumor-Specific Activation and Self-Destruction for Synergistic Tumor Ablation. *Angewandte Chemie (International ed. in English)* **2017**, *56* (45), 14025–14030. <https://doi.org/10.1002/anie.201706964>.
- (130) Trippier, P. C.; McGuigan, C. Boronic Acids in Medicinal Chemistry: Anticancer, Antibacterial and Antiviral Applications. *MedChemComm* **2010**, *1* (3), 183–198. <https://doi.org/10.1039/C0MD00119H>.
- (131) Plescia, J.; Moitessier, N. Design and Discovery of Boronic Acid Drugs. *European journal of medicinal chemistry* **2020**, *195*, 112270. <https://doi.org/10.1016/j.ejmech.2020.112270>.
- (132) Andersen, K. A.; Smith, T. P.; Lomax, J. E.; Raines, R. T. Boronic Acid for the Traceless Delivery of Proteins into Cells. *ACS chemical biology* **2016**, *11* (2), 319–323. <https://doi.org/10.1021/acscchembio.5b00966>.
- (133) Ellis, G. A.; Palte, M. J.; Raines, R. T. Boronate-Mediated Biologic Delivery. *Journal of the American Chemical Society* **2012**, *134* (8), 3631–3634. <https://doi.org/10.1021/ja210719s>.
- (134) Liu, P.; Xu, B.; Quilley, J.; Wong, P. Y. Peroxynitrite Attenuates Hepatic Ischemia-Reperfusion Injury. *American journal of physiology. Cell physiology* **2000**, *279* (6), C1970–7. <https://doi.org/10.1152/ajpcell.2000.279.6.C1970>.
- (135) Szabó, C.; Ischiropoulos, H.; Radi, R. Peroxynitrite: Biochemistry, Pathophysiology and Development of Therapeutics. *Nature reviews. Drug discovery* **2007**, *6* (8), 662–680. <https://doi.org/10.1038/nrd2222>.

- (136) Sztatowski, T. P.; Nathan, C. F. Production of Large Amounts of Hydrogen Peroxide by Human Tumor Cells. *Cancer research* **1991**, *51* (3), 794–798.
- (137) Xu, W. C.; Liang, J. Z.; Li, C.; He, Z. X.; Yuan, H. Y.; Huang, B. Y.; Liu, X. L.; Tang, B.; Pang, D. W.; Du, H. N.; Yang, Y. Pathological Hydrogen Peroxide Triggers the Fibrillization of Wild-Type SOD1 via Sulfenic Acid Modification of Cys-111. **2018**, *9* (2), 67. <https://doi.org/10.1038/s41419-017-0106-4>.
- (138) Bienert, G. P.; Schjoerring, J. K.; Jahn, T. P. Membrane Transport of Hydrogen Peroxide. *Biochimica et biophysica acta* **2006**, *1758* (8), 994–1003. <https://doi.org/10.1016/j.bbamem.2006.02.015>.
- (139) D’Auréaux, B.; Toledano, M. B. ROS as Signalling Molecules: Mechanisms That Generate Specificity in ROS Homeostasis. *Nature Reviews Molecular Cell Biology* **2007**, *8* (10), 813–824. <https://doi.org/10.1038/nrm2256>.
- (140) Brooks, A. D.; Yeung, K.; Lewis, G. G.; Phillips, S. T. A Strategy for Minimizing Background Signal in Autoinductive Signal Amplification Reactions for Point-of-Need Assays. *Analytical methods : advancing methods and applications* **2015**, *7* (17), 7186–7192. <https://doi.org/10.1039/c5ay00508f>.
- (141) Liu, J.; Zheng, S.; Akerstrom, V. L.; Yuan, C.; Ma, Y.; Zhong, Q.; Zhang, C.; Zhang, Q.; Guo, S.; Ma, P.; Skripnikova, E. V.; Bratton, M. R.; Pannuti, A.; Miele, L.; Wiese, T. E.; Wang, G. Fulvestrant-3 Boronic Acid (ZB716): An Orally Bioavailable Selective Estrogen Receptor Downregulator (SERD). *Journal of medicinal chemistry* **2016**, *59* (17), 8134–8140. <https://doi.org/10.1021/acs.jmedchem.6b00753>.
- (142) Zhang, C.; Guo, S.; Yang, L.; Liu, J.; Zheng, S.; Zhong, Q.; Zhang, Q.; Wang, G. Metabolism, Pharmacokinetics, and Bioavailability of ZB716, a Steroidal Selective Estrogen Receptor Downregulator (SERD). *Oncotarget* **2017**, *8* (61), 103874–103889. <https://doi.org/10.18632/oncotarget.21808>.
- (143) Luo, L.; Zhong, Q.; Guo, S.; Zhang, C.; Zhang, Q.; Zheng, S.; He, L.; Wang, G. Development of a Bioavailable Boron-Containing PI-103 Bioisostere, PI-103BE. *Bioorganic & medicinal chemistry letters* **2020**, *30* (14), 127258. <https://doi.org/10.1016/j.bmcl.2020.127258>.
- (144) Wang et al. Boron-Based Prodrug Strategy for Increased Bioavailability and Lower-Dosage Requirements for Drug Molecules Containing at Least One Phenol (or Aromatic Hydroxyl) Group. *Patent WO2016/004166* **2016**.
- (145) Li, X.; Wu, S.; Dong, G.; Chen, S.; Ma, Z.; Liu, D.; Sheng, C. Natural Product Evodiamine with Borate Trigger Unit: Discovery of Potent Antitumor Agents against Colon Cancer. *ACS Med Chem Lett* **2020**, *11* (4), 439–444. <https://doi.org/10.1021/acsmedchemlett.9b00513>.
- (146) Giang, I.; Boland, E. L.; Poon, G. M. K. Prodrug Applications for Targeted Cancer Therapy. *AAPS J* **2014**, *16* (5), 899–913. <https://doi.org/10.1208/s12248-014-9638-z>.
- (147) Wilson, W. R.; Hay, M. P. Targeting Hypoxia in Cancer Therapy. *Nat. Rev. Cancer* **2011**, *11* (6), 393–410. <https://doi.org/10.1038/nrc3064>.
- (148) Sun, I.-C.; Yoon, H. Y.; Lim, D.-K.; Kim, K. Recent Trends in In Situ Enzyme-Activatable Prodrugs for Targeted Cancer Therapy. *Bioconjug. Chem.* **2020**, *31* (4), 1012–1024. <https://doi.org/10.1021/acs.bioconjchem.0c00082>.
- (149) Singh, Y.; Palombo, M.; Sinko, P. J. Recent Trends in Targeted Anticancer Prodrug and Conjugate Design. *Curr. Med. Chem.* **2008**, *15* (18), 1802–1826. <https://doi.org/10.2174/092986708785132997>.
- (150) Sherwood, R. F. Advanced Drug Delivery Reviews: Enzyme Prodrug Therapy. *Advanced Drug Delivery Reviews* **1996**, *22* (3), 269–288. [https://doi.org/10.1016/S0169-409X\(96\)00450-4](https://doi.org/10.1016/S0169-409X(96)00450-4).
- (151) *Prodrugs: Challenges and Rewards*; Stella, V., Borchardt, R., Hageman, M., Oliyai, R., Maag, H., Tilley, J., Eds.; Biotechnology: Pharmaceutical Aspects; Springer-Verlag: New York, 2007. <https://doi.org/10.1007/978-0-387-49785-3>.
- (152) Kavanaugh, W. M. Antibody Prodrugs for Cancer. *Expert Opinion on Biological Therapy* **2020**, *20* (2), 163–171. <https://doi.org/10.1080/14712598.2020.1699053>.

- (153) Maslah, H.; Skarbek, C.; Pethe, S.; Labruère, R. Anticancer Boron-Containing Prodrugs Responsive to Oxidative Stress from the Tumor Microenvironment. *European Journal of Medicinal Chemistry* **2020**, *207*, 112670. <https://doi.org/10.1016/j.ejmech.2020.112670>.
- (154) Adam, C.; Pérez-López, A. M.; Hamilton, L.; Rubio-Ruiz, B.; Bray, T. L.; Sieger, D.; Brennan, P. M.; Unciti-Broceta, A. Bioorthogonal Uncaging of the Active Metabolite of Irinotecan by Palladium-Functionalized Microdevices. *Chemistry* **2018**, *24* (63), 16783–16790. <https://doi.org/10.1002/chem.201803725>.
- (155) Prijovich, Z. M.; Burnouf, P.-A.; Chou, H.-C.; Huang, P.-T.; Chen, K.-C.; Cheng, T.-L.; Leu, Y.-L.; Roffler, S. R. Synthesis and Antitumor Properties of BQC-Glucuronide, a Camptothecin Prodrug for Selective Tumor Activation. *Mol. Pharmaceutics* **2016**, *13* (4), 1242–1250. <https://doi.org/10.1021/acs.molpharmaceut.5b00771>.
- (156) Nicolaou, K. C.; Smith, A. L.; Yue, E. W. Chemistry and Biology of Natural and Designed Eneidyne. *PNAS* **1993**, *90* (13), 5881–5888. <https://doi.org/10.1073/pnas.90.13.5881>.
- (157) Nicolaou, K. C.; Dai, W.-M. Chemistry and Biology of the Eneidyne Anticancer Antibiotics. *Angewandte Chemie International Edition in English* **1991**, *30* (11), 1387–1416. <https://doi.org/10.1002/anie.199113873>.
- (158) Myers, A. G.; Glatthar, R.; Hammond, M.; Harrington, P. M.; Kuo, E. Y.; Liang, J.; Schaus, S. E.; Wu, Y.; Xiang, J.-N. Development of an Enantioselective Synthetic Route to Neocarzinostatin Chromophore and Its Use for Multiple Radioisotopic Incorporation. *J Am Chem Soc* **2002**, *124* (19), 5380–5401. <https://doi.org/10.1021/ja012487x>.
- (159) Myers, A. G.; Liang, J.; Hammond, M.; Harrington, P. M.; Wu, Y.; Kuo, E. Y. Total Synthesis of (+)-Neocarzinostatin Chromophore. *J. Am. Chem. Soc.* **1998**, *120* (21), 5319–5320. <https://doi.org/10.1021/ja980588y>.
- (160) Adhikari, A.; Shen, B.; Rader, C. Challenges and Opportunities to Develop Eneidyne Natural Products as Payloads for Antibody-Drug Conjugates. *Antib Ther* **2021**, *4* (1), 1–15. <https://doi.org/10.1093/abt/tbab001>.
- (161) Franks, A. T.; Franz, K. J. A Prochelator with a Modular Masking Group Featuring Hydrogen Peroxide Activation with Concurrent Fluorescent Reporting. *Chem Commun (Camb)* **2014**, *50* (77), 11317–11320. <https://doi.org/10.1039/c4cc05076b>.
- (162) Gagey, N.; Emond, M.; Neveu, P.; Benbrahim, C.; Goetz, B.; Aujard, I.; Baudin, J.-B.; Jullien, L. Alcohol Uncaging with Fluorescence Reporting: Evaluation of o-Acetoxyphenyl Methyloxazolone Precursors. *Org Lett* **2008**, *10* (12), 2341–2344. <https://doi.org/10.1021/ol800284g>.
- (163) Gagey, N.; Neveu, P.; Benbrahim, C.; Goetz, B.; Aujard, I.; Baudin, J.-B.; Jullien, L. Two-Photon Uncaging with Fluorescence Reporting: Evaluation of the o-Hydroxycinnamic Platform. *J Am Chem Soc* **2007**, *129* (32), 9986–9998. <https://doi.org/10.1021/ja0722022>.
- (164) Meier, C.; Steinhauer, T. N.; Koczian, F.; Pletzko, B.; Jarolim, K.; Girreser, U.; Braig, S.; Marko, D.; Vollmar, A. M.; Clement, B. A Dual Topoisomerase Inhibitor of Intense Pro-Apoptotic and Antileukemic Nature for Cancer Treatment. *ChemMedChem* **2017**, *12* (5), 347–352. <https://doi.org/10.1002/cmdc.201700026>.
- (165) Feng, W.; Satyanarayana, M.; Tsai, Y.-C.; Liu, A. A.; Liu, L. F.; LaVoie, E. J. 11-Substituted 2,3-Dimethoxy-8,9-Methylenedioxybenzo[i]Phenanthridine Derivatives as Novel Topoisomerase I-Targeting Agents. *Bioorganic & Medicinal Chemistry* **2008**, *16* (18), 8598–8606. <https://doi.org/10.1016/j.bmc.2008.08.018>.
- (166) Tumir, L.-M.; Radić Stojković, M.; Piantanida, I. Come-Back of Phenanthridine and Phenanthridinium Derivatives in the 21st Century. *Beilstein J. Org. Chem.* **2014**, *10*, 2930–2954. <https://doi.org/10.3762/bjoc.10.312>.
- (167) Dong, X.-Y.; Zhan, T.-Y.; Jiang, S.-P.; Liu, X.-D.; Ye, L.; Li, Z.-L.; Gu, Q.-S.; Liu, X.-Y. Copper-Catalyzed Asymmetric Coupling of Allenyl Radicals with Terminal Alkynes to Access Tetrasubstituted Allenes. *Angewandte Chemie International Edition* **2021**, *60* (4), 2160–2164. <https://doi.org/10.1002/anie.202013022>.

- (168) Takagi, J.; Takahashi, K.; Ishiyama, T.; Miyaura, N. Palladium-Catalyzed Cross-Coupling Reaction of Bis(Pinacolato)Diboron with 1-Alkenyl Halides or Triflates: Convenient Synthesis of Unsymmetrical 1,3-Dienes via the Borylation-Coupling Sequence. *J Am Chem Soc* **2002**, *124* (27), 8001–8006. <https://doi.org/10.1021/ja0202255>.
- (169) Wirz, J. Kinetic Studies of Keto–Enol and Other Tautomeric Equilibria by Flash Photolysis. In *Advances in Physical Organic Chemistry*; Elsevier, 2010; Vol. 44, pp 325–356. [https://doi.org/10.1016/S0065-3160\(08\)44006-6](https://doi.org/10.1016/S0065-3160(08)44006-6).
- (170) Rios, N.; Piacenza, L.; Trujillo, M.; Martínez, A.; Demicheli, V.; Prolo, C.; Álvarez, M. N.; López, G. V.; Radi, R. Sensitive Detection and Estimation of Cell-Derived Peroxynitrite Fluxes Using Fluorescein-Boronate. *Free Radical Biology and Medicine* **2016**, *101*, 284–295. <https://doi.org/10.1016/j.freeradbiomed.2016.08.033>.
- (171) Bernardo, P. H.; Wan, K.-F.; Sivaraman, T.; Xu, J.; Moore, F. K.; Hung, A. W.; Mok, H. Y. K.; Yu, V. C.; Chai, C. L. L. Structure–Activity Relationship Studies of Phenanthridine-Based Bcl-XL Inhibitors. *J. Med. Chem.* **2008**, *51* (21), 6699–6710. <https://doi.org/10.1021/jm8005433>.
- (172) Dubost, E.; Dumas, N.; Fossey, C.; Magnelli, R.; Butt-Gueulle, S.; Ballandonne, C.; Caignard, D. H.; Dulin, F.; Sopkova de-Oliveira Santos, J.; Millet, P.; Charnay, Y.; Rault, S.; Cailly, T.; Fabis, F. Synthesis and Structure–Affinity Relationships of Selective High-Affinity 5-HT<sub>4</sub> Receptor Antagonists: Application to the Design of New Potential Single Photon Emission Computed Tomography Tracers. *J. Med. Chem.* **2012**, *55* (22), 9693–9707. <https://doi.org/10.1021/jm300943r>.
- (173) Nakanishi, T.; Suzuki, M. Revision of the Structure of Fagaridine Based on the Comparison of UV and NMR Data of Synthetic Compounds. *J. Nat. Prod.* **1998**, *61* (10), 1263–1267. <https://doi.org/10.1021/np980193s>.
- (174) Makhey, D.; Li, D.; Zhao, B.; Sim, S.-P.; Li, T.-K.; Liu, A.; Liu, L. F.; LaVoie, E. J. Substituted Benzo[i]Phenanthridines as Mammalian Topoisomerase-Targeting Agents. *Bioorganic & Medicinal Chemistry* **2003**, *11* (8), 1809–1820. [https://doi.org/10.1016/S0968-0896\(03\)00053-1](https://doi.org/10.1016/S0968-0896(03)00053-1).
- (175) Yu, Y.; Singh, S. K.; Liu, A.; Li, T.-K.; Liu, L. F.; LaVoie, E. J. Substituted Dibenzo[c,h]Cinnolines: Topoisomerase I-Targeting Anticancer Agents. *Bioorganic & Medicinal Chemistry* **2003**, *11* (7), 1475–1491. [https://doi.org/10.1016/S0968-0896\(02\)00604-1](https://doi.org/10.1016/S0968-0896(02)00604-1).
- (176) Lasák, P.; Motyka, K.; Kryštof, V.; Stýskala, J. Synthesis, Bacteriostatic and Anticancer Activity of Novel Phenanthridines Structurally Similar to Benzo[c]Phenanthridine Alkaloids. *Molecules* **2018**, *23* (9), E2155. <https://doi.org/10.3390/molecules23092155>.
- (177) Li, D.; Zhao, B.; Sim, S.-P.; Li, T.-K.; Liu, A.; Liu, L. F.; LaVoie, E. J. 8,9-Methylenedioxybenzo[i]Phenanthridines: Topoisomerase I-Targeting Activity and Cytotoxicity. *Bioorganic & Medicinal Chemistry* **2003**, *11* (17), 3795–3805. [https://doi.org/10.1016/S0968-0896\(03\)00394-8](https://doi.org/10.1016/S0968-0896(03)00394-8).
- (178) Zhu, S.; Ruchelman, A. L.; Zhou, N.; Liu, A. A.; Liu, L. F.; LaVoie, E. J. Esters and Amides of 2,3-Dimethoxy-8,9-Methylenedioxy-Benzo[i]Phenanthridine-12-Carboxylic Acid: Potent Cytotoxic and Topoisomerase I-Targeting Agents. *Bioorganic & Medicinal Chemistry* **2005**, *13* (24), 6782–6794. <https://doi.org/10.1016/j.bmc.2005.07.033>.
- (179) Chinnagolla, R. K.; Jeganmohan, M. Ruthenium-Catalyzed Ortho-Arylation of Acetanilides with Aromatic Boronic Acids: An Easy Route to Prepare Phenanthridines and Carbazoles. *Chem Commun (Camb)* **2014**, *50* (19), 2442–2444. <https://doi.org/10.1039/c3cc49398a>.
- (180) Ueber eine neue Synthese der Phenanthridinbasen - Pictet - 1896 - Berichte der deutschen chemischen Gesellschaft - Wiley Online Library <https://chemistry-europe.onlinelibrary.wiley.com/doi/abs/10.1002/cber.18960290206> (accessed 2021 -12 -02).
- (181) Candito, D. A.; Lautens, M. Palladium-Catalyzed Domino Direct Arylation/N-Arylation: Convenient Synthesis of Phenanthridines. *Angew Chem Int Ed Engl* **2009**, *48* (36), 6713–6716. <https://doi.org/10.1002/anie.200902400>.

- (182) Gerfaud, T.; Neuville, L.; Zhu, J. Palladium-Catalyzed Annulation of Acyloximes with Arynes (or Alkynes): Synthesis of Phenanthridines and Isoquinolines. *Angew Chem Int Ed Engl* **2009**, *48* (3), 572–577. <https://doi.org/10.1002/anie.200804683>.
- (183) Maestri, G.; Larraufie, M.-H.; Derat, É.; Ollivier, C.; Fensterbank, L.; Lacôte, E.; Malacria, M. Expeditious Synthesis of Phenanthridines from Benzylamines via Dual Palladium Catalysis. *Org Lett* **2010**, *12* (24), 5692–5695. <https://doi.org/10.1021/ol102509n>.
- (184) Grigg, R. D.; Van Hoveln, R.; Schomaker, J. M. Copper-Catalyzed Recycling of Halogen Activating Groups via 1,3-Halogen Migration. *J Am Chem Soc* **2012**, *134* (39), 16131–16134. <https://doi.org/10.1021/ja306446m>.
- (185) Mehta, B. K.; Yanagisawa, K.; Shiro, M.; Kotsuki, H. Unprecedented Hydrothermal Reaction of O-Phenylaniline and Related Derivatives with Cyclic Ketones. A Novel Approach to the Construction of Phenanthridine and Quinoline Ring Systems. *Org Lett* **2003**, *5* (10), 1605–1608. <https://doi.org/10.1021/ol0300120>.
- (186) Shou, W.-G.; Yang, Y.-Y.; Wang, Y.-G. Cascade Approach to Substituted 6-Aryl-Phenanthridines from Aromatic Aldehydes, Anilines, and Benzenediazonium-2-Carboxylate. *J Org Chem* **2006**, *71* (24), 9241–9243. <https://doi.org/10.1021/jo061648i>.
- (187) Sripada, L.; Teske, J. A.; Deiters, A. Phenanthridine Synthesis via [2+2+2] Cyclotrimerization Reactions. *Org Biomol Chem* **2008**, *6* (2), 263–265. <https://doi.org/10.1039/b716519f>.
- (188) Alonso, R.; Campos, P. J.; García, B.; Rodríguez, M. A. New Light-Induced Iminyl Radical Cyclization Reactions of Acyloximes to Isoquinolines. *Org Lett* **2006**, *8* (16), 3521–3523. <https://doi.org/10.1021/ol061258i>.
- (189) Budén, M. E.; Dorn, V. B.; Gamba, M.; Pierini, A. B.; Rossi, R. A. Electron-Transfer-Mediated Synthesis of Phenanthridines by Intramolecular Arylation of Anions from N-(Ortho-Halobenzyl)Arylamines: Regiochemical and Mechanistic Analysis. *J Org Chem* **2010**, *75* (7), 2206–2218. <https://doi.org/10.1021/jo9025918>.
- (190) Linsenmeier, A. M.; Williams, C. M.; Bräse, S. Synthesis of Phenanthridine Derivatives via Photolysis. *J Org Chem* **2011**, *76* (21), 9127–9132. <https://doi.org/10.1021/jo201542x>.
- (191) Wang, L.; Sha, W.; Dai, Q.; Feng, X.; Wu, W.; Peng, H.; Chen, B.; Cheng, J. The Benzoyl Peroxide Promoted Dual C-C Bond Formation via Dual C-H Bond Cleavage:  $\alpha$ -Phenanthridinylation of Ether by Isocyanide. *Org Lett* **2014**, *16* (8), 2088–2091. <https://doi.org/10.1021/ol500277u>.
- (192) Zhang, Z.; Tang, X.; Dolbier, W. R. Photoredox-Catalyzed Tandem Insertion/Cyclization Reactions of Difluoromethyl and 1,1-Difluoroalkyl Radicals with Biphenyl Isocyanides. *Org Lett* **2015**, *17* (18), 4401–4403. <https://doi.org/10.1021/acs.orglett.5b02061>.
- (193) Ge, J.; Wang, X.; Liu, T.; Shi, Z.; Xiao, Q.; Yin, D. Assembly of Substituted Phenanthridines via a Cascade Palladium-Catalyzed Coupling Reaction, Deprotection and Intramolecular Cyclization. *RSC Advances* **2016**, *6* (23), 19571–19575. <https://doi.org/10.1039/C6RA00249H>.
- (194) Zhang, X.; Sarkar, S.; Larock, R. C. Synthesis of Naphthalenes and 2-Naphthols by the Electrophilic Cyclization of Alkynes. *The Journal of Organic Chemistry* **2006**, *71* (1), 236–243. <https://doi.org/10.1021/jo051948k>.
- (195) Mee, S. P. H.; Lee, V.; Baldwin, J. E. Stille Coupling Made Easier-the Synergic Effect of Copper(I) Salts and the Fluoride Ion. *Angew Chem Int Ed Engl* **2004**, *43* (9), 1132–1136. <https://doi.org/10.1002/anie.200352979>.
- (196) Rawal, V. H.; Cava, M. P. Thermolytic Removal of T-Butyloxycarbonyl (BOC) Protecting Group on Indoles and Pyrroles. *Tetrahedron Letters* **1985**, *26* (50), 6141–6142. [https://doi.org/10.1016/S0040-4039\(00\)95036-6](https://doi.org/10.1016/S0040-4039(00)95036-6).
- (197) Nath, S.; Devi, G. R. Three-Dimensional Culture Systems in Cancer Research: Focus on Tumor Spheroid Model. *Pharmacology & Therapeutics* **2016**, *163*, 94–108. <https://doi.org/10.1016/j.pharmthera.2016.03.013>.
- (198) Dahlgren, M. K.; Schyman, P.; Tirado-Rives, J.; Jorgensen, W. L. Characterization of Biaryl Torsional Energetics and Its Treatment in OPLS All-Atom Force Fields. *J. Chem. Inf. Model.* **2013**, *53* (5), 1191–1199. <https://doi.org/10.1021/ci4001597>.

- (199) Henry, C. M.; Hollville, E.; Martin, S. J. Measuring Apoptosis by Microscopy and Flow Cytometry. *Methods* **2013**, *61* (2), 90–97. <https://doi.org/10.1016/j.ymeth.2013.01.008>.
- (200) Martin, H. L.; Adams, M.; Higgins, J.; Bond, J.; Morrison, E. E.; Bell, S. M.; Warriner, S.; Nelson, A.; Tomlinson, D. C. High-Content, High-Throughput Screening for the Identification of Cytotoxic Compounds Based on Cell Morphology and Cell Proliferation Markers. *PLOS ONE* **2014**, *9* (2), e88338. <https://doi.org/10.1371/journal.pone.0088338>.
- (201) Rojas Wahl, R. U. Decomposition Mechanism of 3-N-Morpholinosydnonimine (SIN-1)—a Density Functional Study on Intrinsic Structures and Reactivities. *J Mol Model* **2004**, *10* (2), 121–129. <https://doi.org/10.1007/s00894-004-0178-9>.
- (202) Martin-Romero, F. J.; Gutiérrez-Martin, Y.; Henao, F.; Gutiérrez-Merino, C. Fluorescence Measurements of Steady State Peroxynitrite Production upon SIN-1 Decomposition: NADH versus Dihydrodichlorofluorescein and Dihydrorhodamine 123. *J Fluoresc* **2004**, *14* (1), 17–23. <https://doi.org/10.1023/b:jofl.0000014655.89256.bd>.
- (203) Lin, X.; Zheng, W.; Liu, J.; Zhang, Y.; Qin, H.; Wu, H.; Xue, B.; Lu, Y.; Shen, P. Oxidative Stress in Malignant Melanoma Enhances Tumor Necrosis Factor- $\alpha$  Secretion of Tumor-Associated Macrophages That Promote Cancer Cell Invasion. *Antioxid Redox Signal* **2013**, *19* (12), 1337–1355. <https://doi.org/10.1089/ars.2012.4617>.
- (204) Denicola, A.; Souza, J. M.; Radi, R. Diffusion of Peroxynitrite across Erythrocyte Membranes. *Proc Natl Acad Sci U S A* **1998**, *95* (7), 3566–3571. <https://doi.org/10.1073/pnas.95.7.3566>.

# Publications

- In-Cell Generation of Anticancer Phenanthridine Through Bioorthogonal Cyclization in Antitumor Prodrug Development. *Angew. Chem. Int. Ed.*, **2021**, 60, 24043-24047  
→ <https://onlinelibrary.wiley.com/doi/abs/10.1002/anie.202110041>
- Anticancer Boron-Containing Prodrugs Responsive to Oxidative Stress from the Tumor Microenvironment. *Eur. J. Med. Chem.*, **2020**, 112670  
→ <https://www.sciencedirect.com/science/article/abs/pii/S0223523420306425>
- Arylboronate prodrugs of doxorubicin as promising chemotherapy for pancreatic cancer. *Bioorg. Chem.*, **2019**, 91, 103158  
→ <https://www.sciencedirect.com/science/article/abs/pii/S0045206819309381?via%3Dihub>
- Boronic acid/boronate prodrugs for cancer treatment: current status and perspectives. *Future Med. Chem.*, **2021**, 13, 859-861  
→ <https://www.future-science.com/doi/abs/10.4155/fmc-2021-0037>